

EFFECTS OF VALPROIC ACID ON FATTY ACID
PRODUCTION IN MICROORGANISMS AND BIOACTIVE
COMPOUNDS FROM *Feroniella lucida* (Scheff.) Swingle
AND TERMITE-ASSOCIATED FUNGUS ISFB10



Miss Prapassorn Poolchanuan

จุฬาลงกรณ์มหาวิทยาลัย
CHULALONGKORN UNIVERSITY

A Dissertation Submitted in Partial Fulfillment of the Requirements
for the Degree of Doctor of Philosophy in Biotechnology

Common Course

FACULTY OF SCIENCE

Chulalongkorn University

Academic Year 2020

Copyright of Chulalongkorn University

ผลของ valproic acid ต่อการผลิตกรดไขมันในจุลินทรีย์และสารออกฤทธิ์ทางชีวภาพจาก
มะสังและราที่อยู่ร่วมกับปลวก ISFB10



วิทยานิพนธ์นี้เป็นส่วนหนึ่งของการศึกษาตามหลักสูตรปริญญาวิทยาศาสตรดุษฎีบัณฑิต
สาขาวิชาเทคโนโลยีชีวภาพ ไม่สังกัดภาควิชา/เทียบเท่า
คณะวิทยาศาสตร์ จุฬาลงกรณ์มหาวิทยาลัย
ปีการศึกษา 2563
ลิขสิทธิ์ของจุฬาลงกรณ์มหาวิทยาลัย

Thesis Title EFFECTS OF VALPROIC ACID ON FATTY ACID
PRODUCTION IN MICROORGANISMS AND
BIOACTIVE COMPOUNDS FROM *Feroniella lucida*
(Scheff.) Swingle AND TERMITE-ASSOCIATED
FUNGUS ISFB10
By Miss Prapassorn Poolchanuan
Field of Study Biotechnology
Thesis Advisor Associate Professor NATTAYA
NGAMROJANAVANICH, Ph.D.
Thesis Co Advisor Associate Professor Prasat Kittakoop, Ph.D.

Accepted by the FACULTY OF SCIENCE, Chulalongkorn University in
Partial Fulfillment of the Requirement for the Doctor of Philosophy

..... Dean of the FACULTY OF
SCIENCE
()

DISSERTATION COMMITTEE

..... Chairman
(CHOMPOONIK KANCHANABANCA, Ph.D.)
..... Thesis Advisor
(Associate Professor NATTAYA
NGAMROJANAVANICH, Ph.D.)
..... Thesis Co-Advisor
(Associate Professor Prasat Kittakoop, Ph.D.)
..... Examiner
(Associate Professor SEHANAT PRASONGSUK,
Ph.D.)
..... Examiner
(Professor KHANITHA PUDHOM, Ph.D.)
..... External Examiner
(Damrong Sommit, Ph.D.)

ประภัสสร พูลฉนวน : ผลของ valproic acid ต่อการผลิตกรดไขมันในจุลินทรีย์และสารออกฤทธิ์ทางชีวภาพจากมะสังและราที่อยู่ร่วมกับปลวก ISFB10. (EFFECTS OF VALPROIC ACID ON FATTY ACID PRODUCTION IN MICROORGANISMS AND BIOACTIVE COMPOUNDS FROM *Feroniella lucida* (Scheff.) Swingle AND TERMITE-ASSOCIATED FUNGUS ISFB10) อ.ที่ปรึกษาหลัก : รศ. ดร. นาดยา งามโรจนวิชย์, อ.ที่ปรึกษาร่วม : รศ. ดร.ประสพ กิตตะคุปต์

ยา Valproic acid หรือ VPA เป็นยาที่ใช้ในการรักษาโรคลมชัก ไบโพล่า ไมเกรน และภาวะที่ร่างกายมีอาการปวดที่เกิดจากความผิดปกติของระบบประสาท ซึ่งยาตัวนี้มีผลข้างเคียงหลายอย่าง ในการศึกษาพบว่ากรดไขมันบางชนิดเปลี่ยนแปลงอย่างมีนัยสำคัญเมื่อเติมยา VPA ในอาหารเลี้ยงเชื้อที่ความเข้มข้น 100 μM ในการศึกษาพบว่ายา VPA มีผลต่อการสร้างกรดไขมันบางชนิดในแบคทีเรีย เชื้อรา และยีสต์ โดยการไปกระตุ้นการสร้างกรดไขมันที่มากขึ้น ลดลง หรือมีผลยับยั้งการสร้างกรดไขมันบางชนิดอีกด้วย ยา VPA ไปกระตุ้นการผลิตกรดไขมันชนิด *trans-9-elaidic acid* ซึ่งเป็นกรดไขมันที่มีการรายงานก่อนหน้านี้ว่าส่งผลต่อระบบภูมิคุ้มกันของมนุษย์ นอกจากนี้ยังพบว่ายา VPA มีผลต่อการผลิตสารกลุ่ม polyketide บางชนิดในเชื้อรา การศึกษานี้ยังได้ศึกษาสารออกฤทธิ์ทางชีวภาพจากดินมะสังและเชื้อราที่อยู่ร่วมกับปลวกอีกด้วย candicine (7) และสารอนุพันธ์ candicine (8) ถูกแยกจากสารสกัดของมะสังส่วนหนาม สารประกอบที่แยกได้ (8) มีฤทธิ์ยับยั้ง xanthine oxidase อ่อน มีค่า IC_{50} $473.8 \pm 13.4 \mu\text{M}$ roridin A (9) และ verrucarin A (10) ถูกแยกออกจากสารสกัดของเชื้อราที่แยกจากปลวก ISFB10 สารประกอบที่แยกได้ (9) แสดงความเป็นพิษต่อเซลล์มะเร็ง HuCCA-1 A549 MOLT-3 HepG2 ด้วยค่า IC_{50} 0.016 ± 0.0007 0.0055 ± 0.0001 0.005 ± 0.0003 และ $0.024 \pm 0.002 \mu\text{M}$ ตามลำดับ และสารประกอบ (10) แสดงความเป็นพิษต่อเซลล์มะเร็ง HuCCA-1 A549 MOLT-3 HepG2 ด้วยค่า IC_{50} 0.014 ± 0.0005 0.0047 ± 0.0005 0.008 ± 0.0002 และ 0.019 ± 0.001 ตามลำดับ แต่ roridin A (9) และ verrucarin A (10) ก็แสดงความเป็นพิษต่อเซลล์ปกติ MRC-5 ด้วยค่า IC_{50} 0.038 ± 0.006 และ 0.012 ± 0.0004 ตามลำดับ

จุฬาลงกรณ์มหาวิทยาลัย
CHULALONGKORN UNIVERSITY

สาขาวิชา เทคโนโลยีชีวภาพ
ปีการศึกษา 2563

ลายมือชื่อนิสิต
ลายมือชื่อ อ.ที่ปรึกษาหลัก
ลายมือชื่อ อ.ที่ปรึกษาร่วม

5872854623 : MAJOR BIOTECHNOLOGY

KEYWORD Valproic acid fatty acid polyketide microorganisms bioactive
D: compounds

Prapassorn Poolchanuan : EFFECTS OF VALPROIC ACID ON FATTY ACID PRODUCTION IN MICROORGANISMS AND BIOACTIVE COMPOUNDS FROM *Feroniella lucida* (Scheff.) Swingle AND TERMITE-ASSOCIATED FUNGUS ISFB10. Advisor: Assoc. Prof. NATTAYA NGAMROJANAVANICH, Ph.D. Co-advisor: Assoc. Prof. Prasat Kittakoop, Ph.D.

Valproic acid or valproate (VPA) is a drug for the treatment of epilepsy, bipolar disorder, migraine headaches and neuropathic pain. Unfortunately, VPA has many side effects. In this work, it was found that productions of some fatty acids were significantly affected by VPA at the concentration of 100 μM . Further exploration of VPA on fatty acid production in microorganisms including fungi, yeast, and bacteria, as well as representative gut microbiome. This work showed that VPA could enhance, reduce or completely inhibit the production of some fatty acids. VPA could induce the production of *trans*-9-elaidic acid that was previously found to have cellular effects in human macrophages. Moreover, VPA was found to inhibit the production of some polyketides produced by a model fungus. This work also investigated bioactive compounds from a plant, *Feroniella lucida* (Scheff.) Swingle and a termite-associated fungus ISFB10. Candicine (7) and candicine derivative (8) were isolated from spine part of *F. lucida*. Compound 8 exhibited weak cancer chemoprevention activity in the xanthine oxidase assay (XXO) with an IC_{50} value of $473.8 \pm 13.4 \mu\text{M}$. Roridin A (9) and verrucarin A (10) were isolated from the termite-associated fungus ISFB10. Compounds 9 exhibited strong cytotoxic activities toward HuCCA-1, A549, MOLT-3 and HepG2 cancer cell lines with IC_{50} values of 0.016 ± 0.0007 , 0.0055 ± 0.0001 , 0.005 ± 0.0003 and $0.024 \pm 0.002 \mu\text{M}$, respectively. Compounds 10 also exhibited strong cytotoxic activities toward HuCCA-1, A549, MOLT-3 and HepG2 cancer cell lines with IC_{50} values of 0.014 ± 0.0005 , 0.0047 ± 0.0005 , 0.008 ± 0.0002 and $0.019 \pm 0.001 \mu\text{M}$, respectively. Unfortunately, compounds 9 and 10 were also exhibited strong cytotoxic activity toward normal cell line MRC-5 with IC_{50} values of 0.038 ± 0.006 and 0.012 ± 0.0004 , respectively.

Field of Study: Biotechnology

Student's Signature

Academic Year: 2020

.....
Advisor's Signature

Year:

.....
Co-advisor's Signature

.....

ACKNOWLEDGEMENTS

I would like to express my deepest and sincere gratitude to my advisor, Assoc. Prof. Nattaya Ngamrojanavanich and my co-advisor, Assoc. Prof. Prasat Kittakoop, for giving me an opportunity to pursue this research, their kind supervision, valuable guidance and encouragement throughout this work. I would also like to express my gratitude to Mr. Sanya Surerum and Mr. Surasak Prachya, for their special care, valuable advice and suggestion. Special thanks to Dr. Sanit Thongnest for his suggestion and structure elucidation of compound 5. I would also like to express my gratitude to Dr. Panida Unagul for research collaboration. My appreciation is also extended to Prof. Dr. Thammarat Aree for X-ray analysis, and Prof. Dr. Suthep Wiyakrutta for identification of fungi.

I would like to thank the 100th Anniversary Chulalongkorn University Fund for Doctoral Scholarship for financial support.

I am very grateful to the laboratory of natural products, Chulabhorn Research Institute (CRI), laboratory of chemical biology, Chulabhorn Graduate Institute (CGI) for giving me an opportunity to use advanced equipments and technology. Special thanks to Miss Somkid Sitthimonchai, Miss Busakorn Saimanee, Miss Pakamas Intachote and Miss Suchada Sengsai for the bioassay of cytotoxicity and cancer chemoprevention.

I would like to thank all members of CRI Natural Product Laboratory and CRI and CGI staffs for their kind suggestion and warm relationship. I would also like to express my gratitude to Mr. Nitirat Chimnoi for MS analysis and Miss Kittiporn Trisupphakant for UV and IR spectroscopy analysis.

Thanks also go to all friends for their love, support and encouragement, as well as all Blackpink members, my beloved artist, who fill my energy, my soul, encouragement and happiness throughout this work. Thank you for being a part in my life.

Finally, I am deep grateful to my family for being admirable role model, for their infinite support, entire care and love, encouragement and valuable suggestion. Thank you for showing me how much you love me.

Prapassorn Poolchanuan



จุฬาลงกรณ์มหาวิทยาลัย
CHULALONGKORN UNIVERSITY

TABLE OF CONTENTS

	Page
ABSTRACT (THAI)	iii
ABSTRACT (ENGLISH).....	iv
ACKNOWLEDGEMENTS.....	v
TABLE OF CONTENTS.....	vii
LIST OF FIGURES	1
LIST OF TABLES.....	2
Chapter I Introduction.....	3
Chapter II Literature review.....	8
2.1 Valproic acid (VPA).....	8
2.2 <i>Feroniella lucida</i> (Scheff.) Swingle	13
2.3 Termite-associated fungus ISFB10.....	19
Chapter III Materials and methods.....	26
3.1 General experiment method.....	26
3.2 Chemicals	26
3.3 Material and methodology in the study of effects of VPA on the biosynthesis of fatty acids and polyketides in microorganisms	27
3.3.1 Materials for the preparation of culture medium.....	27
3.3.2 Microorganisms used in the study.....	27
3.3.3. Cultivation of microorganisms	29
3.3.3.1. Cultivation of fungi	29
3.3.3.2 Cultivation of yeast	29
3.3.3.3 Cultivation of bacteria	30
3.3.4 Extraction of lipid and analysis of fatty acids	30
3.3.5 Isolation of mevalonolactone (Compound 1).....	31
3.3.6 Isolation of compound 2-6	31
3.3.7 Structure elucidation of fungal metabolites by spectroscopic techniques	32

3.3.8 Antibacterial activity	32
3.3.9 Statistical analysis method	32
3.4 Material and methodology for the study of bioactive compounds from <i>Feroniella lucida</i> (Scheff.) Swingle	33
3.4.1 Plant extraction and isolation	33
3.4.2 Investigation of chemical constituents and biological evaluation of plant extracts.....	34
3.5 Termite-associated fungus ISFB10 (unidentified).....	36
3.5.1 Collection and isolation of fungi	36
3.5.2 Fungal cultivation, extraction and isolation	36
3.5.3 Investigation of chemical constituents and biological evaluation of fungal extracts.....	38
Chapter IV Results and discussion	39
4.1 Effects of VPA on biosynthesis of fatty acids and polyketides.....	39
4.1.1 Effect of VPA on fatty acid biosynthesis	39
4.1.2 Effect of VPA on polyketide biosynthesis	56
4.1.3 Structure elucidation of compound 1 isolated from the fungus <i>Trichoderma reesei</i> and compounds 2-6, isolated from the fungus <i>Dothideomycete</i> sp.	60
4.1.3.1 Structure elucidation of compound 1	60
4.1.3.2 Structure elucidation of compound 2	62
4.1.3.3 Structure elucidation of compound 3	64
4.1.3.4 Structure elucidation of compound 4	66
4.1.3.5 Structure elucidation of compound 5	68
4.1.3.6 Structure elucidation of compound 6	70
4.1.4 Antibacterial activity	72
4.1.5 Cancer chemoprevention activity	73
4.1.6 Cytotoxic activity	73
4.2 Bioactive compounds from <i>Feroniella lucida</i> (Scheff.) Swingle.....	74
4.2.1 Structure elucidation of compound 7	74
4.2.2 Structure elucidation of compound 8	76

4.2.3 Biological activities of compounds isolated from <i>F. lucida</i>	78
4.3 Bioactive compounds from termite-associated fungus ISFB10	79
4.3.1 Structure elucidation of compound 9	79
4.3.2 Structure elucidation of compound 10	82
4.3.3 Biological activities of compounds isolated from termite-associated fungus ISFB10.....	85
Chapter V Conclusion.....	87
5.1 Effects of VPA on biosynthesis of fatty acids and polyketides.....	87
5.1.1 Effects of VPA on biosynthesis of fatty acids.....	87
5.1.2 Effects of VPA on biosynthesis of polyketides.....	88
5.2 Bioactive compounds from <i>Feroniella lucida</i> (Scheff.) Swingle.....	88
5.3 Bioactive compounds from termite-associated fungus ISFB10	89
REFERENCES	90
Appendix.....	97
VITA.....	163

LIST OF FIGURES

Figure 1 <i>Feroniella lucida</i> (Scheff.) Swingle.....	6
Figure 2 Schematic representation of mitochondrial β -oxidation of valproic acid (VPA), this picture is adapted from Silva (2008) ⁴	9
Figure 3 Chemical structures of compounds isolated from <i>Z. limonella</i>	14
Figure 4 Luteolin isolated from <i>F. limonia</i>	15
Figure 5 Chemical structures of compounds isolated from <i>F. lucida</i> (Scheff.) Swingle	17
Figure 6 Chemical structures of compounds isolated from <i>F. lucida</i> (Scheff.) Swingle	18
Figure 7 Chemical structures of antibiotics isolated from marine fungi	20
Figure 8 Chemical structures of compounds isolated from <i>Dothideomycete</i> sp.	21
Figure 9 Chemical structures of compounds isolated from termite-associated fungi..	23
Figure 10 Structures (R)-(-)-Mevalonolactone isolated from the marine-derived fungus <i>Trichoderma reesei</i>	40
Figure 11 Structures of compounds 2-6 isolated from the endophytic fungus <i>Dothideomycete</i> sp.....	58
Figure 12 Metabolite profile of the fungus <i>Dothideomycete</i> sp. (A) a control culture and (B) VPA (100 μ M) treated culture.....	59

LIST OF TABLES

Table 1 Lists of microorganisms used in this research	28
Table 2 Effect of VPA (100 μ M) on fatty acid profile of the fungus <i>Trichoderma reesei</i>	40
Table 3 Effect of VPA (100 μ M) on fatty acid profile of fungi	44
Table 4 Effect of VPA (100 μ M) on fatty acid profile of yeast.....	46
Table 5 Effect of VPA (100 μ M) on fatty acid profile of bacteria	47
Table 6 Effect of VPA (100 μ M) on fatty acid profile of representative gut fungi.....	51
Table 7 Effect of VPA (100 μ M) on fatty acid contents of representative gut yeast ..	54
Table 8 ^1H and ^{13}C NMR spectral data (400 MHz, in acetone- d_6) of compound 1	61
Table 9 ^1H and ^{13}C NMR spectral data (400 MHz, in CDCl_3) of compound 2	63
Table 10 ^1H and ^{13}C NMR spectral data (400 MHz, in CDCl_3) of compound 3	65
Table 11 ^1H and ^{13}C NMR spectral data (400 MHz, in CDCl_3) of compound 4	67
Table 12 ^1H and ^{13}C NMR spectral data (400 MHz, in CDCl_3) of compound 5	69
Table 13 ^1H and ^{13}C NMR spectral data (400 MHz, in CDCl_3) of compound 6	71
Table 14 Antibacterial activity of compounds 3-6	72
Table 15 Cancer chemoprevention activity of compounds 3, 4, 5 and 6.....	73
Table 16 Cytotoxic activity of compounds 3, 4, 5 and 6.....	73
Table 17 ^1H and ^{13}C NMR spectral data (400 MHz, in acetone- d_6) of compound 7 ..	75
Table 18 ^1H and ^{13}C NMR spectral data (400 MHz, in acetone- d_6) of compound 8 ..	77
Table 19 Cancer chemoprevention activity of compound 8 isolated from <i>F. lucida</i> ...	78
Table 20 ^1H and ^{13}C NMR spectral data (400 MHz, in acetone- d_6) of compound 9 ..	81
Table 21 ^1H and ^{13}C NMR spectral data (400 MHz, in acetone- d_6) of compound 10 ..	84
Table 22 Cytotoxic activities of compounds isolated from termite-associated fungus ISFB10	85

Chapter I

Introduction

Valproic acid (VPA) or valproate is an anticonvulsive drug and it has been widely used as drug for the treatment of many disorders, for example, epilepsy, and for the prevention of migraine headaches. VPA has been reported to have many side effects such as hepatic steatogenesis in rats¹, and negative influence on hepatic carbohydrate and lipid metabolism was also observed in the patient under VPA treatment². Moreover, there were numerous deadly cases of hyperammonemia in patients under VPA treatment³. Basically, VPA undergoes fatty acid β -oxidation in mitochondria and causes toxicity due to the interference with mitochondrial β -oxidation. Furthermore, VPA treatment also causes many serious inborn errors of metabolism⁴. Patients under VPA treatment could have hepatotoxicity and weight gain due to the interference of VPA with carnitine palmitoyl-transferase I, a key enzyme in mitochondrial fatty acid β -oxidation pathway⁵. VPA could also inhibit *N*-acetyl glutamate synthetase, the interference with this enzyme resulting in the inhibition of urea synthesis^{6,7}. Abnormal autism-like behaviors in mice was observed in mice treated with VPA when compared with the valpromide, a VPA analog lacking histone deacetylase inhibition activity⁸. Nowadays, the risk of VPA on autism spectrum disorders has been gained much attention from numerous of research groups^{9, 10, 11, 12, 13, 14}. VPA is a histone deacetylase inhibitor, which is a drug candidate targeting anticancer therapy. VPA could alter the biosynthesis of fungal metabolites with enhanced chemical diversity, so VPA treatment with microorganisms is an effective strategy for controlling gene expression of fungal biosynthetic pathway¹⁵. Previous works have revealed the effectiveness of epigenetic modifiers for the production of new secondary metabolites in microorganisms, for example, proteasome inhibitor^{16, 17} and histone deacetylase inhibitor^{18, 19, 20}; this technique is known as “one strain many compound” (OSMAC) approach.

VPA was found to enhance ten-fold production of a fungal alkaloid, fumiquinazoline C²¹, and could induce new secondary metabolite production in endophytic fungus²² and enhance antimicrobial activity of the fungal metabolites^{23, 24}.

This discovery has challenged the scientific community worldwide to deeply investigate the mechanisms of VPA in various aspects^{25, 26}. Recently, there were many studies about drug repurposing of VPA for the treatment many diseases such as of breast cancer²⁷, colon cancer associated with diabetes mellitus²⁸, diffuse intrinsic pontine glioma²⁹, hypertension induced from high-fat diet³⁰, and HIV infection³¹. In addition, VPA inhibits cell cycle progression and MAP kinase signaling in the yeast model³². Beside the activities mentioned above, VPA also sensitized hepatocellular carcinoma cells to proton therapy through the suppression of NRF2 activation³³. Recently, the combination of VPA with other anticancer drugs has been subjected to Phase II clinical study for cancer therapy³⁴.

Gut microbiome plays an important role on human health, for example, food digestion and immune system. Moreover, gut microbiome can implicate health and diseases status of host such as cancer, diabetes and obesity, and now it has gradually received attention over the past 15 years^{35, 36}. Many studies have reported the role of gut microbiome in food allergy³⁷, liver disease³⁸ and anti-tumor immunity³⁹. Therefore, drug-microbiome interactions have recently received attention from the scientific community. There were many studies about drug-microbiome interactions, for example, interaction of atypical, antipsychotic drug, with the gut microbiome in a bipolar disease cohort⁴⁰, interaction of metformin, antidiabetic drug, with human gut microbiome⁴¹, and interaction of proton-pump inhibitor drugs with gut microbiome⁴². Non-antibiotic drugs have significant effect on the growth of gut microbiome. This correlation guided the potential risk of non-antibiotics in stimulating antibiotics resistance⁴³. Recent investigation revealed the ability of gut microbiome on drug metabolism due to gut microbiome could encode enzymes that can directly metabolize various types of drug⁴⁴. The fungus *Trichoderma reesei* was initially cultivated in the PDB culture media and only mevalonolactone was produced as a secondary metabolite.

So OSMAC approach was applied by adding VPA in the culture media; it was expected that the fungus would produce a variety of secondary metabolites. However, VPA was found to change certain fatty acid production in this fungus.

Based on the basic knowledge that fatty acid and polyketide biosynthesis share the similarities of enzyme by using the similar catalytic elements, utilization of common precursors, similar structures, similar chemistry and overall architectural design⁴⁵. Upon our preliminary results from the fungus *Trichoderma reesei*, this research aimed to investigate the effects of an anticonvulsive drug VPA on the production of fatty acids and polyketides in microorganisms, as well as the effects of VPA on representative gut microbiome.

In the past decades, natural bioactive compounds have played an important role throughout the world in treating and preventing diseases. A number of structurally and pharmacologically bioactive compounds have been isolated from natural resources including terrestrial plants, terrestrial microorganisms and marine organisms; these natural products possess antioxidant, antimicrobial, anticancer, chemoprevention, tyrosinase inhibition, and apoptosis induction. The world's biosphere is still challenging scientists to explore the novel bioactive compounds with potentially therapeutic properties that might be used as therapeutic agents in the future⁴⁶. Many synthetic drugs currently used in treatment, for example, doxorubicin (anticancer drug), provide undesirable side effects such as cardiotoxicity and tumor-drug resistance. And it is interesting to note that more than 50% of drugs used in cancer treatment are from medicinal plants. *Feroniella lucida* (Scheff.) Swingle is the tropical plant. Pulp of this plant is eaten as vegetable, the pericarp is used medicinally as traditional medicine and leaves are used in the treatment of flatulence and wound healing.

From the preliminary evaluation on anticancer and cancer chemoprevention activities, CH₂Cl₂ extracts from spine and leave of this plant exhibited their biological activities. *Feroniella lucida* (Scheff.) Swingle is therefore an interesting source to investigate bioactive compounds which might be useful for therapeutic purposes.



Figure 1 *Feroniella lucida* (Scheff.) Swingle

มหาวิทยาลัย
CHULALONGKORN UNIVERSITY

Feroniella lucida (Scheff.) Swingle (Figure 1) is the plant in Rutaceae family, locally known as “Ma-sung” in Thai. It is medium-sized tree distributed widely in Northeast of Thailand. Rutaceae family comprises almost 150 genera and 1600 species of trees, shrubs and climbers distributed throughout the temperate and tropical regions of the world⁴⁷.

There are many interesting sources for bioactive compounds from natural product such as plants, marine organisms, algae and microorganisms. Beside the isolation of bioactive compounds from *Feroniella lucida* (Scheff.) Swingle mentioned above, termite associated fungi are also interesting source for the investigation of bioactive compounds. The enormous symbiotic microbial communities play essential roles for hosts in digestion, immune system, production of vitamins and cofactors and the production of some compounds or antibiotics against host antagonists⁴⁸.

Furthermore, these microbial networks also involve the balance within termite communities such as the cleanliness of termite nest. This symbiotic association could lead to the discovery of novel bioactive compounds from termite-associated fungi.

Therefore, the aims of this study are to study the effects of VPA on fatty acid synthesis in microorganisms and the effect of VPA on polyketide biosynthesis in the fungus model. Moreover, we aim to investigate the bioactive compounds from plants and termite-associated fungus and to study their biological activities which might be useful for medical, pharmaceutical and cosmetic purposes.

Chapter II

Literature review

2.1 Valproic acid (VPA)

Valproic acid (VPA), or valproate is an anticonvulsive drug. It has been used as drug for the treatment of epilepsy and bipolar disorder and for the prevention of migraine headaches. Unfortunately, VPA has side effects, for example, the administration of high dose VPA (750 mg per Kg) significantly induced microvesicular steatosis in mice after 48 h of VPA intake. On the other hand, steatosis was not seen in mice treated with low dose of VPA (350 mg per Kg) ¹. VPA has negative influence on hepatic carbohydrate and lipid metabolism by the inhibition of lactate gluconeogenesis, fatty acid oxidation and fatty acid synthesis. VPA increased medium-chain acyl-CoA ester fraction whereas coenzyme A, acetyl-CoA and long-chain acyl CoA were decreased ². There were a number of fatal cases of hyperammonemic encephalopathy (VHE) for patients treated with VPA. The symptoms of VHE are acute onset of impaired consciousness, focal neurogenic symptoms and increase seizure frequency ³. VPA undergoes fatty acid β -oxidation pathway in mitochondria. Briefly, VPA is metabolized to be active intermediate forms (Figure 2), and those intermediates are finally changed into 3-hydroxy-VPA and 3-keto-VPA, and these metabolites were found in the urine of rat treated with VPA, whereas $\Delta^{2(E)}$ -VPA is the metabolite found in human urine for the patient under VPA treatment. VPA metabolism affected the enzyme fatty acid β -oxidation (FAO) and their cofactors, and VPA also induced plasma carnitine deficiency; this interference can cause many serious inborn errors of metabolism ⁴.

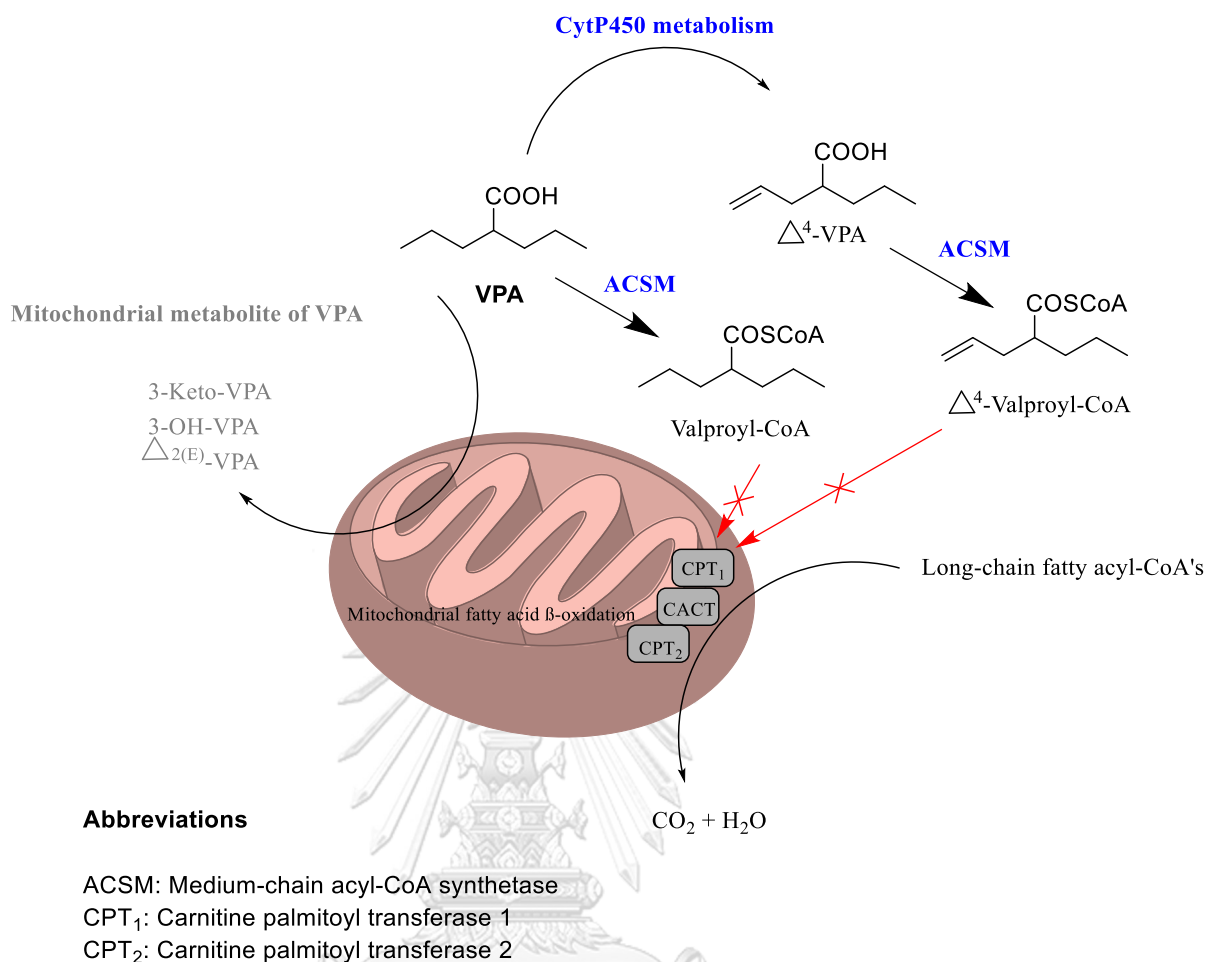


Figure 2 Schematic representation of mitochondrial β -oxidation of valproic acid (VPA), this picture is adapted from Silva (2008)⁴.

In 2009, Aires and co-workers reported that VPA interfered carnitine palmitoyl-transferase I, a key enzyme in mitochondrial fatty acid β -oxidation, which maybe a crucial mechanism inducing hepatotoxicity and weight gain for patients under VPA therapy⁵. Moreover, patients receiving VPA for one year had significantly higher body weight when compared with lamotrigine, another prescribed drug for epilepsy treatment⁴⁹. VPA could inhibit *N*-acetyl glutamate synthetase, resulting in the inhibition of urea synthesis^{6,7}.

Moreover, VPA was found to induce abnormal autism-like behaviors in mice when compared to mice with prenatal exposure to valpromide, a VPA analog lacking histone deacetylase inhibition activity. Valpromide did not affect the behaviors in mice.

Noted that maternal used of VPA during pregnancy has been implicated autism spectrum disorders (ASD) in children, and mice prenatal with exposure to VPA showed behavioral alterations similar to human case with autism⁸.

There were many studies on the risk of VPA on autism spectrum disorders (ASD)^{9, 10, 11, 12, 13, 14}. VPA exhibits anticancer activity, and it is a promising anticancer candidate. Clinical trials on VPA treating some forms of cancer have been carried out. Recently, VPA in the combination with other anticancer drugs such as cisplatin and cetuximab has been subjected to phase II clinical study for cancer therapy, and the result showed that the drug combination provided less toxic and more effective first-line chemotherapy regimen in patients³⁴.

VPA could inhibit proliferation and induce differentiation of numerous transformed cell lines, for example, neuroblastoma, erythroleukemia, carcinomas of the skin, breast, prostate, bladder, lung, colon, cervix, hematopoietic progenitor cells and leukemic blast cells. In addition, VPA also suppressed tumor growth and metastasis formation. Nowadays, drug repurposing of VPA has been intensively investigated for the treatment of various diseases, for example, VPA inhibited breast cancer cell migration and metastasis, as well as induced cell cycle arrest and apoptosis²⁷. VPA prevented hyperglycemia, hyperinsulinemia, and TNF- α and IL-1 β production, and also prevented colony formation and cell migration in mice with colon cancer associated with diabetes mellitus²⁸. Diffuse intrinsic pontine glioma (DIPG) was studied with VPA, and it showed that VPA induced histone H3 acetylation, resulting in apoptosis induction and reduction of cell viability in DIPG cells²⁹. VPA is also used in the treatment of high-fat diet-induced hypertension by downregulating angiotensin II and its receptors via inhibition of HDAC1³⁰. VPA repurposing of HIV infection is in progress, and studies showed that VPA therapy has significant effect on reversing HIV-1 latent reservoirs³¹.

The study from yeast model revealed that VPA could induce growth inhibition by modulating the expression of many genes responsible for protein folding, sexual reproduction, cell wall organization and cell cycle progression. Moreover, VPA inhibited MAP kinase signaling which is a crucial mechanism for mating pheromone pathway³². Besides the treatment of various diseases mentioned above, VPA could also sensitize hepatocellular carcinoma cells to proton therapy through the suppression of NRF2 activation, resulting in proton-induced apoptotic cell death and tumor growth delay³³.

Gut microbiome plays an important role for human health and diseases. Although gut microbiome has been investigated for several decades about their roles for host, for example, gut microbiome has capacities in digestion, fermentation of non-digestible substrates, immune system and classical infection diseases by pathogen, but gut microbiome still has received increasing attention from the scientific community worldwide, because it can directly implicate health and diseases status of host, e.g., cancer, diabetes, obesity and liver disease^{35, 36}. Number of publications reported that there were correlation between microbiota association and medication specific effects of some diseases, for example, gut microbiome more than 2700 species of the deeply phenotyped Twins UK cohort were studied, and it was found that those microbiome associated with 38 common diseases and 51 medication⁵⁰. In 2019, Feehley and co-workers reported that gut microbiome regulated food allergy in human. The experiment was studied on germ-free mice colonized with feces from healthy or cow's milk allergic (CMA) infants, and found that germ-free mice colonized with bacteria from healthy infants were protected against anaphylactic responses to cow's milk allergen³⁷. Moreover, infants born to obese mothers have different microbiome diversity compared with infants born to normal weight mothers. Microbiome dysbiosis led to increased gut permeability, and reduced macrophage phagocytic activity and bacterial translocation to liver, resulting in increased hepatic inflammatory responses and trigger non-alcoholic fatty liver disease (NAFLD)³⁸. Gut microbiome has been found to have the role in anti-tumor immunity and limiting tumor expansion³⁹.

Previous works have demonstrated the drug interaction with human gut microbiome, such as atypical antipsychotics (AAP) drug interacting with gut microbiome in bipolar disease cohort. Gut microbiome were significantly different between AAP-treated and non AAP-treated cohort, especially, AAP treatment decreased species richness of bacteria *Lachnospiraceae*, *Akkermansia* and *Sutterella*, respectively⁴⁰. Antidiabetic drug, metformin, has been investigated for the interaction with human gut microbiome, and found that this drug induced gut microbiome shifts with a depletion of butyrate-producing taxa⁴¹. Proton-pump inhibitor drug, drug for the treatment of peptic ulcers and gastroesophageal reflux disease, has also been investigated drug interacting with gut microbiome. It was found that this drug altered the composition of gut microbiome by decreasing microbial diversity and abundance in gut commensals, whereas, the abundance of *Streptococcaceae* of oral and upper GI tract commensal was increased⁴². There is a significant impact of non-antibiotic drugs on gut microbiome in human.

More than 100 marketed drugs were studied against 40 strains of representative gut bacteria. The result showed that 24% of drugs inhibited the growth of at least one strain of bacteria. This correlation guided the potential risk of non-antibiotics in stimulating antibiotics resistance⁴³. Interestingly, gut microbiome was found to encode enzymes responsible for drug metabolism⁴⁴.

Previous works have reported the significant correlation between the biosynthesis of fatty acid and polyketides, indicating that there are similarities of enzymes responsible for the biosynthesis of fatty acid and polyketide natural products. The differences between polyketide and fatty acid biosynthesis are the number and type of acyl precursors used, as well as the cyclization pattern and the position of keto-group reductions in the products⁵¹. There are three types of polyketide biosynthesis; type I fatty acid and polyketide synthases which mostly found in bacteria⁴⁵, type II fatty acid and polyketide synthases which broadly found in fungi and plant plastids⁵² and type III polyketide synthases of plant⁵³. Furthermore, type III polyketide synthases were also found in gram-positive, filamentous bacterium *Streptomyces griseus*, the fungi *Aspergillus oryzae* and *Neurospora crassa*, and the yeasts *Saccharomyces cerevisiae* and *Schizosaccharomyces pombe*⁵³.

Based on our preliminary result from the fungus *Dothideomycete* sp. as mentioned earlier and the similarities of fatty acid and polyketide biosynthesis, so this thesis research aimed to investigate the effects of an anticonvulsive drug VPA on the production of fatty acids and polyketides in microorganisms. In this work, apart from representative gut microbiome, microorganisms including yeast, fungi and bacteria involved in food and beverage production were also investigated. It should be noted that endophytic fungus *Dothideomycete* sp. is known as a source of polyketides in our laboratory. This fungus provided a tricyclic polyketide, azaphilone, hybrid azaphilone-pyrone, calbistrin, and isochromanone, and it produced large amount of austdiol^{54, 55, 56}.

2.2 *Feroniella lucida* (Scheff.) Swingle

For a thousand of years, natural products have played an important role for the treatment of human diseases. Thailand is one of the most biodiversity-rich countries in Southeast Asia. Natural product medicines have come from various sources including terrestrial plants, terrestrial microorganisms and marine organisms. A number of structurally and pharmacologically bioactive compounds have been isolated from natural resources, and some of which display antioxidant, antimicrobial, anticancer, chemoprevention, apoptosis induction and tyrosinase inhibitory activities.

Feroniella lucida (Scheff.) Swingle is the plant in Rutaceae family, locally known as “Ma-sung” in Thai. It is medium-sized tree distributed widely in the Northeast of Thailand. Rutaceae family comprises almost 150 genera and 1600 species of trees, shrubs and climbers, and they distribute throughout the temperate and tropical regions of the world. There are many phytochemical constituents isolated from this family. For example, *Zanthoxylum limonella* is the plant belongs to Rutaceae family, and various types of secondary metabolites were isolated from stem bark and fruit of this plant. Numerous compounds were isolated from *Z. limonella*, as shown in Figure 3. Some compounds from *Z. limonella* exhibited antimicrobial, antioxidant, antitumor and larvicidal activities⁵⁷.

Another plant belongs to Rutaceae family is *Feronia limonia*, and the major secondary metabolite isolated from this plant was luteolin (Figure 4), which belongs to a flavone group of flavonoids⁵⁸.

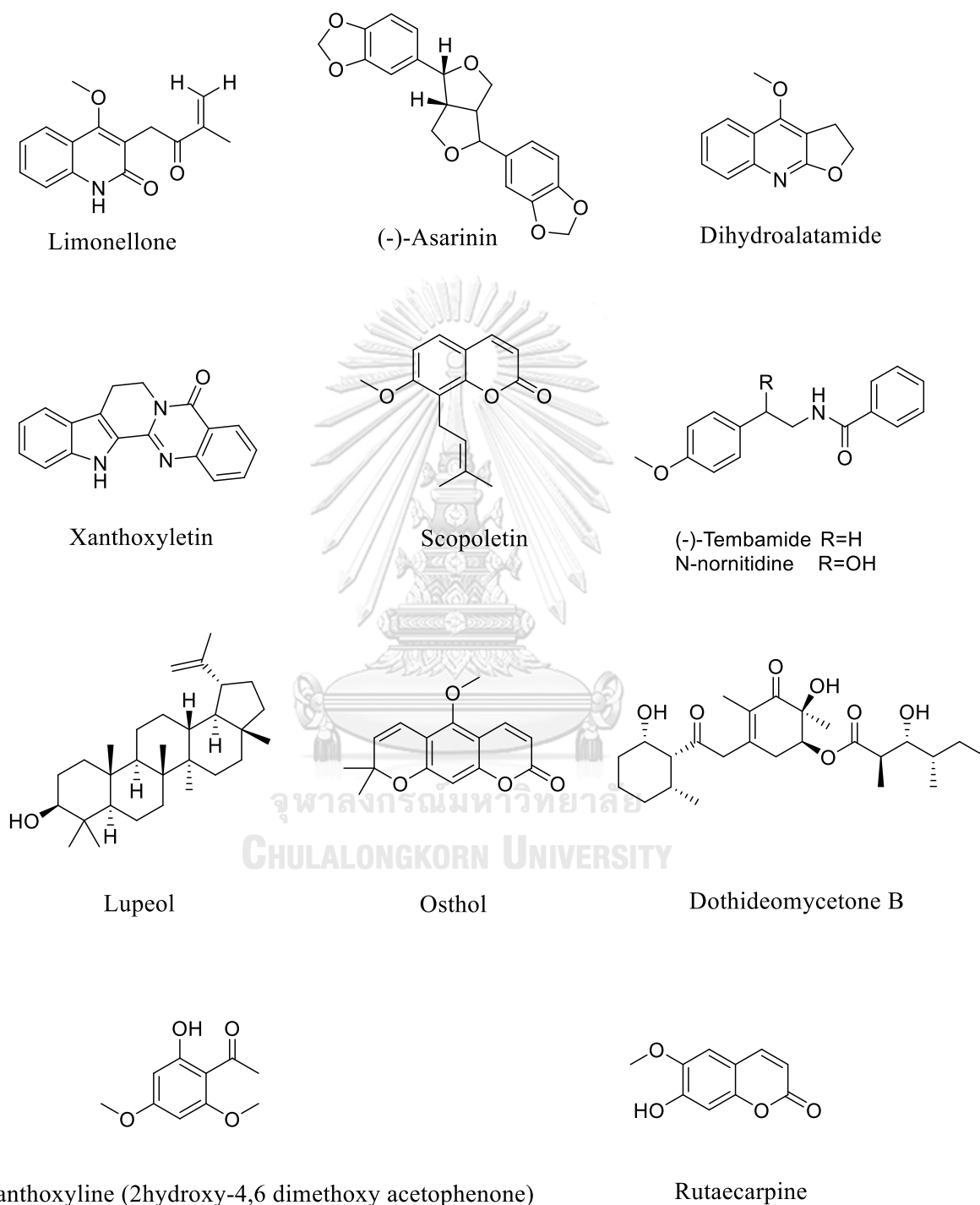
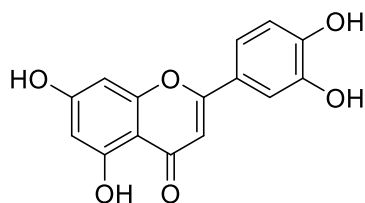


Figure 3 Chemical structures of compounds isolated from *Z. limonella*



Luteolin

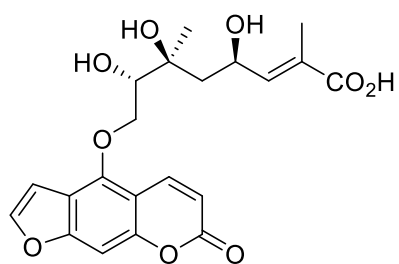
Figure 4 Luteolin isolated from *F. limonia*

Previous phytochemical studies of *F. lucida* reported that this plant had various types of secondary metabolites, for example, coumarins isolated from roots and twigs of this plant, namely, feronielllic acid A-C, feroniellin A-C, and lucidafuranocoumarin A-C^{59, 60, 61, 62}, alkaloids, namely, (Z)-N-(4-methoxystyryl)nicotinamide, lignans, namely, lucidenal and lucidanin, flavanone, namely, (2S)-3'-formyl-4',5,7-trihydroxyflavanone isolated from roots and twigs⁶³ (Figure 5), and triterpenoids, namely, feroniellide A-B isolated from root⁶⁴, and feroniellide C-D from the stem bark of *F. lucida*⁶⁵ (Figure 6).

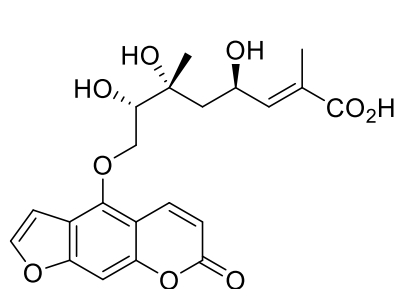
Many compounds isolated from *F. lucida* (Scheff.) Swingle exhibited interesting biological activities including antibacterial, antitumor, antimycobacterial, antifungal and anti-HIV activities. Feroniellin A induced apoptosis in human A549 lung cancer cell lines⁵⁹. Beside apoptosis induction, feroniellins A and B exhibited in vivo cytotoxicity against human KB carcinoma cells with IC₅₀ values of 0.13 and 0.23 mM, respectively. Moreover, feroniellins A and B were cytotoxic toward HeLa cells with IC₅₀ values of 0.14 and 0.19 mM, respectively⁵⁹. Lucidinal exhibited cytotoxicity against HuCCA-1, A549, MOLT-3 and HepG2 cancer cell lines with IC₅₀ values of 4.27, 9.59, 2.31 and 6.50 µg/mL, respectively⁶³.

Lucidafuranocoumarin exhibited cytotoxicity toward KB carcinoma cells, NCI-H187 and MCF-7 cell lines with IC_{50} values of 5.23, 3.16 and 13.13 μ M, respectively⁶¹. Feroniellides A and B exhibited cytotoxicity toward KB carcinoma cells with IC_{50} values of 60 and 49 μ g/mL, and against HeLA carcinoma cells with IC_{50} values of 46 and 40 μ g/mL, respectively⁶⁴. In addition, Feroniellides C, D, and E exhibited cytotoxicity toward KB carcinoma cells with IC_{50} values of 25.5, 4.1, and 3.4 μ g/mL, and also exhibited cytotoxicity against HeLA carcinoma cells with IC_{50} values of 27.5, 10.0, and 14.2 μ g/mL, respectively⁶⁵.

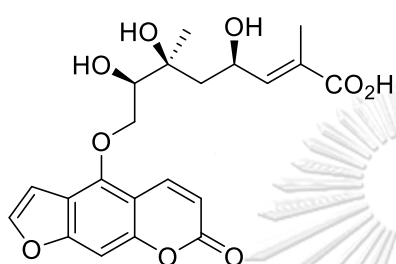




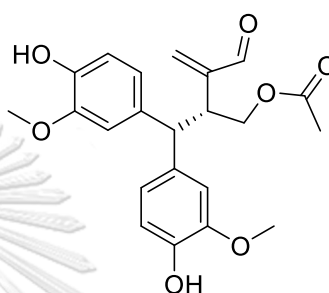
Feronielllic acid A



Feronielllic acid B



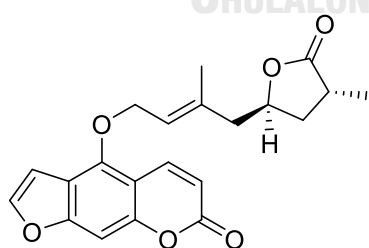
Feronielllic acid C



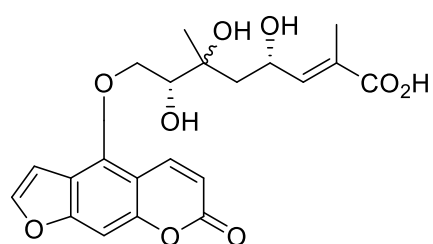
Lucidenal



(Z)-N-(4-Methoxystyryl)nicotinamide (2S)-3'-Formyl-4',5,7-trihydroxyflavanone



Lucidafuranocoumarin B 1



Lucidafuranocoumarin B 2

Figure 5 Chemical structures of compounds isolated from *F. lucida* (Scheff.) Swingle

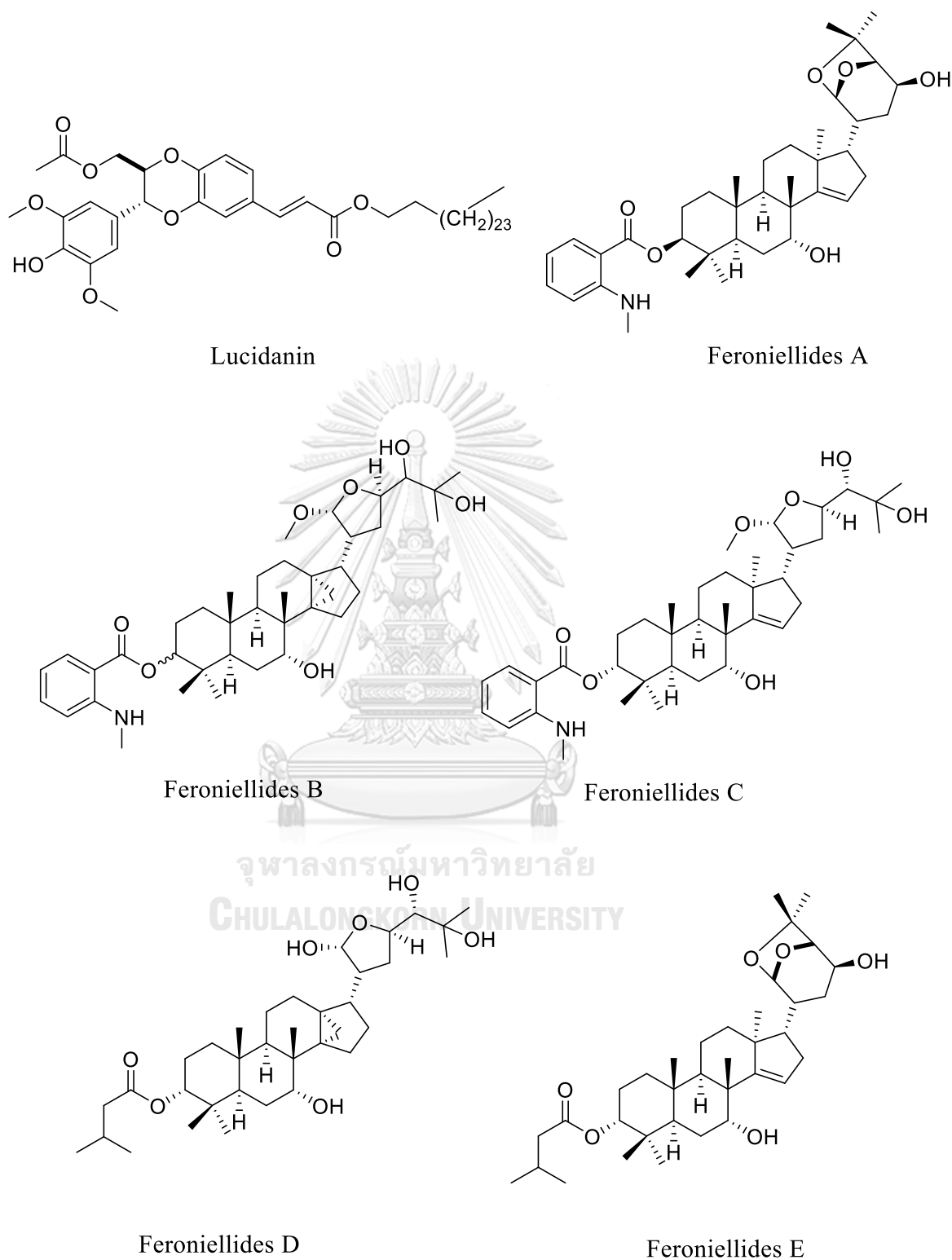
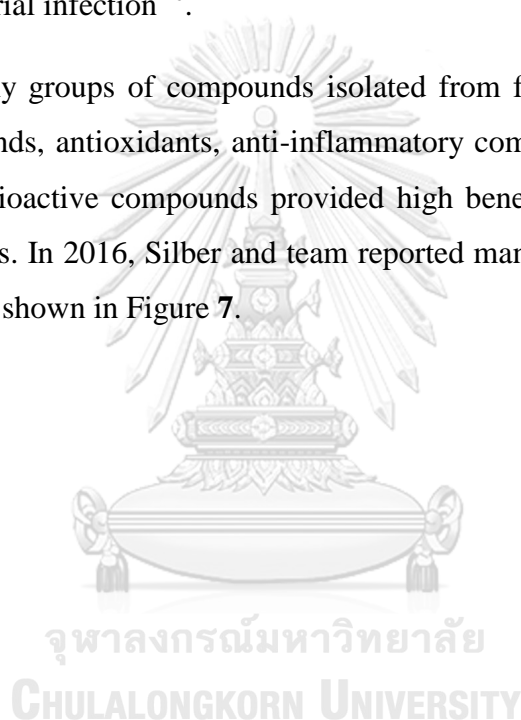


Figure 6 Chemical structures of compounds isolated from *F. lucida* (Scheff.) Swingle

2.3 Termite-associated fungus ISFB10

The second large kingdom of eukaryotic organisms is fungi kingdom. Taxonomists recently estimated that fungal kingdom has more than 5 million species but only approximately 100,000 species have been formally classified. There are many novel bioactive secondary metabolites isolated from fungi which are very useful in therapeutic purpose. In 1928, the discovery of penicillin from *Penicillium chrysogenum* was one of the most important discoveries in medicinal history to find drug against bacterial infection⁴⁶.

There are many groups of compounds isolated from fungi including antibiotics, cytotoxic compounds, antioxidants, anti-inflammatory compounds and other medical leads, and these bioactive compounds provided high benefit for medical purpose to treat many diseases. In 2016, Silber and team reported many antibiotics isolated from marine fungi,⁶⁶ as shown in Figure 7.



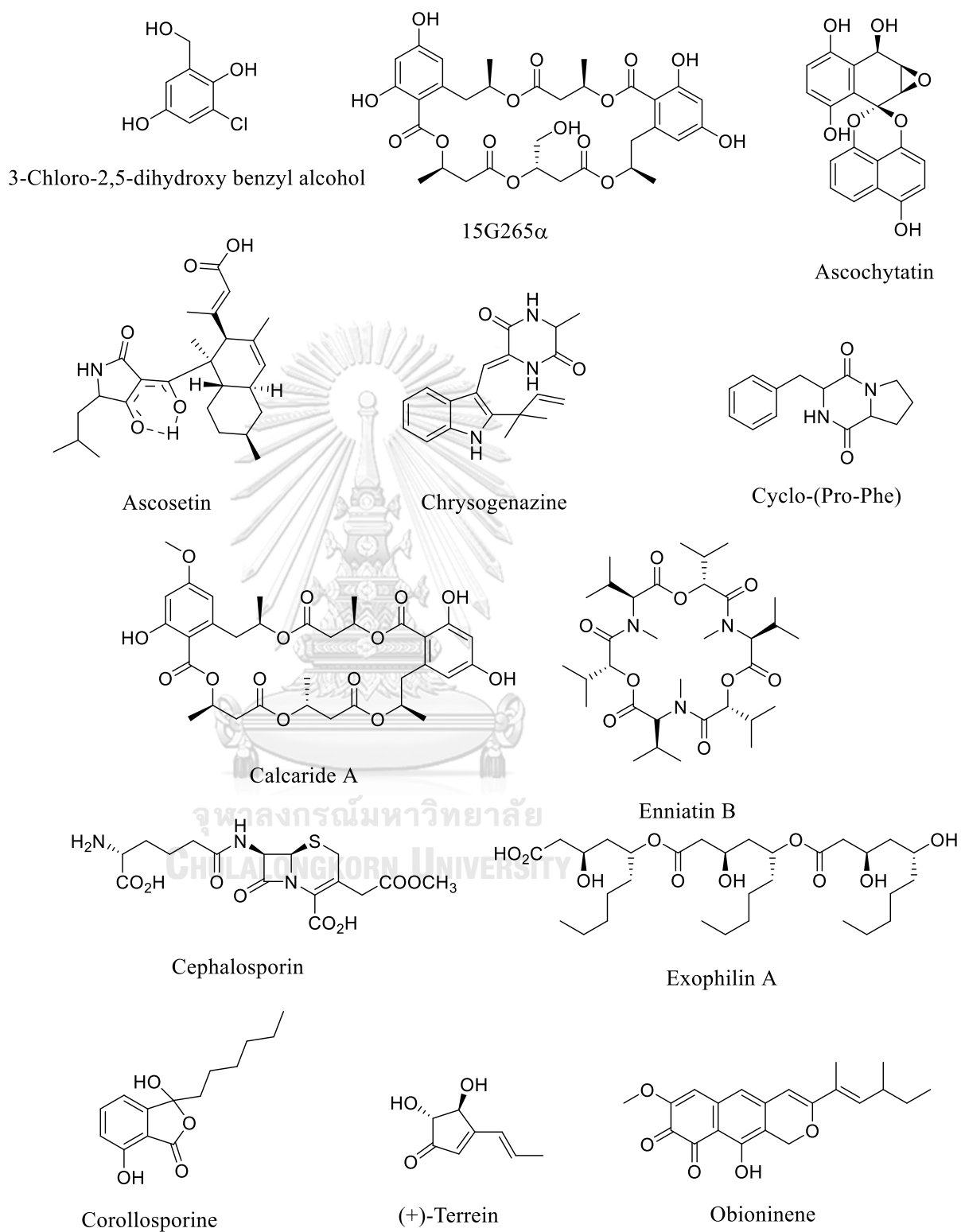


Figure 7 Chemical structures of antibiotics isolated from marine fungi

In addition to antibiotics, fungi also produced cytotoxic compounds. In 2012, Kittakoop et. al. reported a novel tricyclic polyketide (dothideomycetide A) and azaphilone derivatives (dothideomycetone A and dothideomycetone B) from the fungus *Dothideomycete* sp. (isolated from a Thai medicinal plant, *Tiliacora triandra*)⁵⁴ (Figure 8).

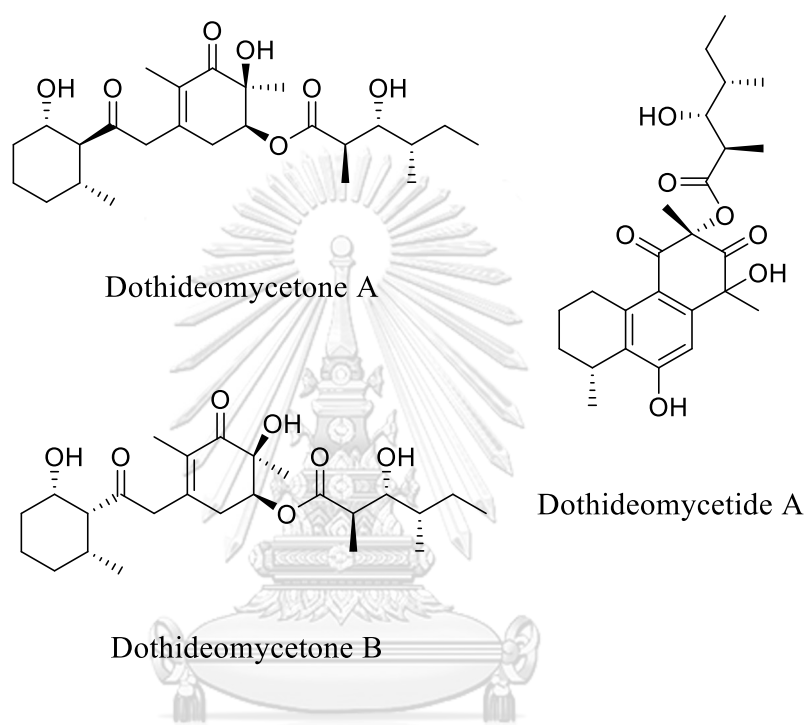


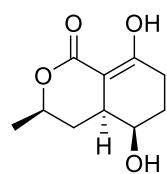
Figure 8 Chemical structures of compounds isolated from *Dothideomycete* sp.

Dothideomycetone A (Figure 8) exhibited cytotoxic activities against MOLT-3 (acute lymphoblastic leukemia) cancer cell line with IC_{50} value of 24 $\mu\text{g/mL}$ while dothideomycetide A exhibited cytotoxic activity against HuCCA-1, A549, HepG2, and MOLT-3 cell lines with IC_{50} values of 33, 36, 35, and 15 $\mu\text{g/mL}$, respectively. Moreover dothideomycetide A showed antibacterial activity against *Staphylococcus aureus* ATCC 25923 and ATCC 33591 (methicillin resistant strain) with respective MIC values of 128 and 256 $\mu\text{g/mL}$ ⁵⁴.

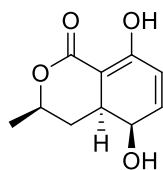
Beside bioactive compounds from marine and endophytic fungi mentioned above, termite associated fungi are one of the most interesting sources for the discovery of novel bioactive compounds. The association between hosts and internalized microbial symbiosis is very interesting. The most diverse communities are found in host digestive tract where microbial symbiosis plays important roles for hosts including digestion, immune system and production of vitamins and cofactors and the production of some compounds or antibiotics against host antagonists^{48, 67, 68, 69}. Furthermore, these microbial networks also involve the balance within termite communities such as the cleanliness of termite nest. This symbiotic association could lead to the discovery of novel bioactive compounds from termite-associated fungi.

In 2020, Xu *et. al.* recently reported bioactive compounds, namely, [5-hydroxyramulosin, biatriosporin M and 1-(2,5-Dihydroxyphenyl)-3-hydroxybutan-1-one isolated from termite-associated fungi⁷⁰. Chang and group also revealed the six new eremophilane-type sesquiterpenes, namely, nigriterpenes A-F and a new phenolic compound, namely, 2-hydroxymethyl-3-pentylphenol from the termite-associated fungus *Xylaria nigripes* in 2017⁷¹.

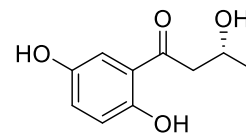
Termite-associated fungus *Xylaria fimbriata* also produced seven new isoprenyl phenolic ethers, namely, fimbriethers A-G⁷² (Figure 9). Moreover, 4,8-dihydroxy-3,4-dihyronaphthalen-1(2*H*)-one was produced from the termite-associated fungus *Xylaria escharoidea*⁷³.



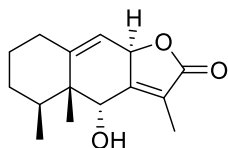
5-Hydroxyramulosin



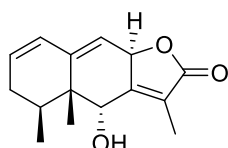
Biatriosporin M



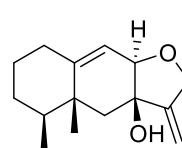
1-(2,5-Dihydroxyphenyl)-3-hydroxybutan-1-one



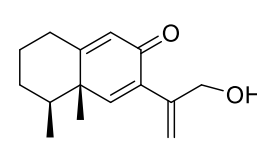
Nigriterpene A



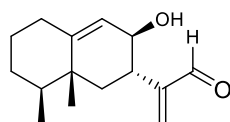
Nigriterpene B



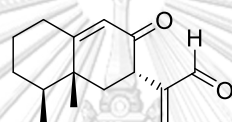
Nigriterpene C



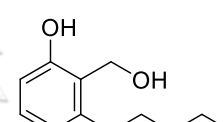
Nigriterpene D



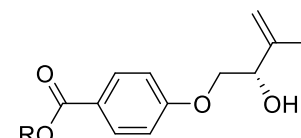
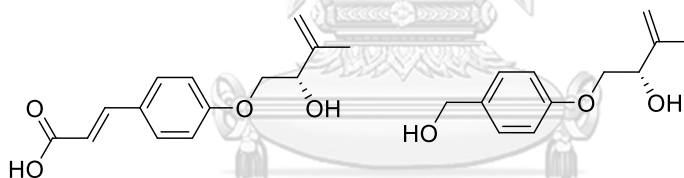
Nigriterpene E



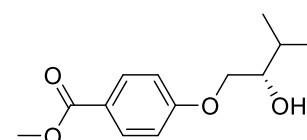
Nigriterpene F



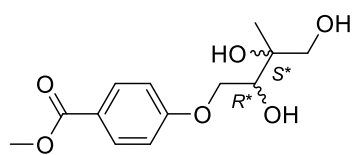
2-Hydroxymethyl-3-pentylphenol

Fimbriether A, R=H
Fimbriether B, R=CH₃

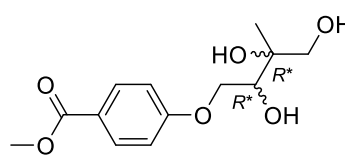
Fimbriether C Fimbriether D



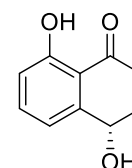
Fimbriether E



Fimbriether F



Fimbriether G



4,8-Dihydroxy-3,4-dihydronaphthalen-1(2H)-one

Figure 9 Chemical structures of compounds isolated from termite-associated fungi

In 2020, Xu et. al. reported that 5-hydroxyramulosin and biatriosporin M (Figure 9) isolated from termite-associated fungi exhibited antimicrobial and antifungal activities against *E. coli*, *B. subtilis*, *S. aureus* and *C. albicans* with the inhibition zone diameter of 13.67, 12.17, 11.33 and 14.33 mm, respectively⁷⁰. The compound, 1-(2,5-dihydroxyphenyl)-3-hydroxybutan-1-one (Figure 9), was found active against *B. subtilis* and *S. aureus* with the inhibition zone diameter of 8.32 and 9.13 mm, respectively⁷⁰.

Nigriterpene C (Figure 9) from termite-associated fungus *Xylaria nigripes* inhibited nitric oxide (NO) production, inducible nitric oxide synthase (iNOS) and cyclooxygenase-2 expression (COX-2) with the IC₅₀ value of 21.7±4.9, 8.1±2.3 and 16.6±5.5 µM, respectively⁷¹. Fimbriethers A-G (Figure 9) inhibited NO production in lipopolysaccharide (LPS)-induced murine macrophage RAW 264.7 cells with the percentage inhibition of 4.6±2.0, 31.3±1.3, 7.7±5.9, 7.3±2.8, 38.9±0.1, 6.0±3.9 and 49.7±0.5, respectively. Interestingly, fimbriethers A-G inhibited NO production without significant cytotoxicity as observed in percentage of cell viability, and every compound exhibited more than 90% of cell viability⁷².

Moreover, 4,8-dihydroxy-3,4-dihydroxynaphthalen-1(2H)-one (Figure 9) produced by the termite-associated fungus *Xylaria escharoidea* exhibited antifungal and antibacterial activities against *C. albicans*, *P. aeruginosa*, *S. aureus* and *B. subtilis* with the inhibition zone diameter of 15.3±0.1, 15.5±0.05, 16.5±0.05 and 16.6±0.05, respectively⁷³.

From the literature reviews, it can be noted that there were many bioactive compounds isolated from termite-associated fungi. The diversity of secondary metabolites production could obtain from termite communities. Beside the novel compounds from termite-associated fungi, scientists have also paid the attention on termite-associated bacteria^{48, 74, 75, 76, 77}. Secondary metabolites isolated from fungi exhibited many biological activities such as antioxidant, anticancer, antifungal, anti-leishmanial, and anti-inflammatory activities^{66, 78}.

Taxol, a well-known anticancer drug was originally derived from barks of the Pacific yew, *Taxus brevifolia*, but Taxol in the present can be produced from many strains of fungi^{79, 80}. These data support that bioactive compounds or medical leads producing from fungi are important chemicals, and fungi are the alternative sources of bioactive compounds.



Chapter III

Materials and methods

3.1 General experiment method

The ^1H , ^{13}C , DEPT, HSQC, HMBC, COSY, and NOESY NMR spectra were obtained from a Bruker Advance 400 MHz (^1H at 400 MHz, ^{13}C at 100 MHz), or Bruker Advance 600 (^1H at 600 MHz, ^{13}C at 150 MHz). HRMS data were obtained from a Bruker micro TOF mass spectrometer. UV spectra were recorded on a Shimadzu UV-1700 PharmaSpect UV-Vis spectrophotometer. IR spectra were obtained from a Perkin Elmer Spectrum One spectrophotometer using a Universal Attenuated Total Reflectance (UATR) technique. High performance liquid chromatography (HPLC) was carried out using Waters e2695 and Waters 1525 separation modules coupled with Waters 2998 photodiode array detector. Column chromatography was performed on Sephadex LH-20 (GE Health Care Bio-Science AB) or silica gel 60 (Merck Code No. 7734). Optical rotations were measured on a JASCO P-1020 polarimeter. Aseptic technique was performed on BSL-2 biosafety cabinet (SafeFAST Classic model). Shaking cultivation of microorganisms was carried out using shaker incubator (Vision). All cultures were sterilized using autoclave (HIRAYAMA model).

3.2 Chemicals

All solvents used in this experiment were distilled using commercial grade solvents, and spectral grade solvents were used for spectroscopic analysis. Valproic acid is pharmaceutical grade from SIGMA-ALDRICH, Catalog number: PHR1061-1G. Polysorbate 80, ammonium citrate, sodium acetate, magnesium sulfate, manganese sulfate, dipotassium phosphate were purchased from SIGMA-ALDRICH

3.3 Material and methodology in the study of effects of VPA on the biosynthesis of fatty acids and polyketides in microorganisms

3.3.1 Materials for the preparation of culture medium

- Proteose Peptone No.3
- Beef extract
- Yeast extract
- Dextrose
- Glucose
- Malt extract
- Potato dextrose broth
- Fresh tubers of potato from Foodland, IT square, Bangkok
- Sea water collected from Bangsean, Chonburi

3.3.2 Microorganisms used in the study

Microorganisms used in this study were received from the Culture Collection of Thailand Bioresource Research Center (TBRC), Thailand, except that *Trichoderma reesei* and *Dothideomycete* sp. are the fungi available in our laboratory.

Table 1 Lists of microorganisms used in this research

Microorganism strain	Purpose of use
<i>Trichoderma reesei</i>	Investigation of secondary metabolite production and the study of effects of VPA on fatty acid biosynthesis in fungi
<i>Dothideomycete</i> sp.	Study of effects of VPA on polyketide biosynthesis in fungi
<i>Pediococcus acidilactici</i> TBRC 7580	Study of effects of VPA on fatty acid biosynthesis in bacteria
<i>Bacillus amyloliquefaciens</i> TBRC 293	Study of effects of VPA on fatty acid biosynthesis in bacteria
<i>Acetobacter cerevisiae</i> TBRC 6687	Study of effects of VPA on fatty acid biosynthesis in bacteria
<i>Fusarium oxysporum</i> TBRC 4265	Study of effects of VPA on fatty acid biosynthesis in fungi
<i>Aspergillus aculeatus</i> TBRC 2535	Study of effects of VPA on fatty acid biosynthesis in fungi
<i>Xylaria globosa</i> TBRC 6767	Study of effects of VPA on fatty acid biosynthesis in fungi
<i>Cordyceps militaris</i> TBRC 6930	Study of effects of VPA on fatty acid biosynthesis in fungi
<i>Aureobasidium pullulans</i> TBRC 4786	Study of effects of VPA on fatty acid biosynthesis in fungi
<i>Phialemonium</i> sp. TBRC 4709	Study of effects of VPA on fatty acid biosynthesis in fungi
<i>Cladosporium</i> sp. TBRC 4134	Study of effects of VPA on fatty acid biosynthesis in fungi
<i>Penicillium shearii</i> TBRC 2865	Study of effects of VPA on fatty acid biosynthesis in fungi
<i>Aspergillus flavipes</i> BCC 28681	Study of effects of VPA on fatty acid biosynthesis in fungi
<i>Saccharomyces cerevisiae</i> TBRC 1563	Study of effects of VPA on fatty acid biosynthesis in yeast
<i>Candida utilis</i> TBRC 360	Study of effects of VPA on fatty acid biosynthesis in yeast
<i>Lachancea thermotolerans</i> TBRC 4347	Study of effects of VPA on fatty acid biosynthesis in yeast
<i>Candida butyri</i> TBRC 221	Study of effects of VPA on fatty acid biosynthesis in yeast
<i>Candida catenulata</i> TBRC 223	Study of effects of VPA on fatty acid biosynthesis in yeast
<i>Saccharomyces ludwigii</i> TBRC 2149	Study of effects of VPA on fatty acid biosynthesis in yeast

3.3.3. Cultivation of microorganisms

3.3.3.1. Cultivation of fungi

Fungus *Fusarium oxysporum* TBRC 4265, *Aspergillus aculeatus* TBRC 2535, *Xylaria globosa* TBRC 6767, *Cordyceps militaris* TBRC 6930, *Aureobasidium pullulans* TBRC 4786, *Phialemonium* sp. TBRC 4709, *Cladosporium* sp. TBRC 4134, *Penicillium shearii* TBRC 2865 and *Aspergillus flavipes* BCC 28681 were cultivated in 250 mL of potato dextrose broth (PDB) medium (Supplementary table A1) supplemented with or without 100 μ M of VPA. The cultivation was performed in three replications for each condition, and was incubated with shaking condition at 30 °C for 21 days, except that the fungus *Cordyceps militaris* TBRC 6930 was cultivated at 25 °C for 21 days. Noted that the fungus *Fusarium oxysporum* TBRC 4265 is a marine fungus, and it was cultivated in PDB medium prepared from seawater instead of deionized water.

The endophytic fungus *Dothideomycete* sp. was cultivated in 250 mL of potato dextrose broth (PDB) medium supplemented with or without 100 μ M of VPA, and was incubated at 30 °C for 30 days under static condition. The fungus *Trichoderma reesei* was cultivated in the same manner as that of the endophytic fungus *Dothideomycete* sp., except that seawater was used instead of deionized water for the preparation of culture medium.

3.3.3.2 Cultivation of yeast

All yeast strains were grown in 250 mL of YM medium (Supplementary table A2) supplemented with or without 100 μ M of VPA, and three replications for each condition were performed. The cultivation was incubated at 30 °C for 14 days.

3.3.3.3 Cultivation of bacteria

The bacterium *Pediococcus acidilactici* was grown in MRS medium (Supplementary table A3), while *Bacillus amyloliquefaciens* was cultivated in NA medium (Supplementary table A4). *Acetobacter cerevisiae* was grown in GPY medium (Supplementary table A5). All bacterial strains were cultivated in 250 mL of culture medium supplemented with or without 100 μ M of VPA, and three replications for each condition were carried out. *Pediococcus acidilactici* was incubated at 30 °C for 5 days under anaerobic condition, whereas the bacterial strains *Bacillus amyloliquefaciens* and *Acetobacter cerevisiae* were incubated with shaking condition at 30 °C for 5 days. Cells of filamentous fungi were separated by filtration using Whatman paper, whereas cells of yeast and bacteria were collected by centrifuge at 8000 rpm for 25 minutes. Cells of microorganisms were dried by freeze drying, and lipid in dried cell was extracted twice by hexane.

3.3.4 Extraction of lipid and analysis of fatty acids

Dried cells of microorganisms were extracted twice by maceration in hexane overnight at room temperature. Crude fat extract was individually transesterified with 4% sulphuric acid in methanol. A fat extract was dissolved in methanol containing 4% of sulphuric acid, and the mixture was heated at 90 °C for 1h. Nonadecanoic acid (C19:0) was used as an internal standard. The esterified products were analyzed by gas chromatography (GC) technique using a 30 m x 0.25 mm OmegawaxTM 250 fused silica capillary column. The GC instrument was equipped with an automatic sampler and flame ionization detector (FID).

The injector and detector temperatures were kept at 250 °C and 260 °C, respectively, and helium was used as a carrier gas at a linear velocity of 30 cm/s. The initial temperature for GC column at 200 °C was held for 10 min, and then increased at 20°C/min to 230 °C, where it was held for 17 min. Individual fatty acid esters were identified based on the retention times relative to fatty acid methyl ester standards (Supelco 37 Component FAME Mix as the standard for methyl ester).

3.3.5 Isolation of mevalonolactone (Compound **1**)

A crude broth extract (198 mg) of the fungus *Trichoderma reesei* was separated by Sephadex LH-20 column chromatography (CC) (size 2 x 132 cm), eluted with methanol, yielding twelve fractions (F1-F12). A fraction 8 (79 mg) was further separated by Sephadex LH-20 column chromatography (CC) (size 1.5 x 126 cm), eluted with methanol to give nine fractions (F81-F89). A fraction F81 was purified by C18 reversed phase HPLC, eluted with a solvent system of MeOH:H₂O (60:40), to give mevalonolactone (**1**) (11.7 mg).

3.3.6 Isolation of compound **2-6**

Crude broth extract (107.6 mg) of the fungus *Dothideomycete* sp. was separated by C18 reversed phase HPLC using MeOH:H₂O (60:40) as a mobile phase to yield compounds **1** (9.2 mg), **4** (4.8 mg) and **5** (5.7 mg), respectively. However, compounds **2** and **3** were obtained as a mixture when it was separated by MeOH:H₂O (60:40) system, this mixture was further purified by HPLC using MeOH:H₂O (40:60) as a mobile phase to yield compound **2** (12.8 mg) and compound **3** (7.1 mg).

3.3.7 Structure elucidation of fungal metabolites by spectroscopic techniques

Structure elucidation of the isolated compounds were performed using ^1H , ^{13}C and 2D NMR spectroscopic data obtained from Bruker AM400 (^1H at 400 MHz, ^{13}C at 100 MHz), or Bruker Avance (^1H at 600 MHz, ^{13}C at 150 MHz). Deuterated CDCl_3 was used as an NMR solvent. HRMS data obtained from a Bruker micro TOF mass spectrometer were also used for structure elucidation.

3.3.8 Antibacterial activity

Bacterial samples were streaked on NA plate and incubated for 24 h. Then single colonies of bacteria were dissolved in 0.85% saline solution. Bacterial samples were prepared in the same turbidity as 0.5 McFarland standard using UV spectroscopy in the measurement. Each strain of bacteria sample was spread on NA plate. Drugs and isolated compounds were prepared at the concentration of 10 mg/100 μL . Each solution was dropped on disc 10 μL and put on NA plate which it was then incubated at 37 °C for 20 h. and measured the clear zone.

3.3.9 Statistical analysis method

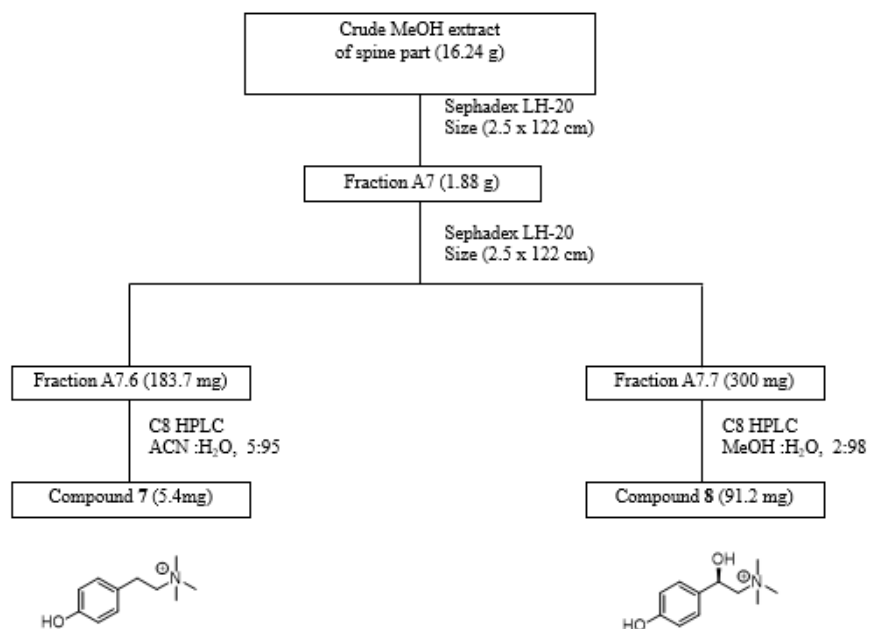
Statistical analysis of all data, three replications per each condition of an individual microorganism, was performed using the IBM SPSS Statistics 22 software, Independent-Samples T test method. Differences of fatty acid content between each group (control without VPA or with 100 μM of VPA) were determined by two-tailed *t* test, and data are reported as mean \pm s.d. with the significance set at $p < 0.01$ or at $p < 0.05$.

3.4 Material and methodology for the study of bioactive compounds from *Feroniella lucida* (Scheff.) Swingle

3.4.1 Plant extraction and isolation

Plant materials were collected from Lam Luk Ka District, Pathumthani Province, Thailand, in December 2016. Air-dried plants were ground into powder form. The powdered spine (0.45 kg), leaf (1.5 kg), and stem (5.2 kg) were soaked in CH₂Cl₂ (2 times) at room temperature to yield crude extracts of 3.92 g (spine), 34.37 g (leaf) and 33.59 g (stem). Plant materials were further soaked in MeOH (2 times) at room temperature to yield a crude extract of 16.24 g (spine), 182.62 g (leaf) and 177.19 g (stem).

Crude MeOH extract from spine part was separated by Sephadex LH-20 (2.5x122 cm), eluted with MeOH to give twenty three fractions (A1-A23). Fraction A7 (1881 mg) was separated by Sephadex LH-20 (2.5x122 cm), eluted with MeOH to give 15 fractions (A7.1-A7.15). Fraction A7.6 (187.3 mg) was further separated by C8 HPLC with a solvent system of acetonitrile:H₂O (5:95) to give compound **7** (5.4 mg). Fraction A7.7 (300 mg) was further separated by C8 HPLC with a solvent system of MeOH:H₂O (2:98) to give compound **8** (91.2 mg) as shown in scheme **1**.



Scheme 1 The isolation procedure of a crude MeOH extract of spine part of *F. lucida*

3.4.2 Investigation of chemical constituents and biological evaluation of plant extracts

Pure compounds were characterized by spectroscopic techniques including NMR spectroscopy, mass spectrometry and IR spectroscopy. Structure elucidations of the isolated compounds were performed using ¹H, ¹³C and 2D NMR spectroscopic data obtained from a Bruker Advance 400 MHz (¹H at 400 MHz, ¹³C at 100 MHz), or Bruker Advance 600 (¹H at 600 MHz, ¹³C at 150 MHz). Deuterated CDCl₃ and acetone-d₆ were used as NMR solvents.

The isolated compounds were examined for their biological activities including cytotoxic, cancer chemoprevention and anti-bacterial activities. Cytotoxic activities were evaluated against HepG2 (liver hepatocellular carcinoma), MOLT-3 (acute lymphoblastic leukemia), A549 (human lung cancer), HuCCA-1 (human cholangiocarcinoma cell line) and MRC-5 (normal fibroblast cell). Cytotoxic activity for adhesive cell lines including HepG2, A549, and HuCCA-1 cancer cell lines was evaluated with the MTT assay. For non-adhesive cell such as MOLT-3 cell line, the cytotoxicity was assessed using the XTT assay⁸¹. Etoposide and doxorubicin were used as the reference drugs.

Inhibition of superoxide anion radical formation by xanthine/ xanthine oxidase (XXO assay) was performed following the previous work⁸². Superoxide dismutase was used as a control. Inhibition of 12-O-tetradecanoylphorbol-13-acetate (TPA)- induced superoxide anion radical generation in differentiated HL-60 cells (HL-60 assay) was evaluated. TPA-induced superoxide anion radical formation in differentiated HL-60 human promyelocytic leukemia cells, was performed by photometric determination of cytochrome c reduction, following the method of previous work⁸². Superoxide dismutase was used as a positive control.

Measurement of oxygen radical absorbance capacity (ORAC) was determined by a method modified from previous work⁸². Antioxidant potential of the test compounds (IM) was compared with that of 6-hydroxy-2,5,7,8-tetramethylchromane-2-carboxylic acid (Trolox), a water soluble vitamin E analog. Results were expressed as ORAC units, where 1 ORAC unit equals the net protection of β -phycoerythrin produced by IM of Trolox. Aromatase inhibitory assay (AIA assay) was performed following the previous work⁸³ by using CYP19/methoxy-4-trifluoromethyl-coumarin (MFC) high throughput inhibition screening kit (BD Biosciences, Woburn MA, USA).

The isolated compounds from *F. lucida* were also tested for antibacterial activity; bacterial samples were streaked on nutrient agar plate and incubated for 24 h. Single colonies of bacteria were dissolved in 0.85% saline solution. Bacterial samples were prepared in the same turbidity as 0.5 McFarland standard using UV spectroscopy in the measurement. Then each strain of bacteria was spread on nutrient agar plate and drugs and isolated compounds were prepared at the concentration of 10 mg/100 μ L. Each sample was dropped on disc 10 μ L and put on nutrient agar plate, and incubated at 37 $^{\circ}$ C for 20 h. The clear zone was measured.

3.5 Termite-associated fungus ISFB10 (unidentified)

3.5.1 Collection and isolation of fungi

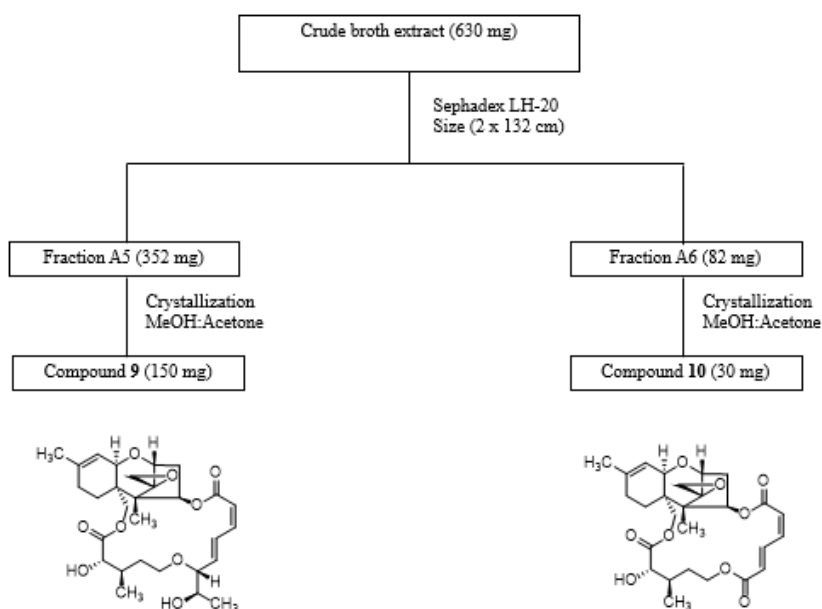
Termite was collected from Lam Luk Ka District, Pathumthani Province, Thailand, in May 2018. Outer surface disinfection was performed by soaking sample in 5% sodium hypochlorite, then rinsed with distilled water and further soaked in 70% ethanol, and samples were then rinsed with distilled water. Termite samples were crushed in order to investigate internal microorganisms, especially a digestive tract. Then, serial dilution was performed and samples from each dilution were poured on PDA-RO containing antibacterial agent. Fungi grown on this PDA-RO were isolated until obtaining of pure culture. Each pure culture was preliminary screened for the metabolite production by cultivating each fungus in a flask containing 50 mL of PDB culture media. Broth part was extracted by EtOAc and analyzed by 1 H NMR spectrum. Termite-associated fungus ISFB10 used in this research was chosen based on interesting metabolite profile as indicated by 1 H NMR spectrum.

3.5.2 Fungal cultivation, extraction and isolation

Initially, termite associated fungus ISFB10 was sub-cultured on PDA-RO and cultivated for 7 days, and it was then inoculated aseptically in 1000 mL Erlenmeyer flask, each containing 250 mL of potato dextrose broth prepared from fresh tuber of potatoes (PDB).

A total volume was 3 L of culture. Termite-associated fungus ISFB10 was cultivated at room temperature under static condition for 4 weeks. Fermentation broth and mycelia were separated by filtration. Cultured broth was extracted with an equal volume of EtOAc (3 times) to give 630 mg of a crude broth extract. Mycelia were soaked in MeOH (2 times) followed by CH₂Cl₂ (2 times), and extracts from these two parts were combined and then extracted with hexane to remove fatty acid. An aqueous part was further extracted with EtOAc (3 times) to give 326 mg of a crude mycelial extract.

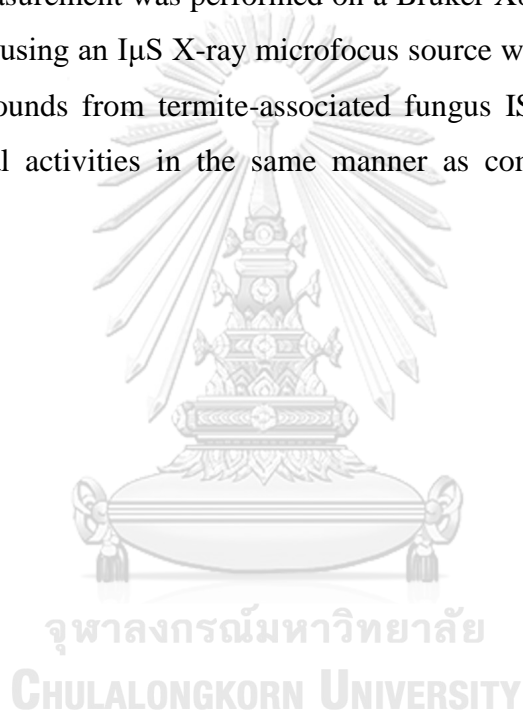
Crude broth extract (630 mg) was separated by Sephadex LH-20 (CC) (size 2 x 132 cm), eluted with methanol, yielding seventeen fractions (A1-A17). A fraction A5 (352 mg) was re-crystallized from a solvent mixture of MeOH:acetone to give roridin A, compound **9** (150 mg). A fraction A6 (82 mg) was also purified by re-crystallization from a solvent mixture of MeOH:acetone to give verrucarin A, compound **10** (30 mg) as shown in scheme 2.



Scheme 2 The isolation procedure of a crude broth extract from the termite-associated fungus ISFB10 (unidentified)

3.5.3 Investigation of chemical constituents and biological evaluation of fungal extracts

Pure compounds were characterized by analysis of spectroscopic data obtained from NMR spectroscopy, mass spectrometry and IR spectroscopy. Structure elucidation of the isolated compounds were performed using ^1H , ^{13}C and 2D NMR spectroscopic data obtained from Bruker AM400 (^1H at 400 MHz, ^{13}C at 100 MHz), or Bruker Avance (^1H at 600 MHz, ^{13}C at 150 MHz). Deuterated CDCl_3 and acetone- d_6 were used as NMR solvents. Single-crystal X-ray diffraction measurement was performed on a Bruker X8 Prospector KAPPA CCD diffractometer using an $\text{I}\mu\text{S}$ X-ray microfocus source with multilayer mirrors. The isolated compounds from termite-associated fungus ISFB10 were evaluated for their biological activities in the same manner as compounds isolated from *F. lucida*.



Chapter IV

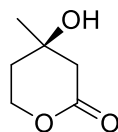
Results and discussion

4.1 Effects of VPA on biosynthesis of fatty acids and polyketides

4.1.1 Effect of VPA on fatty acid biosynthesis

Valproic acid, histone deacetylase inhibitor, could alter the biosynthesis of fungal metabolites with enhanced chemical diversity, so VPA treatment with microorganisms is an effective strategy for controlling gene expression of fungal biosynthetic pathway¹⁵. Previous works have revealed the effectiveness of epigenetic modifiers for the production of new secondary metabolites in microorganisms, for example, proteasome inhibitor^{16, 17} and histone deacetylase inhibitor^{18, 19, 20}; this technique is known as “one strain many compound” (OSMAC) approach. Previous work has reported that VPA was found to enhance ten-fold production of a fungal alkaloid, fumiquinazoline C²¹, and could induce new secondary metabolite production in endophytic fungus²² and enhance antimicrobial activity of the fungal metabolites^{23, 24}.

Initially, our work preliminary investigated the effect of VPA on the metabolite production of marine-derived fungus *Trichoderma reesei*, which produced mevalonolactone (compound **1**) as a secondary metabolite (Figure **10**). So the aim of this work is to use VPA, histone deacetylase inhibitor, to diversify secondary metabolites production through mevalonate biosynthesis pathway, which is the common pathway of terpene and steroid production. Previous works used VPA concentration of 50 μM , 60 μM , 100 μM and 500 μM to study effect of VPA on the metabolite profile^{21, 22, 23, 24}. In this work we initially fed VPA in the concentration of 100 μM and 300 μM , however the growth of fungus was inhibited when VPA at the concentration of 300 μM or higher was used in the cultivation. Therefore, VPA at the concentration of 100 μM was performed in this work. Unfortunately, we could not obtain new terpenes and steroids from VPA treatment with the fungus *Trichoderma reesei*, but VPA interestingly showed the effect on fatty acid profiles as observed from ¹H NMR spectrum of a crude cell extract.



(R)-(-)-Mevalonolactone (1)

Figure 10 Structures (R)-(-)-Mevalonolactone isolated from the marine-derived fungus *Trichoderma reesei*

Then liquid extract of the fungus *T. reesei* was subjected to gas chromatography technique for analysis of fatty acid profile, and the result revealed that VPA significantly induced the production of palmitic acid (C16:0) from 9.39% in a control (without VPA) to 19.89% (2.11 times increase) in the fungus treated with VPA, while oleic acid (C18:1) was significantly reduced from 71.51% in a control to 57.19% (1.25 times decrease), as shown in Table 2. The amount of palmitoleic acid (C16:1), stearic acid (C18:0), linoleic acid (C18:2), and α -linolenic acid (C18:3) of a control were relatively the same as that in the VPA treated fungus. Total fatty acid production of a control (65.26%) was higher than the fungus treated with VPA (49.99%), as shown in Table 2.

Table 2 Effect of VPA (100 μ M) on fatty acid profile of the fungus *Trichoderma reesei*

Condition	Fatty acid content (%), mean \pm s.d. (n=3)						
	C16:0	C16:1	C18:0	C18:1	C18:2	C18:3	Total fatty acid (%)
Control (without VPA)	9.39 \pm 1.42*	0.37 \pm 0.1 1	3.47 \pm 0.58 *	71.51 \pm 6.24 *	8.62 \pm 2.0 4	0.06 \pm 0.0 2	65.26 \pm 6.52 *
VPA, 100 μ M	19.89 \pm 2.96 *	0.46 \pm 0.1 1	4.73 \pm 0.63 *	57.19 \pm 5.41 *	7.22 \pm 1.4 1	0.05 \pm 0.0 2	49.99 \pm 5.69 *

* $p \leq 0.05$ was selected as the minimum criterion for significance.

* $p \leq 0.01$ was selected as the minimum criterion for significance.

As mentioned above, it was reported in previous work that VPA caused side effect related to fatty acid metabolism in patients, for example, the influence on lipid metabolism². VPA interfered with mitochondrial β -oxidation, and fatty acid β -oxidation enzyme (FAO) and their cofactors, and thus causing serious inborn errors of metabolism after VPA treatment⁴, and inducing hepatotoxicity and weight gain for patients under VPA treatment^{5, 49}. Therefore, the interferences of VPA on fatty acid metabolism in patients and our preliminary data of VPA on the fatty acid profile of the fungus *Trichoderma reesei* (Table 2) inspired us to study the effect of VPA on fatty acid profile in other microorganisms including representative gut microbiome, microorganisms used in food and beverage productions, and microorganisms from marine, soil, plant and insect ecosystem.

Microorganisms used in this work were from the culture collection of Thailand Bioresource Research Center (TBRC), Thailand. The first group of microorganisms is fungi including *Fusarium oxysporum* TBRC 4265 (marine fungi), *Aspergillus aculeatus* TBRC 2535 (soil fungi), *Xylaria globosa* TBRC 6767 (endophytic fungi), *Cordyceps militaris* TBRC 6930 (entomopathogenic/ insect fungi), and *Aureobasidium pullulans* TBRC 4786 (epiphytic of endophytic fungi of plants). Each strain of fungus was cultivated in PDB under shaking condition in the presence (100 μ M) or absence (control) of VPA, and fatty acid profiles of each culture are in Table 3. The marine fungus *Fusarium oxysporum* TBRC 4265 produced ten fatty acids including palmitic acid (C16:0) for 29.40%, palmitoleic acid (C16:1) for 0.71%, stearic acid (C18:0) for 15.09%, oleic acid (C18:1) for 32.93%, linoleic acid (C18:2) for 19.94%, α -linolenic acid (C18:3) for 0.44%, arachidic acid (C20:0) for 0.65%, docosanoic acid (C22:0) for 0.43%, erucic acid (C22:1) for 0.09%, and lignoceric acid (C24:0) for 0.33%. After VPA treatment (100 μ M) with the marine fungus *F. oxysporum* TBRC 4265, it was found that the fungus completely stopped the production of palmitoleic acid (C16:1), α -linolenic acid (C18:3), arachidic acid (C20:0), and lignoceric acid (C24:0). However, VPA significantly enhanced the production of some fatty acids, for example, palmitic acid (C16:0) from 29.40% (control) to 51.79% (1.76 times of the control), docosanoic acid (C22:0) from 0.43% (control) to 0.97% (2.25 times of the control), and erucic acid (C22:1) from 0.09%

(control) to 1.44% (16.0 times of the control). On the other hand, VPA reduced the production of linoleic acid (C18:2) from 19.94% (control) to 5.27% (3.78 times less than the control), as shown in Table 3.

The soil fungus *Aspergillus aculeatus* TBRC 2535 did not produce α -linolenic acid (C18:3) when fungus was cultivated in the control, whereas it was enhanced to produce α -linolenic acid (C18:3) after feeding with 100 μ M of VPA. VPA also enhanced the production of linoleic acid (C18:2) from 2.80% (control) to 27.20% (9.71 time of the control) and lignoceric acid (C24:0) from 6.88% (control) to 11.30% (1.64 times of the control).

In contrast, the reduction of palmitic acid (C16:0) from 41.52% (control) to 22.01% (1.88 times less than the control), palmitoleic acid (C16:1) from 0.28% (control) to 0.14% (2.00 times less than the control), stearic acid (C18:0) from 17.29% (control) to 8.81% (1.96 times less than the control), and arachidic acid (C20:0) from 0.84% (control) to 0.24% (3.5 times less than the control) was observed in the VPA treated culture of *A. aculeatus* TBRC 2535, as shown in Table 3. The production of arachidic acid (C20:0) in the endophytic fungus *Xylaria globosa* TBRC 6767 was completely inhibited when this fungus was treated with VPA. Arachidic acid (C20:0) of 0.39% was found in the control, whereas none was found in VPA treated culture (Table 3). VPA also inhibited the production of lignoceric acid (C24:0) in the insect fungus *Cordyceps militaris* TBRC 6930; 0.28% of lignoceric acid (C24:0) was produced in the control, but none was detected in the fungus treated culture (Table 3).

In contrast, VPA did not have significant effects on fatty acid profile of the fungus *Aureobasidium pullulans* TBRC 4786, an epiphyte or endophyte of plants, as shown in Table 3. For the total fatty acid content, VPA reduced the total fatty acid production in *F. oxysporum* TBRC 4265 from 45.33% (control) to 9.85% (4.60 times less than the control), whereas the total fatty acid of *A. aculeatus* TBRC 2535 and *A. pullulans* TBRC 4786 were increased from 12.73% (control) to 29.13 % (2.28 times of the control) and from 27.62% (control) to 40.16% (1.45 times of the control), respectively (Table 3).

VPA did not give significant effects on the total fatty acid of *X. globosa* TBRC 6767 and *C. militaris* TBRC 6930. From the result, it indicated that VPA could inhibit or enhance the production of some fatty acids in fungi.

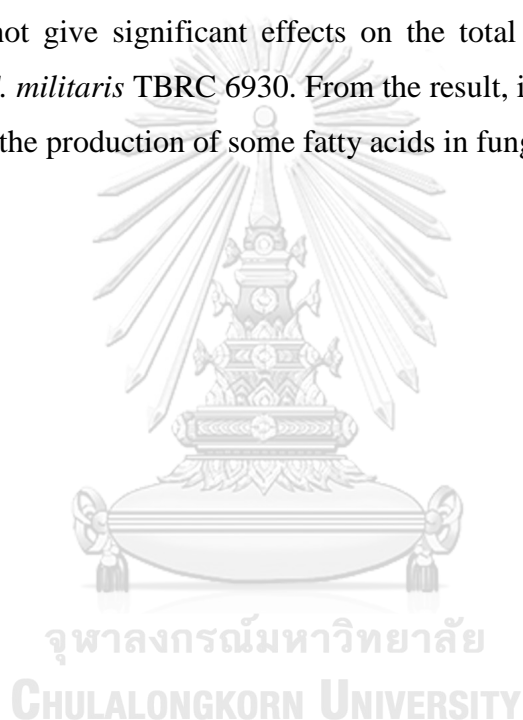


Table 3 Effect of VPA (100 μ M) on fatty acid profile of fungi

Fungi, condition	Fatty acid content (%), mean \pm s.d. (n = 3)													Total fatty acid (%)
	C16:0	C16:1	C18:0	C18:1	C18:2	C18:3	C20:0	C22:0	C22:1	C24:0				
<i>Fusarium oxysporum</i> , control (without VPA)	29.40 \pm 4.91*	0.71 \pm 0.06*	15.09 \pm 3.82	32.93 \pm 4.39*	19.94 \pm 3.45*	0.44 \pm 0.05*	0.65 \pm 0.18*	0.43 \pm 0.11*	0.09 \pm 0.02*	0.33 \pm 0.10*			45.33 \pm 4.84*	
<i>F. oxysporum</i> , 100 μ M of VPA	51.79 \pm 5.14*	0.00*	20.29 \pm 3.29	20.24 \pm 2.17*	5.27 \pm 0.60*	0.00*	0.00*	0.97 \pm 0.09*	1.44 \pm 0.07*	0.00*			9.85 \pm 2.53*	
<i>Aspergillus aculeatus</i> , control (without VPA)	41.52 \pm 1.61*	0.28 \pm 0.03*	17.29 \pm 2.11*	29.46 \pm 3.93	2.80 \pm 0.13*	0.00*	0.84 \pm 0.13*	0.93 \pm 0.08*	0.00	6.88 \pm 0.54*			12.73 \pm 1.56*	
<i>A. aculeatus</i> , 100 μ M of VPA	22.01 \pm 1.85*	0.14 \pm 0.04*	8.81 \pm 1.16*	27.83 \pm 5.33	27.20 \pm 4.36*	1.27 \pm 0.10*	0.24 \pm 0.01*	1.20 \pm 0.08*	0.00	11.30 \pm 1.55*			29.13 \pm 2.49*	
<i>Xylaria globosa</i> , control (without VPA)	20.98 \pm 1.83	0.00	21.57 \pm 2.88	33.77 \pm 1.61*	21.31 \pm 3.46	0.00	0.39 \pm 0.05*	0.00	0.00	1.98 \pm 0.14*			47.08 \pm 6.00	
<i>X. globosa</i> , 100 μ M of VPA	20.82 \pm 4.50	0.00	22.36 \pm 2.29	30.2 \pm 1.37*	24.08 \pm 3.41	0.00	0.00*	0.00	0.00	2.55 \pm 0.13*			48.67 \pm 8.71	
<i>Cordyceps militaris</i> , control (without VPA)	36.38 \pm 3.27	0.54 \pm 0.08*	7.84 \pm 0.63	36.94 \pm 1.42*	18.03 \pm 2.60	0.00	0.00	0.00	0.00	0.28 \pm 0.06*			61.55 \pm 2.23	
<i>C. militaris</i> , 100 μ M of VPA	31.85 \pm 4.45	0.74 \pm 0.09*	6.56 \pm 1.03	41.97 \pm 2.45*	18.88 \pm 2.81	0.00	0.00	0.00	0.00	0.00*			58.45 \pm 0.57	
<i>Aureobasidium pullulans</i> , control (without VPA)	29.6 \pm 2.01	0.70 \pm 0.05*	9.05 \pm 0.67*	41.14 \pm 1.17	17.36 \pm 1.39	0.00	0.00	0.00	0.00	2.15 \pm 0.11			27.62 \pm 3.65*	
<i>A. pullulans</i> , 100 μ M of VPA	29.08 \pm 0.70	0.52 \pm 0.05*	11.94 \pm 0.79*	41.29 \pm 0.52	15.08 \pm 0.14	0.00	0.00	0.00	0.00	2.08 \pm 0.24			40.16 \pm 5.01*	

*p \leq 0.05 was selected as the minimum criterion for significance.*p \leq 0.01 was selected as the minimum criterion for significance.

Next, we tried to investigate the effects of VPA on the fatty acid profile of yeast, as shown in Table 4. Three strains of yeast were used as a model; *Saccharomyces cerevisiae* TBRC 1563, *Candida utilis* TBRC 360, and *Lachancea thermotolerans* TBRC 4347, and these strains of yeast are normally used in food and beverage productions. As presented in Table 4, VPA completely stopped the production of α -linolenic acid (C18:3) in the yeast *S. cerevisiae* TBRC 1563 and *C. utilis* TBRC 360; 1.97% and 1.28% of α -linolenic acid (C18:3) were found in the control, respectively, whereas none was found in VPA treated culture. VPA also stopped the production of palmitoleic acid (C16:1) in the yeast *C. utilis* TBRC 360; 0.35% of palmitoleic acid (C16:1) was produced in the control, but none was detected in VPA treated culture. The productions of palmitic acid (C16:0) and stearic acid (C18:0) were increased from 29.03% (control) to 47.16% (1.62 times of the control), and from 6.60% (control) to 10.91% (1.65 times of the control), respectively, after feeding the yeast *C. utilis* TBRC 360 with VPA. In contrast, the decreased levels of oleic acid (C18:1) from 46.89% (control) to 34.21% (1.37 times less than the control) and linoleic acid (C18:2) from 15.86% (control) to 7.72% (2.05 times less than the control) were observed in VPA treated culture of *C. utilis* TBRC 360 (Table 4). Moreover, the decreased level of the total fatty acid from 24.35% (control) to 15.62% (1.55 times less than the control) was observed in VPA treated culture of *C. utilis* TBRC 360 (Table 4). VPA did not have effects on fatty acid profile and the total fatty acid of the yeast *L. thermotolerans* TBRC 4347, as shown in Table 4. Interestingly, previous work has reported that *C. utilis* TBRC 360 was found as gut microbiome in pediatric patients with inflammatory bowel disease ⁸⁴.

Table 4 Effect of VPA (100 μ M) on fatty acid profile of yeast

Yeast, condition	Fatty acid content (%), mean \pm s.d. (n = 3)									
	C16:0	C16:1	C18:0	C18:1	C18:2	C18:3	Total fatty acid (%)			
<i>Saccharomyces cerevisiae</i> , control (without VPA)	15.25 \pm 2.81	27.98 \pm 2.17	7.52 \pm 1.26	39.31 \pm 2.11	7.96 \pm 2.73	1.97 \pm 0.21*	39.68 \pm 6.09			
<i>S. cerevisiae</i> , 100 μ M of VPA	14.80 \pm 1.54	30.42 \pm 4.63	6.37 \pm 1.38	41.13 \pm 2.75	7.28 \pm 1.83	0.00*	41.39 \pm 8.34			
<i>Candida utilis</i> , control (without VPA)	29.03 \pm 3.40*	0.35 \pm 0.09*	6.60 \pm 1.17*	46.89 \pm 4.82*	15.86 \pm 1.50*	1.28 \pm 0.08*	24.35 \pm 2.29*			
<i>C. utilis</i> , 100 μ M of VPA	47.16 \pm 4.31*	0.00*	10.91 \pm 1.85*	34.21 \pm 2.92*	7.72 \pm 0.36*	0.00*	15.62 \pm 1.84*			
<i>Lachancea thermotolerans</i> , control (without VPA)	22.04 \pm 2.89	25.52 \pm 3.07	7.53 \pm 1.52	15.65 \pm 0.84*	27.30 \pm 1.73	1.97 \pm 0.25	39.22 \pm 6.39			
<i>L. thermotolerans</i> , 100 μ M of VPA	22.10 \pm 2.78	24.63 \pm 0.70	7.35 \pm 0.98	19.64 \pm 0.71*	24.65 \pm 3.22	1.64 \pm 0.19	39.29 \pm 2.88			

*p \leq 0.05 was selected as the minimum criterion for significance.

*p \leq 0.01 was selected as the minimum criterion for significance.

Table 5 Effect of VPA (100 μ M) on fatty acid profile of bacteria

Bacteria, condition	Fatty acid content (%), mean \pm s.d. (n = 3)									
	C16:0	C16:1	C18:0	C18:1	C18:2	C20:0	C24:0	Total fatty acid (%)		
<i>Pediococcus acidilactici</i> , control (without VPA)	52.02 \pm 4.34	0.00	39.44 \pm 4.04	0.00	7.00 \pm 0.44*	0.00	1.53 \pm 0.06*	7.92 \pm 0.48*		
<i>P. acidilactici</i> , 100 μ M of VPA	48.52 \pm 1.90	0.00	40.60 \pm 3.14	0.00	10.87 \pm 1.27*	0.00	0.00*	3.24 \pm 0.10*		
<i>Bacillus amyloliquefaciens</i> , control (without VPA)	49.96 \pm 1.35	9.72 \pm 1.14*	30.20 \pm 5.63	0.00	10.12 \pm 1.49	0.00	0.00	5.09 \pm 1.06		
<i>B. amyloliquefaciens</i> , 100 μ M of VPA	49.18 \pm 1.14	4.41 \pm 0.40*	34.12 \pm 4.19	0.00	12.29 \pm 2.16	0.00	0.00	3.35 \pm 0.76		
<i>Acetobacter cerevisiae</i> , control (without VPA)	56.17 \pm 6.30	0.00	37.02 \pm 6.66	0.61 \pm 0.05*	5.76 \pm 1.08	0.43 \pm 0.07*	0.00	8.59 \pm 2.79		
<i>A. cerevisiae</i> , 100 μ M of VPA	60.34 \pm 0.65	0.00	33.27 \pm 1.65	0.00*	6.39 \pm 1.55	0.00*	0.00	5.50 \pm 0.89		

*p \leq 0.01 was selected as the minimum criterion for significance.

The effects of VPA on the fatty acid profile of bacteria were also investigated (Table 5). The bacteria *Pediococcus acidilactici* TBRC 7580, *Bacillus amyloliquefaciens* TBRC 293, and *Acetobacter cerevisiae* TBRC 6687, were used as model bacteria. The bacteria *P. acidilactici* TBRC 7580 and *A. cerevisiae* TBRC 6687 are normally used in fermented dairy products (yoghurt production) and meat (Thai fermented pork sausage or “Naem” in Thai), whereas *B. amyloliquefaciens* TBRC 293 is used in food industry, being a source of α -amylase for the starch hydrolysis. VPA completely inhibited the production of lignoceric acid (C24:0) in the bacterium *P. acidilactici* TBRC 7580; 1.53% of lignoceric acid (C24:0) was produced in the control, while none was produced in the VPA treated culture of *P. acidilactici* TBRC 7580. Moreover, VPA also completely inhibited the production of oleic acid (C18:1) and arachidic acid (C20:0) in the VPA treated culture of *A. cerevisiae* TBRC 6687; 0.61% and 0.43% of oleic acid (C18:1) and arachidic acid (C20:0) were produced in the control, respectively. In addition, decreased level of palmitoleic acid (C16:1) from 9.72% (control) to 4.41% (2.20 times less than the control) was observed in the VPA treated culture of *B. amyloliquefaciens* TBRC 293, as shown in Table 5.

Nowadays, gut microbiome has received attention worldwide^{35, 36}. As mentioned earlier, previous works revealed that there were drug-microbiome interactions, for example, metformin and proton inhibitor drugs interacting with human gut microbiome^{41, 42}. Therefore, we studied the effects of VPA on fatty acid profile of certain representative gut microbiome, e.g., fungi and yeast. Four strains of gut fungi including *Penicillium shearii* TBRC 2865, *Cladosporium sp.* TBRC 4134, *Phialemonium sp.* TBRC 4709, and *Aspergillus flavipes* BCC 28681 were investigated for the effects of VPA on fatty acid profile. The genera *Penicillium*, *Cladosporium*, *Phialemonium*, and *Aspergillus* are the most prevalent fungi in human gut^{85, 86, 87}. VPA could enhance the production of linoleic acid (C18:2) from 12.46% (control) to 23.60% (1.89 times of the control) in the fungus *P. shearii* TBRC 2865, as shown in Table 6, while it reduced the production of palmitic acid (C16:0) from 24.29% (control) to 16.86% (1.44 less than the control), stearic acid (C18:0) from 17.09% (control) to 13.37% (1.28 times less than the control), arachidic acid (C20:0) from 1.65% (control) to 1.08% (1.53 times less than the control), heneicosanoic acid

(C21:0) from 1.61% (control) to 1.02% (1.58 times less than the control), docosanoic acid (C22:0) from 1.30% (control) to 0.67% (1.94 times less than the control), and lignoceric acid (C24:0) from 1.66% (control) to 1.17% (1.42 times less than the control), respectively, in the fungus *P. shearii* TBRC 2865 (Table 6).

The productions of oleic acid (C18:1), arachidic acid (C20:0), and lignoceric acid (C24:0) were increased in the VPA treated culture of *Phialemonium sp.* TBRC 4709, increasing from 43.27% (control) to 57.95% (1.34 of the control), 0.36% (control) to 0.58% (1.61 times of the control), and from 0.61% (control) to 0.83% (1.36 times of the control), respectively, in the VPA treated culture of *Phialemonium sp.* TBRC 4709 (Table 6). In contrast, VPA reduced the production of palmitic acid (C16:0) from 28.73% (control) to 22.16% (1.30 times less than the control), linoleic acid (C18:2) from 14.85% (control) to 7.47% (1.99 times less than the control), and α -linolenic acid (C18:3) from 2.53% (control) to 1.52% (1.66 times less than the control), as shown in Table 6.

The productions of stearic acid (C18:0), α -linolenic acid (C18:3), and lignoceric acid (C24:0) in the fungus *Cladosporium sp.* TBRC 4134 were reduced after feeding the culture with VPA, reducing from 17.62% (control) to 9.90% (1.78 times less than the control), 0.20% (control) to 0.10% (2.00 times less than the control), and from 0.34% (control) to 0.16% (2.13 times less than the control), respectively, but VPA enhanced the production of linoleic acid (C18:2) from 12.55% (control) to 15.20% (1.21 times of the control), arachidic acid (C20:0) from 0.52% (control) to 0.80% (1.54 times of the control), heneicosanoic acid (C21:0) from 0.44% (control) to 0.77% (1.75 times of the control), and docosanoic acid (C22:0) from 0.35% (control) to 0.53% (1.51 times of the control) in the fungus *Cladosporium sp.* TBRC 4134 (Table 6). VPA reduced the production of palmitic acid (C16:0) from 21.30% (control) to 18.34% (1.16 times less than the control), oleic acid (C18:1) from 42.17% (control) to 39.13% (1.08 times less than the control), and linoleic acid (C18:2) from 26.58% (control) to 20.85% (1.27 times less than the control) in VPA treated culture of *A. flavipes* BCC 28681, as shown in Table 6. On the other hand, VPA enhanced the production of stearic acid (C18:0) from 8.70% (control) to 16.09% (1.85 times of the control), arachidic acid (C20:0) from 0.24% (control) to 1.77%

(7.38 times of the control), docosanoic acid (C22:0) from 0.24% (control) to 2.10% (8.75 times of the control), and lignoceric acid (C24:0) from 0.29% (control) to 1.19% (4.10 times of the control) in the VPA treated culture of *A. flavipes* BCC 28681 (Table 6). Moreover, VPA also had the effects on the total fatty acid of some gut fungi; the total fatty acids of *P. shearii* TBRC 2865 and *Phialemonium sp.*

TBRC 4709 were increased from 49.13% (control) to 54.31% (1.11 times of the control) and from 64.44% (control) to 72.17% (1.12 times of the control) when the fungus was treated with VPA, while the total fatty acid of the fungus *Cladosporium sp.* TBRC 4134 was reduced from 73.50% (control) to 58.34% (1.26 times less than the control) in the VPA treated culture, as shown in Table 6.



Table 6 Effect of VPA (100 μ M) on fatty acid profile of representative gut fungi

Fungi, condition	C16:0	C18:0	C18:1 C	C18:2	C18:3	C20:0	C21:0	C22:0	C24:0	%TFA
TBRC 2865 (<i>Penicillium shearii</i>) control	24.29 \pm 0.73*	17.09 \pm 2.94	39.94 \pm 4.29	12.46 \pm 1.43*	0	1.65 \pm 0.10*	1.61 \pm 0.19*	1.30 \pm 0.18*	1.66 \pm 0.37	49.13 \pm 3.14*
TBRC 2865 (<i>Penicillium shearii</i>) 100 μ M VPA	16.86 \pm 0.79*	13.37 \pm 1.98	42.23 \pm 3.62	23.60 \pm 3.49*	0	1.08 \pm 0.05*	1.02 \pm 0.14*	0.67 \pm 0.16*	1.17 \pm 0.13	54.31 \pm 1.60*
TBRC 4709 (<i>Phialemonium sp.</i>) control	28.73 \pm 0.36*	8.23 \pm 0.43	43.27 \pm 0.92*	14.85 \pm 0.56*	2.53 \pm 0.05*	0.36 \pm 0.02*	0.58 \pm 0.09	0.84 \pm 0.08*	0.61 \pm 0.06*	64.44 \pm 5.15
TBRC 4709 (<i>Phialemonium sp.</i>) 100 μ M VPA	22.16 \pm 0.38*	7.94 \pm 0.24	57.95 \pm 0.48*	7.47 \pm 0.29*	1.52 \pm 0.06*	0.58 \pm 0.02*	0.51 \pm 0.09	1.05 \pm 0.01*	0.83 \pm 0.03*	72.17 \pm 3.64
TBRC 4134 (<i>Cladosporium sp.</i>) control	35.29 \pm 1.97	17.62 \pm 1.74*	32.69 \pm 1.57	12.55 \pm 2.13	0.20 \pm 0.05*	0.52 \pm 0.02*	0.44 \pm 0.14*	0.35 \pm 0.03*	0.34 \pm 0.06*	73.50 \pm 3.86*
TBRC 4134 (<i>Cladosporium sp.</i>) 100 μ M VPA	38.77 \pm 2.50	9.90 \pm 0.81*	33.78 \pm 2.30	15.20 \pm 1.79	0.10 \pm 0.02*	0.80 \pm 0.07*	0.77 \pm 0.11*	0.53 \pm 0.03*	0.16 \pm 0.07*	58.34 \pm 1.27*
BCC 28681 (<i>Aspergillus flavipes</i>) control	21.30 \pm 0.69*	8.70 \pm 0.46*	42.17 \pm 1.78	26.58 \pm 1.10*	0	0.24 \pm 0.03*	0.49 \pm 0.02	0.24 \pm 0.02*	0.29 \pm 0.05*	72.03 \pm 5.77
BCC 28681 (<i>Aspergillus flavipes</i>) 100 μ M VPA	18.34 \pm 0.59*	16.09 \pm 1.74*	39.13 \pm 3.33	20.85 \pm 1.76*	0	1.77 \pm 0.05*	0.53 \pm 0.03	2.10 \pm 0.06*	1.19 \pm 0.07*	74.77 \pm 6.00

*p \leq 0.05 was selected as the minimum criterion for significance.

*p \leq 0.01 was selected as the minimum criterion for significance.

Three representative gut yeasts were *Candida catenulate* TBRC223, *Candida butyri* TBRC 221 (syn. *Candida aaseri*), and *Saccharomyces ludwigii* TBRC 2149. The genera *Candida* and *Saccharomyces* are commonly found as gut yeasts^{88, 89}, particular the yeast *Saccharomyces cerevisiae*⁹⁰. The yeast *C. catenulate* TBRC223 is one of the most prevalent species of yeast found in human gastrointestinal tract⁹¹, whereas *C. butyri* TBRC 221 is found as microbiota in green olive fermentations⁹². In this study, the yeast *S. cerevisiae* TBRC 1563 previously mentioned above would be one of the representative gut yeasts (Table 4). We found that VPA had significant effect on α -linolenic acid (C18:3) as it completely stopped the production of this fatty acid in the VPA treated culture of *S. cerevisiae* TBRC 1563 (Table 4). As shown in Table 7, VPA completely stopped the production of palmitoleic acid (C16:1) and α -linolenic acid (C18:3); 5.54% and 1.33% of palmitoleic acid (C16:1) and α -linolenic acid (C18:3) were produced in the control, respectively, while none were produced in the VPA treated culture of *C. catenulate* TBRC 223. Palmitic acid (C16:0) production was increased from 31.35% (control) to 48.10% (1.53 times of the control), whereas the production of oleic acid (C18:1) was reduced from 29.90% (control) to 19.74% (1.51 times less than the control), as shown in Table 7. VPA completely enhanced the production of palmitoleic acid (C16:1) when the yeast *C. butyri* TBRC 221 was treated with VPA. On the other hand, the production of palmitic acid (C16:0) was reduced from 38.52% (control) to 33.84% (1.14 times less than the control) in the VPA treated culture of *C. butyri* TBRC 221 (Table 7). In the yeast *S. ludwigii* TBRC 2149, VPA reduced the production of stearic acid (C18:0) from 6.32% (control) to 4.70% (1.34 times less than the control), oleic acid (C18:1) from 48.75% (control) to 23.63% (2.06 times less than the control), and linoleic acid (C18:2) from 5.61% (control) to 0.35% (16.03 times less than the control), respectively (Table 7). In contrast, VPA induced the production of *trans*-9-elaidic acid (*trans*-C18:1) in the VPA treated culture of the yeast *S. ludwigii* TBRC 2149; 29.97% of this fatty acid was produced but none observed in the control, as shown in Table 7. Normally, *trans*-9-elaidic acid (*trans*-C18:1) is present in yeast and is degraded by peroxisomal multifunctional enzymes⁹³. It was found that *trans*-9-elaidic acid is less toxic than its *cis* isomer, oleic acid, and that it exhibited distinct effects in gene expression regulation and processing of excess fatty acids in yeast⁹⁴. In addition, *trans*-9-elaidic

acid (*trans*-C18:1) could also inhibit β -oxidation in human peripheral macrophages and increase intracellular Zn^{2+} level in human macrophages^{95, 96}. Interestingly, the present work revealed that VPA could induce the production of *trans*-9-elaidic acid (*trans*-C18:1) in *S. ludwigii* TBRC 2149, the representative gut yeast (Table 7).

Although this study has not investigated the effects of VPA on fatty acid profile of the representative gut bacteria, it is more likely that VPA may have effects on the biosynthesis of fatty acid of gut bacteria. The genus *Pediococcus* is normally found in humans and animals as intestinal flora⁹⁷. Therefore, *P. acidilactici* TBRC 7580 as mentioned earlier in Table 5 may be used as the representative gut bacterium. It was found that VPA completely stopped the production of lignoceric acid (C24:0) after feeding VPA with the culture of *P. acidilactici* TBRC 7580 (Table 5). The bacterium *P. acidilactici* is usually used as probiotic. From the previous work, this bacterium strain could survive in a gastrointestinal tract of volunteers about 2 weeks after oral feeding⁹⁸.

The total fatty acid contents in *C. catenulate* TBRC223 and *S. ludwigii* TBRC 2149 were decreased from 15.41% (control) to 10.32% (1.49 times less than the control), and from 36.87% (control) to 31.54% (1.17 times less than the control), respectively, in the VPA treated culture of those two bacterial strains. In contrast, VPA increased the production of the total fatty acid in the bacterium *C. butyri* TBRC 221 from 7.39% (control) to 14.18% (1.92 times of the control), as shown in Table 7.

Table 7 Effect of VPA (100 μ M) on fatty acid contents of representative gut yeast

Yeast, condition	C16:0	C16:1	C18:0	C18:1 T	C18:1 C	C18:2	C18:3	%TFA
TBRC 223 (<i>Candida catenulata</i>) control	31.35 \pm 1.53*	5.54 \pm 0.35*	15.13 \pm 1.07	0	29.90 \pm 1.89*	16.75 \pm 1.70	1.33 \pm 0.13*	15.41 \pm 1.36*
TBRC 223 (<i>Candida catenulata</i>) 100 μ M VPA	48.10 \pm 2.12*	0*	15.66 \pm 1.31	0	19.74 \pm 1.78*	16.51 \pm 1.06	0*	10.32 \pm 1.12*
TBRC 221 (<i>Candida butyri</i>) control	38.52 \pm 1.91*	0*	9.35 \pm 0.72	0	21.69 \pm 1.31	30.44 \pm 1.82	0	7.39 \pm 1.01*
TBRC 221 (<i>Candida butyri</i>) 100 μ M VPA	33.84 \pm 1.59*	1.32 \pm 0.29*	8.87 \pm 0.47	0	23.25 \pm 1.49	32.72 \pm 1.46	0	14.18 \pm 1.12*
TBRC 2149 (<i>Saccharomyces ludwigii</i>) control	13.92 \pm 1.90	25.40 \pm 0.63	6.32 \pm 0.61*	0*	48.75 \pm 1.51*	5.61 \pm 0.16*	0	36.87 \pm 2.20*
TBRC 2149 (<i>Saccharomyces ludwigii</i>) 100 μ M VPA	13.42 \pm 1.49	27.94 \pm 0.32	4.70 \pm 0.46*	29.97 \pm 2.12*	23.63 \pm 1.13*	0.35 \pm 0.06*	0	31.54 \pm 1.60*

*p \leq 0.05 was selected as the minimum criterion for significance.

*p \leq 0.01 was selected as the minimum criterion for significance.

Recently, a number of works have demonstrated drug-microbiome interactions, for example, antidiabetic drug metformin and proton-pump inhibitor drugs^{41, 42}, on which gut microbiome can encode enzymes responsible for drug metabolism⁴⁴. VPA has many side effects for the patients under VPA treatment, for example, the effect on lipid metabolism²; VPA interferes β -oxidation pathway of fatty acid, and thus causing toxicity. The negative impact on serious inborn errors of metabolism is induced from VPA treatment⁴, the hepatotoxicity and weight gain in patients are also induced from VPA. VPA interferes carnitine palmitoyl-transferase I which is a key enzyme in fatty acid β -oxidation⁵. The present work revealed that an anticonvulsive drug, VPA, at the concentration of 100 μ M, has effects on fatty acid profile of fungi, bacteria, and yeast, suggesting that VPA affects the biosynthesis of fatty acid in microorganisms. Besides VPA has the effects on fatty acid profile of the microorganisms mentioned earlier, and VPA also has the effects on fatty acid biosynthesis in certain representative gut microbiome.

Normally, oral administration of VPA in epilepsy treatment is usually treated at doses of 10 to 15 mg/kg/day; 600 to 900 mg for patients with 60 kg weight. However, prophylaxis of migraine headaches is normally treated with VPA at doses of 250-500 mg/day, while the treatment of manic episodes associated with bipolar disorder uses the doses up to 750 mg/day. It is possible that when patients receiving high doses of VPA, i.e., 600 mg to 900 mg, the quantity of VPA in a gastrointestinal tract of patients may reach at the concentration of 100 μ M, which may affect the fatty acid biosynthesis in gut microbiome of patients. Nevertheless, changing in fatty acid profile in microorganisms induced from VPA in this present work is not predictable according to the enhancement or reduction of fatty acid production by VPA observed differently in an individual microorganism. The data from this work demonstrated that certain fatty acids were completely inhibited in some strains of microorganisms, while those of some fatty acids were enhanced by VPA in some microorganisms. Moreover, the present work revealed that *trans*-9-elaidic acid (*trans*-C18:1) production in the yeast *S. ludwigii* TBRC 2149 is induced by VPA, as shown in Table 7.

The production of *trans*-9-elaidic acid (*trans*-C18:1) is worth mentioning because this fatty acid was previously found to inhibit β -oxidation in human peripheral blood macrophages, and it induced the increase of intracellular Zn^{2+} in human macrophages^{95, 96}. Therefore, the fatty acid induction or inhibition by VPA may have direct effects to patients under VPA treatment.

Fatty acid metabolism has a crucial role for human because it can keep the homeostasis balance and the negative perturbations that might cause disease development⁹⁹. Especially, short-chain fatty acids have many critical roles in human, for example, it might have a role in microbiota-gut-brain crosstalk¹⁰⁰. Short-chain fatty acids also possess key roles in regulating host metabolism, immune system and cell proliferation¹⁰¹.

4.1.2 Effect of VPA on polyketide biosynthesis

It is known that enzymes responsible for fatty acid and polyketide biosynthesis shared the similarities of enzymes by using the similar catalytic elements⁴⁵. According to data mentioned above, it was found that VPA has effects on the production of fatty acids in microorganisms, and therefore VPA may have effects on the biosynthesis of polyketide natural products because fatty acid synthases and polyketide synthases have similar catalytic elements, for example, these two enzymes may use similar common precursors and catalytic roles. From this hypothesis, it inspired us to investigate another part of this present work, the study of effects of VPA on the natural product polyketide biosynthesis using the endophytic fungus *Dothideomycete* sp. as a fungal model; this strain of fungus is known as a source of polyketide production in our laboratory^{54, 55, 56}. As mentioned earlier in the literature review that the fungus *Dothideomycete* sp. produced a tricyclic polyketide, and others polyketides including azaphilone, hybrid azaphilone-pyrone, calbistrin, isochromanone, and austdiol (compound **2**) as a major compound^{54, 55, 56}.

However, in the present work after feeding the fungus *Dothideomycete* sp. with 100 μ M VPA, in addition to austdiol (compound **2**), the fungus *Dothideomycete* sp. produced other types of polyketide, e.g., known isobenzofuranone polyketides **3**, **4** and **6**, and a polyketide **5** (Figure 11). Compounds **3** and **4** were previously isolated as a mixture (ratio 1:1), these two polyketides were not completely separated by reversed phase HPLC in the previous study¹⁰². In the present work, compounds **3** and **4** were separated by repeated HPLC separation using MeOH:H₂O (40:60) as a mobile phase.

The structures of compounds **3** and **4** were elucidated by analysis of 1D and 2D NMR spectra, as well as by the comparison with data of previous study¹⁰². The absolute configurations of compounds **3**, **4** and **6** were established by the modified Mosher's method and CD spectra after derivatization¹⁰³, as well as X-ray analysis for compound **6**¹⁰⁴. It was found that compounds **3** and **6** were the isomer with 3*R* and 8*S* because it had negative values, whereas compound **4** was the isomer with 3*R* and 8*R* according to the positive values^{103, 104}. Therefore, the absolute configuration of compound **3** was 3*R* and 8*S* due to the negative optical rotation, $[\alpha]^{27.1}_{\text{D}} -38.1$ ($c = 0.22$, CHCl₃), while compound **4** had 3*R* and 8*R* configuration with a positive optical rotation, $[\alpha]^{27.1}_{\text{D}} +38.9$ ($c = 0.25$, CHCl₃). Compound **5** was a papyracillic acid derivative which was previously isolated from the fungus *Ascochyta agropyrina* Var. *nana*¹⁰⁵. Based on structure elucidation and the comparison with previous works^{103, 104, 106}, compound **2**, **3**, **4** and **6** were derived from polyketide biosynthesis pathway whereas the biosynthesis of compound **5** is still unclear. There is no report on the biosynthesis of this compound.

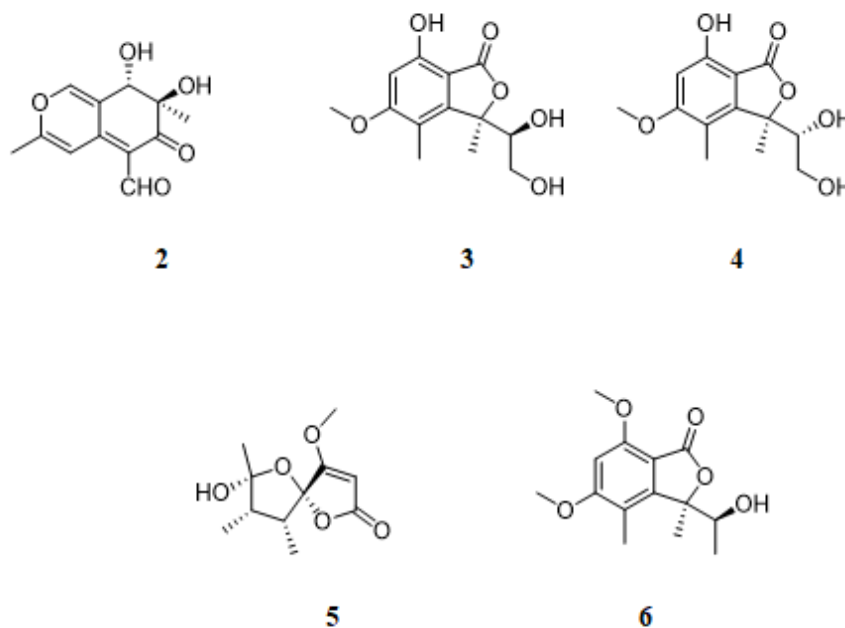


Figure 11 Structures of compounds 2-6 isolated from the endophytic fungus *Dothideomycete* sp.

The endophytic fungus *Dothideomycete* sp. was cultivated in 100 μ M of VPA. The comparison of the metabolite profile by HPLC analysis between the VPA treated culture and the control (without VPA) was investigated and shown in Figure 12. As presented in Figure 12A, HPLC chromatogram of the control fungal culture showed a peak at retention time (t_R) of 6.5 min for austdiol (compound 2), at t_R of 7.4 min for compounds 3 and 4, at t_R of 8.0 min for compound 5, and at t_R of 10.2 min for quadricinctone A (compound 6). Figure 12B showed HPLC chromatogram of VPA treated culture of the fungus *Dothideomycete* sp. which polyketide austdiol (compound 2) was markedly reduced more than 90% and quadricinctone A (compound 6) was reduced almost 50% production.

VPA did not give significant effects on the production of polyketides 3, 4, and 5. From the data mentioned above, this experiment demonstrated that VPA had the effects on polyketide production in the fungus *Dothideomycete* sp., as shown in Figure 12.

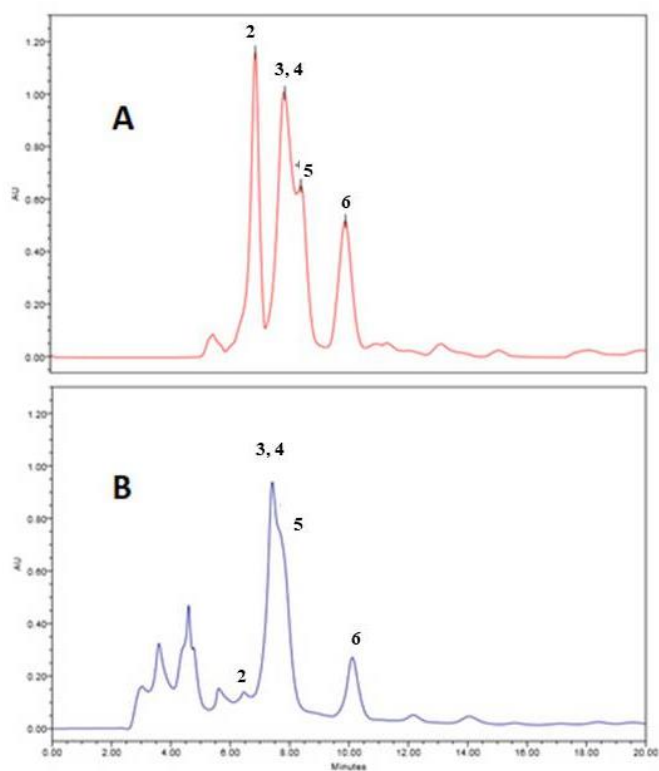
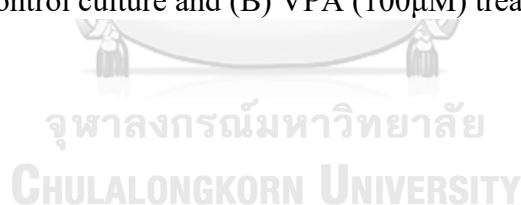


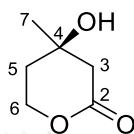
Figure 12 Metabolite profile of the fungus *Dothideomycete* sp. (A) a control culture and (B) VPA (100 μ M) treated culture.



Previously, we hypothesized that VPA may have effects on the biosynthesis of polyketide natural products because fatty acid synthases and polyketide synthases may have similar catalytic elements. Interestingly, as we hypothesized, VPA has the effects on the biosynthesis of certain polyketide natural products in the endophytic fungus *Dothideomycete* sp. This knowledge is very interesting and useful to apply in natural production research.

4.1.3 Structure elucidation of compound **1** isolated from the fungus *Trichoderma reesei* and compounds **2-6**, isolated from the fungus *Dothideomycete* sp.

4.1.3.1 Structure elucidation of compound **1**

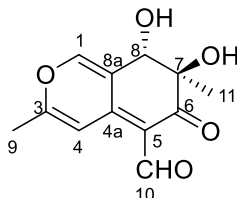


Compound **1** was obtained as brown-orange amorphous solid. The molecular formula of $C_6H_{11}O_3$ was determined by HRESI-MS showing m/z 131.0713 $[M+H]^+$ (calcd. for 131.0708). IR spectrum showed the absorption bands at 3425 cm^{-1} and 1704 cm^{-1} , indicating the presence of $-OH$ and carbonyl functional groups, respectively. The UV spectrum absorption was at 203.50 nm. The 1H NMR spectrum of compound **1** showed three sp^3 methylene groups at δ_H 1.83 and 1.93 (1H, m, H-5), 4.20 and 4.50 (1H, ddd, td, $J=16, 12, 4$ and $J=12, 4$, H-6) and 2.50 (1H, s, H-3), and methyl group at δ_H 1.30 (3H, s, 7-Me). The $^1H-^1H$ COSY spectrum revealed the correlation of H-5 and H-6. The HMBC correlations were observed from H-3 (δ_H 2.50) to C-2; from H-5 (δ_H 1.83 and 1.93) to C-6; and from 7-Me (δ_H 1.30) to C-3, C-4, and C-5. On the basis of these spectroscopic data, the structure of compound **1** was established, and this compound was previously isolated from marine fungi¹⁰⁷. Spectroscopic data of compound **1** are identical to those reported in the literatures¹⁰⁷.

Table 8 ^1H and ^{13}C NMR spectral data (400 MHz, in acetone-d6) of compound 1

Position	δ_{H} , mult. (J in Hz)	δ_{C}	HMBC
2	-	170.2	-
3	2.50, s	44.9	C-2
4	-	67.8	-
5	1.83, 1.93, m	36.1	C-6, C-7
6	4.20, 4.50, ddd, td (16, 12, 4), (12, 4)	66.0	-
7	1.30, s	29.0	C-3, C-4, C-5

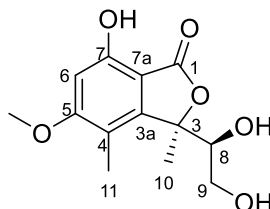


4.1.3.2 Structure elucidation of compound **2**

Compound **2** was obtained as brown-red amorphous solid. The molecular formula of $C_{12}H_{12}O_5$ was determined by HRESI-MS showing m/z 259.0577 $[M+H]^+$ (calcd. for 259.0582). IR spectrum showed the absorption bands at 3474 cm^{-1} and 1734 cm^{-1} which indicated the presence of $-OH$ and carbonyl functional groups, respectively. The UV spectrum absorptions were observed at 378.50, 255.50 and 203.50 nm. The 1H NMR spectrum of compound **2** showed signals of one oxygenated sp^3 methine group at δ_H 4.66 (H, s, H-8), one oxygenated methine group at δ_H 10.16 (H, s, H-10), two aromatic methine protons at δ_H 8.02 (H, s, H-1) and 8.39 (H, s, H-4), one methyl group at δ_H 2.44 (H, s, Me-9) and one sp^3 methyl at δ_H 1.18 (H, s, Me-11). The HMBC correlations were observed from H-1 (δ_H 8.02) to C-3, C-8a and C-9; from H-4 (δ_H 8.39) to C-3 and C-8a; from H-8 (δ_H 4.66) to C-1, C-8a and C-11; from Me-9 (δ_H 2.44) to C-3 and C-4; from H-10 (δ_H 10.16) to C-4a, C-5 and C-8a and from Me-11 (δ_H 1.18) to C-6, C-7 and C-8. Compound **2**, namely austdiol, was previously isolated from the endophytic fungus *Mycoleptodiscus indicus*¹⁰⁶. On the basis of these spectroscopic data and the data comparison with previous work¹⁰⁶, the structure of compound **2** was established.

Table 9 ^1H and ^{13}C NMR spectral data (400 MHz, in CDCl_3) of compound 2

Position	δ_{H} , mult. (J in Hz)	δ_{C}	HMBC
1	8.02, s	150.8	C-3, C-4, C-5, C-8a, C-9
2	-	-	-
3	-	166.3	-
4	8.39, s	107.9	C-3, C-4, C-7, C-8a
4a	-	144.9	-
5	-	108.3	-
6	-	198.2	-
7	-	72.1	-
8	4.66, s	75.0	C-1, C-8, C-8a, C-11
8a	-	120.9	-
9	2.44, s	20.4	C-3, C-4
10	10.16, s	189.8	C-4a, C-5, C-8a
11	1.18, s	18.3	C-6, C-7, C-8

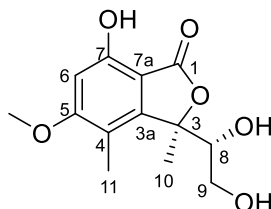
4.1.3.3 Structure elucidation of compound **3**

Compound **3** was obtained as yellow amorphous semi-solid. The molecular formula of $C_{13}H_{16}O_6$ was determined by HRESI-MS showing m/z 291.0838 $[M+H]^+$ (calcd. for 291.0845). IR spectrum showed the absorption bands at 3460 cm^{-1} and 1751 cm^{-1} which indicated the presence of $-OH$ and carbonyl functional groups, respectively. The UV spectrum absorptions were observed at 299.5, 259.5 and 217.0 nm. The 1H NMR spectrum of compound **2** showed signals of one methoxy group at δ_H 3.88 (3H, s, 5-OMe), two methyl groups at δ_H 1.81 (3H, s, 10-Me) and 2.13 (3H, s, 11-Me), one aromatic methine at δ_H 6.44 (1H, s, H-6), one sp^3 methine at δ_H 4.12 (1H, d, $J=16$, H-8), and one sp^3 methylene group at δ_H 3.35 (1H, d, $J=8$, H-9). The 1H - 1H COSY spectrum revealed the correlation of H-8 and H-9. The HMBC correlations were observed from H-6 (δ_H 6.44) to C-4, C-5, C-7 and C-7a; from 10-Me (δ_H 1.81) to C-3, C-3a and C-8; from 11-Me (δ_H 2.13) to C-3a, C-4, and C-5; and from 5-OMe (δ_H 3.88) to C-5. On the basis of these spectroscopic data, the structure of compound **3** was established, and this compound was previously isolated from the fungus *Entrophospora* sp.¹⁰² Unfortunately, the previous work obtained compounds **3** and **4** as a mixture with the ratio of 1:1¹⁰². In this work, compounds **3** and **4** were completely separated by repeated HPLC separation using MeOH:H₂O (40:60) as a mobile phase. The absolute configurations of compounds **3**, **4** and **6** were confirmed by comparing our data with previous work¹⁰⁴. It was found that the isomer with 3*R* and 8*S* (compound **3**) had negative values, whereas the isomer with 3*R* and 8*R* (compound **4**) had positive values^{103, 104}. Therefore, the absolute configuration of compound **3** was 3*R* and 8*S* due to the negative optical rotation, $[\alpha]^{27.1}_D -38.1$ ($c = 0.22$, CHCl₃).

Table 10 ^1H and ^{13}C NMR spectral data (400 MHz, in CDCl_3) of compound 3

Position	δ_{H} , mult. (<i>J</i> in Hz)	δ_{C}	HMBC
1	-	170.8	-
3	-	90.2	-
3a	-	148.7	-
4	-	112.7	-
5	-	165.5	-
6	6.44, s	98.5	C-7a, C-4, C-7, C-5
7	-	156.6	-
7a	-	102.6	-
8	4.12, d (3.8)	74.5	-
9	3.35, d, (8.1)	62.4	-
10	1.81, s	21.6	C-8, C-3, C-3a
11	2.13, s	11.3	C-4, C-3a, C-5
5-OMe	3.88, s	56.3	C-5

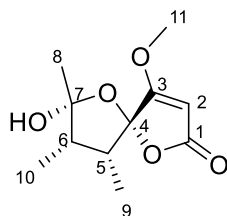


4.1.3.4 Structure elucidation of compound **4**

Compound **4** was obtained as yellow amorphous semi-solid. The molecular formula of $C_{13}H_{16}O_6$ was determined by HRESI-MS showing m/z 291.0839 $[M+H]^+$ (calcd. for 291.0845). IR spectrum showed the absorption bands at 3394 cm^{-1} and 1717 cm^{-1} which indicated the presence of $-OH$ and carbonyl functional groups, respectively. The UV spectrum absorptions were at 298.5, 259.0 and 216.0 nm. The 1H NMR spectrum of compound **4** showed signals of one methoxy group at δ_H 3.87 (3H, s, 5-OMe), two methyl groups at δ_H 1.70 (3H, s, 10-Me) and 2.17 (3H, s, 11-Me), one aromatic methine at δ_H 6.43 (1H, s, H-6), one sp^3 methine at δ_H 4.17 (1H, d, $J=4$, H-8), and one sp^3 methylene group at δ_H 3.80 (1H, d, $J=8$, H-9). The 1H - 1H COSY spectrum revealed the correlation of H-8 and H-9. The HMBC correlations were observed from H-6 (δ_H 6.43) to C-4, C-5, C-7 and C-7a; from 10-Me (δ_H 1.70) to C-3, C-3a and C-8; from 11-Me (δ_H 2.17) to C-3a, C-4, and C-5; from H-8 (δ_H 4.17) to C-3 and C-9, and from 5-OMe (δ_H 3.87) to C-5. On the basis of these spectroscopic data and by data comparison with previous works as mentioned above^{102, 103, 104}, the structure of compound **4** was established. The absolute configuration of compound **4** was $3R$ and $8R$ due to the positive optical rotation, $[\alpha]^{27.1}_D +38.9$ (0.25, $CHCl_3$).

Table 11 ^1H and ^{13}C NMR spectral data (400 MHz, in CDCl_3) of compound 4

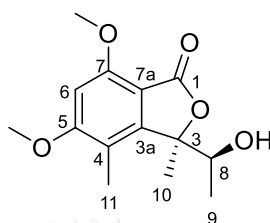
Position	δ_{H} , mult. (J in Hz)	δ_{C}	HMBC
1	-	171.2	-
3	-	90.4	-
3a	-	149.4	-
4	-	112.5	-
5	-	165.3	-
6	6.43, s	98.3	C-7a, C-4, C-7, C-5, C-1
7	-	156.4	-
7a	-	103.2	-
8	4.17, d (4.3)	73.6	C-9, C-3
9	3.80, d, (8.0)	62.1	C-3
10	1.70, s	21.1	C-8, C-3, C-3a
11	2.17, s	10.9	C-4, C-3a, C-5
5-OMe	3.87, s	56.2	C-5

4.1.3.5 Structure elucidation of compound **5**

Compound **5** was obtained as yellow amorphous semi-solid. The molecular formula of $C_{11}H_{16}O_5$ was determined by HRESI-MS showing m/z 251.0883 $[M+H]^+$ (calcd. for 251.0895). IR spectrum showed the absorption bands at 3396 cm^{-1} and 1737 cm^{-1} which indicated the presence of $-OH$ and carbonyl functional groups, respectively. The UV spectrum absorption was observed at 223.0 nm. The 1H NMR spectrum of compound **5** showed signals of one methine group at δ_H 5.11 (1H, s, H-2), one methoxy group at δ_H 3.91 (3H, s, 11-Me), and three methyl groups at δ_H 1.55 (3H, s, H-8), 0.93 (3H, s, 9-Me), and 1.07 (3H, s, 10-Me). The 1H - 1H COSY spectrum revealed the fragment of H-10/ H-6/ H-5/ H-9. The HMBC correlations were observed from H-2 (δ_H 5.11) to C-1 and C-4; from H-5 (δ_H 2.38) to C-4; from H-6 (δ_H 1.96) to C-5 and C-7; from 8-Me (δ_H 1.55) to C-6 and C-7; from 9-Me (δ_H 0.93) to C-4 and C-5; from 10-Me (δ_H 1.07) to C-5, C-6 and C-7; and from 11-Me (δ_H 3.91) to C-3. Compound **5** was a derivative of papyracillic acid, which was previously isolated from *Ascochyta agropyrina* var. *nana*^{105, 109}. On the basis of these spectroscopic data and from the comparison of our data with previous works^{105, 109}, the structure of compound **5** was established as shown.

Table 12 ^1H and ^{13}C NMR spectral data (400 MHz, in CDCl_3) of compound 5

Position	δ_{H} , mult. (J in Hz)	δ_{C}	HMBC
1	-	169.3	-
2	5.11, s	90.5	C-1, C-4
3	-	176.2	-
4	-	109.7	-
5	2.38, dq (12.4, 6.8)	43.6	C-6, C-4
6	1.96, dq (12.4, 6.8)	47.0	C-5, C-7, C-9
7	-	107.7	-
8	1.55, s	26.3	C-6, C-7
9	0.93, d (6.8)	10.1	C-4, C-5, C-5
10	1.07, d (6.8)	11.4	C-5, C-6, C-7
11	3.91, s	59.6	C-3

4.1.3.6 Structure elucidation of compound **6**

Compound **6** was obtained as yellow amorphous semi-solid. The molecular formula of $C_{14}H_{18}O_5$ was determined by HRESI-MS showing m/z 289.1020 $[M+H]^+$ (calcd. for 289.1052). IR spectrum showed the absorption bands at 3419 cm^{-1} and 1726 cm^{-1} , indicating the presence of $-OH$ and carbonyl functional groups, respectively. The UV spectrum absorptions were observed at 299.0, 260.5 and 221.0 nm. The 1H NMR spectrum of compound **6** showed characteristic signal of two methoxy groups at δ_H 3.93 (3H, s, 5-OMe) and 3.98 (3H, s, 7-OMe), three methyl groups at δ_H 0.88 (3H, d, $J=6.4$, 9-Me), 1.77 (3H, s, 10-Me) and 2.13 (3H, s, 11-Me), one aromatic methine at δ_H 6.41 (1H, s, H-6), and one sp^3 methine at δ_H 4.22 (1H, d, $J=6.4$, H-8). The 1H - 1H COSY spectrum revealed the correlation of H-8 and 9-Me. The HMBC correlations were observed from H-6 (δ_H 6.41) to C-4, C-5, C-7 and C-7a; from 9-Me (δ_H 0.88) to C-3, C-8 and C-10; from 10-Me (δ_H 1.77) to C-3, C-3a and C-8; from 11-Me (δ_H 2.13) to C-3a, C-4, and C-5; from H-8 (δ_H 4.22) to C-3, C-9 and C-10; from 5-OMe (δ_H 3.93) to C-5 and C-6; and from 7-OMe (δ_H 3.98) to C-6 and C-7. Compound **6** was previously isolated from *Leptosphaeria* sp.¹⁰³. The absolute configuration of compound **6** was confirmed by comparing our data with previous work¹⁰³. It was found that the absolute configuration of compound **6** was 3*R* and 8*S* due to the negative optical rotation, $[\alpha]^{25.5}_D -18.0$ (0.14, $CHCl_3$).

Table 13 ^1H and ^{13}C NMR spectral data (400 MHz, in CDCl_3) of compound 6

Position	δ_{H} , mult. (J in Hz)	δ_{C}	HMBC
1	-	168.0	-
3	-	88.6	-
3a	-	152.8	-
4	-	111.7	-
5	-	164.5	-
6	6.41, s	94.4	C-7a, C-4, C-7, C-5, C-1
7	-	158.3	-
7a	-	105.7	-
8	4.22, d (6.4)	70.9	C-9, C-10, C-3
9	0.88, d, (6.4)	17.8	C-10, C-8, C-3
10	1.77, s	21.5	C-8, C-3, C-3a
11	2.13, s	11.1	C-4, C-3a, C-5
5-OMe	3.93, s	55.9	C-6, C5
7-OMe	3.98, s	56.1	C-6, C-7

4.1.4 Antibacterial activity

Table 14 Antibacterial activity of compounds 3-6

Bacterial strains	Inhibition zone (mm)					
	Tetracycline	Chloramphenicol	Compound 3	Compound 4	Compound 5	Compound 6
<i>Pseudomonas aeruginosa</i> (-)	24	25	Inactive	Inactive	8	10
<i>Salmonella enterica</i> (-)	26	26	Inactive	Inactive	10	11
<i>Bacillus cereus</i> (+)	24	27	Inactive	Inactive	8	8

Compounds 3-6 were investigated for their antibacterial activity against *P. aeruginosa*, *S. enterica* and *B. cereus*. It was found that compound 5 showed weak antibacterial activity against *P. aeruginosa*, *S. enterica* and *B. cereus* with inhibition zones of 8, 10 and 8 mm, respectively. Moreover, compound 6 also exhibited weak antibacterial activity against *P. aeruginosa*, *S. enterica* and *B. cereus* with inhibition zones of 10, 11 and 8 mm, respectively, as shown in Table 14.

4.1.5 Cancer chemoprevention activity

The isolated compounds were evaluated for cancer chemoprevention properties. It was found that compound **5** exhibited weak activity for the xanthine oxidase assay (XXO) with an IC_{50} value of $365.9 \pm 5.9 \mu\text{M}$. Compound **6** exhibited moderate activity for the XXO assay with an IC_{50} value of $117.9 \pm 2.5 \mu\text{M}$, as shown in Table **15**.

Table **15** Cancer chemoprevention activity of compounds **3**, **4**, **5** and **6**

Compounds	IC_{50} (μM)
	XXO assay
3	Inactive
4	Inactive
5	365.9 ± 5.9
6	117.9 ± 2.5

4.1.6 Cytotoxic activity

Compounds **3-6** were also investigated for their cytotoxic activity, and it was found that compound **6** showed moderate cytotoxic activity against MOLT-3 cell line with IC_{50} value of $170.32 \pm 1.07 \mu\text{M}$, as shown in Table **16**.

Table **16** Cytotoxic activity of compounds **3**, **4**, **5** and **6**

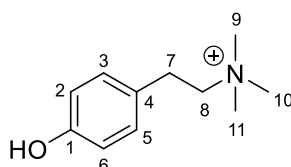
Compounds	Cytotoxic activity, IC_{50} (μM); values are expressed as mean \pm s.d., n = 3
	MOLT-3
3	Inactive
4	Inactive
5	Inactive
6	170.32 ± 1.07
Etoposide ($\mu\text{g/ml}$)	0.008 ± 0.000
Doxorubicin ($\mu\text{g/ml}$)	ND

ND= Not determined

MOLT-3 (acute lymphoblastic leukemia)

4.2 Bioactive compounds from *Feroniella lucida* (Scheff.) Swingle

4.2.1 Structure elucidation of compound **7**

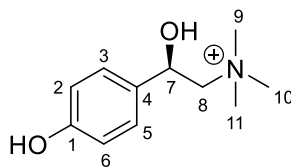


Compound **7** was obtained as yellow solid. The molecular formula of $C_{11}H_{18}NO$ was determined by HRESI-MS showing m/z 180.1367 $[M+H]^+$ (calcd. for 180.1383). IR spectrum showed absorption band at 3365 cm^{-1} which indicated the presence of -OH functional group. The UV spectrum absorptions were observed at 267.0 and 202.5 nm. The ^1H NMR spectrum of compound **7** showed signals of three methyl groups at δ_{H} 3.26 (3H, s, 9-Me), 3.26 (3H, s, 10-Me) and 3.26 (3H, s, 11-Me), para-substituted aromatic methine protons at δ_{H} 6.74 (2H, d, $J=8$, H-2 or H-6) and 7.11 (2H, d, $J=8$, H-3 or H-5) and two groups of non-equivalent methylene protons at δ_{H} 3.06 and 3.54. It should be noted that H-7 was overlapped with H-8. ^1H - ^1H COSY spectrum revealed the correlation of H-2 or H-6 and H-3 or H-5. The HMBC correlations were observed from H-2 or H-6 (δ_{H} 6.74) to C-1, C-2 and C-4; from H-3 or H-5 (δ_{H} 7.11) to C-1, C-5, C-6 and C-7; from H-7 (δ_{H} 3.06 and 3.54) to C-3, C-4 and C-8; from H-8 (δ_{H} 3.06 and 3.54) to C-4, C-7 and C-10; from 9-Me (δ_{H} 3.26) to C-7, C-8, C-10 and C-11; from 10-Me (δ_{H} 3.26) to C-7, C-8, C-9 and C-11 and from 11-Me (δ_{H} 3.26) to C-7, C-8, C-9 and C-10. Compound **7**, namely *N,N,N*-trimethyltyramine or candicine, was previously isolated from *Ginkgo biloba*¹¹⁰, *Stapelia hirsuta* L., cactus-like plant¹¹¹ and citrus plant^{112, 113}. On the basis of these spectroscopic data and from the comparison of our data with previous works^{110, 111, 112, 113}, the structure of compound **7** was established.

Table 17 ^1H and ^{13}C NMR spectral data (400 MHz, in acetone- d_6) of compound 7

Position	δ_{H} , mult. (J in Hz)	δ_{C}	HMBC
1	-	156.7	-
2	6.74, d (8)	116.2	C-1, C-2, C-4
3	7.11, d (8)	130.7	C-1, C-5, C-6, C-7
4	-	126.8	
5	7.11, d (8)	130.7	C-1, C-5, C-6, C-7
6	6.74, d (8)	116.2	C-1, C-2, C-4
7	3.06, 3.54, dd (9, 9)	28.6	C-3, C-4, C-8, C-9
8	3.06, 3.54, dd (9, 9)	67.9	C-4, C-7, C-10
9	3.26, s	53.5	C-7, C-8, C-10, C-11
10	3.26, s	53.5	C-7, C-8, C-9, C-11
11	3.26, s	53.5	C-7, C-8, C-9, C-10

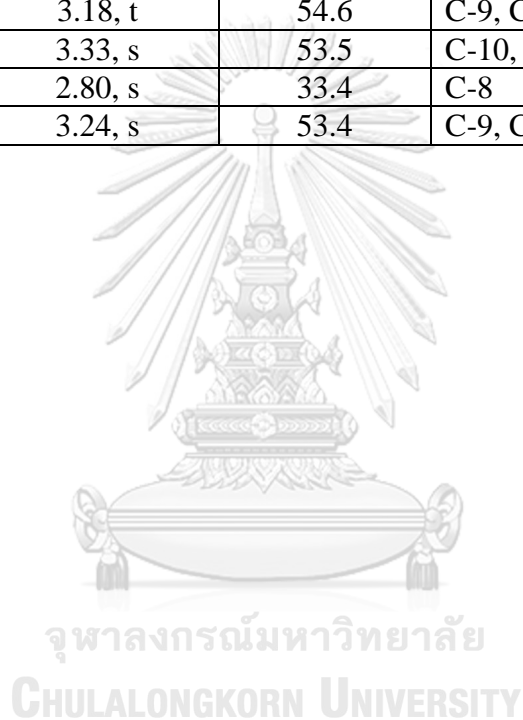


4.2.2 Structure elucidation of compound **8**

Compound **8** was obtained as yellow solid. The molecular formula of $C_{11}H_{19}NO_2$ was determined by HRESI-MS showing m/z 196.1332 $[M+H]^+$ (calcd. for 196.1388). IR spectrum showed absorption band at 3222 cm^{-1} , indicating the presence of -OH functional group. The UV spectrum absorptions were observed at 276.5 and 225.5 nm. The ^1H NMR spectrum of compound **8** showed signals of three methyl groups at δ_{H} 3.33 (3H, s, 9-Me), 2.80 (3H, s, 10-Me) and 3.24 (3H, s, 11-Me), para-substituted aromatic protons at δ_{H} 6.78 (2H, d, $J=8$, H-2 or H-6) and 7.25 (2H, d, $J=8$, H-3 or H-5), one sp^3 methine at δ_{H} 5.0 (1H, dd, $J=8$ and 12, H-7) and methylene protons at δ_{H} 3.18 (2H, t, H-8). The ^1H - ^1H COSY spectrum revealed the correlations of H-5 or H-3 and H-6 or H-2 and H-7 and H-8. The HMBC correlations were observed from H-2 or H-6 (δ_{H} 6.78) to C-1, C-4, C-5 and C-6; from H-3 or H-5 (δ_{H} 7.25) to C-1, C-2, C-5 and C-7; from H-7 (δ_{H} 5.0) to C-3, C-4 and C-8; from H-8 (δ_{H} 3.18) to C-9 and C-10; from 9-Me (δ_{H} 3.33) to C-10 and C-11; from 10-Me (δ_{H} 2.80) to C-8 and from 11-Me (δ_{H} 3.24) to C-9 and C-10. On the basis of these spectroscopic data and from the comparison of our data with previous works^{114, 115, 116}, the structure of compound **8** was established.

Table 18 ¹H and ¹³C NMR spectral data (400 MHz, in acetone-d₆) of compound 8

Position	δ_{H} , mult. (<i>J</i> in Hz)	δ_{C}	HMBC
1	-	157.3	-
2	6.78, d (8)	115.8	C-1, C-4, C-5, C-6
3	7.25 d (8)	127.8	C-1, C-2, C-3, C-7
4	-	131.9	-
5	7.25 d (8)	127.8	C-1, C-2, C-3, C-7
6	6.78, d (8)	115.8	C-1, C-4, C-5, C-6
7	5.0, dd (8, 12)	68.6	C-3, C-4, C-8
8	3.18, t	54.6	C-9, C-10
9	3.33, s	53.5	C-10, C-11
10	2.80, s	33.4	C-8
11	3.24, s	53.4	C-9, C-10



4.2.3 Biological activities of compounds isolated from *F. lucida*

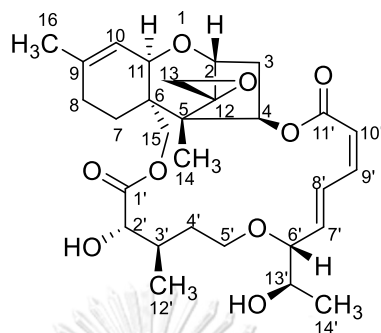
The isolated compounds were evaluated for cancer chemoprevention properties. It was found that compound **8** exhibited weak activity for the xanthine oxidase assay (XXO) with an IC₅₀ value of 473.8±13.4 μM, as shown in Table **19**.

Table **19** Cancer chemoprevention activity of compound **8** isolated from *F. lucida*

Compounds	Assay/IC ₅₀
	XXO
Compound 8	473.8±13.4 μM

4.3 Bioactive compounds from termite-associated fungus ISFB10

4.3.1 Structure elucidation of compound **9**



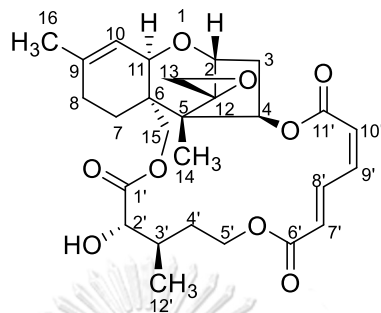
Compound **9** was obtained as yellow crystal solid. The molecular formula of $C_{29}H_{40}O_9$ was determined by HRESI-MS showing m/z 555.2562 $[M+Na]^+$ (calcd. for 555.2570). IR spectrum showed absorption bands at 3437 cm^{-1} and 1732 cm^{-1} which indicated the presence of -OH and carbonyl functional groups, respectively. The UV spectrum absorption was observed at 262 nm. The ^1H NMR spectrum of compound **9** showed signals of four oxygenated sp^3 methines at δ_{H} 3.71 (H, t, H-11), 3.73 (H, t, H-2), 3.80 (H, t, H-6') and 5.80 (H, dd, $J=8$ and 9, H-4), five sp^2 methines at δ_{H} 6.19 (H, dd, $J=16$ and 16, H-7'), 7.61 (H, t, H-8'), 6.79 (H, t, H-9'), 5.75 (H, d, $J=12$, H-10') and 5.37 (H, d, $J=5$, H-10), three sp^3 methines at δ_{H} 2.06 (H, dd, $J=9$ and 9, H-3'), 3.72 (H, t, H-13') and 4.07 (H, d, t, H-2'), four methyl groups at δ_{H} 0.8 (3H, s, 14-Me), 1.68 (3H, s, 16-Me), 1.06 (3H, dd, $J=7$, 12'-Me) and 1.05 (3H, dd, $J=7$, 14'-Me), methylene protons at δ_{H} 1.92 (2H, m, H-8), and six non-equivalent methylene protons at δ_{H} 2.05 and 2.47 (H, dd, $J=15$ and 15, H-3), 1.80 and 1.85 (H, m, H-7), 2.80 and 3.0 (H, d, $J=4$, H-13), 4.29 and 4.40 (H, d, $J=12$, H-15), 1.55 and 1.75 (H, m, H-4'), and 3.50 and 3.72 (H, m, H-5'). The ^1H - ^1H COSY spectrum revealed the correlations of H-3 and H-4, H-7' and H-8', H-8' and H-9', and H-9' and H-10'. The HMBC correlations were observed from H-2 (δ_{H} 3.73) to C-4, C-5 and C-11; from H-3 (δ_{H} 2.05 and 2.47) to C-2, C-5 and C-12; from H-4 (δ_{H} 5.8) to C-6, C-12 and C-11'; from H-7 (δ_{H} 1.80 and 1.85) to C-6, C-7, C-8, C-11, C-12 C-15 and C-16; from H-8 (δ_{H} 1.92) to C-6, C-7, C-9 and C-10; from H-10 (δ_{H} 5.37) to C-6, C-8 and C-11; from H-11 (δ_{H} 3.71) to C-5, C-9, C-10 and C-16; from H-13 (δ_{H} 2.8 and 3.0) to C-2 and C-12;

from 14-Me (δ_{H} 0.8) to C-4, C-5, C-6 and C-12; from H-15 (δ_{H} 4.29 and 4.4) to C-5, C-6, C-7, C-11 and C-1'; from 16-Me (δ_{H} 1.68) to C-9 and C-10; from H-2' (δ_{H} 4.07) to C-1'; from H-3' (δ_{H} 2.06) to C-2'; from H-4' (δ_{H} 1.55 and 1.75) to C-2', C-3', C-5' and C-12'; from H-6' (δ_{H} 3.8) to C-5', C-7' and C-8'; from H-7' (δ_{H} 6.19) to C-6', C-8', and C-9'; from H-8' (δ_{H} 7.61) to C-6', C-9' and C-10'; from H-9' (δ_{H} 6.79) to C-7', and C-11'; from H-10' (δ_{H} 5.75) to C-8' and C-11'; from H-12' (δ_{H} 1.06) to C-2', C-3', C-4' and C-5' and from H-14' (δ_{H} 1.05) to C-6'. Compound **9**, namely roridin A, was previously isolated from *Myrothecium verrucaria*¹¹⁷. On the basis of these spectroscopic data and from the comparison of our data with previous works^{117, 118}, the structure of compound **9** was established.



Table 20 ^1H and ^{13}C NMR spectral data (400 MHz, in acetone- d_6) of compound **9**

Position	δ_{H} , mult. (J in Hz)	δ_{C}	HMBC
2	3.73, t	79.4	C-4, C-5, C-11
3	2.05, 2.47, dd (15, 15)	35.4	C-2, C-5, C-12,
4	5.8, dd (8, 9)	76.8	C-6, C-12, C-11'
5	-	50.0	-
6	-	44.5	-
7	1.8, 1.85, m	20.8	C-6, C-7, C-8, C-11, C-12, C-15, C-16
8	1.92, m	28.2	C-6, C-7, C-9, C-10
9	-	139.1	-
10	5.37, d (5)	120.0	C-6, C-8, C-11
11	3.71, t	67.5	C-5, C-9, C-10, C-16
12	-	65.8	-
13	2.8, 3.0, d (4)	47.7	C-2, C-12
14	0.8, s	7.8	C-4, C-5, C-6, C-12
15	4.29, 4.4, d (12)	64.3	C-5, C-6, C-7, C-11, C-1'
16	1.68, s	23.2	C-9, C-10
1'	-	174.9	-
2'	4.07, t	76.1	C-1'
3'	2.06, dd (9, 9)	37.2	C-2'
4'	1.55, 1.75, m	34.2	C-2', C-3', C-5', C-12'
5'	3.5, 3.72, m	70.2	-
6'	3.8, t	84.3	C-5', C-7', C-8'
7'	6.19, dd (16, 16)	141.4	C-6', C-8', C-9'
8'	7.61, t	126.5	C-6', C-9', C-10'
9'	6.79, t	144.9	C-7', C-11'
10'	5.75, d (12)	117.5	C-8', C-11'
11'	-	167.1	-
12'	1.06, dd (7, 7)	14.8	C-2', C-3', C-4', C-5'
13'	3.72, t	67.5	-
14'	1.05, dd (7, 7)	18.4	C-6'

4.3.2 Structure elucidation of compound **10**

Compound **10** was obtained as yellow crystal solid. The molecular formula of $C_{27}H_{34}O_9$ was determined by HRESI-MS showing m/z 525.2086 $[M+Na]^+$ (calcd. for 525.2101). IR spectrum showed absorption bands at 3482 cm^{-1} and 1712 cm^{-1} , indicating the presence of $-OH$ and carbonyl functional groups, respectively. The UV spectrum absorption was observed at 259 nm. The 1H NMR spectrum of compound **10** showed signals of three oxygenated sp^3 methines at δ_H 5.90 (H, dd, $J=8$ and 8, H-2) and δ_H 3.72 (H, t, H-11) and δ_H 3.71 (H, t, H-4), five sp^2 methines at δ_H 6.20 (H, dd, $J=11$ and 11, H-7'), 6.86 (H, t, H-8'), 8.06 (H, dd, $J=16$ and 16, H-9'), 6.10 (H, d, $J=16$, H-10') and 5.39 (H, d, $J=4$, H-10), two sp^3 methines at δ_H 4.23 (H, d, $J=2$, H-2') and 2.40 (H, d, m, H-3'), three methyl groups at δ_H 0.87 (3H, s, 14-Me), 1.70 (3H, s, 16-Me) and 0.89 (3H, s, 12'-Me), methylene protons at δ_H 1.93 (2H, m, H-8) and six non-equivalent methylene protons at δ_H 2.10 and 2.50 (H, dd, $J=15$ and 8, H-3), 1.82 and 1.91 (H, m, H-7), 2.80 and 3.0 (H, d, $J=4$, H-13), 4.22 and 4.69 (H, d, $J=11$ and 12, H-15), 1.81 and 1.92 (H, m, H-4') and 4.0 and 4.4 (H, m, H-5'). The 1H - 1H COSY spectrum revealed the correlations of H-2 and H-3, H-3 and H-4, H-10 and H-11, H-3' and H-4', H-4' and H-5', H-7' and H-8', H-8' and H-9' and H-9' and H-10'. The HMBC correlations were observed from H-2 (δ_H 5.9) to C-6 and C-12; from H-3 (δ_H 2.1 and 2.5) to C-2, C-4, C-5 and C-12; from H-7 (δ_H 1.82 and 1.91) to C-6, C-8, C-9 and C-11; from H-8 (δ_H 1.93) to C-10; from H-10 (δ_H 5.39) to C-6, C-8, C-11 and

C-16; from H-11 (δ_{H} 3.72) to C-2, C-5, C-7, C-9, C-10 and C-11; from H-13 (δ_{H} 2.8 and 3.0) to C-4 and C-12; from 14-Me (δ_{H} 0.87) to C-2, C-5, C-6 and C-12; from H-15 (δ_{H} 4.22 and 4.69) to C-5, C-6, C-7, C-11 and C-1'; from 16-Me (δ_{H} 1.7) to C-8, C-9 and C-10; from H-2' (δ_{H} 4.23) to C-1', C-3', C-4' and C-12'; from H-3' (δ_{H} 2.4) to C-4' and C-12'; from H-4' (δ_{H} 1.81 and 1.92) to C-3', C-5' and C-12'; from H-5' (δ_{H} 4.0 and 4.4) to C-2', C-3' and C-4'; from H-7' (δ_{H} 6.2) to C-6' and C-9'; from H-8' (δ_{H} 6.86) to C-6', C-9' and C-10'; from H-9' (δ_{H} 8.06) to C-7', C-8' and C-11'; from H-10' (δ_{H} 6.1) to C-8' and C-11' and from H-12' (δ_{H} 0.89) to C-2', C-3' and C-4'. . Compound **10**, namely verrucarin A, was also isolated from *Myrothecium verrucaria*¹¹⁷. On the basis of these spectroscopic data and from the comparison of our data with previous works^{117, 118}, the structure of compound **10** was established.

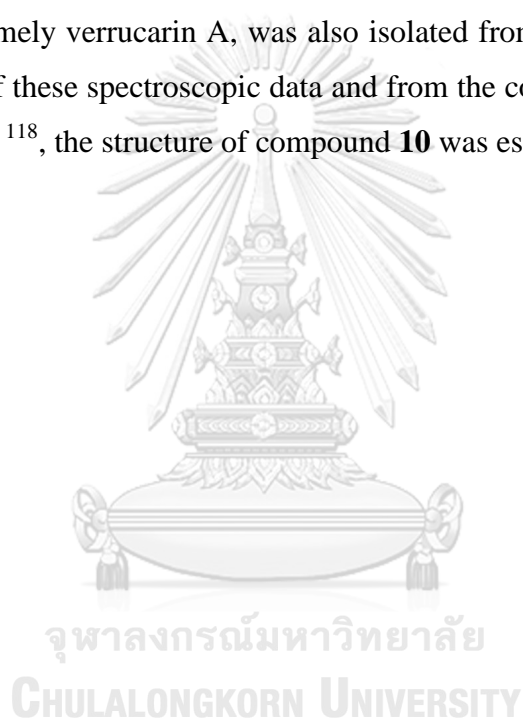


Table 21 ^1H and ^{13}C NMR spectral data (400 MHz, in acetone- d_6) of compound 10

Position	δ_{H} , mult. (J in Hz)	δ_{C}	HMBC
2	5.9, dd (8, 8)	76.8	C-6, C-12
3	2.1, 2.5, dd (15, 8)	35.6	C-2, C-4, C-5, C-12
4	3.71, t	79.4	-
5	-	50.1	-
6	-	44.9	-
7	1.82, 1.91, m, s	20.6	C-6, C-8, C-9, C-11,
8	1.93, s	28.1	C-10
9	-	139.9	-
10	5.39, d (4)	119.9	C-6, C-8, C-11, C-16,
11	3.72, t	67.3	C-2, C-5, C-7, C-9, C-10, C-11
12	-	65.8	-
13	2.8, 3.0, d (4)	47.8	C-4, C-12
14	0.87, s	8.0	C-2, C-5, C-6, C-12,
15	4.22, 4.69, d (11, 12)	63.2	C-5, C-6, C-7, C-11, C-1'
16	1.7, s	23.2	C-8, C-9, C-10
1'	-	174.8	-
2'	4.23, d (2)	74.6	C-1', C-3', C-4', C-12'
3'	2.4, m	33.8	C-4', C-12'
4'	1.81, 1.92, m, s	33.1	C-3', C-5', C-12'
5'	4.0, 4.4, m	61.7	C-2', C-3', C-4'
6'	-	166.7	-
7'	6.2, d (11)	126.9	C-6', C-9'
8'	6.86, t	139.2	C-6', C-9', C-10'
9'	8.06, dd (15, 16)	139.7	C-7', C-8', C-11'
10'	6.1, d (16)	128.1	C-8', C-11'
11'	-	165.7	-
12'	0.89, s	10.6	C-2', C-3', C-4'

4.3.3 Biological activities of compounds isolated from termite-associated fungus ISFB10

Table 22 Cytotoxic activities of compounds isolated from termite-associated fungus ISFB10

Compound	Cytotoxic activity, IC ₅₀ (μM); values are expressed as mean ± s.d., n = 3				
	HuCCA-1	A549	MOLT-3	HepG2	MRC-5
Compound 9	0.016±0.0007	0.0055±0.0001	0.005±0.0003	0.024±0.002	0.038±0.006
Compound 10	0.014±0.0005	0.0047±0.0005	0.008±0.0002	0.019±0.001	0.012±0.0004
Etoposide	ND	ND	0.027±0.002	62.66±1.43	ND
Doxorubicin	1.00±0.044	0.57±0.049	0.0137±0.0000	0.552±0.03	2.380±0.22

ND= Not determined
carcinoma)

HepG2 (liver hepatocellular

MOLT-3 (acute lymphoblastic leukemia)

A549 (human lung cancer)

HuCCA-1 (human cholangiocarcinoma cell line)

MRC-5 (normal fibroblast cell)

Compounds isolated from termite-associated fungus ISFB10 (unidentified) were evaluated for cytotoxic activities toward HuCCA-1, A549, MOLT-3 and HepG2 cell lines. It was found that compounds **9** exhibited strong cytotoxic activities toward HuCCA-1, A549, MOLT-3 and HepG2 with the IC₅₀ values of 0.016±0.0007 μM, 0.0055±0.0001 μM, 0.005±0.0003 μM and 0.024±0.002 μM, respectively. Compounds **10** also exhibited strong cytotoxic activities toward HuCCA-1, A549, MOLT-3 and HepG2 cancer cell lines with IC₅₀ values of 0.014±0.0005 μM, 0.0047±0.0005 μM, 0.008±0.0002 μM and 0.019±0.001 μM, respectively.

These two compounds were also evaluated their cytotoxicity toward normal cell line, MRC-5. Unfortunately, compounds **9** and **10** were also exhibited strong cytotoxic activity toward MRC-5 with the IC_{50} values of $0.038 \pm 0.006 \mu\text{M}$ and $0.012 \pm 0.0004 \mu\text{M}$, respectively. These data indicated that these compounds had no selectivity, and could kill both cancer cells and normal cells. Previous works reported that roridin A and verrucarins A (compounds **9** and **10**) were macrocyclic trichothecene mycotoxins, which can cause many serious problems, for example, inhibiting of protein translation in eukaryote. Moreover, the contamination of macrocyclic trichothecene mycotoxins in livestock production can cause many serious problems to animals, for example, diarrhea, vomiting, leukocytosis and gastrointestinal hemorrhage^{118, 119}.



Chapter V

Conclusion

5.1 Effects of VPA on biosynthesis of fatty acids and polyketides

5.1.1 Effects of VPA on biosynthesis of fatty acids

This work revealed that an anticonvulsive drug, VPA, has effects on biosynthesis of fatty acid in microorganisms including fungi, bacteria, yeast, as well as representative gut microbiome. Biosynthesis of certain fatty acids was completely inhibited by VPA, while that of some fatty acids was induced by VPA. The induction or inhibition of fatty acid biosynthesis was unpredictable in each strain of microorganisms. Interestingly, VPA could induce the production of *trans*-9-elaidic acid in *S. ludwigii* TBRC2149. It is worth mentioning that *trans*-9-elaidic acid was previously found to have many effects on human health, for example, the inhibition of β -oxidation in human peripheral blood macrophages, and the increase of intracellular Zn^{2+} in human macrophages. Therefore, the induction or inhibition of certain fatty acids by VPA drug may have direct effects to patients under VPA treatment. In this study, we found that VPA with the concentration 100 μ M has effects on the biosynthesis of fatty acids in certain representative gut microbiome. Normally, oral administration of VPA for the treatment of epilepsy uses this drug at doses of 10 to 15 mg/kg/day, meaning that 600 mg to 900 mg for the patient with 60 kg weight. It is possible that the amount of VPA in gastrointestinal tract may reach at the concentration of 100 μ M after patients taking high doses of this drug, which may affect the fatty acid biosynthesis in gut microbiome of patients. Research on VPA at the molecular levels should be further studied to reveal the mechanistic action of VPA on changes of fatty acids.

5.1.2 Effects of VPA on biosynthesis of polyketides

From the result, VPA could not diversify secondary metabolite production via mevalonate pathway in the marine-derived fungus *Trichoderma reesei*. This work demonstrated that VPA has effects on the biosynthesis of certain polyketide natural products produced by the fungus *Dothideomycete* sp. As mentioned earlier, fatty acid and polyketide biosynthesis have the similarities of using catalytic elements. Beside the induction or inhibition of fatty acid biosynthesis in microorganisms. VPA it could also affect polyketide biosynthesis in the fungus *Dothideomycete* sp. by inhibiting the production of compound **2** (austdiol), the major compound produced by this fungus, almost 100% inhibition and reducing the production of compound **6** by 50% (approximate). The productions of compounds **3**, **4** and **5** were not affected by VPA.

5.2 Bioactive compounds from *Feroniella lucida* (Scheff.) Swingle

From this work, compounds **7** and **8** were isolated from a crude MeOH extract of spine part. Previous works^{114, 115, 120, 121, 122} reported that compounds **7** and **8** were hordenine and hordenine derivative, respectively. The isolated compounds were evaluated for cancer chemoprevention properties. It was found that compound **8** exhibited weak activity for the xanthine oxidase assay (XXO) with an IC₅₀ value of 473.8±13.4 μM, as shown in Table **23**.

5.3 Bioactive compounds from termite-associated fungus ISFB10

From this work, compounds **9** and **10** were isolated from a broth crude extract. Structure elucidation and the comparison with previous work^{117, 118, 119}, it was found that compounds **9** and **10** were roridin A and verrucarin A, respectively. The isolated compounds were evaluated for biological activities. It was found that compounds **9** exhibited strong cytotoxic activities toward HuCCA-1, A549, MOLT-3 and HepG2 with IC₅₀ values of 0.016±0.0007, 0.0055±0.0001, 0.005±0.0003 and 0.024±0.002 μM, respectively. Compounds **10** also exhibited strong cytotoxic activities toward HuCCA-1, A549, MOLT-3 and HepG2 cancer cell lines with IC₅₀ values of 0.014±0.0005, 0.0047±0.0005, 0.008±0.0002 and 0.019±0.001 μM, respectively.

These two compounds were also evaluated their cytotoxicity toward normal cell lines, MRC-5. Unfortunately, compounds **9** and **10** were also exhibited strong cytotoxic activity toward MRC-5 with IC₅₀ values of 0.038±0.006 and 0.012±0.0004, respectively. Compounds **9** and **10** were macrocyclic trichothecene mycotoxins, and previous reports revealed that they can cause many serious problems to human and animals^{117, 118, 119}.

REFERENCES

1. Lewis JH, et al. Valproate-induced hepatic steatogenesis in rats. *Hepatology*. 1982;2(6):870-3.
2. Becker CM and Harris RA. Influence of valproic acid on hepatic carbohydrate and lipid metabolism. *Archives of biochemistry and biophysics*. 1983;223(2):381-92.
3. Verrotti A, et al. Valproate-Induced Hyperammonemic Encephalopathy. *Metabolic Brain Disease*. 2002;17(4):367-73.
4. Silva MF, et al. Valproic acid metabolism and its effects on mitochondrial fatty acid oxidation: a review. *Journal of Inherited Metabolic Disease*. 2008;31(2):205-16.
5. Aires C, et al. Inhibition of hepatic Carnitine Palmitoyl-Transferase I (CPT IA) by Valproyl-CoA as a possible mechanism of Valproate-induced steatosis. *Biochem Pharmacol*. 2009;79:792-9.
6. Hjelm M, et al. Valproate inhibition of urea synthesis. *Lancet*. 1987;1(8538):923-4.
7. Hjelm M, et al. Valproate-induced inhibition of urea synthesis and hyperammonaemia in healthy subjects. *Lancet*. 1986;2(8511):859.
8. Kataoka S, et al. Autism-like behaviours with transient histone hyperacetylation in mice treated prenatally with valproic acid. *The International Journal of Neuropsychopharmacology*. 2013;16(1):91-103.
9. Sgadò P, et al. Embryonic Exposure to Valproic Acid Impairs Social Predispositions of Newly-Hatched Chicks. *Scientific reports*. 2018;8(1):5919.
10. Sailer L, et al. Consequences of prenatal exposure to valproic acid in the socially monogamous prairie voles. *Scientific reports*. 2019;9(1):2453.
11. Mahmood U, et al. Dendritic spine anomalies and PTEN alterations in a mouse model of VPA-induced autism spectrum disorder. *Pharmacological research*. 2018;128:110-21.
12. Nicolini C and Fahnestock M. The valproic acid-induced rodent model of autism. *Experimental neurology*. 2018;299(Pt A):217-27.
13. Fontes-Dutra M, et al. Abnormal empathy-like pro-social behaviour in the valproic acid model of autism spectrum disorder. *Behavioural brain research*. 2019;364:11-8.
14. Hajisoltani R, et al. Hyperexcitability of hippocampal CA1 pyramidal neurons in male offspring of a rat model of autism spectrum disorder (ASD) induced by prenatal exposure to valproic acid: A possible involvement of Ih channel current. *Brain research*. 2019;1708:188-99.
15. Williams RB, et al. Epigenetic remodeling of the fungal secondary metabolome. *Organic & biomolecular chemistry*. 2008;6(11):1895-7.
16. VanderMolen KM, et al. Epigenetic Manipulation of a Filamentous Fungus by the Proteasome-Inhibitor Bortezomib Induces the Production of an Additional Secondary Metabolite. *RSC advances*. 2014;4(35):18329-35.
17. Li Y, et al. Bortezomib-induced new bergamotene derivatives xylariterpenoids H-K from sponge-derived fungus *Pestalotiopsis maculans* 16F-12. *RSC advances*. 2019;9(2):599-608.
18. Gubiani JR, et al. An epigenetic modifier induces production of (10'S)-verruculide B, an inhibitor of protein tyrosine phosphatases by *Phoma* sp. nov. LG0217, a fungal endophyte of *Parkinsonia microphylla*. *Bioorganic & Medicinal Chemistry*.

2017;25(6):1860-6.

19. El-Hawary SS, et al. Epigenetic Modifiers Induce Bioactive Phenolic Metabolites in the Marine-Derived Fungus *Penicillium brevicompactum*. *Marine Drugs*. 2018;16(8):253.

20. Li G, et al. Epigenetic Modulation of Endophytic *Eupenicillium* sp. LG41 by a Histone Deacetylase Inhibitor for Production of Decalin-Containing Compounds. *Journal of natural products*. 2017;80(4):983-8.

21. Magotra A, et al. Epigenetic modifier induced enhancement of fumiquinazoline C production in *Aspergillus fumigatus* (GA-L7): an endophytic fungus from *Grewia asiatica* L. *AMB Express*. 2017;7(1):43-.

22. Triastuti A, et al. How Histone Deacetylase Inhibitors Alter the Secondary Metabolites of *Botryosphaeria mamane*, an Endophytic Fungus Isolated from *Bixa orellana*, L. *Chemistry & biodiversity*. 2019;16.

23. Zutz C, et al. Fungi Treated with Small Chemicals Exhibit Increased Antimicrobial Activity against Facultative Bacterial and Yeast Pathogens. *BioMed research international*. 2014;2014:540292.

24. Zutz C, et al. Valproic Acid Induces Antimicrobial Compound Production in *Doratomyces microspores*. *Frontiers in microbiology*. 2016;7:510.

25. Phiel C, et al. Histone Deacetylase Is a Direct Target of Valproic Acid, a Potent Anticonvulsant, Mood Stabilizer, and Teratogen. *Journal of Biological Chemistry*. 2001;276:36734-41.

26. Göttlicher M, et al. Valproic acid defines a novel class of HDAC inhibitors inducing differentiation of transformed cells. *The EMBO Journal*. 2001;20(24):6969-78.

27. Heers H, et al. Valproic acid as an adjunctive therapeutic agent for the treatment of breast cancer. *European Journal of Pharmacology*. 2018;835:61-74.

28. Patel MM and Patel BM. Repurposing of sodium valproate in colon cancer associated with diabetes mellitus: Role of HDAC inhibition. *European journal of pharmaceutical sciences : official journal of the European Federation for Pharmaceutical Sciences*. 2018;121:188-99.

29. Killick-Cole C, et al. Repurposing the anti-epileptic drug sodium valproate as an adjuvant treatment for diffuse intrinsic pontine glioma. *PLoS One*. 2017;12:e0176855.

30. Choi J, et al. Role of the histone deacetylase inhibitor valproic acid in high-fat diet-induced hypertension via inhibition of HDAC1/angiotensin II axis. *International journal of obesity (2005)*. 2017;41(11):1702-9.

31. Crosby B and Deas CM. Repurposing medications for use in treating HIV infection: A focus on valproic acid as a latency-reversing agent. *Journal of Clinical Pharmacy and Therapeutics*. 2018;43(5):740-5.

32. Desfossés-Baron K, et al. Valproate inhibits MAP kinase signalling and cell cycle progression in *S. cerevisiae*. *Scientific reports*. 2016;6(1):36013.

33. Yu JI, et al. Valproic Acid Sensitizes Hepatocellular Carcinoma Cells to Proton Therapy by Suppressing NRF2 Activation. *Scientific reports*. 2017;7(1):14986.

34. Caponigro F, et al. Phase II clinical study of valproic acid plus cisplatin and cetuximab in recurrent and/or metastatic squamous cell carcinoma of Head and Neck-V-CHANCE trial. *BMC Cancer*. 2016;16(1):918.

35. Shreiner AB, et al. The gut microbiome in health and in disease. *Current opinion in gastroenterology*. 2015;31(1):69-75.

36. Cani PD. Human gut microbiome: hopes, threats and promises. *Gut*.

2018;67(9):1716-25.

37. Feehley T, et al. Healthy infants harbor intestinal bacteria that protect against food allergy. *Nature Medicine*. 2019;25(3):448-53.
38. Soderborg TK, et al. The gut microbiota in infants of obese mothers increases inflammation and susceptibility to NAFLD. *Nature Communications*. 2018;9(1):4462.
39. Li Y, et al. Gut microbiota dependent anti-tumor immunity restricts melanoma growth in *Rnf5*^{-/-} mice. *Nature Communications*. 2019;10(1):1492.
40. Flowers SA, et al. Interaction Between Atypical Antipsychotics and the Gut Microbiome in a Bipolar Disease Cohort. *Pharmacotherapy*. 2017;37(3):261-7.
41. Forslund K, et al. Disentangling type 2 diabetes and metformin treatment signatures in the human gut microbiota. *Nature*. 2015;528(7581):262-6.
42. Jackson MA, et al. Proton pump inhibitors alter the composition of the gut microbiota. *Gut*. 2016;65(5):749-56.
43. Maier L, et al. Extensive impact of non-antibiotic drugs on human gut bacteria. *Nature*. 2018;555(7698):623-8.
44. Zimmermann M, et al. Mapping human microbiome drug metabolism by gut bacteria and their genes. *Nature*. 2019;570(7762):462-7.
45. Smith S and Tsai SC. The type I fatty acid and polyketide synthases: a tale of two megasynthases. *Natural product reports*. 2007;24(5):1041-72.
46. Dias DA, et al. A historical overview of natural products in drug discovery. *Metabolites*. 2012;2(2):303-36.
47. Kaewpiboon C, et al. Feroniellin A-induced autophagy causes apoptosis in multidrug-resistant human A549 lung cancer cells. *International journal of oncology*. 2014;44(4):1233-42.
48. Um S, et al. The fungus-growing termite *Macrotermes natalensis* harbors bacillaene-producing *Bacillus* sp. that inhibit potentially antagonistic fungi. *Scientific reports*. 2013;3(1):3250.
49. Sidhu HS, et al. Evaluate the effects of long-term valproic acid treatment on metabolic profiles in newly diagnosed or untreated female epileptic patients: A prospective study. *Seizure*. 2017;48:15-21.
50. Jackson MA, et al. Gut microbiota associations with common diseases and prescription medications in a population-based cohort. *Nature Communications*. 2018;9(1):2655.
51. Revill WP, et al. Relationships between fatty acid and polyketide synthases from *Streptomyces coelicolor* A3(2): characterization of the fatty acid synthase acyl carrier protein. *J Bacteriol*. 1996;178(19):5660-7.
52. Chen A, et al. Type II fatty acid and polyketide synthases: deciphering protein-protein and protein-substrate interactions. *Natural product reports*. 2018;35(10):1029-45.
53. Yu D, et al. Type III polyketide synthases in natural product biosynthesis. *IUBMB Life*. 2012;64(4):285-95.
54. Senadeera SP, et al. A novel tricyclic polyketide and its biosynthetic precursor azaphilone derivatives from the endophytic fungus *Dothideomycete* sp. *Organic & biomolecular chemistry*. 2012;10(35):7220-6.
55. Hewage R, et al. One strain-many compounds (OSMAC) method for production of polyketides, azaphilones, and an isochromanone using the endophytic fungus *Dothideomycete* sp. *Phytochemistry*. 2014;108.

56. Wijesekera K, et al. Metabolite diversification by cultivation of the endophytic fungus *Dothideomycete sp.* in halogen containing media: Cultivation of terrestrial fungus in seawater. *Bioorganic & Medicinal Chemistry*. 2017;25(11):2868-77.
57. Supabphol R andTangjitjaroenkun J. Chemical constituents and biological activities of *Zanthoxylum limonella* (Rutaceae): A Review. *Tropical Journal of Pharmaceutical Research*. 2015;13:2119.
58. Hanchinalmath J andLondonkar R. Isolation and identification of a flavone from fruit pulp of *Feronia limonia* linn. 2014;6.
59. Phuwapraisirisan P, et al. Feroniellins A–C, novel cytotoxic furanocoumarins with highly oxygenated C10 moieties from *Feroniella lucida*. *Tetrahedron Letters*. 2006;47(22):3685-8.
60. Phuwapraisirisan P, et al. Feroniellins A–C, three new isomeric furanocoumarins with highly hydroxylated geranyl derived moieties from *Feroniella lucida*. *Tetrahedron Letters*. 2008;49(19):3133-6.
61. Sripisut T, et al. Lucidafuranocoumarins B and C from the twigs of *Feroniella lucida*: Absolute configurations of lucidafuranocoumarin C. *Phytochemistry Letters*. 2012;5(2):309-12.
62. Sripisut T, et al. Chemical constituents from the roots of *Feroniella lucida*. *Journal of Asian natural products research*. 2011;13(6):556-60.
63. Sriyatep T, et al. Two lignans, one alkaloid, and flavanone from the twigs of *Feroniella lucida*. *Tetrahedron*. 2014;70(9):1773-9.
64. Phuwapraisirisan P, et al. Feroniellides A and B, apotirucallane triterpenes with novel cyclic acetals from *Feroniella lucida*. *Tetrahedron Letters*. 2007;48(4):527-30.
65. Phuwapraisirisan P, et al. Feroniellides C-E, new apotirucallane triterpenoids from the stem bark of *Feroniella lucida*. *Natural product research*. 2013;27(8):753-60.
66. Silber J, et al. From discovery to production: Biotechnology of marine fungi for the production of new antibiotics. *Marine Drugs*. 2016;14(7).
67. Da Costa RR andPoulsen M. Mixed-mode transmission shapes termite gut community assemblies. *Trends in Microbiology*. 2018;26(7):557-9.
68. Aanen DK, et al. The evolution of fungus-growing termites and their mutualistic fungal symbionts. *Proceedings of the National Academy of Sciences*. 2002;99(23):14887.
69. Hu H, et al. Fungiculture in Termites Is Associated with a Mycolytic Gut Bacterial Community. *mSphere*. 2019;4(3):e00165-19.
70. Xu X, et al. Diversity, Bacterial Symbionts, and Antimicrobial Potential of Termite-Associated Fungi. *Frontiers in microbiology*. 2020;11:300.
71. Chang J-C, et al. Bioactive Constituents from the Termite Nest-Derived Medicinal Fungus *Xylaria nigripes*. *Journal of natural products*. 2017;80(1):38-44.
72. Chen M-C, et al. Isoprenyl phenolic ethers from the termite nest-derived medicinal fungus *Xylaria fimbriata*. *Journal of Food and Drug Analysis*. 2019;27(1):111-7.
73. Nagam V, et al. Diversity of fungal isolates from fungus-growing termite *Macrotermes barneyi* and characterization of bioactive compound from *Xylaria escharoidea*. *Insect Science*. 2020;n/a(n/a).
74. Beemelmans C, et al. Macrotermycins A–D, Glycosylated Macrolactams from a Termite-Associated *Amycolatopsis sp.* M39. *Organic Letters*. 2017;19(5):1000-3.
75. Kim KH, et al. Natalamycin A, an ansamycin from a termite-associated

- Streptomyces sp. *Chemical Science*. 2014;5(11):4333-8.
76. Carr G, et al. Microtermolides A and B from termite-associated Streptomyces sp. and structural revision of vinylamycin. *Organic Letters*. 2012;14(11):2822-5.
77. Zhang Y-l, et al. Antifungal Activities of Metabolites Produced by a Termite-Associated Streptomyces canus BYB02. *Journal of Agricultural and Food Chemistry*. 2013;61(7):1521-4.
78. Toghueo RMK. Anti-leishmanial and Anti-inflammatory Agents from Endophytes: A Review. *Natural Products and Bioprospecting*. 2019;9(5):311-28.
79. Hao X, et al. Taxol Producing Fungi. In: Ramawat KG, Mérillon J-M, editors. *Natural Products: Phytochemistry, Botany and Metabolism of Alkaloids, Phenolics and Terpenes*. Berlin, Heidelberg: Springer Berlin Heidelberg; 2013. p. 2797-812.
80. Ji Y, et al. Taxol-producing Fungi: A New Approach to Industrial Production of Taxol. *Chinese Journal of Biotechnology*. 2006;22(1):1-6.
81. Chomcheon P, et al. Aromatase inhibitory, radical scavenging, and antioxidant activities of depsidones and diaryl ethers from the endophytic fungus *Corynespora cassiicola* L36. *Phytochemistry*. 2009;70(3):407-13.
82. Gerhäuser C, et al. Mechanism-based in vitro screening of potential cancer chemopreventive agents. *Mutat Res*. 2003;523-524:163-72.
83. Stresser DM, et al. A high-throughput screen to identify inhibitors of aromatase (CYP19). *Anal Biochem*. 2000;284(2):427-30.
84. Chehoud C, et al. Fungal Signature in the Gut Microbiota of Pediatric Patients With Inflammatory Bowel Disease. *Inflammatory bowel diseases*. 2015;21(8):1948-56.
85. Mar Rodríguez M, et al. Obesity changes the human gut mycobiome. *Scientific reports*. 2015;5(1):14600.
86. von Rosenvinge EC, et al. Immune status, antibiotic medication and pH are associated with changes in the stomach fluid microbiota. *The ISME journal*. 2013;7(7):1354-66.
87. Gouba N, et al. Plant and Fungal Diversity in Gut Microbiota as Revealed by Molecular and Culture Investigations. *PLoS One*. 2013;8:e59474.
88. Scanlan PD and Marchesi JR. Micro-eukaryotic diversity of the human distal gut microbiota: qualitative assessment using culture-dependent and -independent analysis of faeces. *The ISME journal*. 2008;2(12):1183-93.
89. Hoffmann C, et al. Archaea and fungi of the human gut microbiome: correlations with diet and bacterial residents. *PLoS One*. 2013;8(6):e66019-e.
90. Nash AK, et al. The gut mycobiome of the Human Microbiome Project healthy cohort. *Microbiome*. 2017;5(1):153.
91. Sokół I, et al. The Prevalence of Yeast and Characteristics of the Isolates from the Digestive Tract of Clinically Healthy Turkeys. *Avian diseases*. 2018;62:286-90.
92. Lucena-Padrós H, et al. Microbial diversity and dynamics of Spanish-style green table-olive fermentations in large manufacturing companies through culture-dependent techniques. *Food Microbiology*. 2014;42:154-65.
93. Gurvitz A, et al. Peroxisomal degradation of trans-unsaturated fatty acids in the yeast *Saccharomyces cerevisiae*. *The Journal of biological chemistry*. 2001;276(2):895-903.
94. Nakamura T, et al. Trans 18-carbon monoenoic fatty acid has distinct effects from its isomeric cis fatty acid on lipotoxicity and gene expression in *Saccharomyces cerevisiae*. *Journal of Bioscience and Bioengineering*. 2017;123(1):33-8.

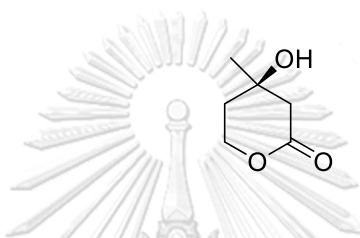
95. Zacherl J, et al. Elaidate, an 18-Carbon trans -Monoenoic Fatty Acid, Inhibits β -Oxidation in Human Peripheral Blood Macrophages. *Journal of cellular biochemistry*. 2014;115.
96. Zacherl J, et al. Elaidate, an 18-Carbon Trans-monoenoic Fatty Acid, but Not Physiological Fatty Acids Increases Intracellular Zn ²⁺ in Human Macrophages. *Journal of cellular biochemistry*. 2014;116.
97. Vaughan E, et al. Diversity, vitality and activities of intestinal lactic acid bacteria and bifidobacteria assessed by molecular approaches. *FEMS Microbiology Reviews* 29 (2005) 3. 2004;29.
98. Balgir PP, et al. *In Vitro* and *In Vivo* Survival and Colonic Adhesion of *Pediococcus acidilactici* MTCC5101 in Human Gut. *BioMed research international*. 2013;2013:583850.
99. Suburu J, et al. Fatty acid metabolism: Implications for diet, genetic variation, and disease. *Food bioscience*. 2013;4:1-12.
100. Dalile B, et al. The role of short-chain fatty acids in microbiota-gut-brain communication. *Nature reviews Gastroenterology & hepatology*. 2019;16(8):461-78.
101. Makki K, et al. The Impact of Dietary Fiber on Gut Microbiota in Host Health and Disease. *Cell Host Microbe*. 2018;23(6):705-15.
102. Gereá AL, et al. Secondary metabolites produced by fungi derived from a microbial mat encountered in an iron-rich natural spring. *Tetrahedron Letters*. 2012;53(32):4202-5.
103. Tayone WC, et al. Stereochemical Investigations of Isochromenones and Isobenzofuranones Isolated from *Leptosphaeria* sp. KTC 727. *Journal of natural products*. 2011;74(3):425-9.
104. Prompanya C, et al. New Polyketides and New Benzoic Acid Derivatives from the Marine Sponge-Associated Fungus *Neosartorya quadricincta* KUFA 0081. *Marine Drugs*. 2016;14(7).
105. Evidente A, et al. Papyracillic Acid, a Phytotoxic 1,6-Dioxaspiro[4,4]nonene Produced by *Ascochyta agropyrina* Var. *nana*, a Potential Mycoherbicide for *Elytrigia repens* Biocontrol. *Journal of Agricultural and Food Chemistry*. 2009;57(23):11168-73.
106. Oliveira L, et al. Antibacterial Activity of Austdiol Isolated from *Mycoleptodiscus indicus* Against *Xanthomonas axonopodis* pv. *Passiflorae*. *Revista Virtual de Química*. 2019;11:596-604.
107. Amagata T, et al. Cytotoxic substances produced by a fungal strain from a sponge: physico-chemical properties and structures. *The Journal of Antibiotics (Tokyo)*. 1998;51(1):33-40.
108. Roy S, et al. An Efficient Asymmetric Route to Tertiary Carbinols: Synthesis of (R)-Mevalonolactone. *Synthesis-stuttgart*. 2007;2007:1082-90.
109. Cimmino A, et al. Papyracillic acid and its derivatives as biting deterrents against *Aedes aegypti* (Diptera: Culicidae): structure–activity relationships. *Medicinal Chemistry Research*. 2015;24(11):3981-9.
110. Könczöl Á, et al. Blood-brain barrier specific permeability assay reveals N-methylated tyramine derivatives in standardised leaf extracts and herbal products of *Ginkgo biloba*. *J Pharm Biomed Anal*. 2016;131:167-74.
111. Shabana M, et al. Phenylalkylamine alkaloids from *Stapelia hirsuta* L. *Natural product research*. 2006;20(8):710-4.
112. Servillo L, et al. Tyramine Pathways in Citrus Plant Defense: Glycoconjugates

- of Tyramine and Its N-Methylated Derivatives. *Journal of Agricultural and Food Chemistry*. 2017;65(4):892-9.
113. Servillo L, et al. N-Methylated Derivatives of Tyramine in Citrus Genus Plants: Identification of N,N,N-Trimethyltyramine (Candicine). *Journal of Agricultural and Food Chemistry*. 2014;62(12):2679-84.
114. Slocum DW and Achermann W. Directed metallation of model adrenaline compounds. *Journal of the Chemical Society, Chemical Communications*. 1974(23):968-9.
115. Chapman NB, et al. The Synthesis, Reactivity, And Pharmacological Properties of some Substituted NN-dimethyl-2-halogeno-2-phenylethylamines, and Related Compounds. *Proceedings of the Royal Society of London Series B, Biological Sciences*. 1965;163(990):116-35.
116. Daly JW, et al. The Chemorelease of Norepinephrine from Mouse Hearts. Structure-Activity Relationships. I. Sympathomimetic and Related Amines. *Journal of Medicinal Chemistry*. 1966;9(3):273-80.
117. Nguyen LTT, et al. Nematicidal activity of verrucarins A and roridin A isolated from *Myrothecium verrucaria* against *Meloidogyne incognita*. *Pesticide Biochemistry and Physiology*. 2018;148:133-43.
118. Märklbauer E, et al. Enzyme immunoassay for the macrocyclic trichothecene roridin A: production, properties, and use of rabbit antibodies. *Applied and Environmental Microbiology*. 1988;54(1):225-30.
119. Kimura M, et al. Molecular and genetic studies of fusarium trichothecene biosynthesis: pathways, genes, and evolution. *Bioscience, Biotechnology, and Biochemistry*. 2007;71(9):2105-23.

Appendix

Part A: Effects of VPA on biosynthesis of fatty acid and polyketides

Physiochemical properties of (*R*)-(-)-Mevalonolactone (**1**) isolated from the marine fungus *Trichoderma reesei*



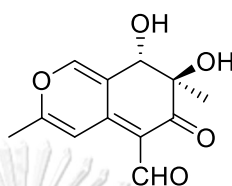
Compound **1** was obtained as yellow liquid (11.7 mg).

ESI-TOF MS: calcd. for $C_6H_{12}O_3$, m/z 131.0708 ($M+H$)⁺, found 131.0713.

UV (MeOH) λ_{max} (log ϵ): 203.50 (2.67) nm.

IR (UATR) ν_{max} : 3425, 2970, 2925, 2150, 1704, 1542, 1473, 1402, 1341, 1305, 1264, 1239, 1159, 1129, 1070, 1024, 987, 970, 935, 906, 882, 829, 805, 760, 723, 662, 675 cm^{-1} .

Physiochemical properties of the isolated compounds from the endophytic fungus *Dothideomycete sp.*

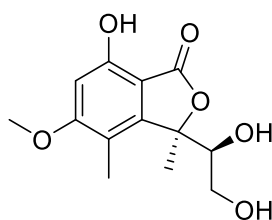


Compound **2** was obtained as brown-red solid (17 mg).

ESI-TOF MS: calcd. for $C_{12}H_{12}O_5Na$, m/z . 259.0582 ($M+Na$)⁺, found 259.0577.

UV (MeOH) λ_{max} (log ϵ): 378.50 (3.73), 255.50 (3.52), 203.50 (3.38) nm.

IR (UATR) ν_{max} : 3474, 3379, 3102, 2924, 2850, 2148, 1734, 1680, 1623, 1605, 1541, 1473, 1434, 1413, 1390, 1351, 1322, 1287, 1260, 1236, 1216, 1198, 1173, 1148, 1128, 1095, 1070, 1044, 1008, 973, 931, 880, 852, 808, 759, 734 cm^{-1} .



Compound **3** was obtained as yellow amorphous semi-solid (7.1 mg).

ESI-TOF MS: calcd. for $C_{13}H_{16}O_6Na$, m/z 291.0845 ($M+Na$)⁺, found 291.0838.

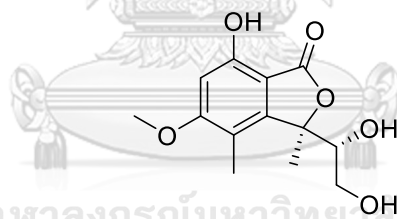
UV (MeOH) λ_{max} (log ϵ): 299.5 (3.76), 259.5 (4.03), 217.0 (4.36) nm.

IR (UATR) ν_{max} : 3749, 3460, 3100, 2946, 1751, 1611, 1457, 1395, 1317, 1219, 1145, 1100, 1039, 994, 921, 899, 836, 720, 689 cm^{-1} .

Optical rotation: $[\alpha]_D^{27.1}$ -31.6 (0.22, CH_3CN)

Optical rotation: $[\alpha]_D^{27.1}$ -38.1 (0.22, $CHCl_3$)

CD: (0.00123 mM, CH_3CN) λ_{max} ($\Delta\epsilon$) 304 (-2.6), 249 (-2.6), 222 (-2.4) nm



Compound **4** was obtained as yellow amorphous semi-solid (12.8 mg).

ESI-TOF MS: calcd. for $C_{13}H_{16}O_6Na$, m/z 291.0845 ($M+Na$)⁺, found 291.0839.

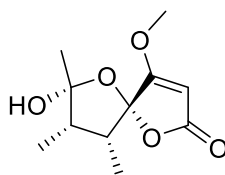
UV (MeOH) λ_{max} (log ϵ): 298.5 (4.07), 259.0 (4.34), 216.0 (4.65) nm.

IR (UATR) ν_{max} : 3749, 3394, 2941, 1717, 1615, 1457, 1369, 1315, 1236, 1217, 1148, 1088, 1055, 924, 837, 796, 736, 689 cm^{-1} .

Optical rotation: $[\alpha]_D^{27.2}$ +13.9 (0.25, CH_3CN)

Optical rotation: $[\alpha]_D^{27.1}$ +38.9 (0.25, $CHCl_3$)

CD: (0.00139 mM, CH_3CN) λ_{max} ($\Delta\epsilon$) 304 (-2.2), 289 (-2.2), 265 (-2.5), 206 (-1.5) nm.



Compound **5** was obtained as yellow amorphous semi-solid (4.8 mg).

ESI-TOF MS: calcd. for $C_{11}H_{16}O_5Na$, m/z 251.0895 ($M+Na$)⁺, found 251.0883.

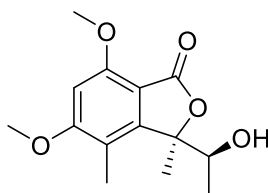
UV (MeOH) λ_{max} ($\log \epsilon$): 223.0 (3.75) nm.

IR (UATR) ν_{max} : 3396, 3121, 2963, 2932, 1758, 1737, 1642, 1456, 1377, 1275, 1254, 1218, 1140, 1063, 1033, 947, 871 cm^{-1} .

Optical rotation: $[\alpha]_D^{27.2}$ -22.8 (0.49, CH_3CN)

Optical rotation: $[\alpha]_D^{27.1}$ -20.7 (0.49, $CHCl_3$)

CD: (0.00128 mM, CH_3CN) λ_{max} ($\Delta\epsilon$) 248 (-3.7), 226 (-2.1) nm.



Compound **6** was obtained as yellow amorphous semi-solid (5.7 mg).

ESI-TOF MS: calcd. for $C_{14}H_{18}O_5Na$, m/z 289.1052 ($M+Na$)⁺, found 289.1020.

UV (MeOH) λ_{max} (log ϵ): 299.0 (3.32), 260.5 (3.50), 221.0 (3.81) nm.

IR (UATR) ν_{max} : 3419, 2936, 2873, 1726, 1600, 1501, 1458, 1437, 1374, 1355, 1318, 1250, 1217, 1184, 1146, 1054, 1007, 942, 894, 847, 822, 720 cm^{-1} .

Optical rotation: $[\alpha]^{27.4}_D$ -9.0 (0.14, CH_3CN)

Optical rotation: $[\alpha]^{25.5}_D$ -18.0 (0.14, $CHCl_3$)

CD: (0.00105 mM, CH_3CN) λ_{max} ($\Delta\epsilon$) 294 (-2.4), 235 (-2.3) nm.

Table A1 Composition of potato dextrose (PDB) culture medium

Ingredients	Amount
Potatoes	200 g
Dextrose	20 g
Deionized water	1000 ml

Table A2 Composition of yeast malt (YM) culture medium

Ingredients	Amount
Yeast extract	3 g
Malt extract	3 g
Peptone	5 g
Glucose	10 g
Deionized water	1000 ml

Table A3 Composition of MRS culture medium

Ingredients	Amount
Proteose Peptone No.3	10 g
Beef extract	10 g
Yeast extract	5 g
Dextrose	20 g
Polysorbate 80	1 g
Ammonium Citrate	2 g
Sodium Acetate	5 g
Magnesium Sulfate	0.1 g
Manganese Sulfate	0.05 g
Dipotassium Phosphate	2 g
Deionized water	1000 ml

Table A4 Composition of nutrient (NA) culture medium

Ingredients	Amount
Peptone	5
Beef extract	3
Deionized water	1000 ml

Table A5 Composition of nutrient Glucose Yeast Peptone broth (GYP) culture medium

Ingredients	Amount
Glucose	25
Yeast extract	3
Peptone	5
Deionized water	1000 ml

Table A6 Weight of dried cells and hexane extracts of fungi

Condition	Dried weight (g)	Crude hexane extract (mg)
<i>Fusarium oxysporum</i> control	7.33	14.40
<i>Fusarium oxysporum</i> 100 μ M valproic acid	3.86	3.16
<i>Aspergillus aculeatus</i> control	7.61	19.03
<i>Aspergillus aculeatus</i> 100 μ M valproic acid	7.40	19.43
<i>Xylaria globosa</i> control	3.66	41.70
<i>Xylaria globosa</i> 100 μ M valproic acid	3.39	34.63
<i>Cordyceps militaris</i> control	3.88	140.60
<i>Cordyceps militaris</i> 100 μ M valproic acid	3.46	86.26
<i>Aureobasidium pullulans</i> control	3.79	49.76
<i>Aureobasidium pullulans</i> 100 μ M valproic acid	3.56	47.56
<i>Phialemonium sp.</i> control	3.77	31.46
<i>Phialemonium sp.</i> 100 μ M valproic acid	3.10	18.33
<i>Cladosporium sp.</i> control	6.67	46.60
<i>Cladosporium sp.</i> 100 μ M valproic acid	8.27	18.36
<i>Penicillium shearii</i> control	3.25	46.43
<i>Penicillium shearii</i> 100 μ M valproic acid	3.57	49.40
<i>Aspergillus flavipes</i> control	5.98	62.76
<i>Aspergillus flavipes</i> 100 μ M valproic acid	4.31	15.96

Table A7 Weight of dried cells and hexane extracts of yeast

Condition	Dried weight (g)	Crude hexane extract (mg)
<i>Saccharomyces cerevisiae</i> control	2.60	8.56
<i>Saccharomyces cerevisiae</i> 100 μ M valproic acid	2.79	10.0
<i>Candida utilis</i> control	2.77	3.23
<i>Candida utilis</i> 100 μ M valproic acid	2.66	2.90
<i>Lachancea thermotolerans</i> control	2.73	11.53
<i>Lachancea thermotolerans</i> 100 μ M valproic acid	2.77	10.30
<i>Candida butyri</i> control	2.04	1.43
<i>Candida butyri</i> 100 μ M valproic acid	1.88	2.13
<i>Candida catenulata</i> control	2.27	2.46
<i>Candida catenulate</i> 100 μ M valproic acid	2.37	1.36
<i>Saccharomyces ludwigii</i> control	2.13	2.10
<i>Saccharomyces ludwigii</i> 100 μ M valproic acid	2.29	4.86

Table A8 Weight of dried cells and hexane extracts of bacteria

Condition	Dried weight (g)	Crude hexane extract (mg)
<i>Pediococcus acidilactici</i> control	112.36	758.0
<i>Pediococcus acidilactici</i> 100 μ M valproic acid	144.0	759.8
<i>Bacillus amyloliquefaciens</i> control	39.93	293.0
<i>Bacillus amyloliquefaciens</i> 100 μ M valproic acid	33.16	270.0
<i>Acetobacter cerevisiae</i> control	79.16	668.7
<i>Acetobacter cerevisiae</i> 100 μ M valproic acid	57.93	520.0

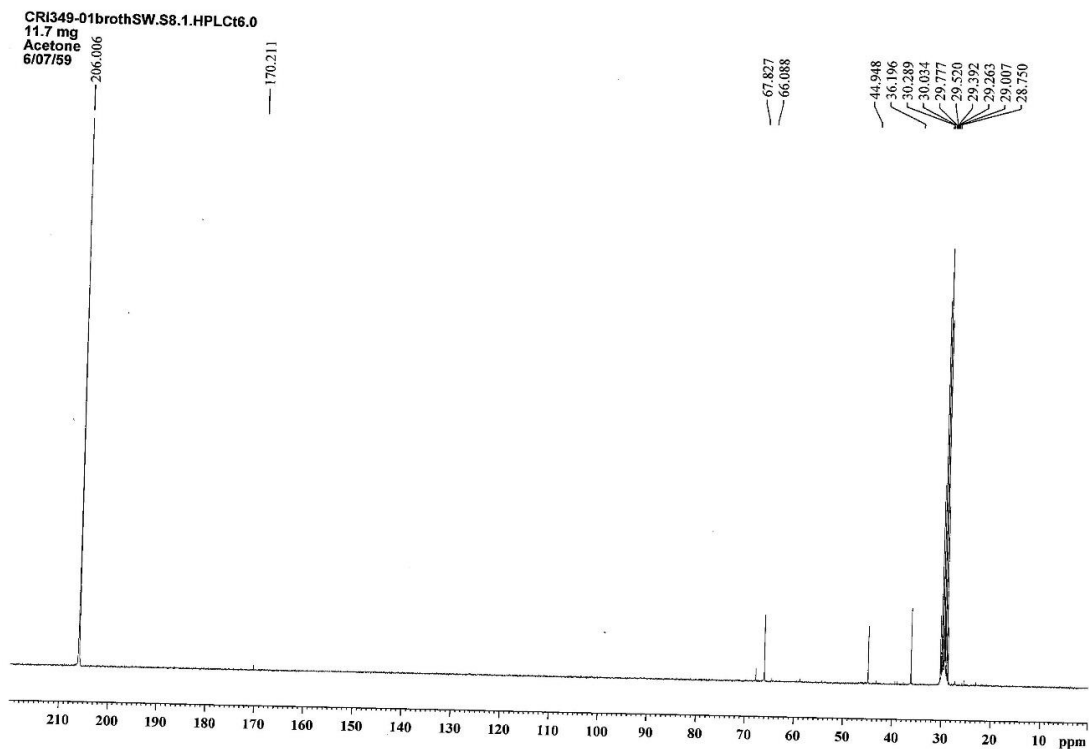
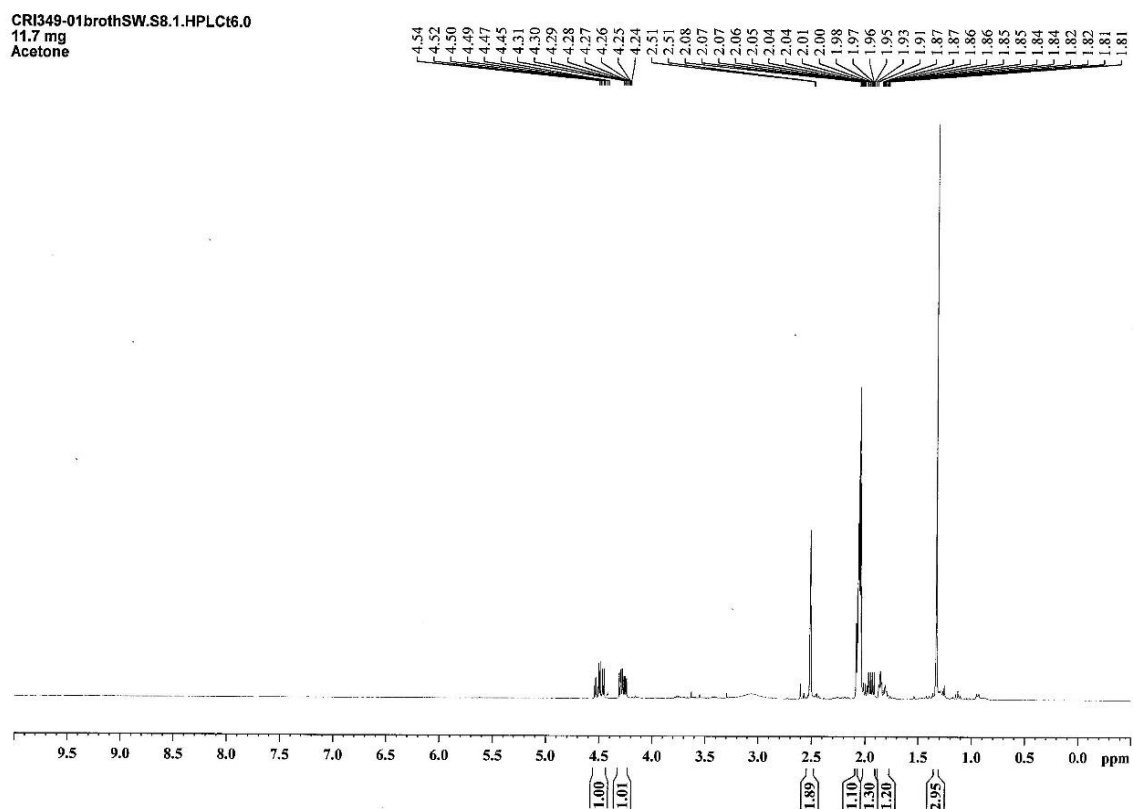
Figure A1 ^1H NMR spectrum (400 MHz, in acetone- d_6) of compound 1Figure A2 ^{13}C NMR spectrum (400 MHz, in acetone- d_6) of compound 1

Figure A3 DEPT 135 (top) and DEPT 90 (bottom) NMR spectrum (400 MHz, in acetone- d_6) of compound **1**

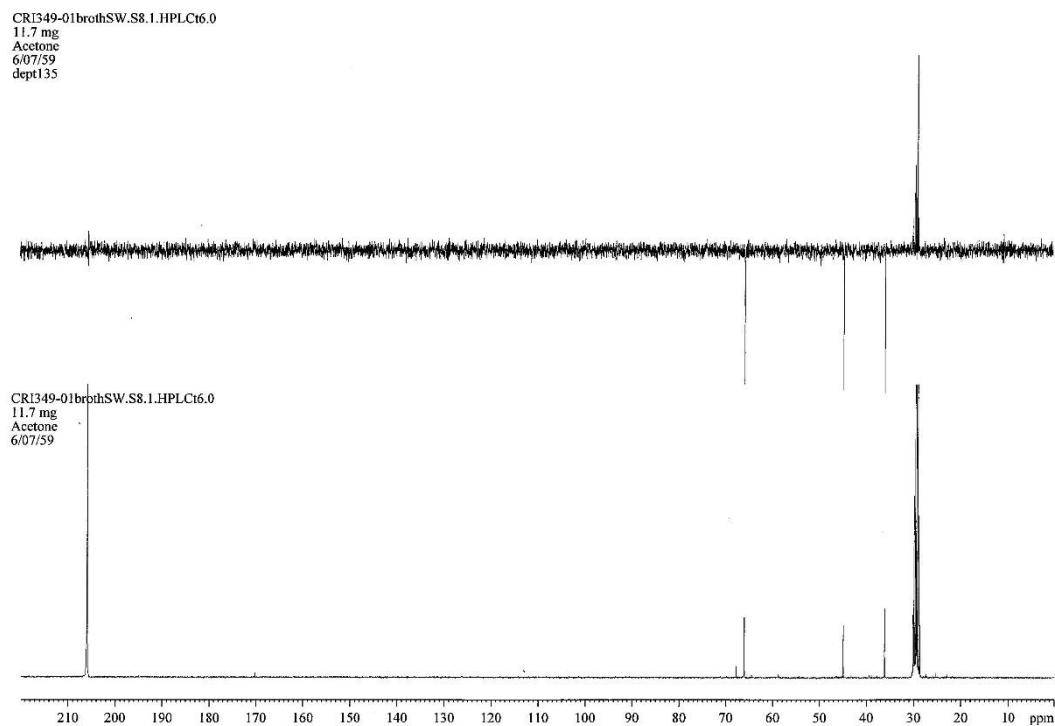


Figure A4 HSQC NMR spectrum (400 MHz, in acetone- d_6) of compound **1**

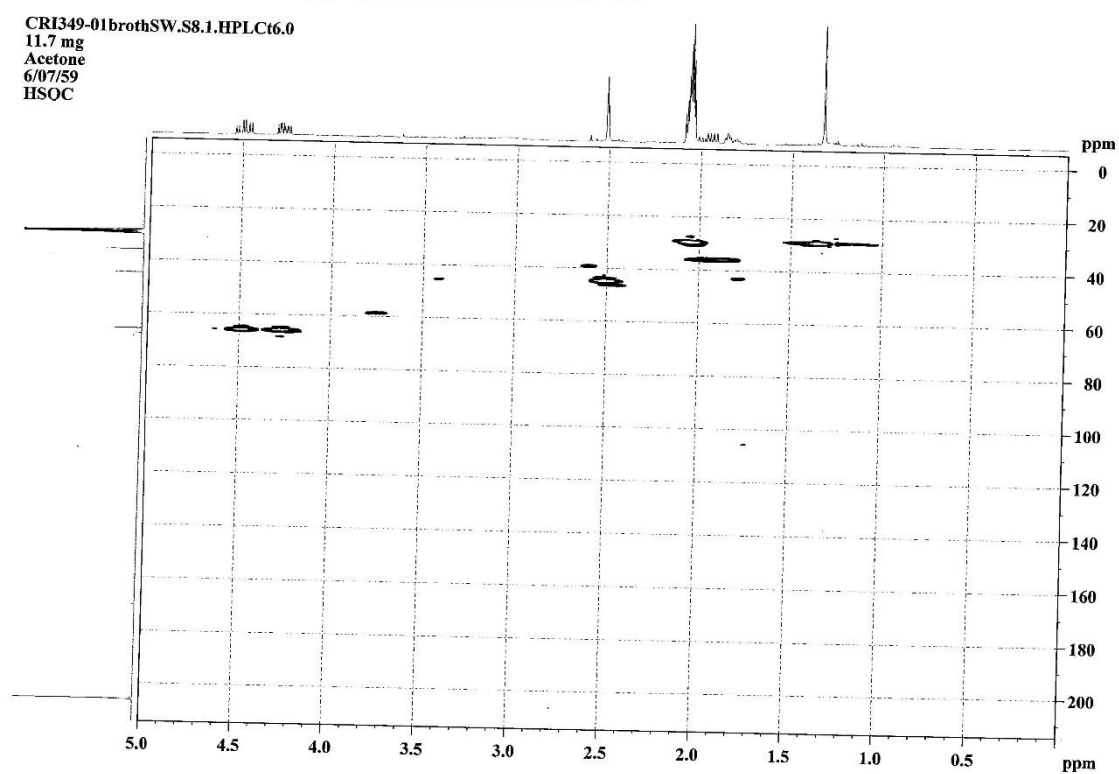


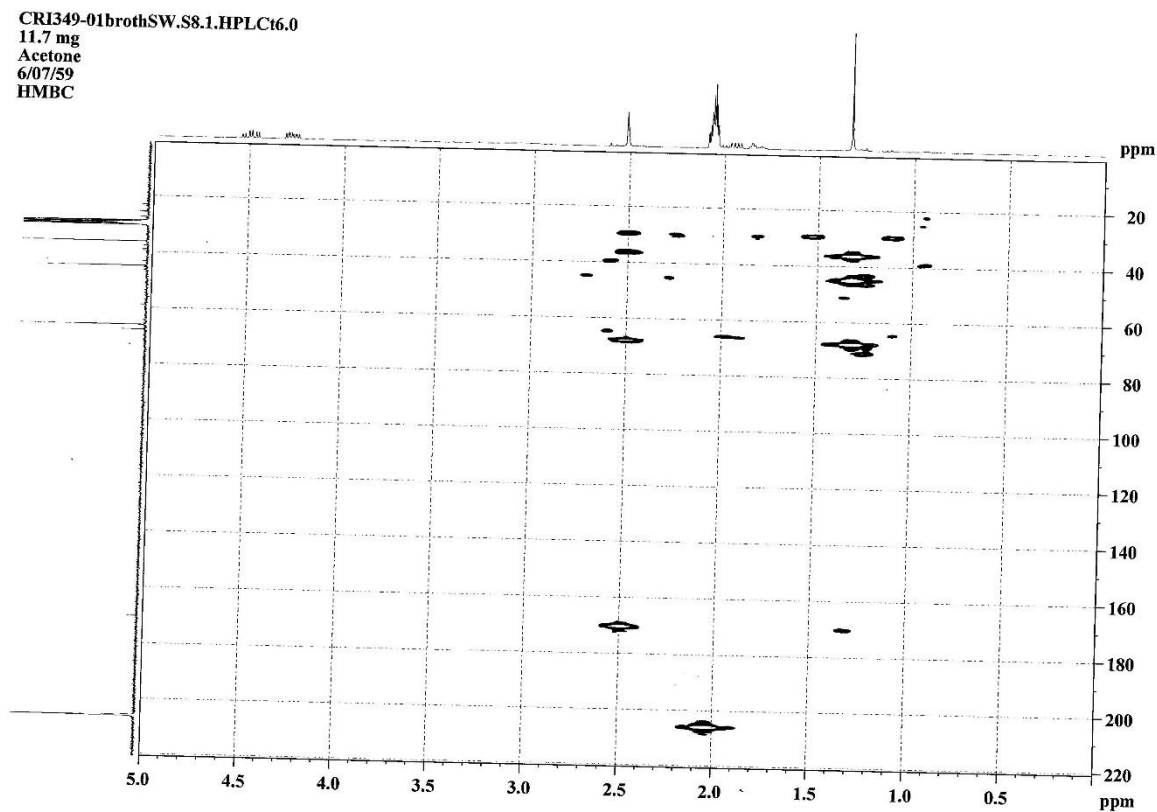
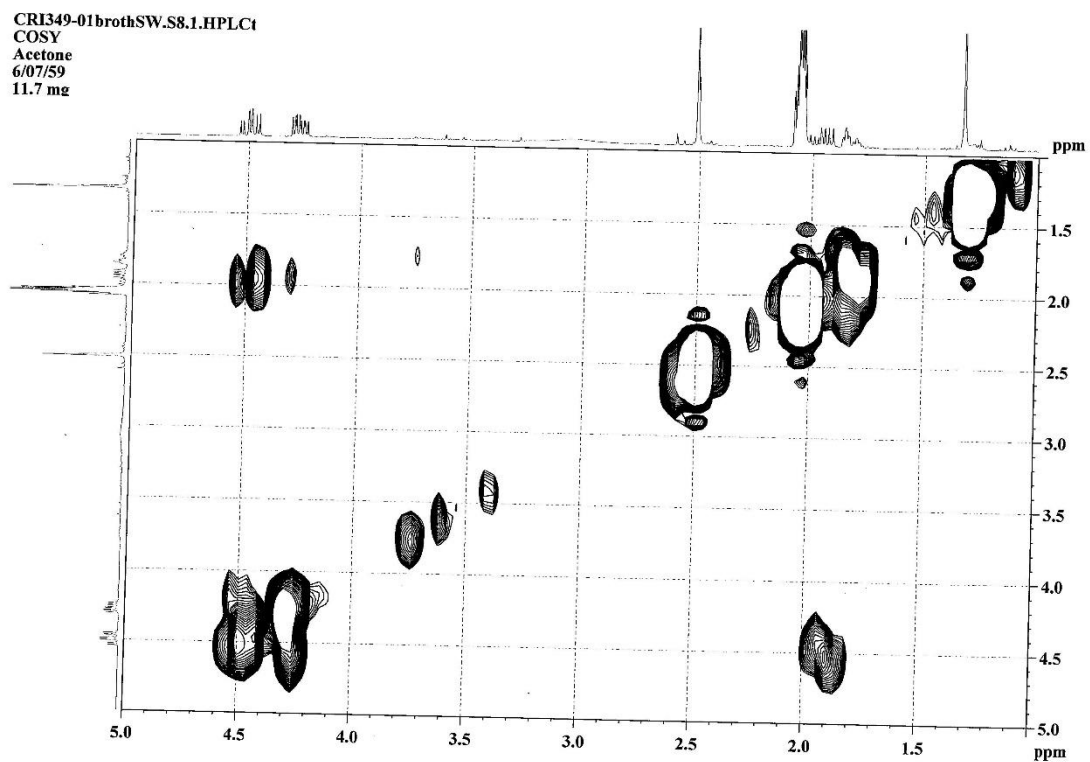
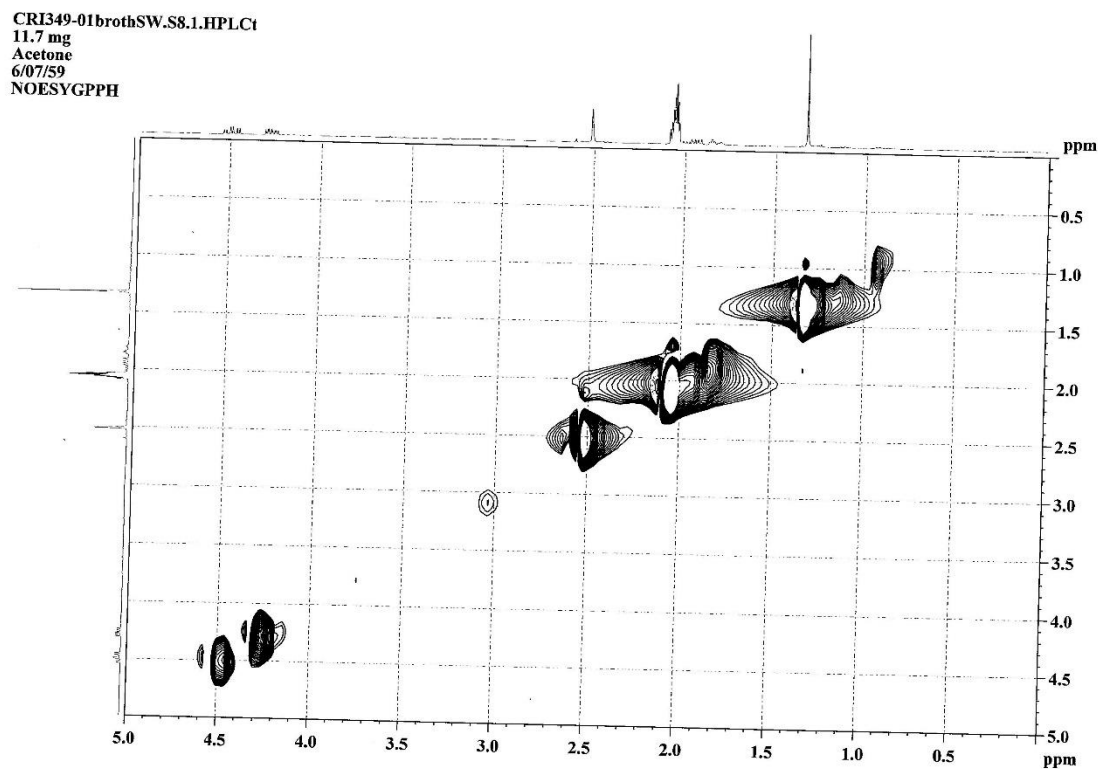
Figure A5 HMBC NMR spectrum (400 MHz, in acetone- d_6) of compound **1**Figure A6 ^1H - ^1H COSY NMR spectrum (400 MHz, in acetone- d_6) of compound **1**

Figure A7 NOESY NMR spectrum (400 MHz, in acetone- d_6) of compound **1**Figure A8 MS spectrum of compound **1**

จุฬาลงกรณ์มหาวิทยาลัย
CHULALONGKORN UNIVERSITY

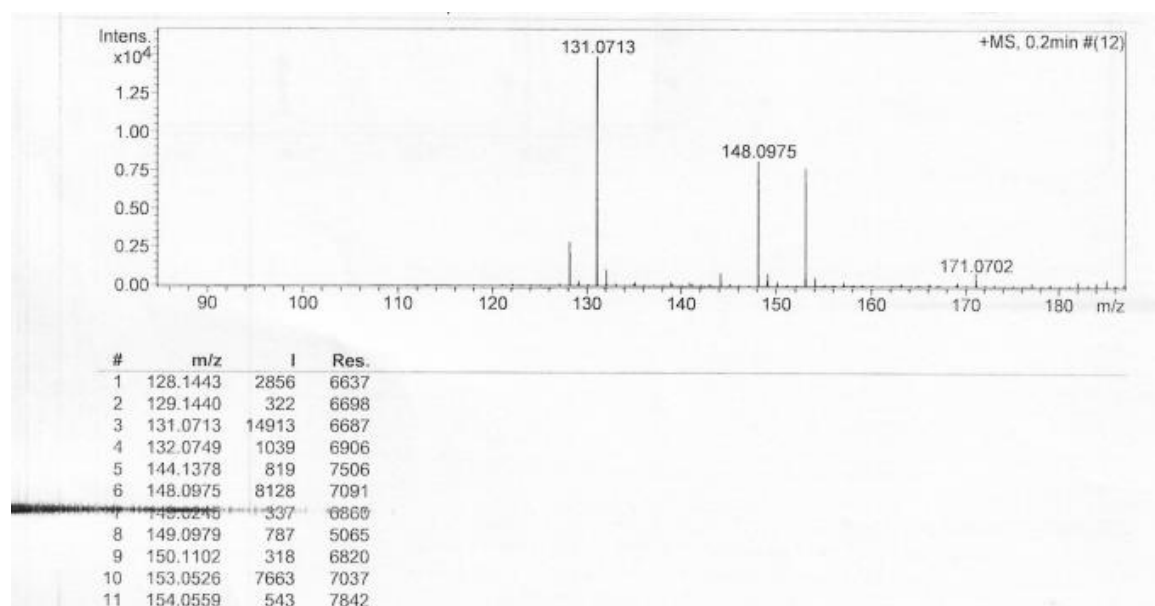


Figure A9 UV spectrum of compound 1

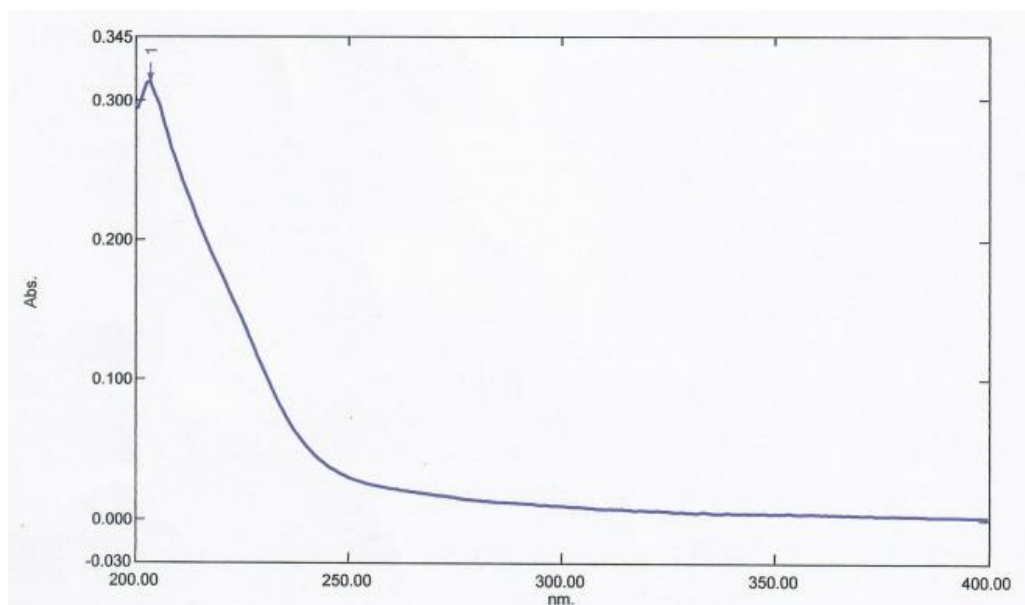


Figure A10 IR spectrum of compound 1

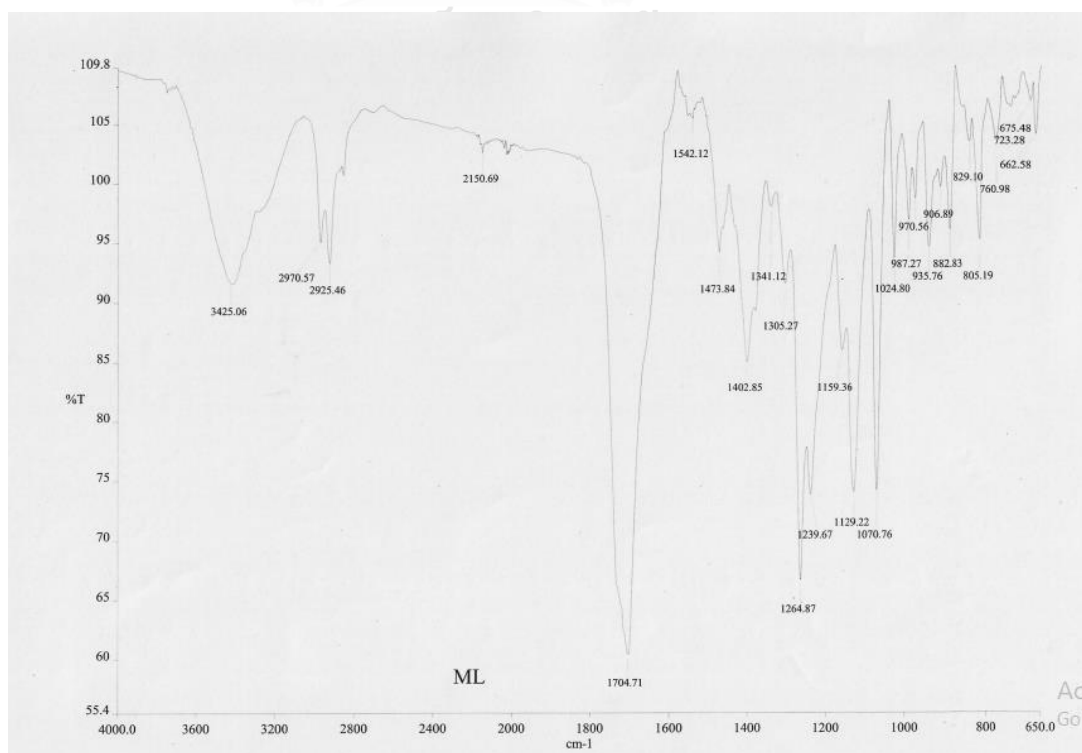


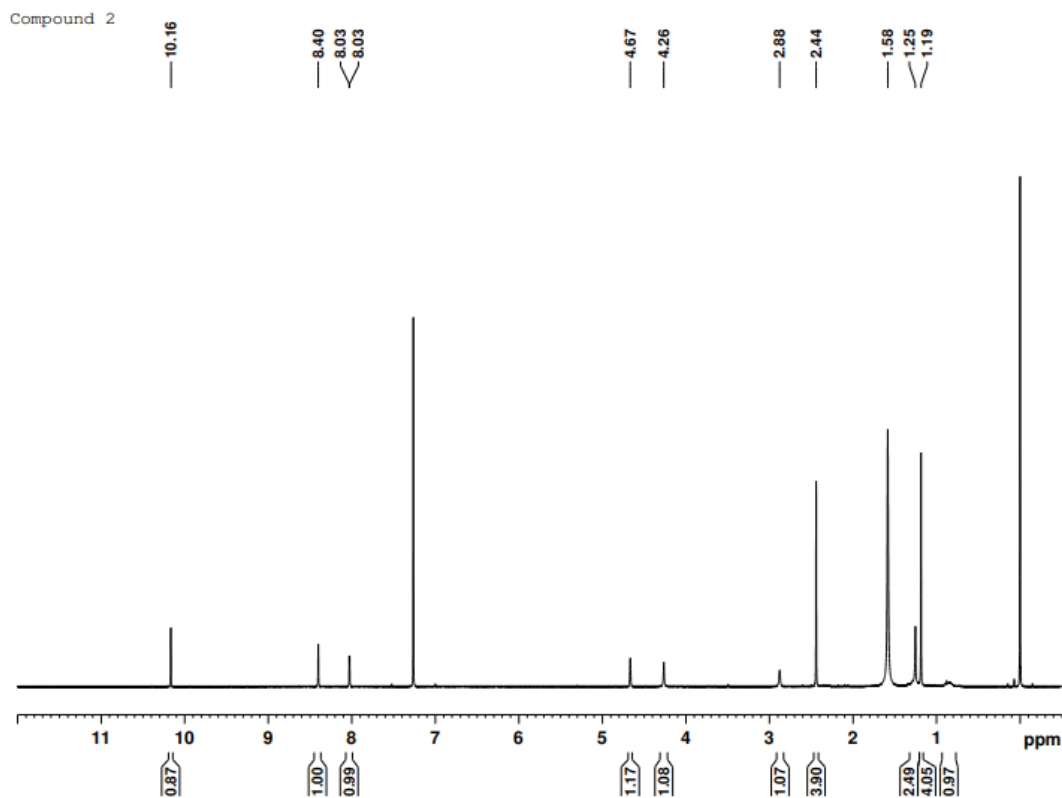
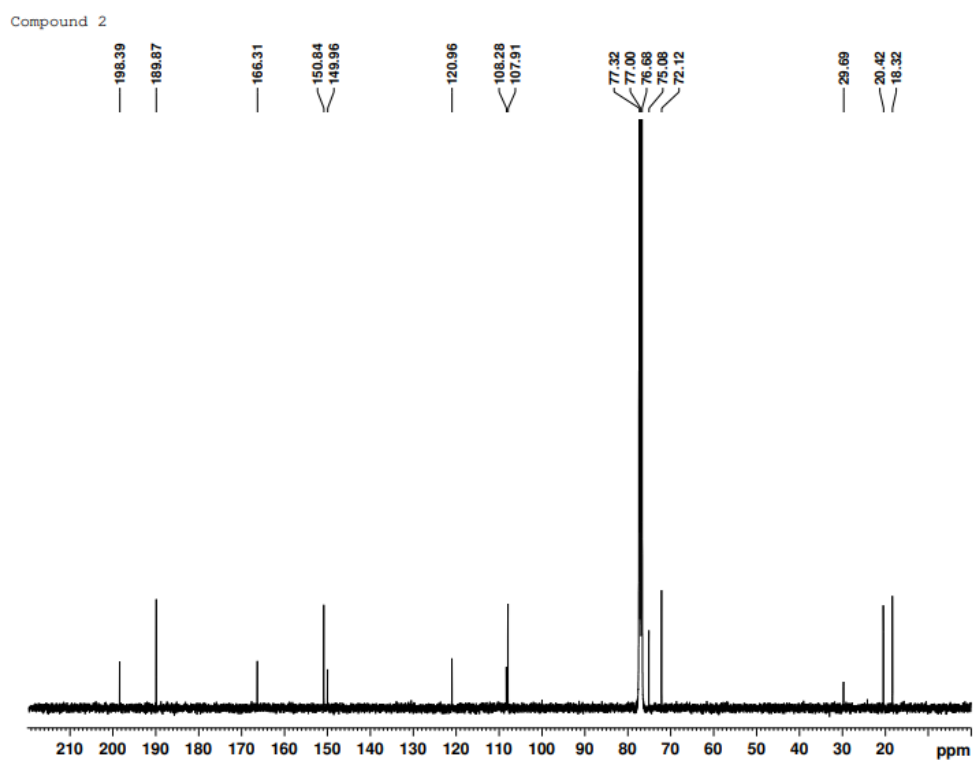
Figure A11 ^1H NMR spectrum (400 MHz, in CDCl_3) of compound 2Figure A12 ^{13}C NMR spectrum (400 MHz, in CDCl_3) of compound 2

Figure A13 DEPT 135 (middle) and DEPT 90 (top) NMR spectrum (400 MHz, in CDCl_3) of compound **2**

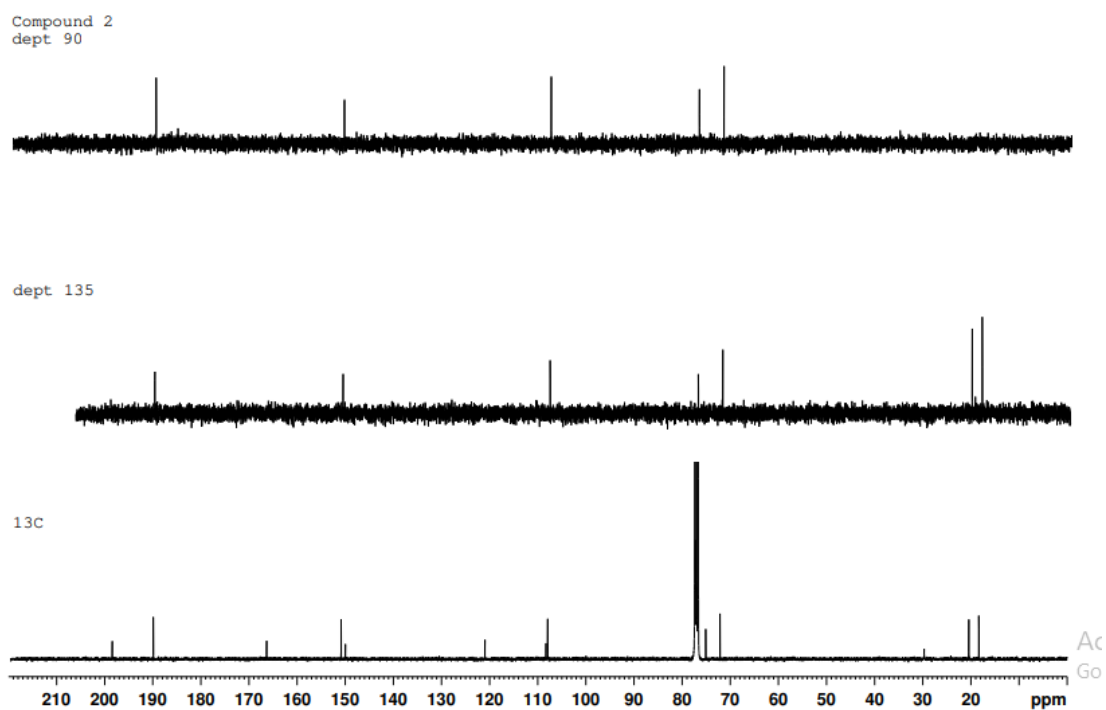


Figure A14 HSQC NMR spectrum (400 MHz, in CDCl_3) of compound **2**

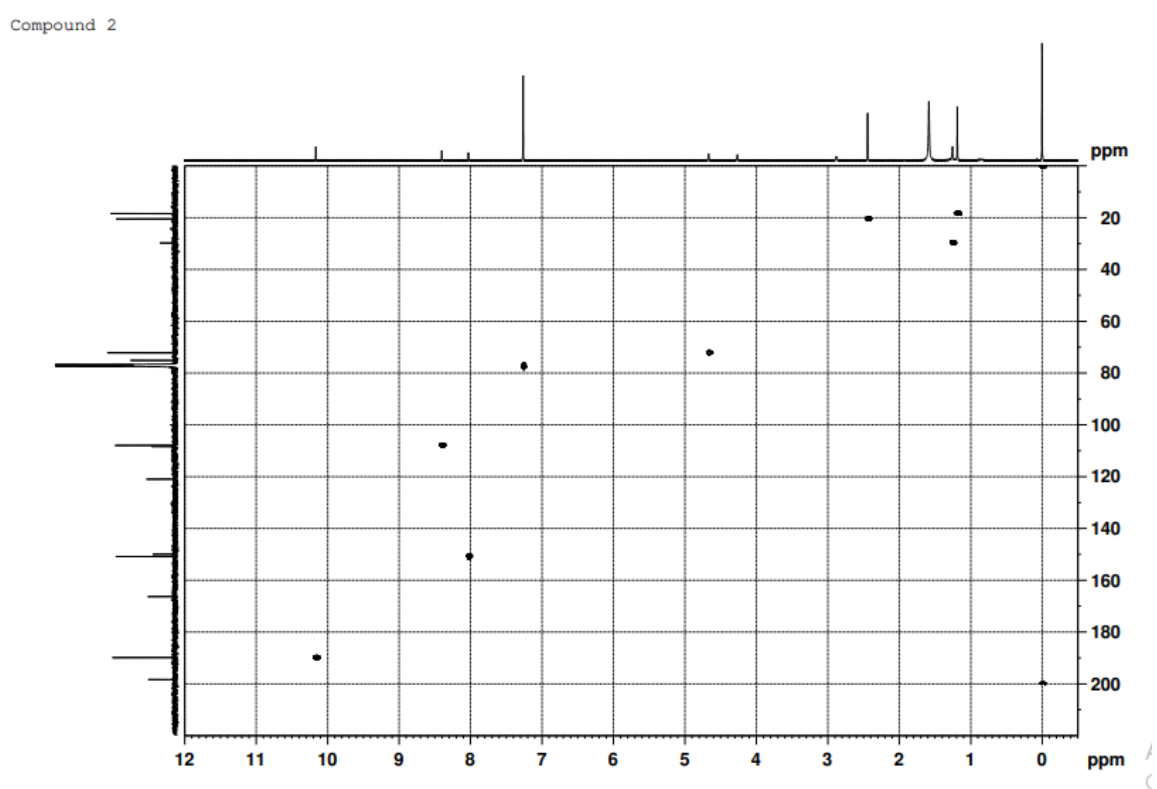


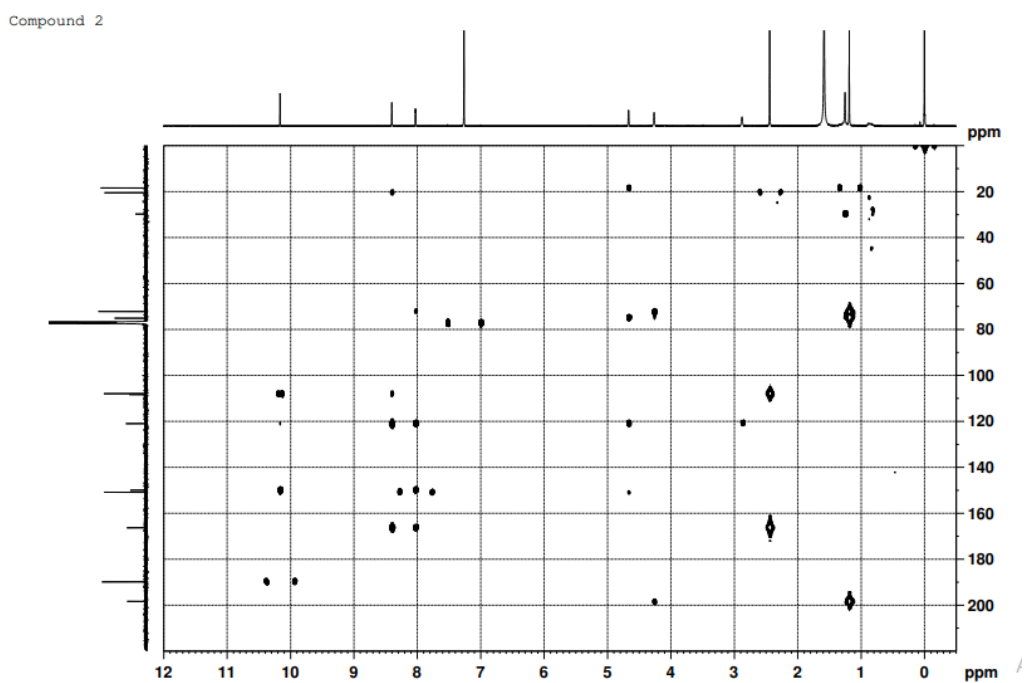
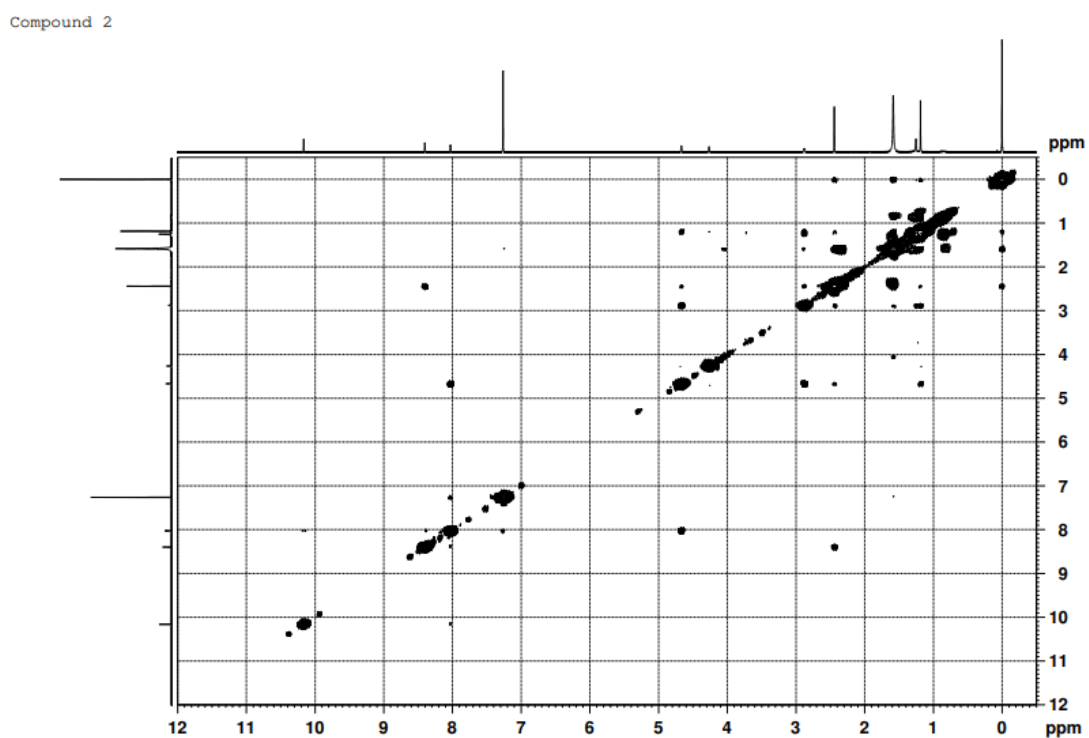
Figure A15 HMBC NMR spectrum (400 MHz, in CDCl₃) of compound 2Figure A16 ¹H-¹H COSY NMR spectrum (400 MHz, in CDCl₃) of compound 2

Figure A19 UV spectrum of compound 2

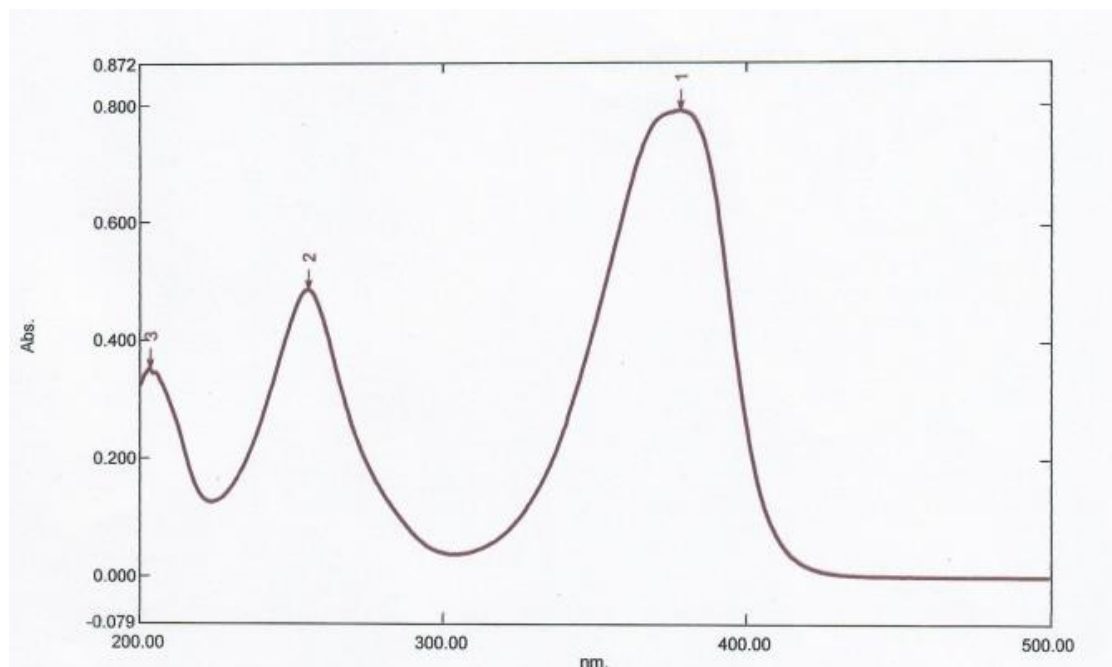


Figure A20 IR spectrum of compound 2

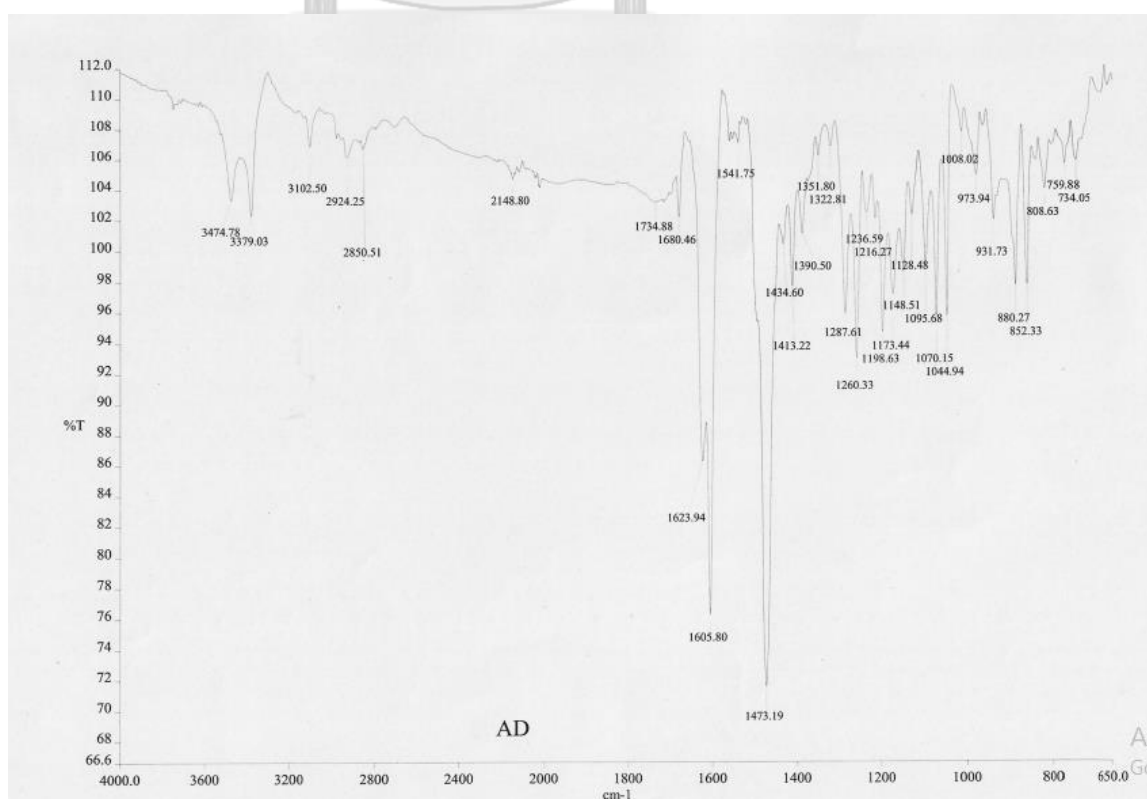


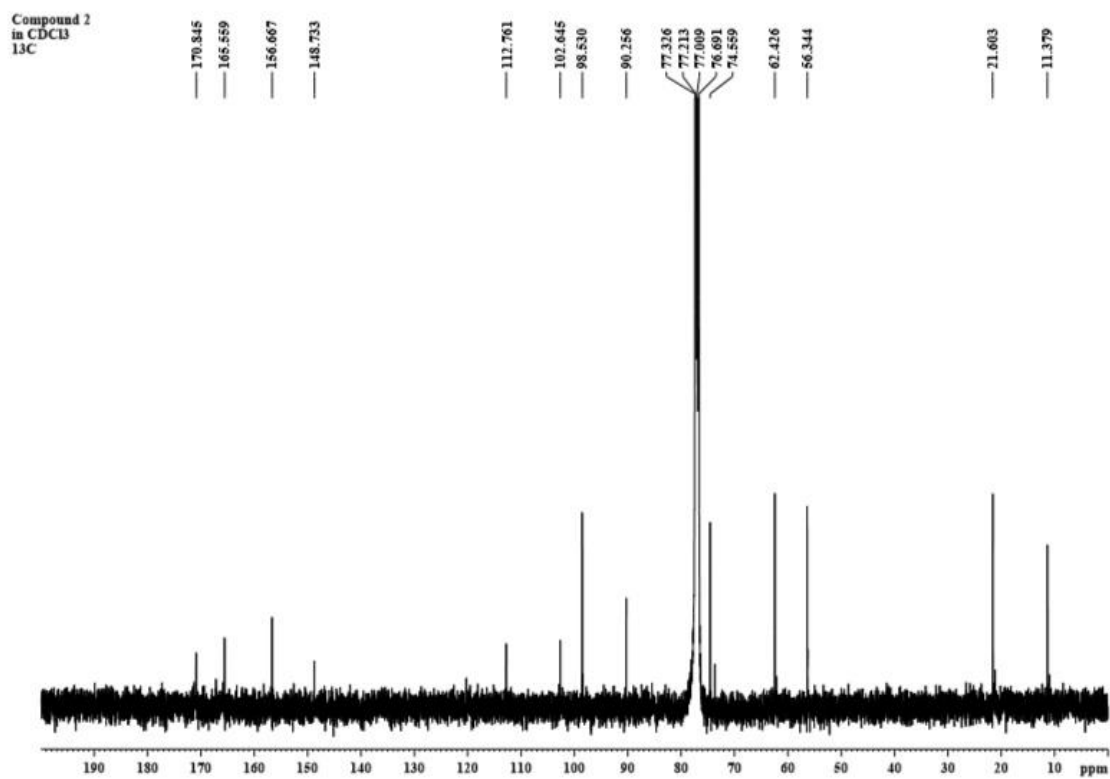
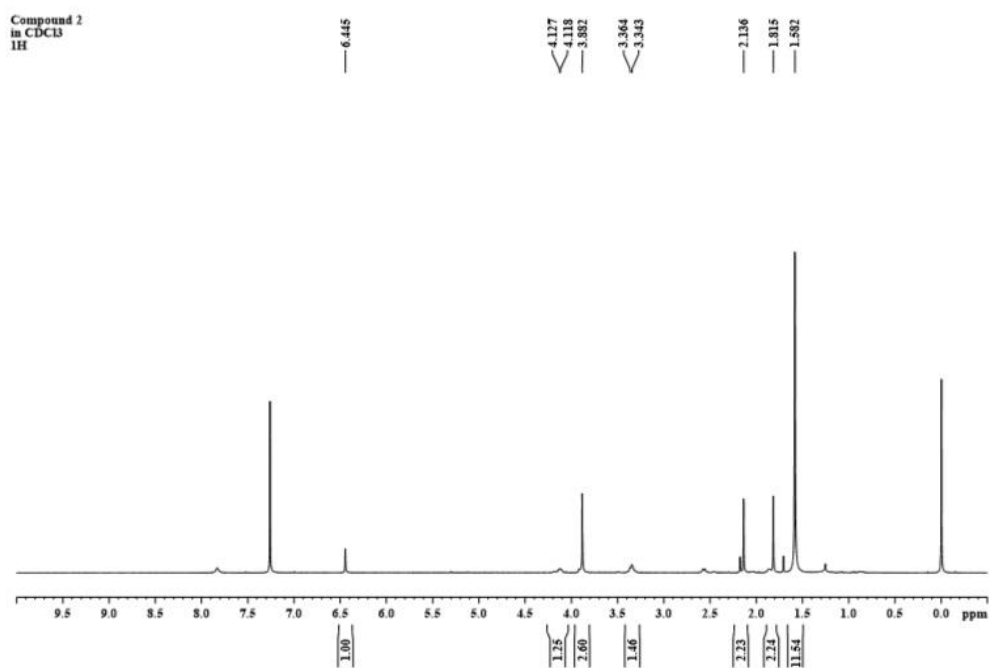
Figure A21 ^1H NMR spectrum (400 MHz, in CDCl_3) of compound 3Figure A22 ^{13}C NMR spectrum (400 MHz, in CDCl_3) of compound 3

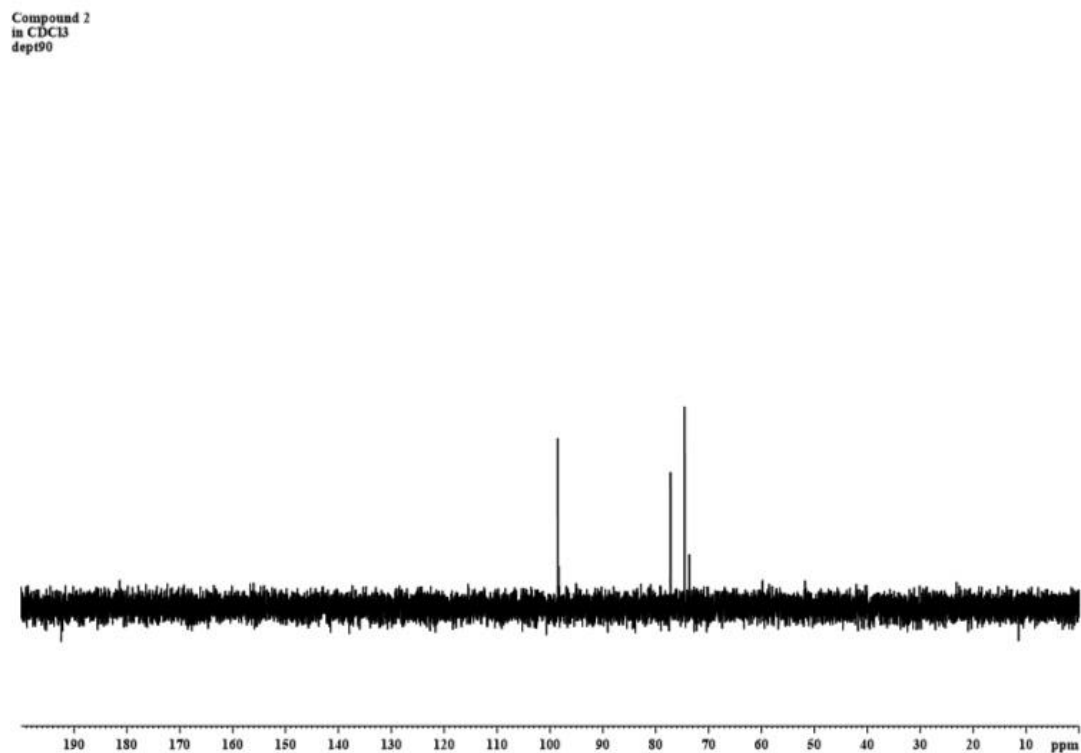
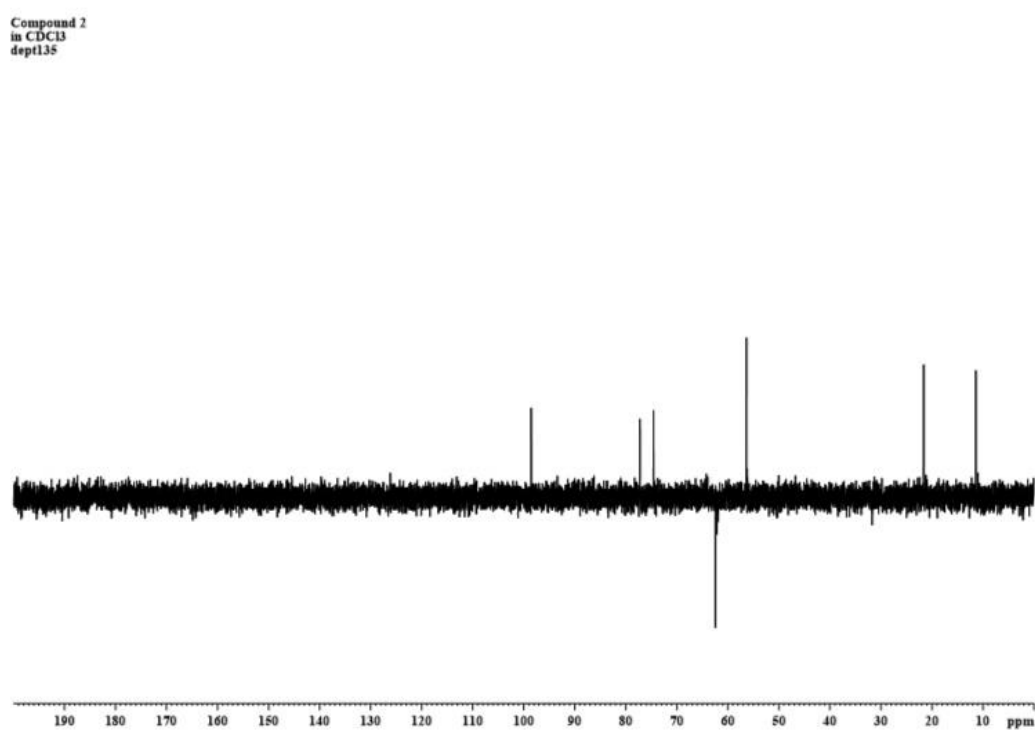
Figure A23 DEPT 135 NMR spectrum (400 MHz, in CDCl₃) of compound **3**Figure A24 DEPT 90 NMR spectrum (400 MHz, in CDCl₃) of compound **3**

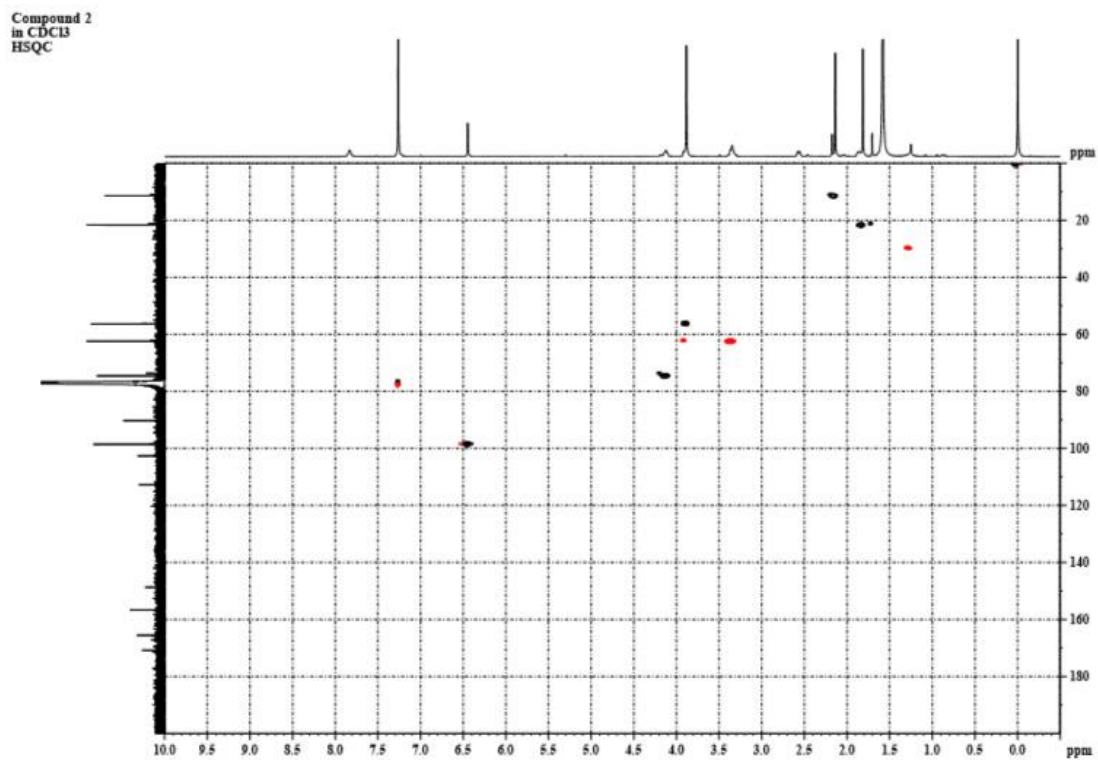
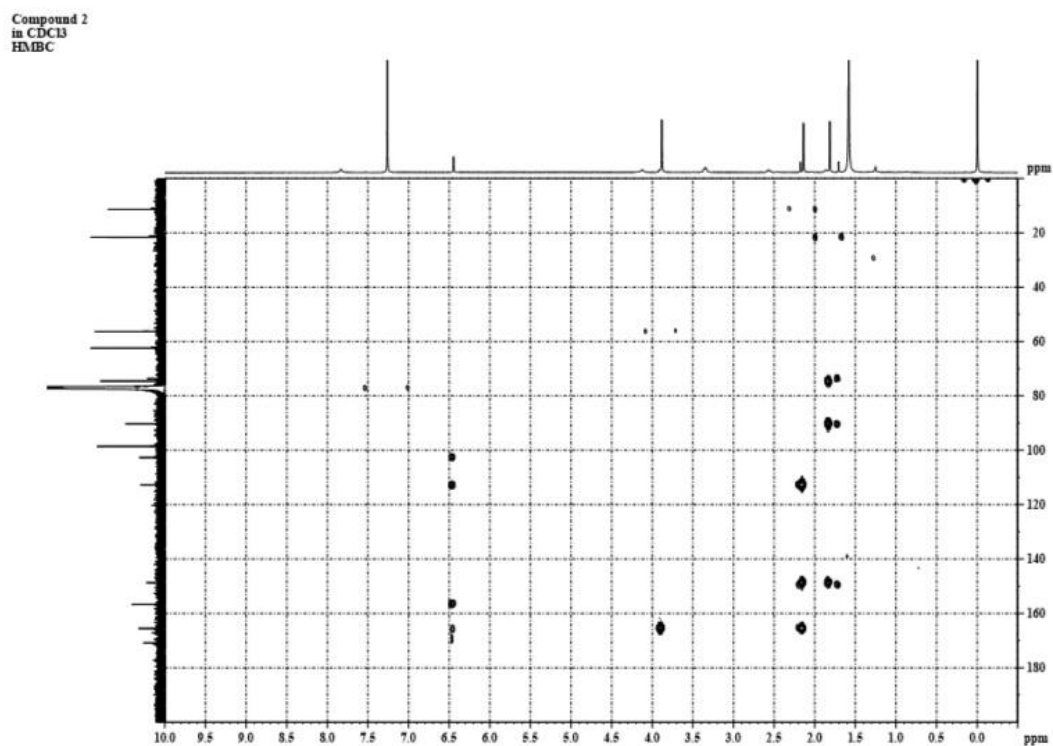
Figure A25 HSQC NMR spectrum (400 MHz, in CDCl₃) of compound 3Figure A26 HMBC NMR spectrum (400 MHz, in CDCl₃) of compound 3

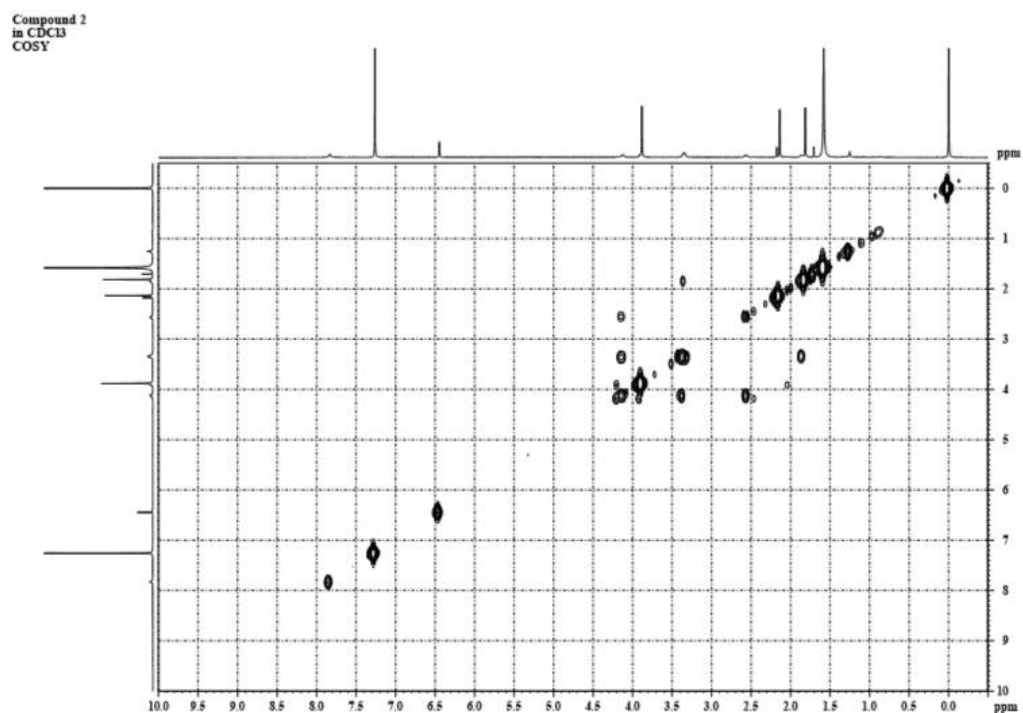
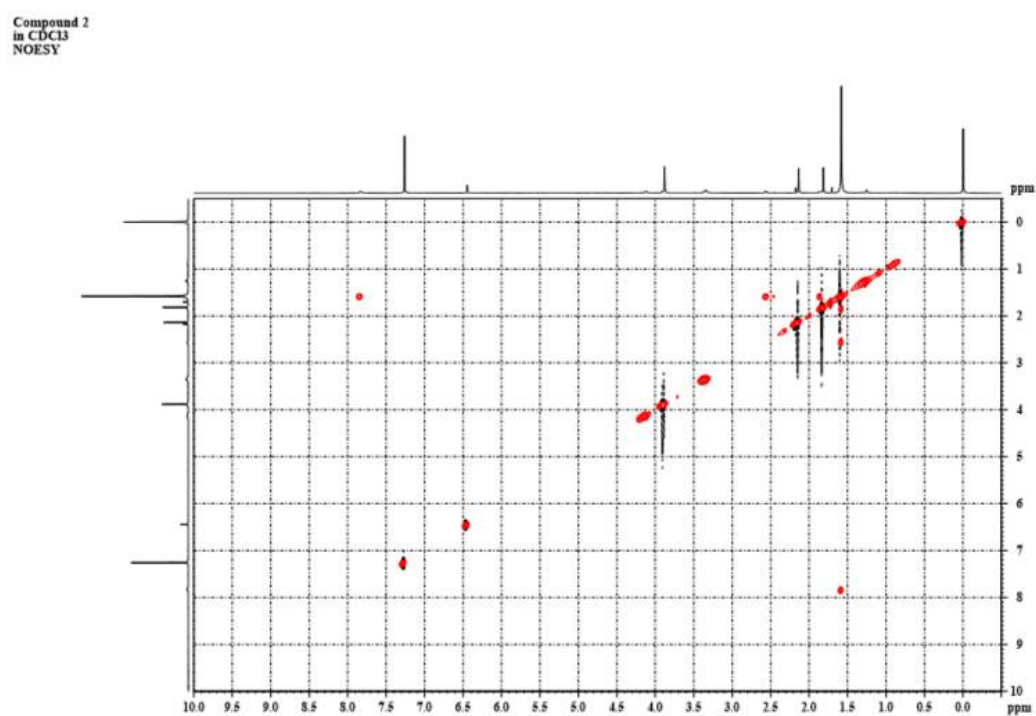
Figure A27 ^1H - ^1H COSY NMR spectrum (400 MHz, in CDCl_3) of compound 3Figure A28 NOESY NMR spectrum (400 MHz, in CDCl_3) of compound 3

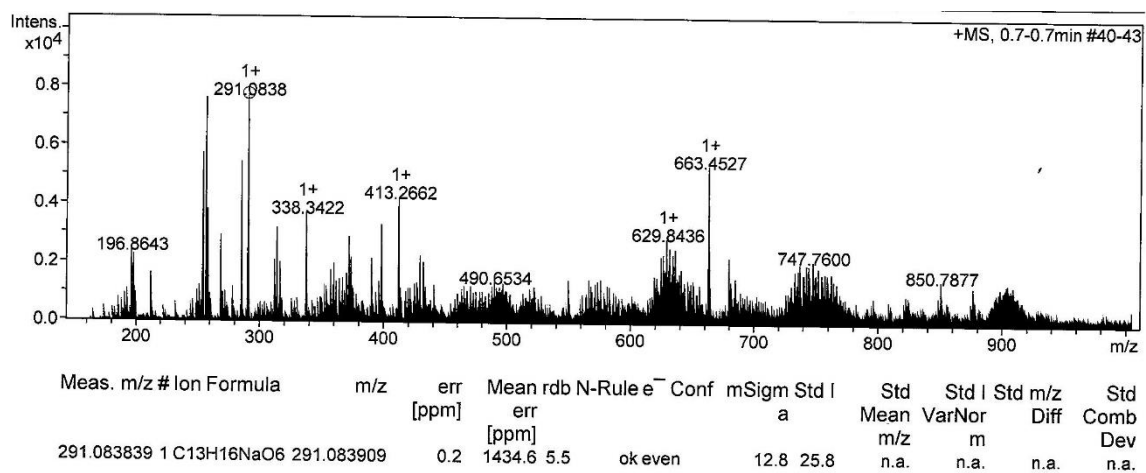
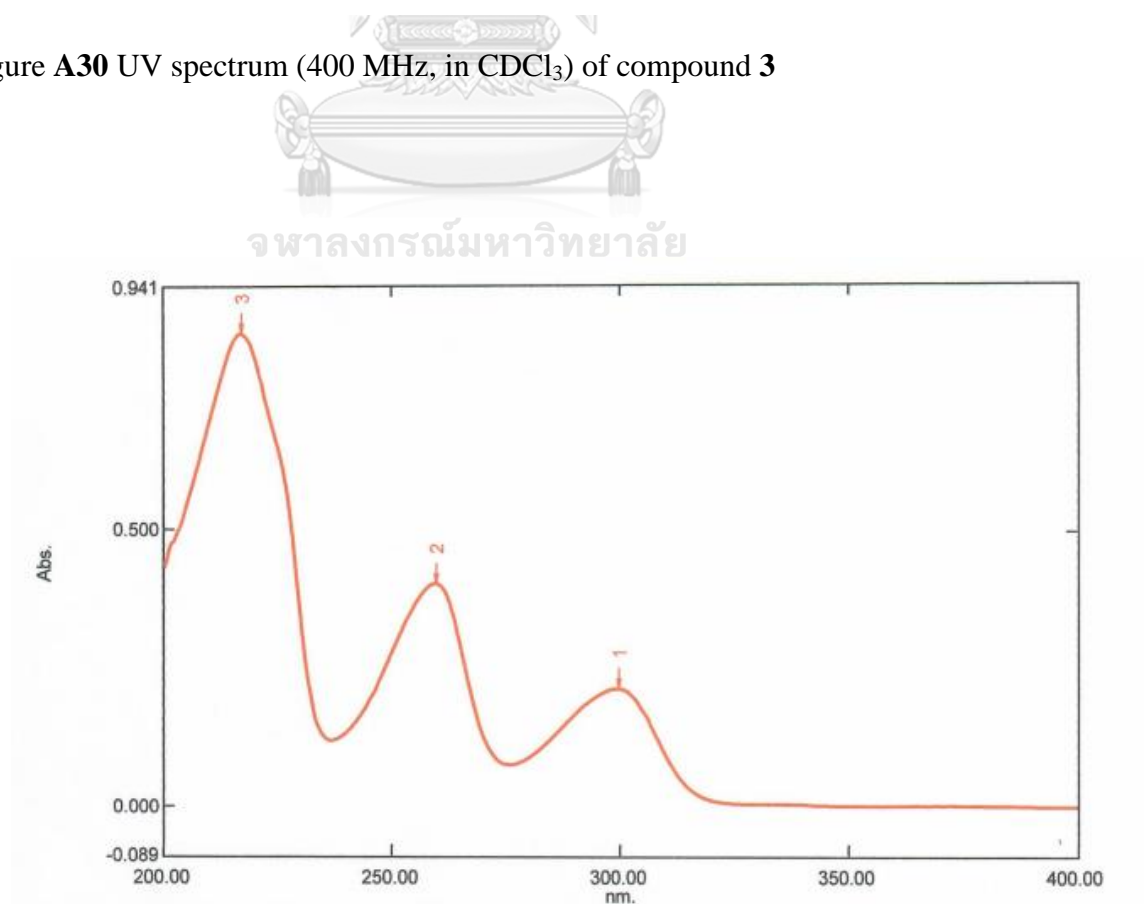
Figure A29 MS spectrum (400 MHz, in CDCl₃) of compound 3Figure A30 UV spectrum (400 MHz, in CDCl₃) of compound 3

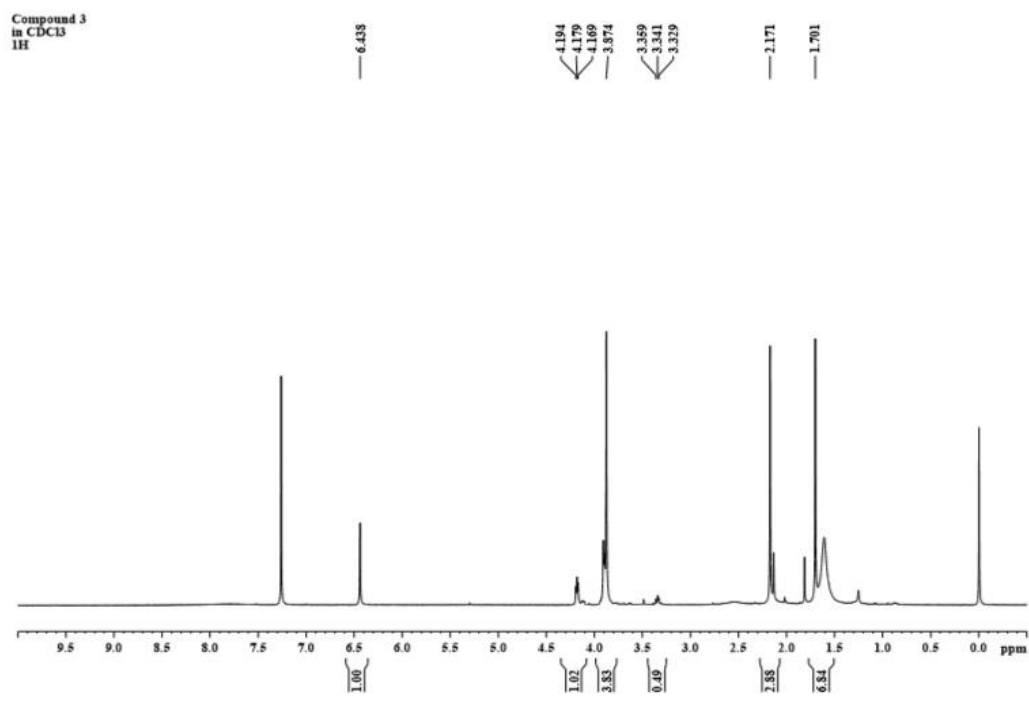
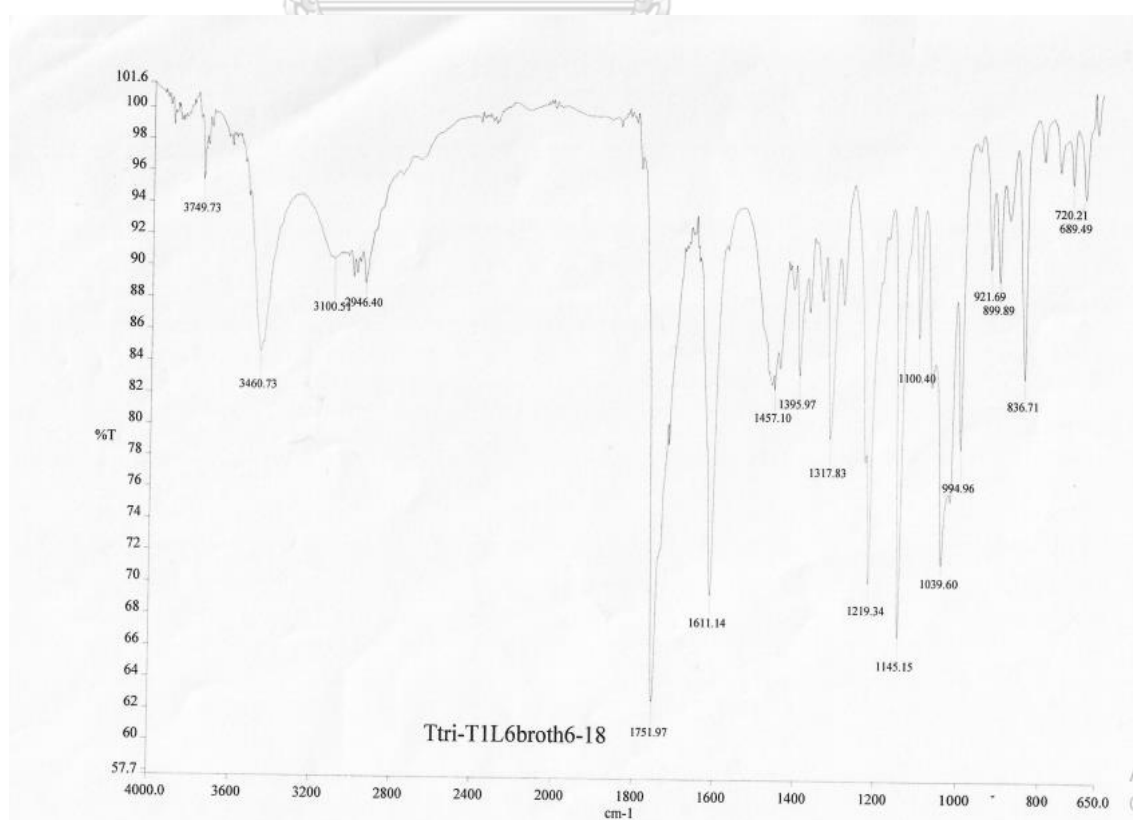
Figure A31 IR spectrum (400 MHz, in CDCl₃) of compound 3Figure A32 ¹H NMR spectrum (400 MHz, in CDCl₃) of compound 4

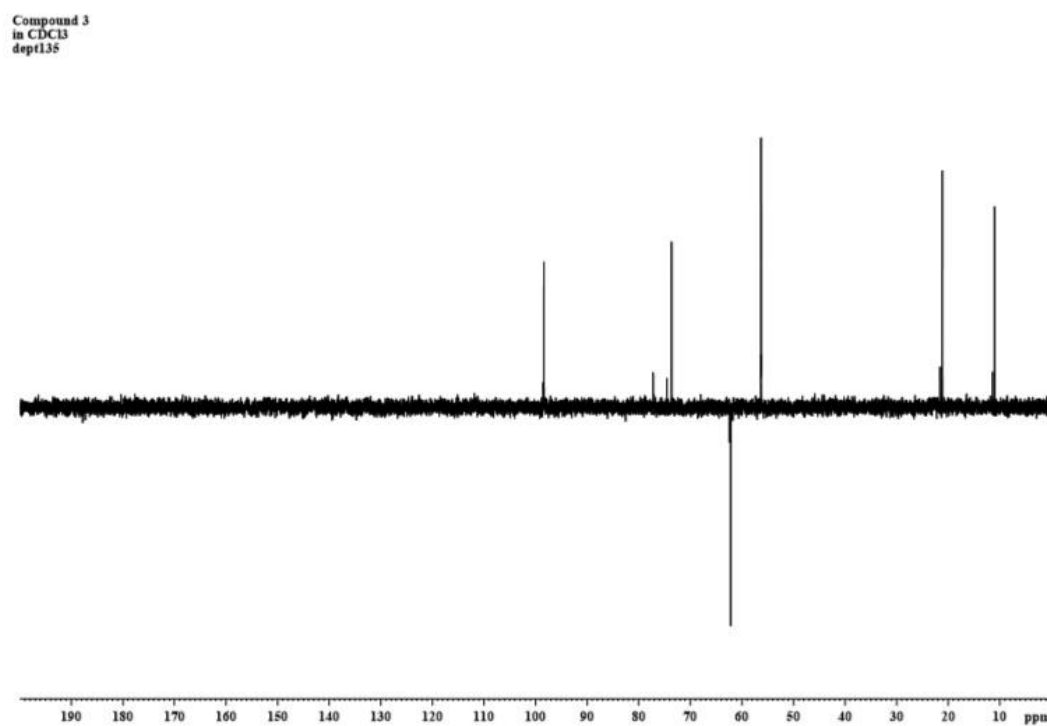
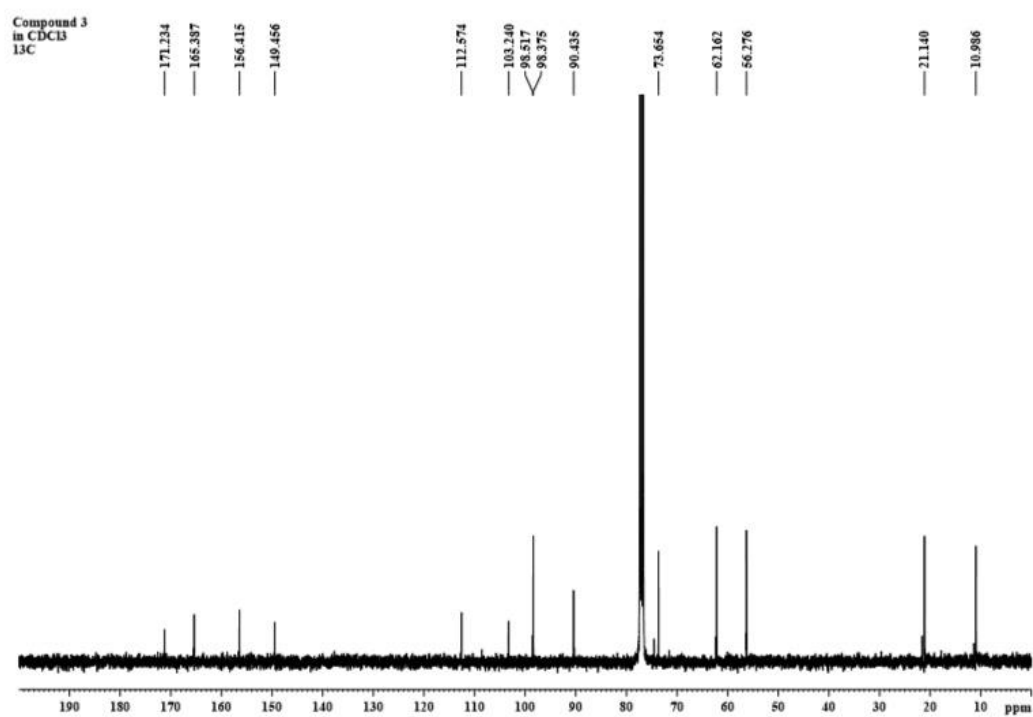
Figure A33 ^{13}C NMR spectrum (400 MHz, in CDCl_3) of compound 4Figure A34 DEPT 135 spectrum (400 MHz, in CDCl_3) of compound 4

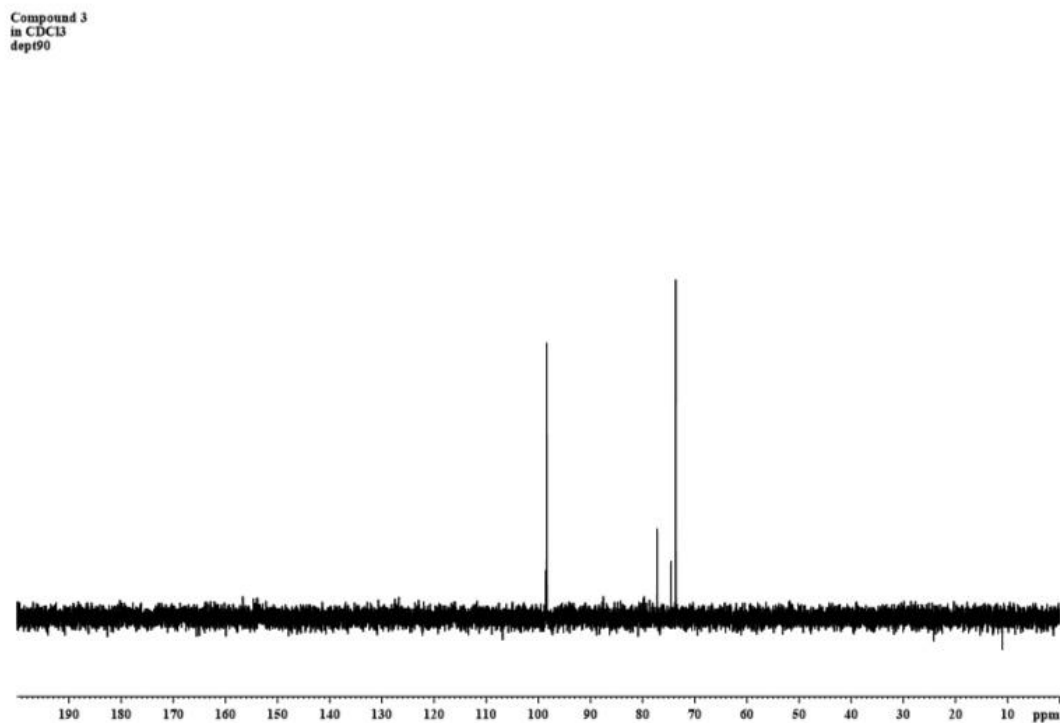
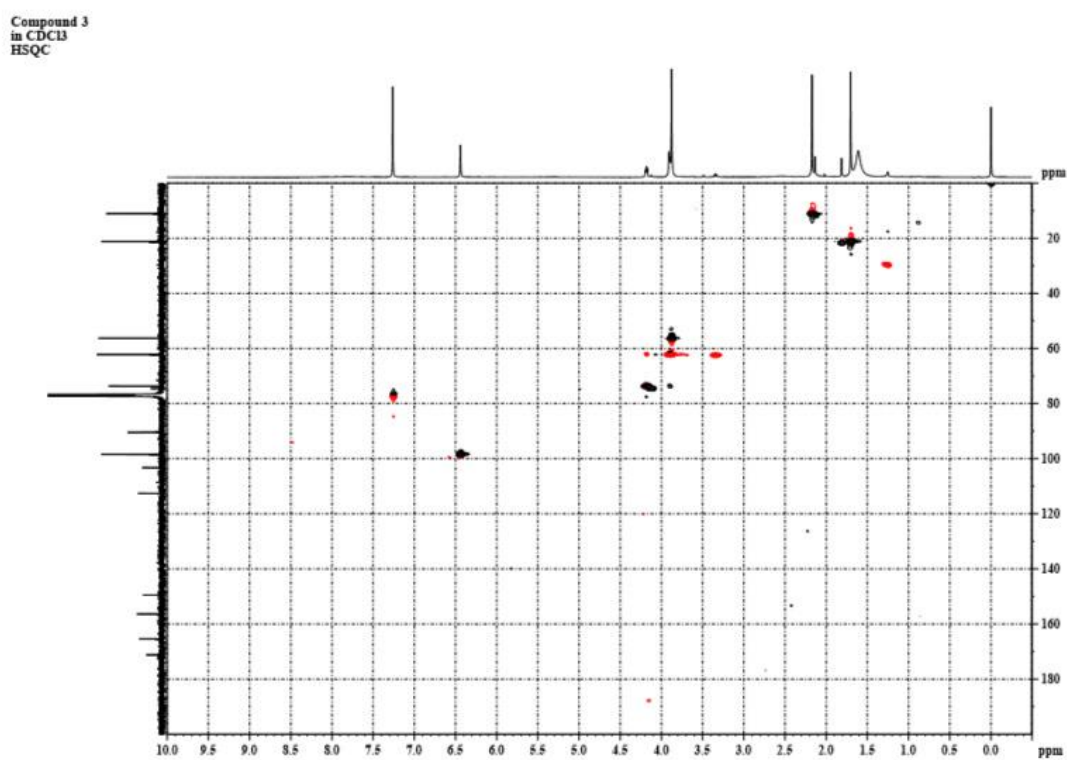
Figure A35 DEPT 90 spectrum (400 MHz, in CDCl₃) of compound 4Figure A36 HSQC NMR spectrum (400 MHz, in CDCl₃) of compound 4

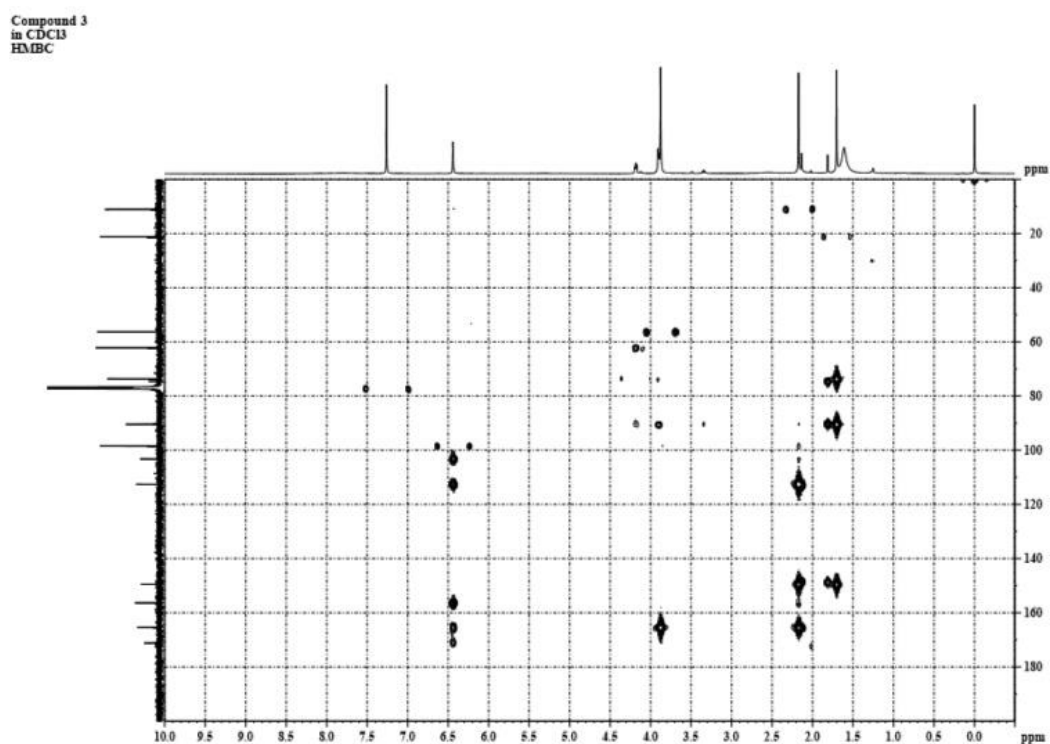
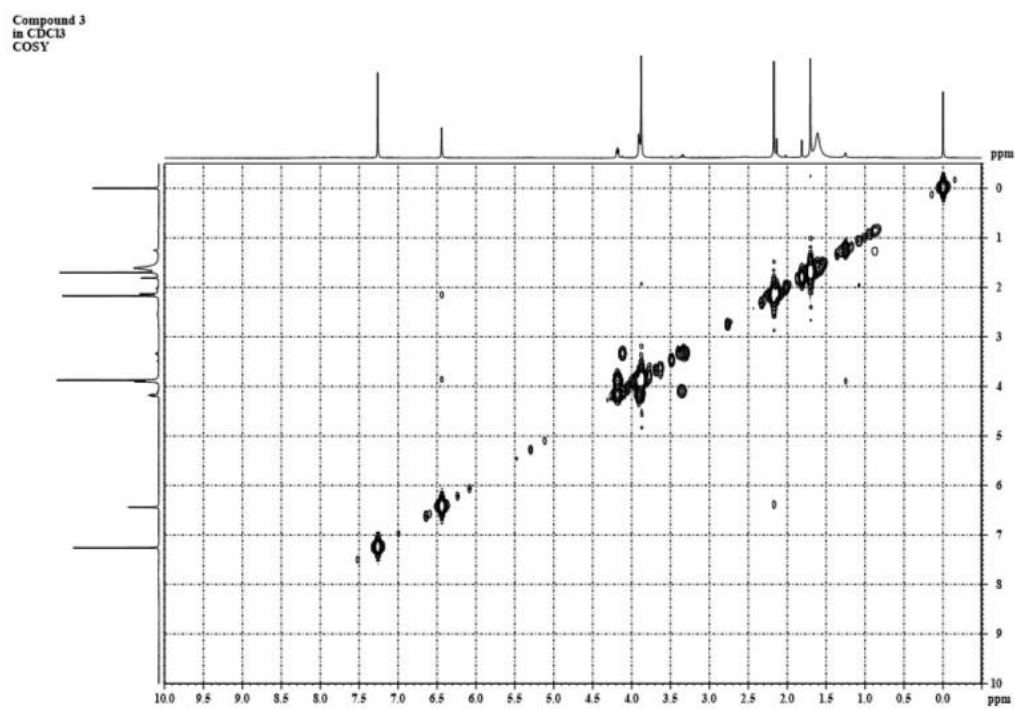
Figure A37 HMBC NMR spectrum (400 MHz, in CDCl₃) of compound 4Figure A38 ¹H-¹H COSY NMR spectrum (400 MHz, in CDCl₃) of compound 4

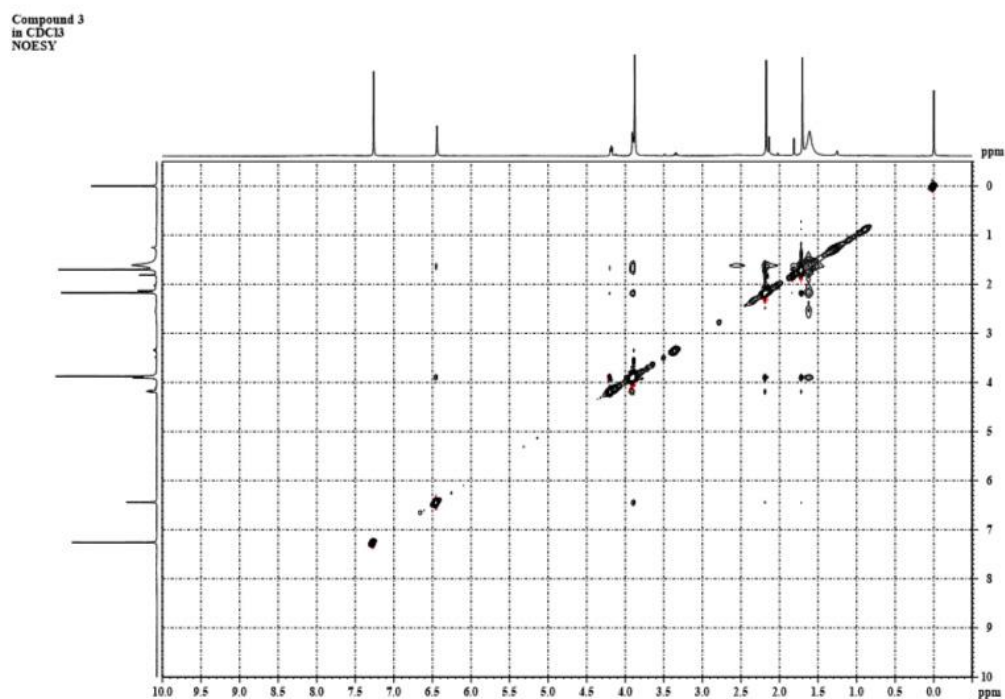
Figure A39 NOESY NMR spectrum (400 MHz, in CDCl₃) of compound 4

Figure A40 MS spectrum of compound 4

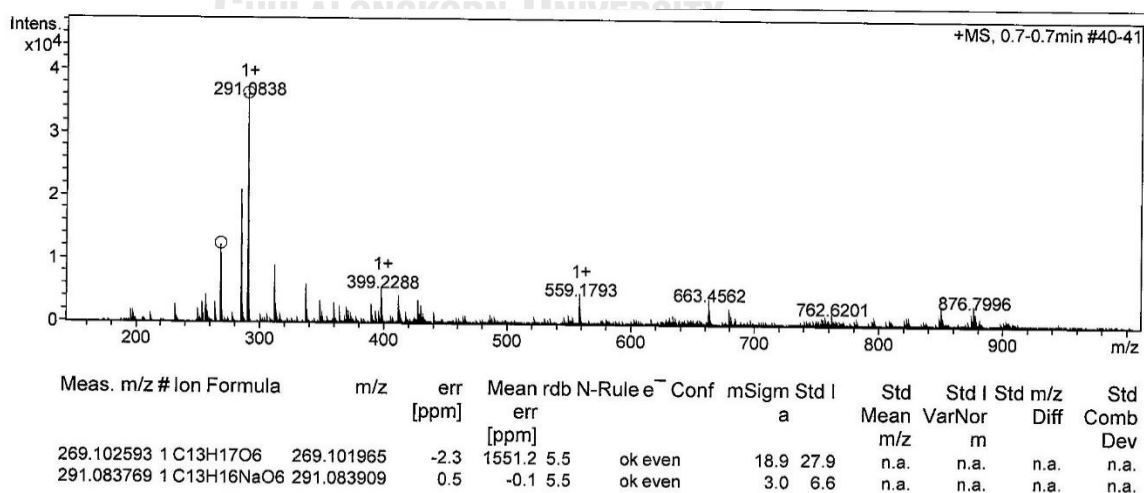


Figure A41 UV spectrum of compound 4

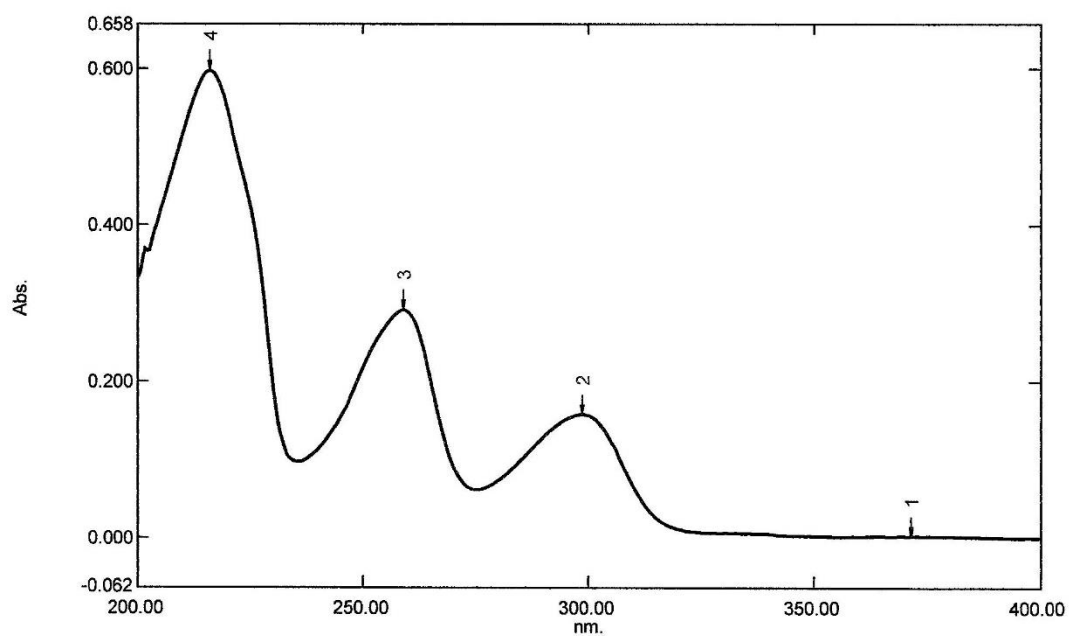


Figure A42 IR spectrum of compound 4

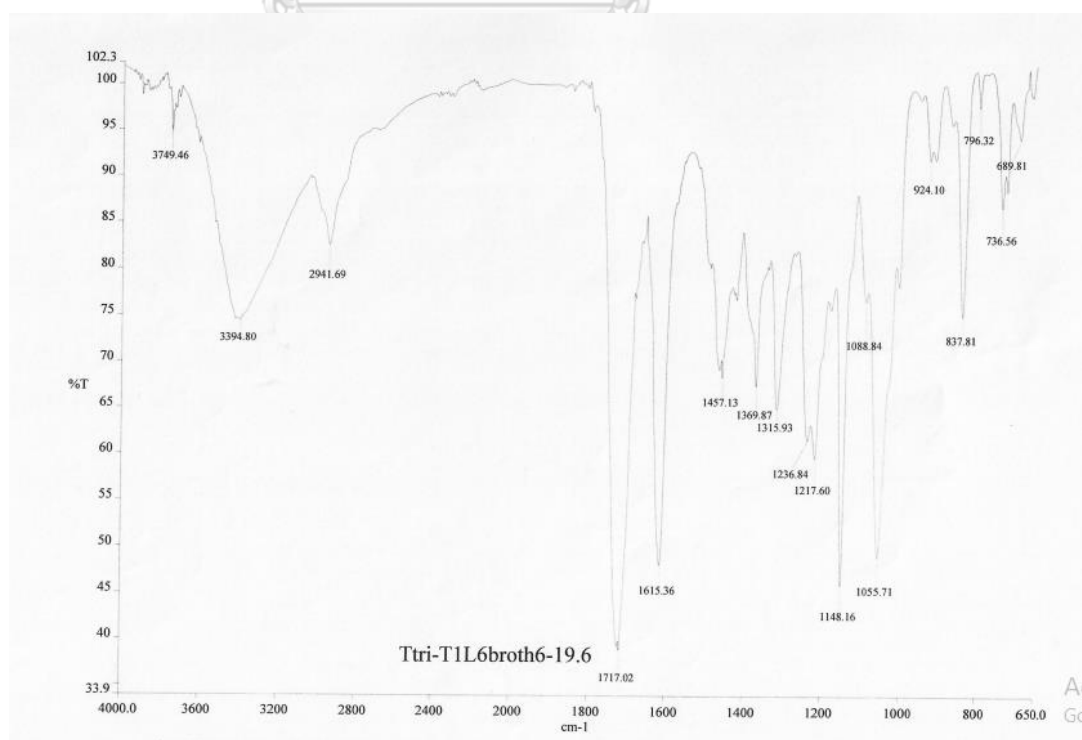


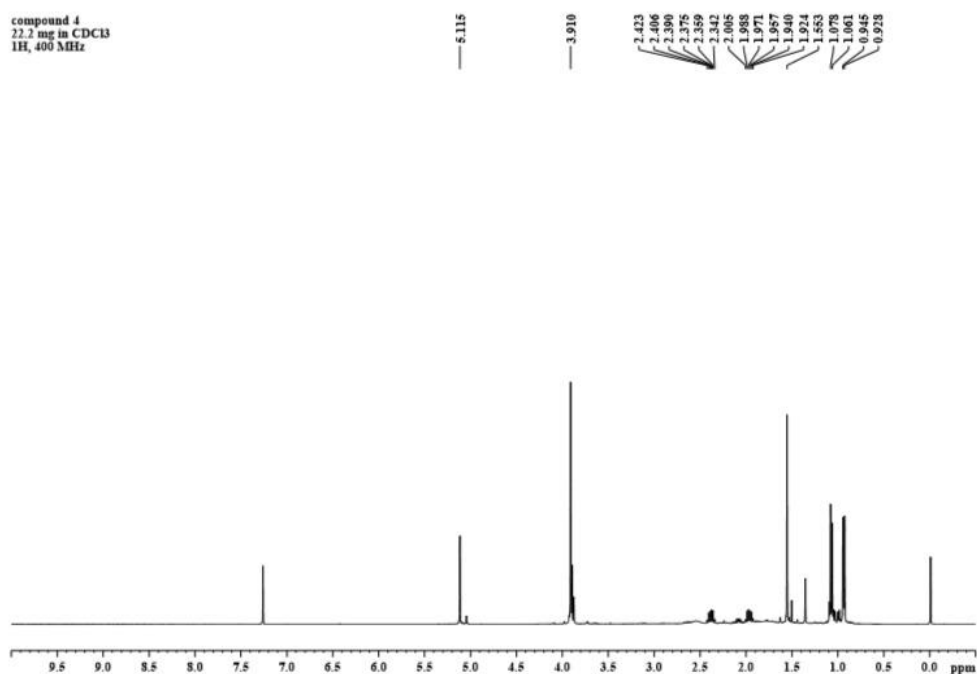
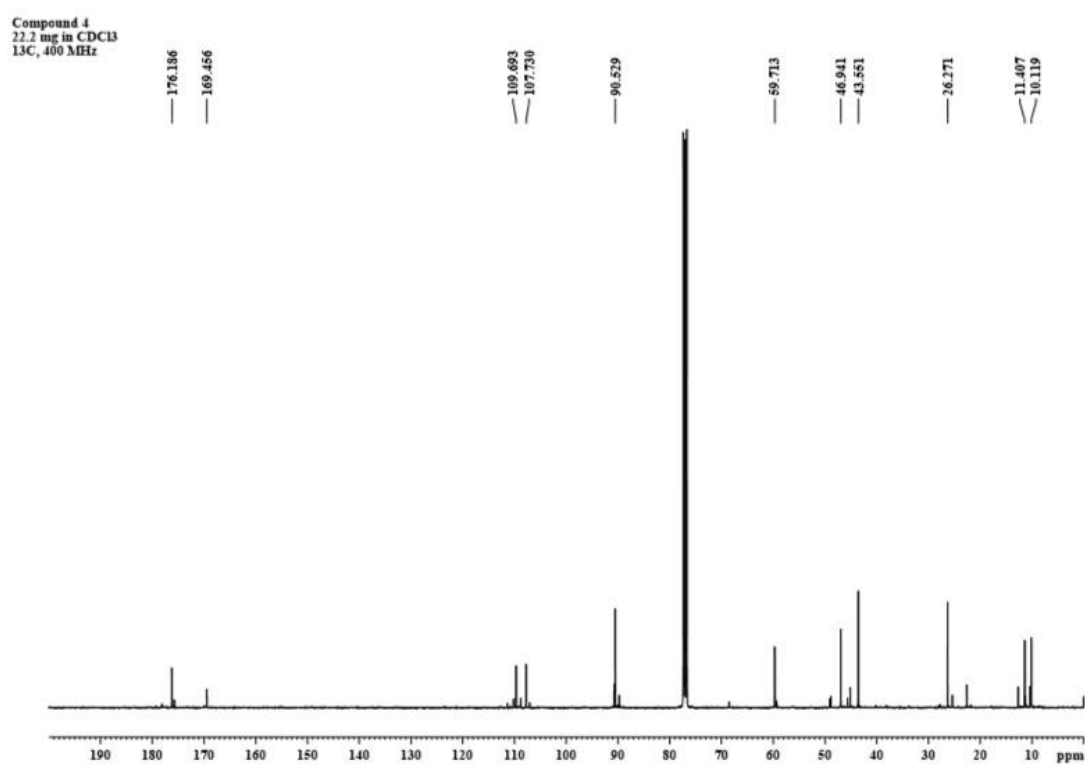
Figure A43 ^1H NMR spectrum (400 MHz, in CDCl_3) of compound 5Figure A44 ^{13}C NMR spectrum (400 MHz, in CDCl_3) of compound 5

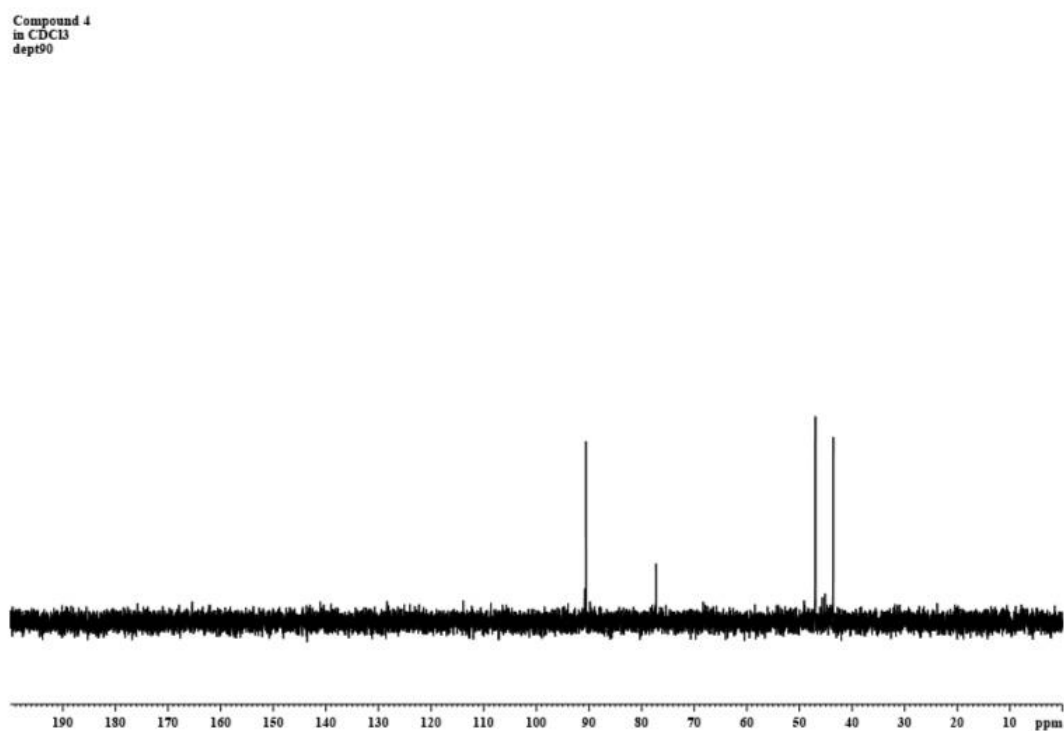
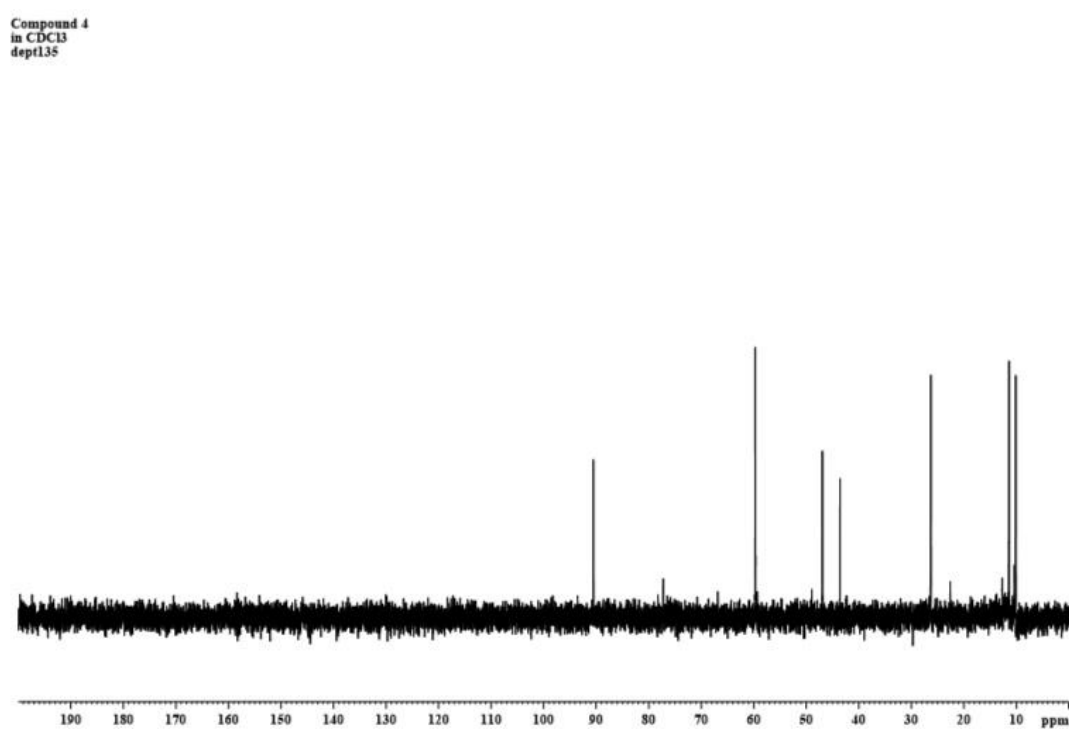
Figure A45 DEPT 135 NMR spectrum (400 MHz, in CDCl₃) of compound 5Figure A46 DEPT 90 NMR spectrum (400 MHz, in CDCl₃) of compound 5

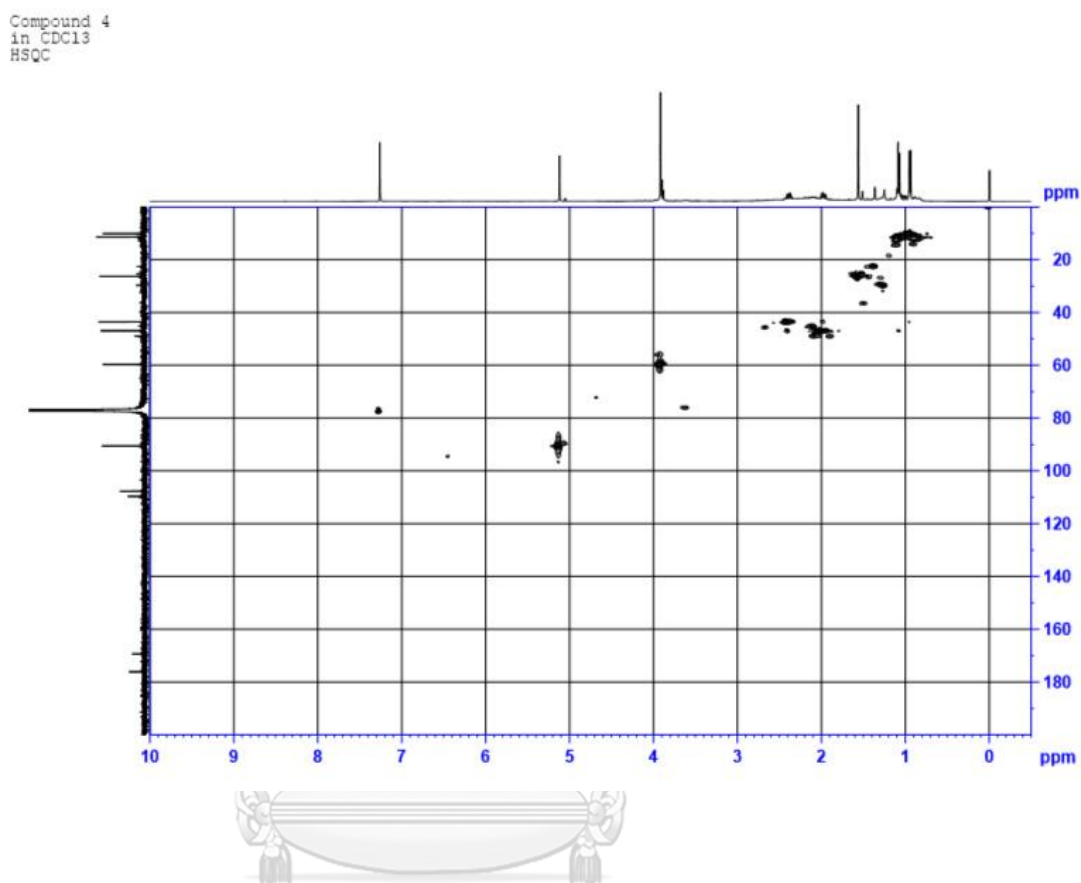
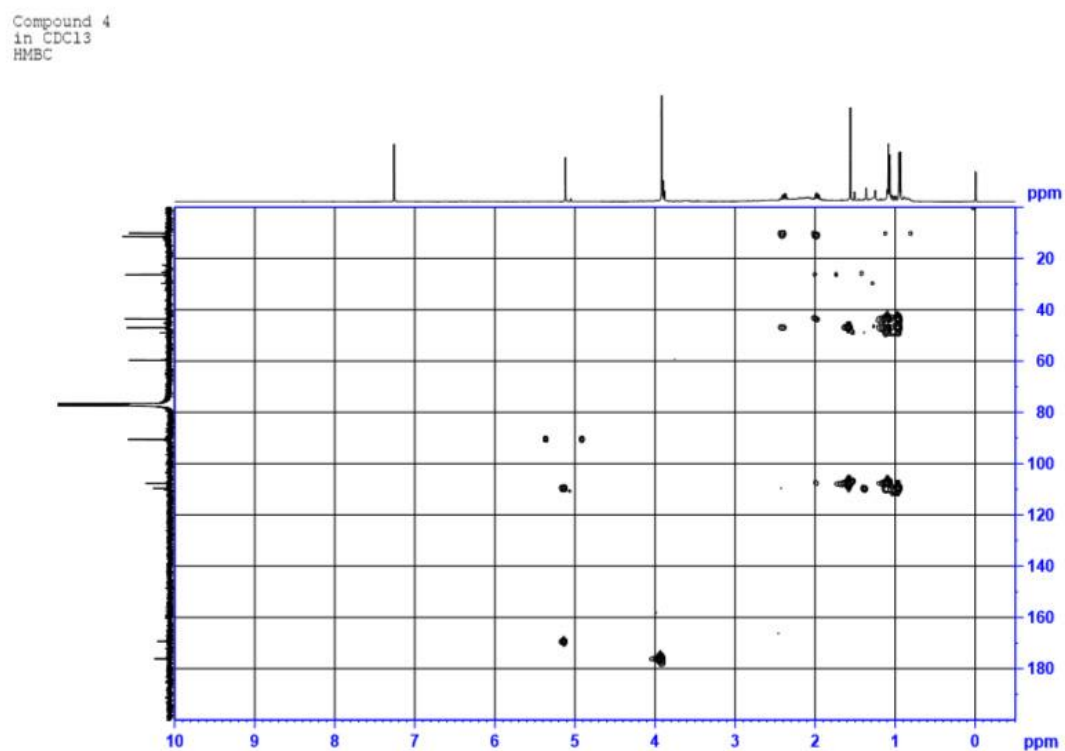
Figure A47 HSQC NMR spectrum (400 MHz, in CDCl₃) of compound 5Figure A48 HMBC NMR spectrum (400 MHz, in CDCl₃) of compound 5

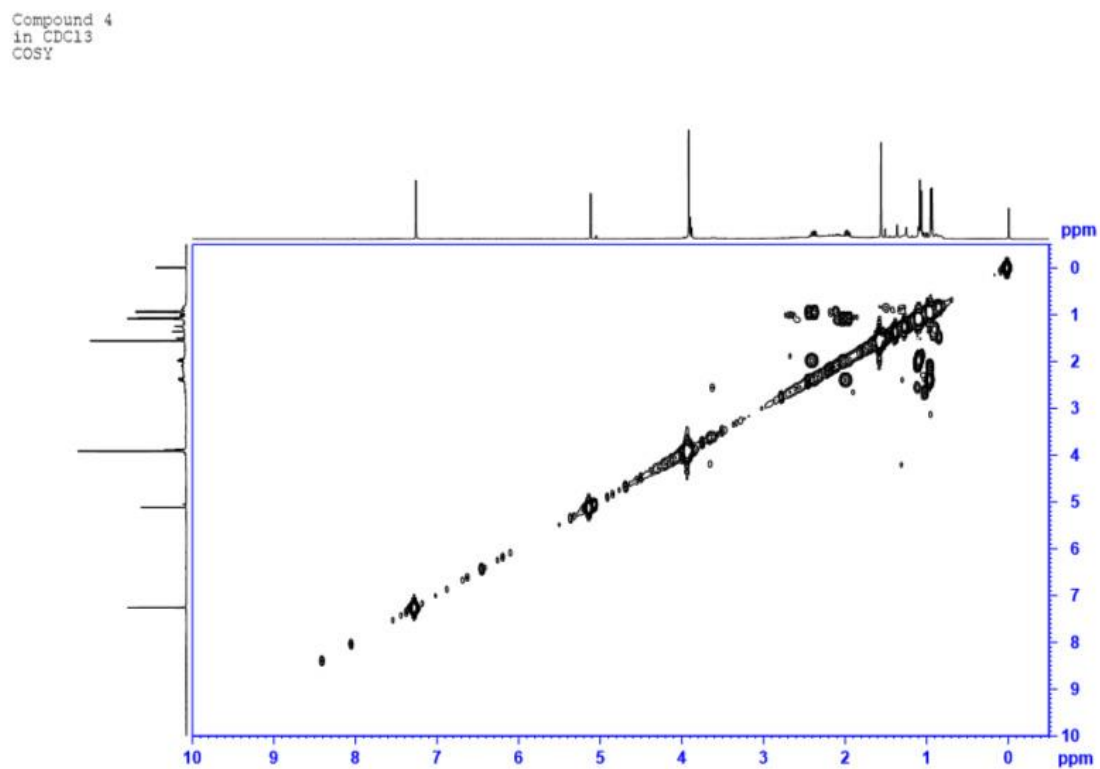
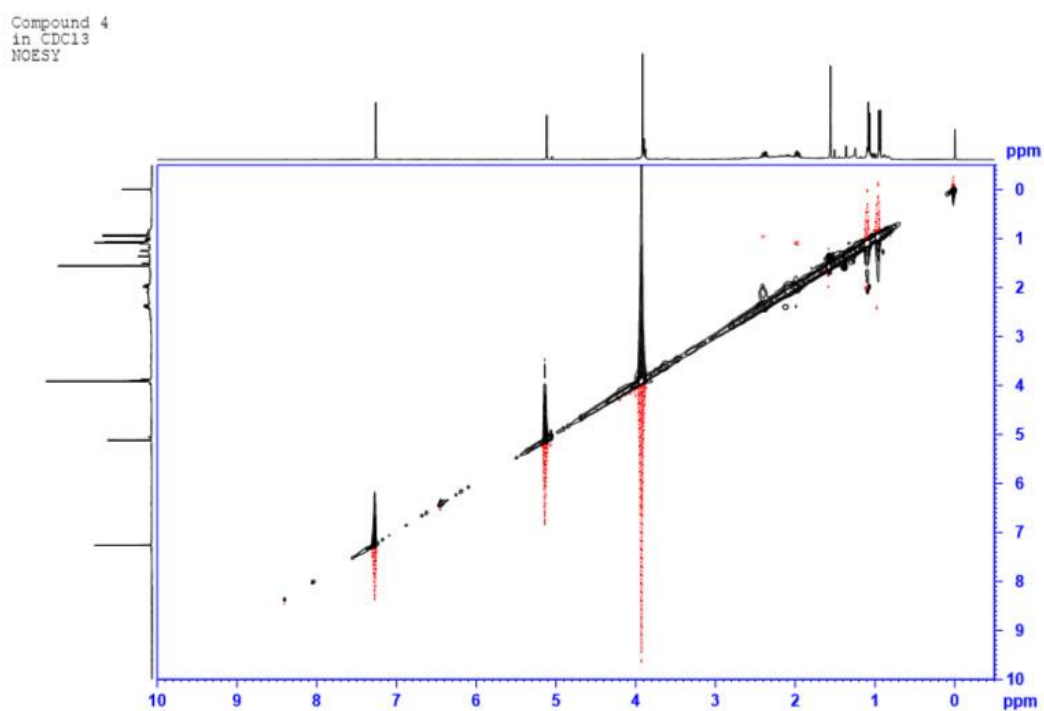
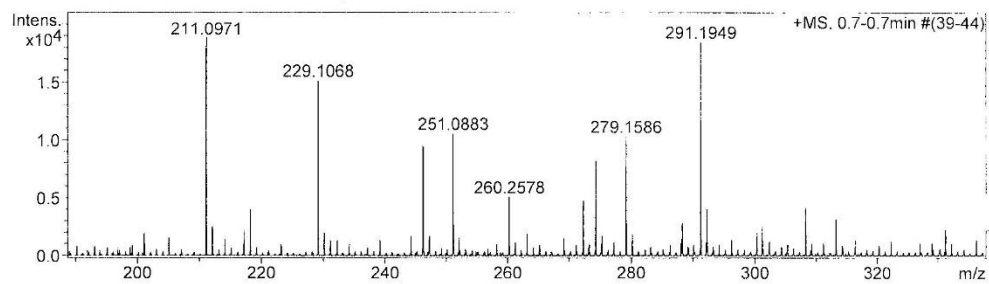
Figure A49 ^1H - ^1H COSY NMR spectrum (400 MHz, in CDCl_3) of compound 5Figure A50 NOESY NMR spectrum (400 MHz, in CDCl_3) of compound 5

Figure A51 MS spectrum of compound 5



#	m/z	I	Res.
1	149.0281	3873	5763
2	157.0874	2236	5677
3	161.0627	2942	5734
4	179.0727	8009	5972
5	201.1053	1983	6188
6	205.0879	1546	6079
7	211.0971	18837	6311
8	212.1008	2509	6490
9	217.1770	2273	5896
10	218.2099	3966	6185
11	229.1068	15087	6782

Figure A52 UV spectrum of compound 5

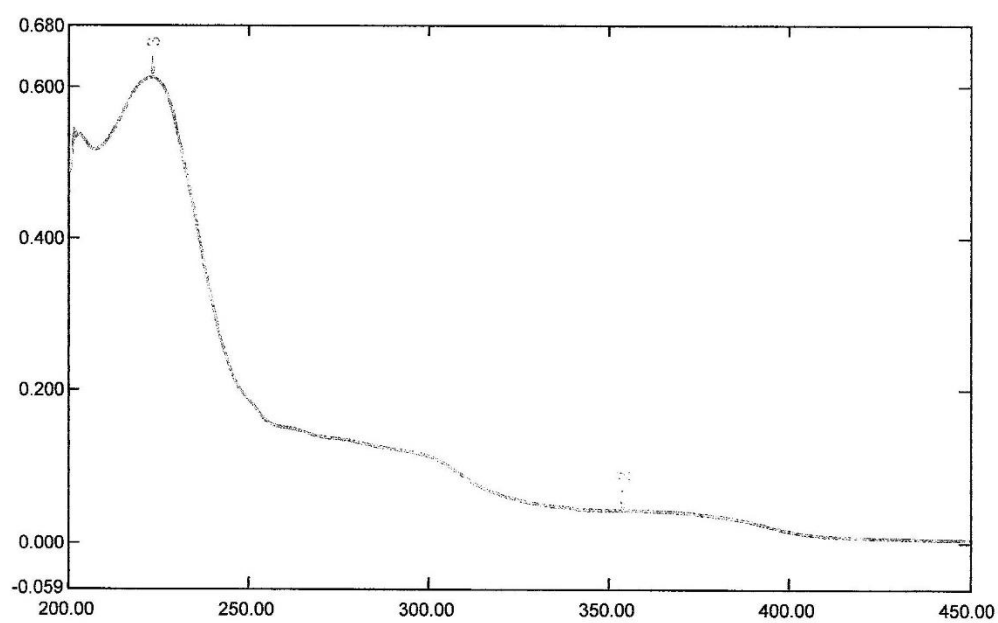


Figure A53 IR spectrum of compound 5

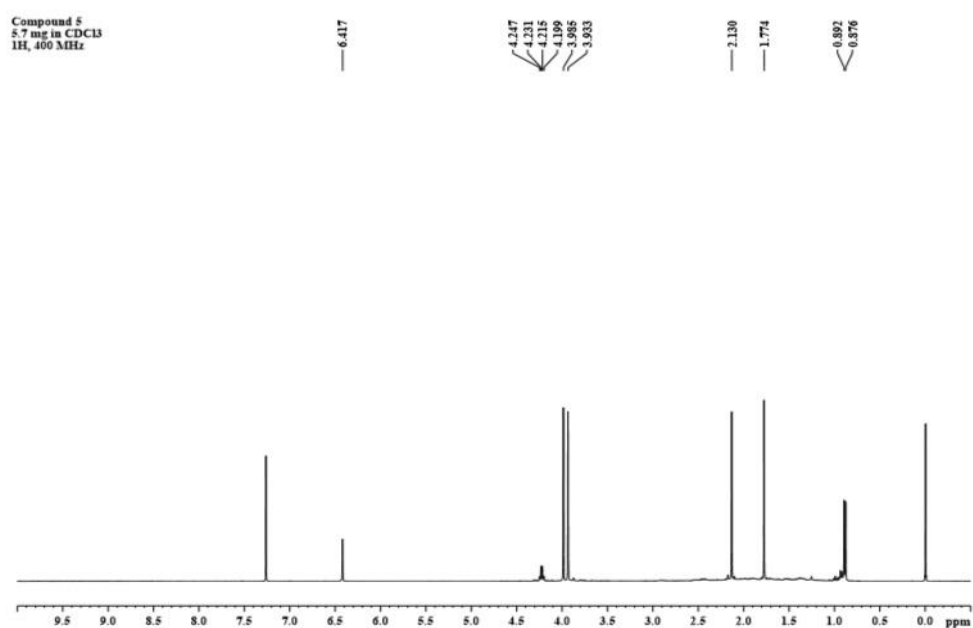
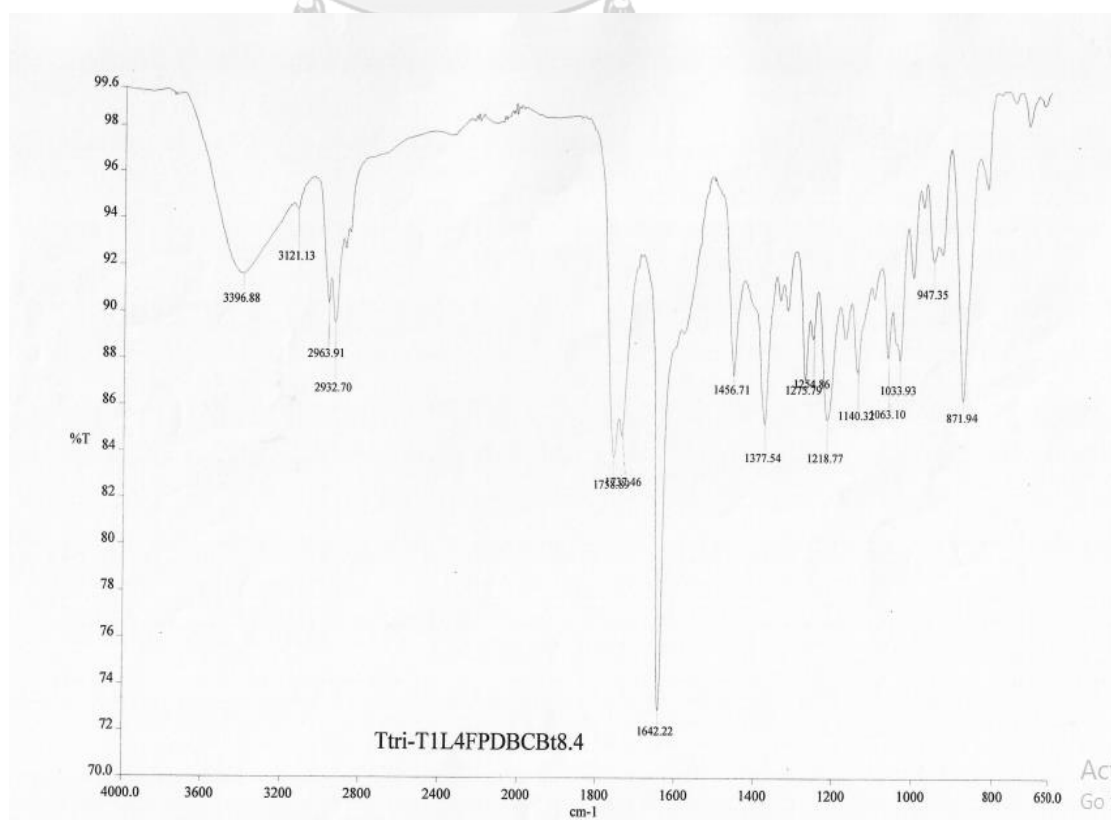
Figure A54 ¹H NMR spectrum (400 MHz, in CDCl₃) of compound 6

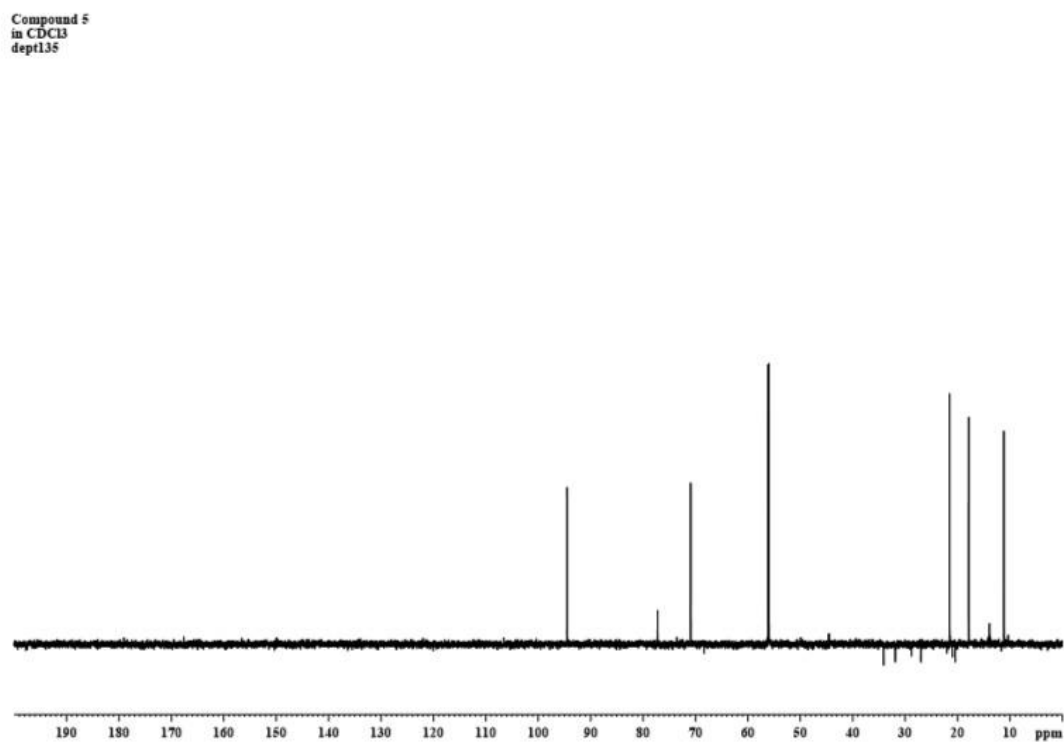
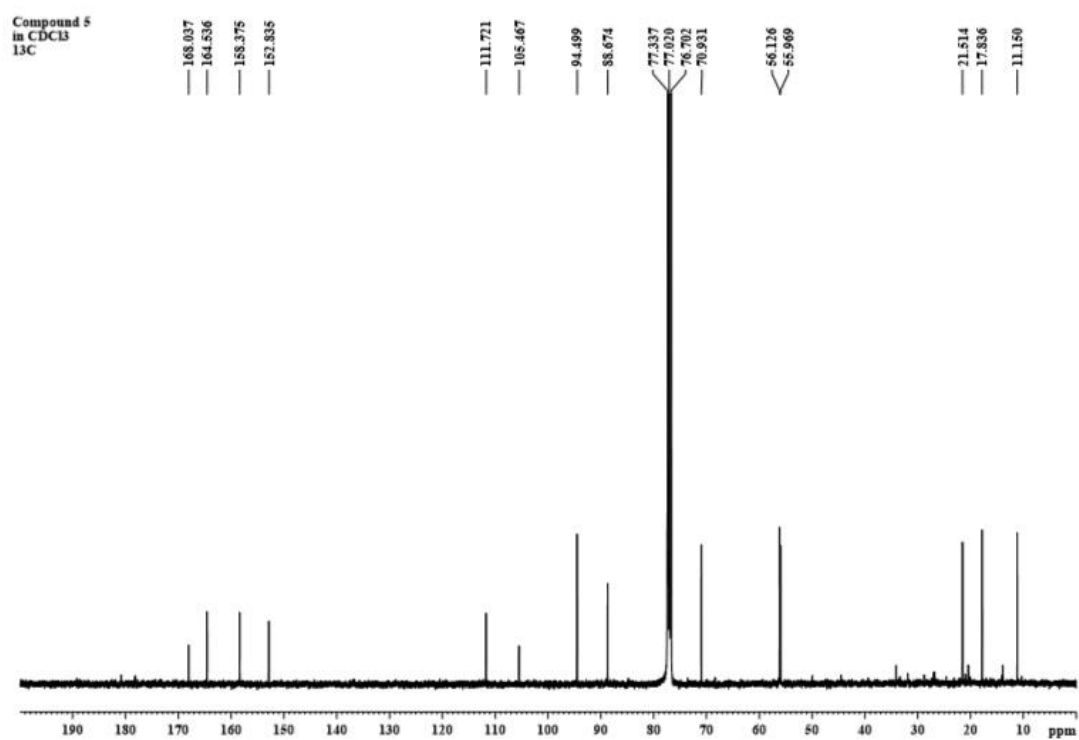
Figure A55 ^{13}C NMR spectrum (400 MHz, in CDCl_3) of compound **6**Figure A56 DEPT 135 NMR spectrum (400 MHz, in CDCl_3) of compound **6**

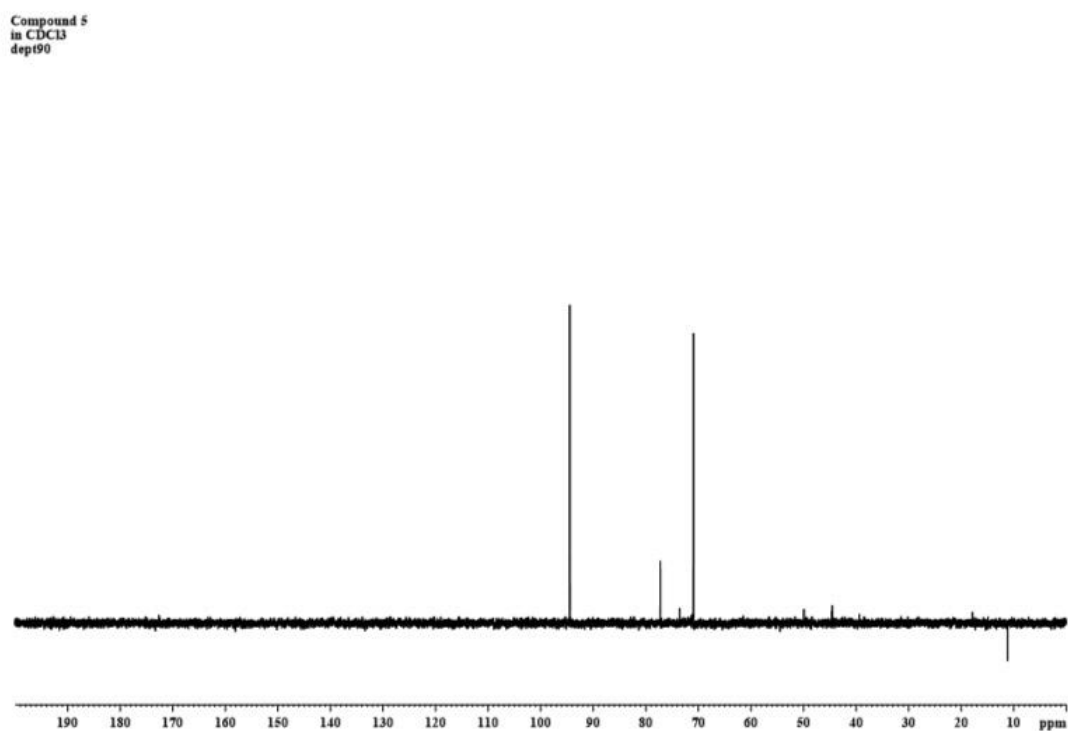
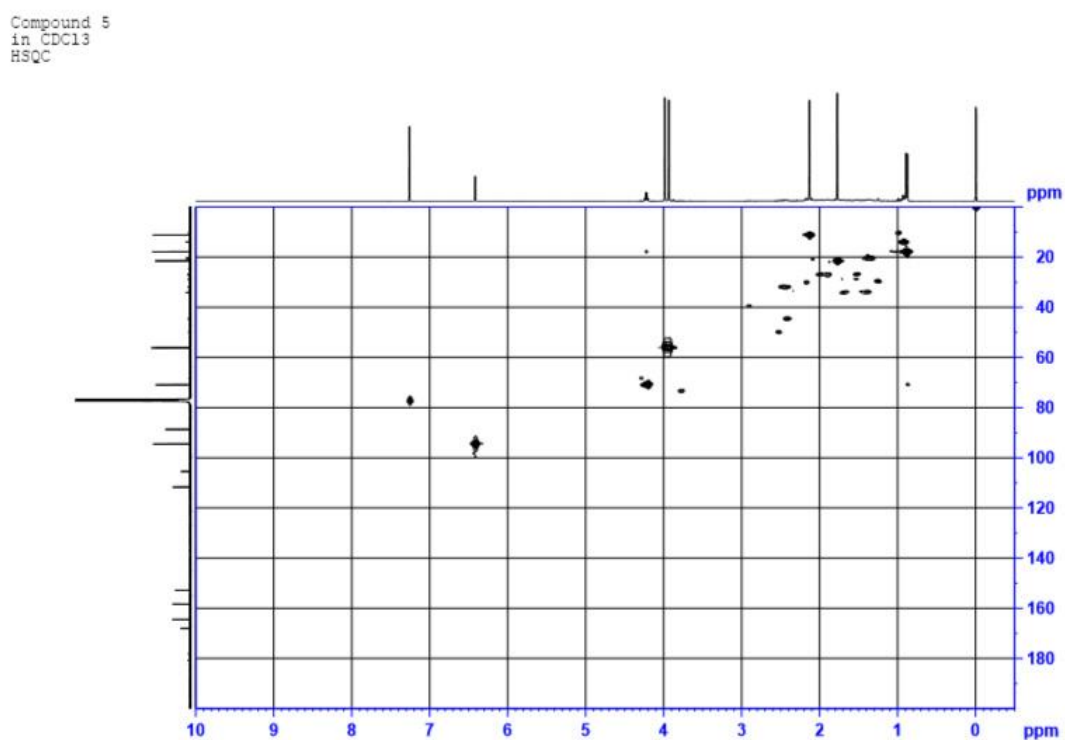
Figure A57 DEPT 90 spectrum (400 MHz, in CDCl₃) of compound 6Figure A58 HSQC NMR spectrum (400 MHz, in CDCl₃) of compound 6

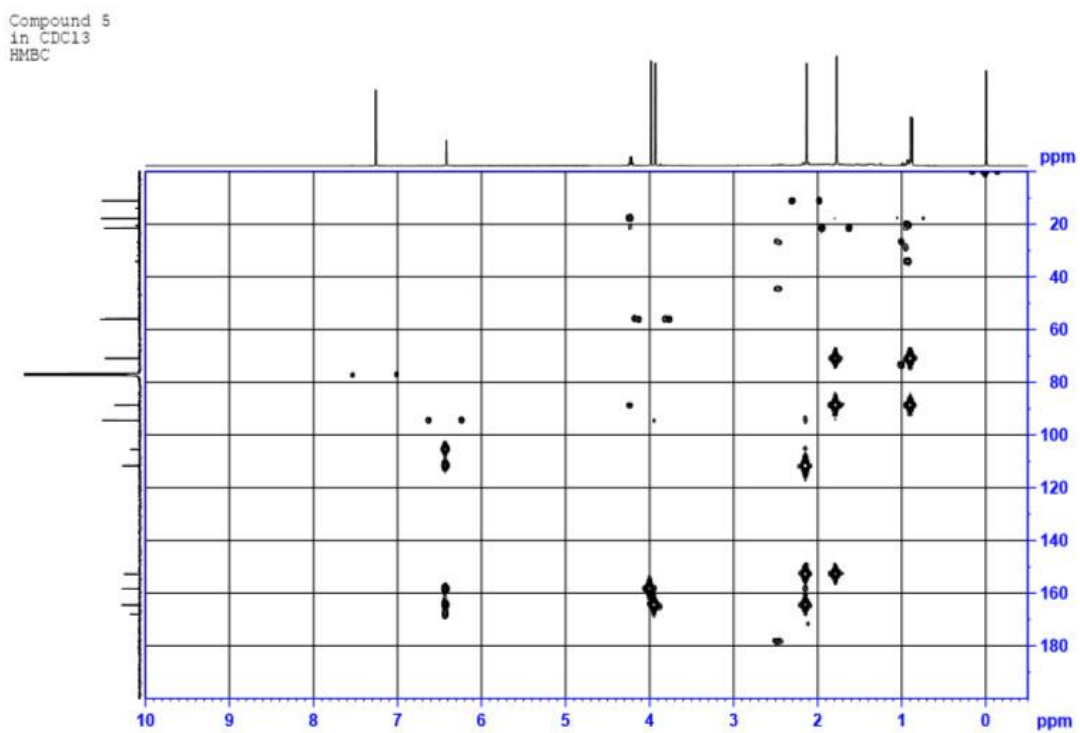
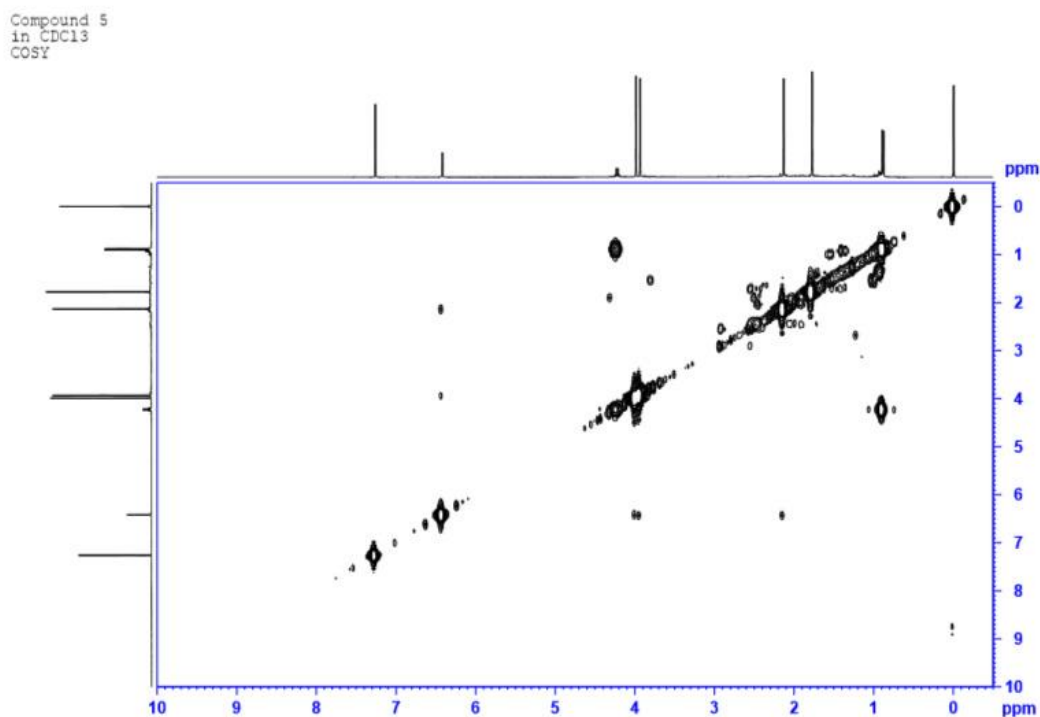
Figure A59 HMBC NMR spectrum (400 MHz, in CDCl₃) of compound 6Figure A60 ¹H-¹H COSY NMR spectrum (400 MHz, in CDCl₃) of compound 6

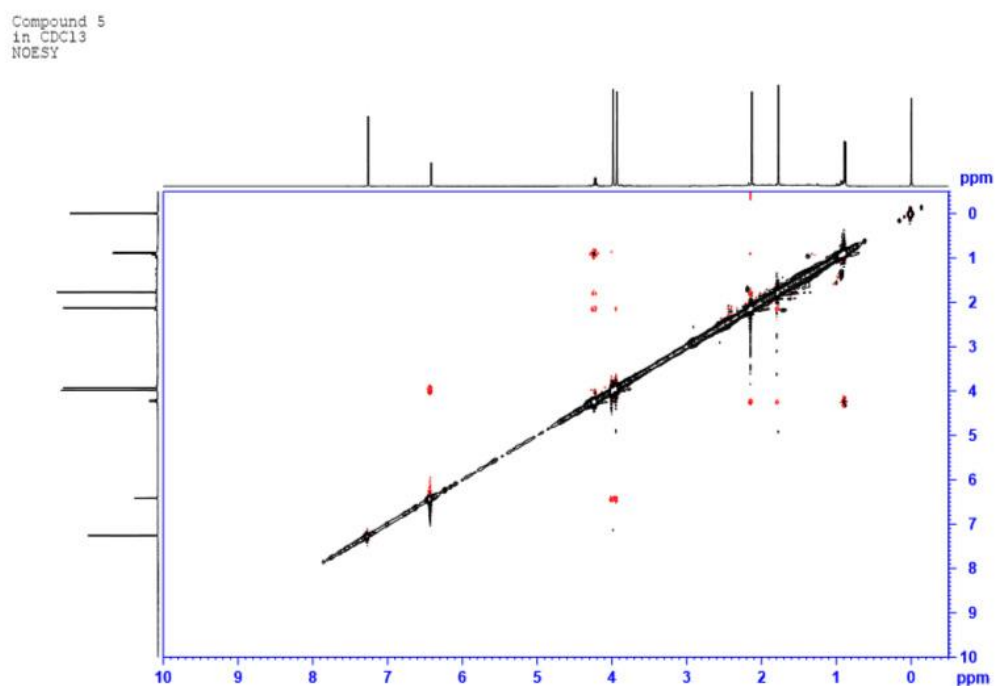
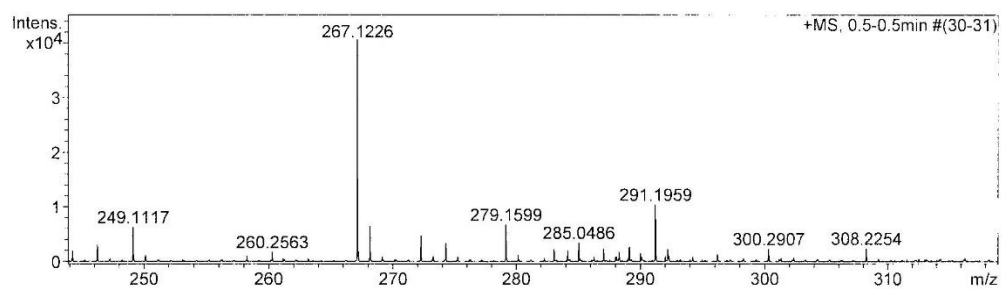
Figure A61 NOESY NMR spectrum (400 MHz, in CDCl₃) of compound 6

Figure A62 MS spectrum of compound 6



#	m/z	I	Res.
1	149.0228	3050	5670
2	177.0443	7519	6014
3	179.0454	7277	4339
4	181.0379	2643	6252
5	246.2409	3062	6791
6	249.1117	6265	7175
7	267.1226	40561	7335

Figure A63 UV spectrum of compound 6

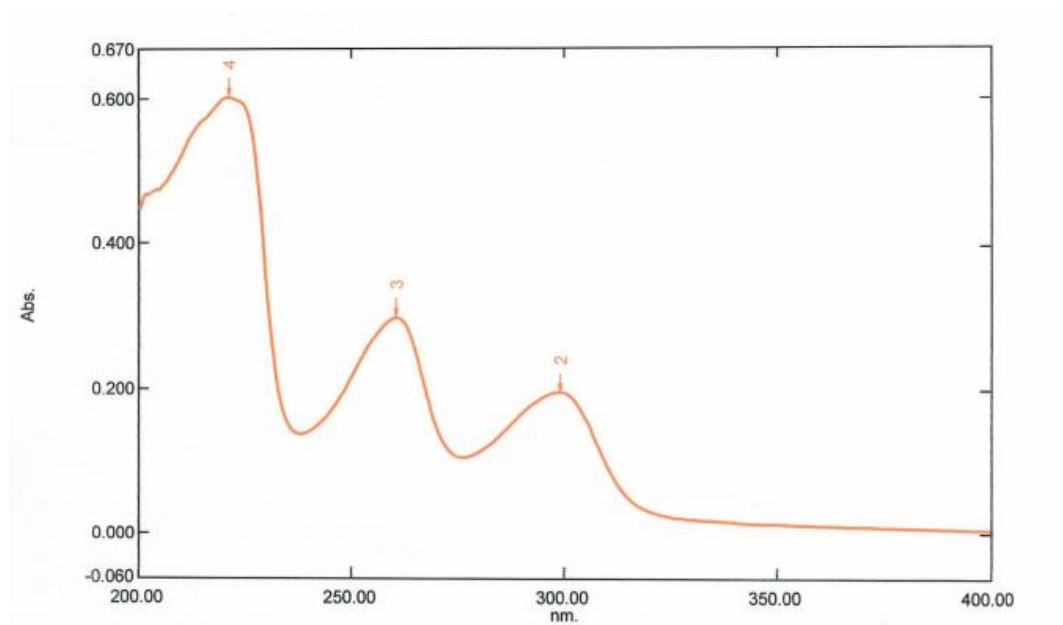
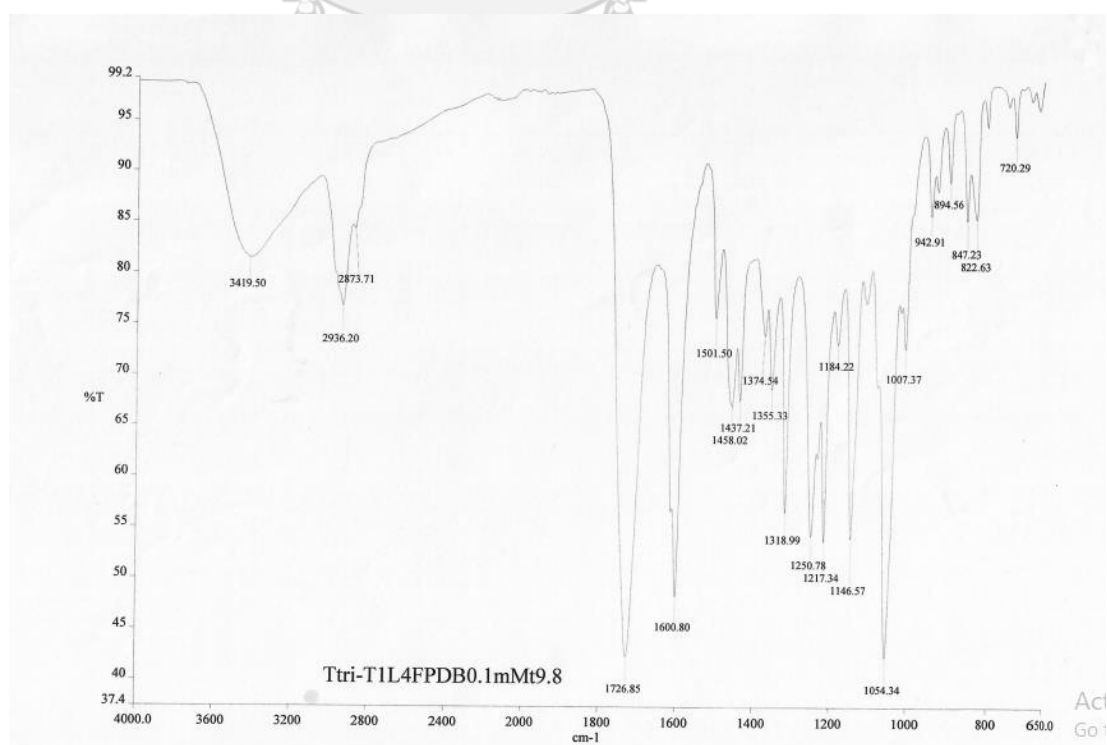
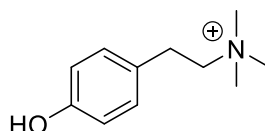


Figure A64 IR spectrum of compound 6



Part B: Bioactive compounds from *Feroniella lucida* (Scheff.) Swingle

Physicochemical properties of compounds isolated from *Feroniella lucida* (Scheff.) Swingle

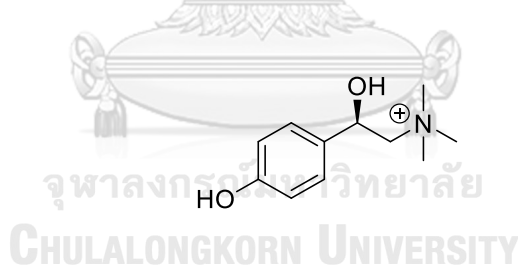


Compound **7** was obtained as yellow solid (5.4 mg)

ESI-TOF MS: calcd. for $C_{11}H_{18}NO$, m/z 180.1388 ($M+H$)⁺, found 180.1367.

UV (MeOH) λ_{max} (log ϵ): 267.0 (1.44), 202.5 (2.09) nm.

IR (UATR) ν_{max} : 3365, 2955, 2924, 2853, 1633, 1473, 1454, 1397, 1337, 1218, 1126, 1083, 1035, 1008, 956, 1054, 879, 866 cm^{-1} .



Compound **8** was obtained as yellow solid (91.2 mg)

ESI-TOF MS: calcd. for $C_{11}H_{19}NO_2$, m/z 196.1388 ($M+H$)⁺, found 196.1332.

UV (MeOH) λ_{max} (log ϵ): 276.5 (1.12), 225.5 (1.83) nm.

IR (UATR) ν_{max} : 3222, 3023, 2805, 2154, 1924, 1614, 1597, 1516, 1451, 1262, 1228, 1172, 1134, 1104, 1074, 1035, 914, 837, 789 cm^{-1} .

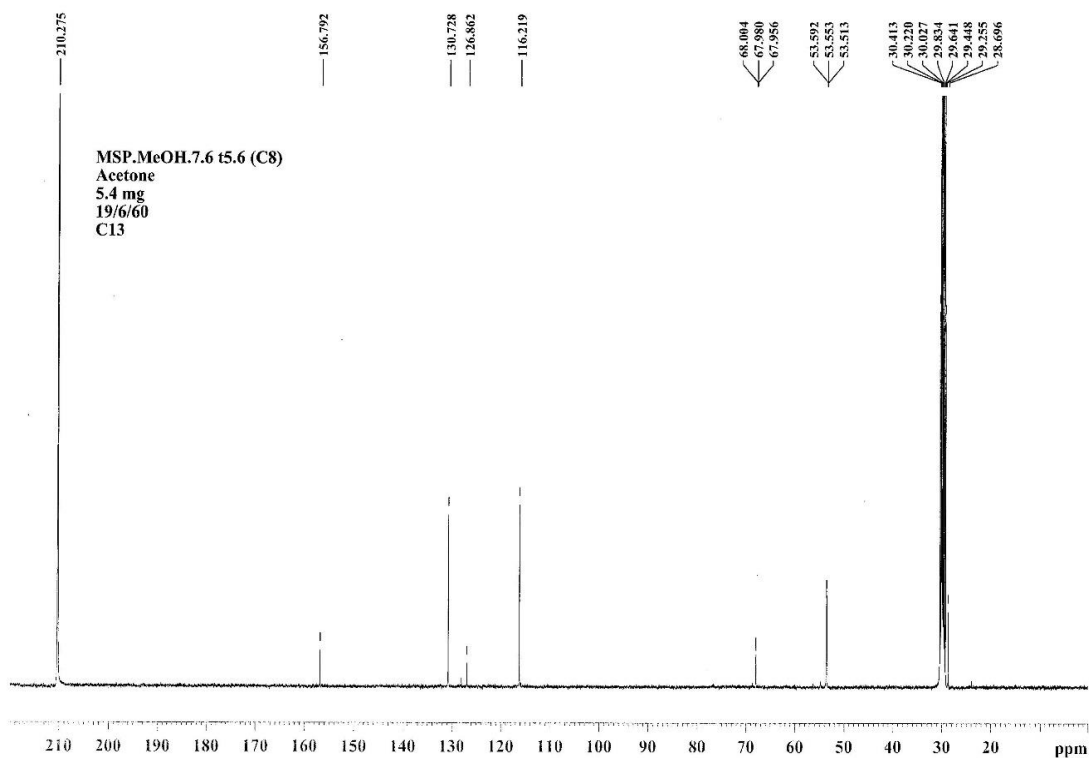
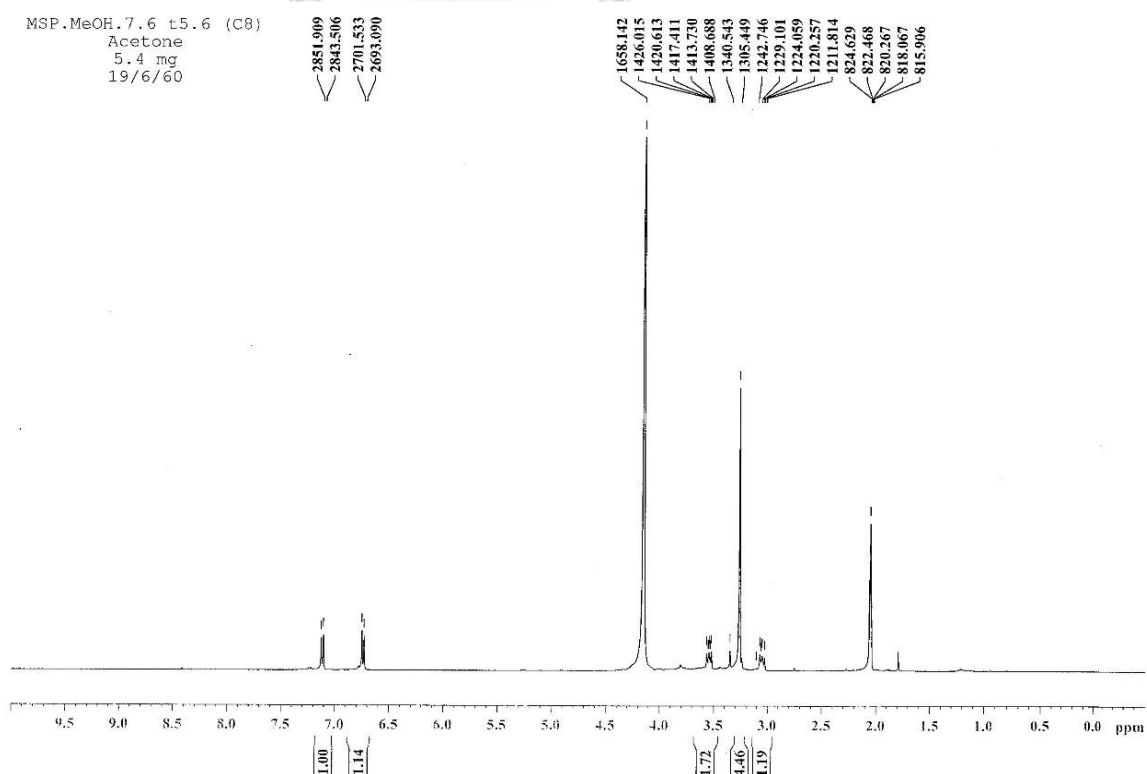
Figure B1 ^1H NMR spectrum (400 MHz, in acetone- d_6) of compound 7Figure B2 ^{13}C NMR spectrum (400 MHz, in acetone- d_6) of compound 7

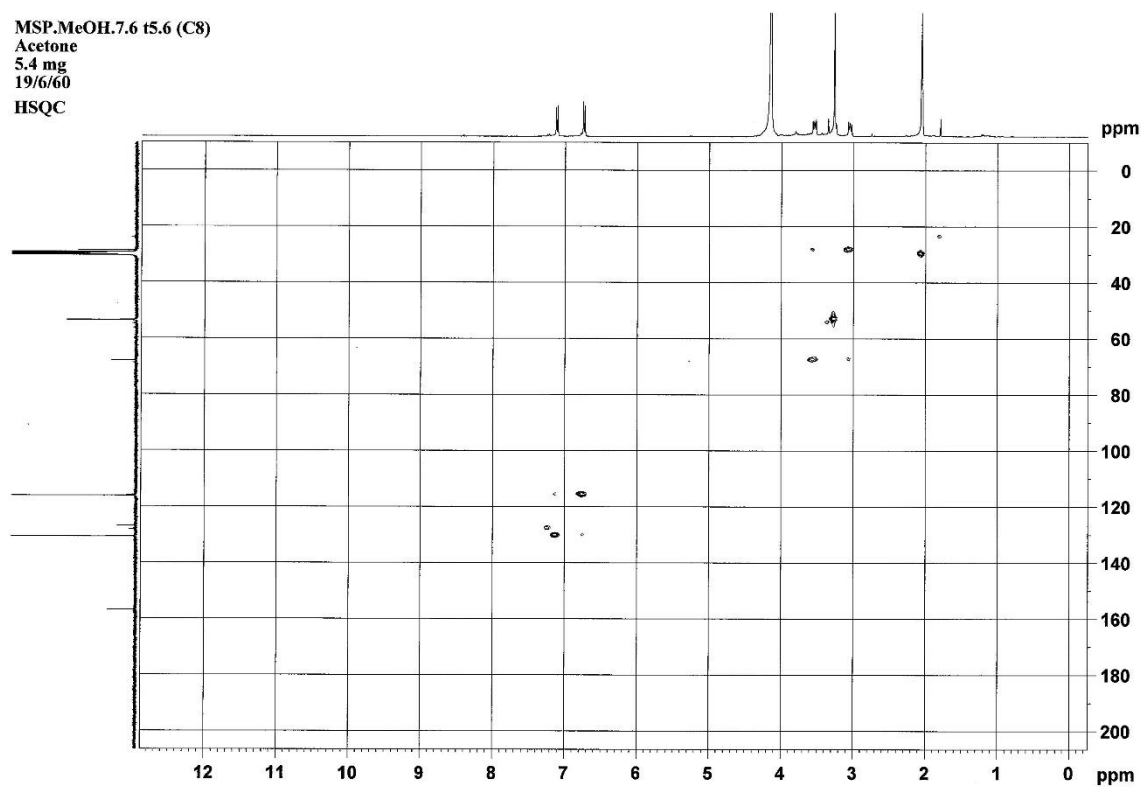
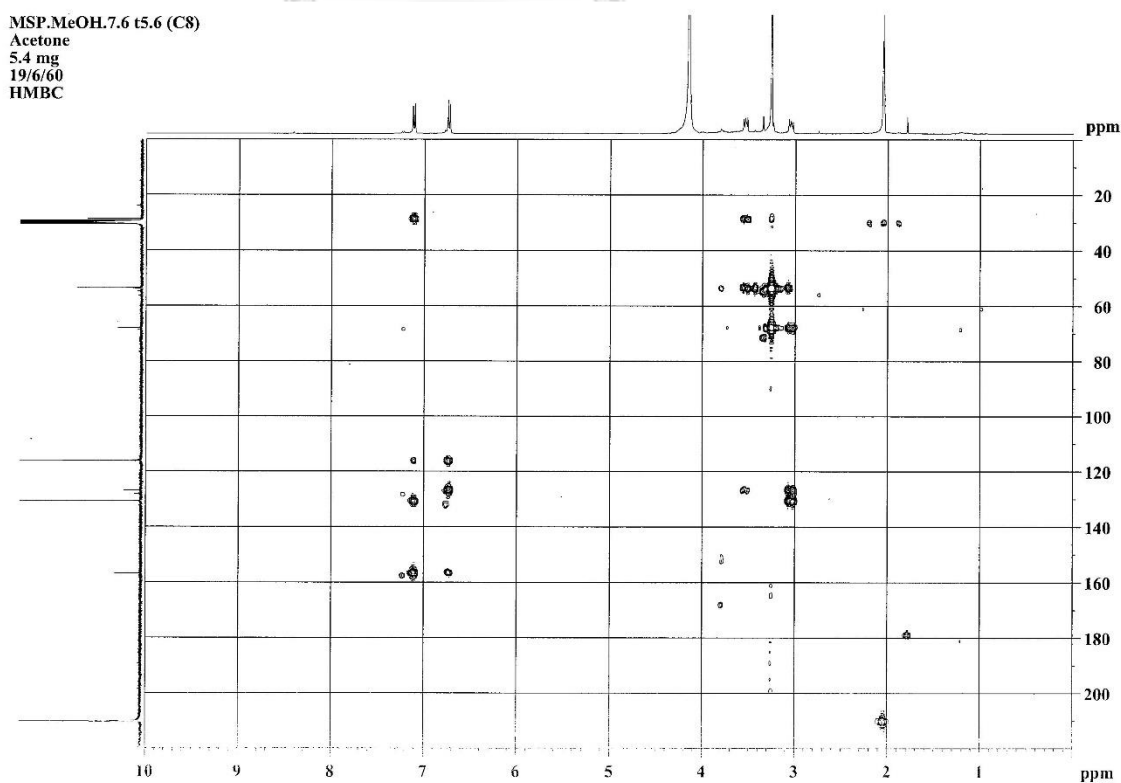
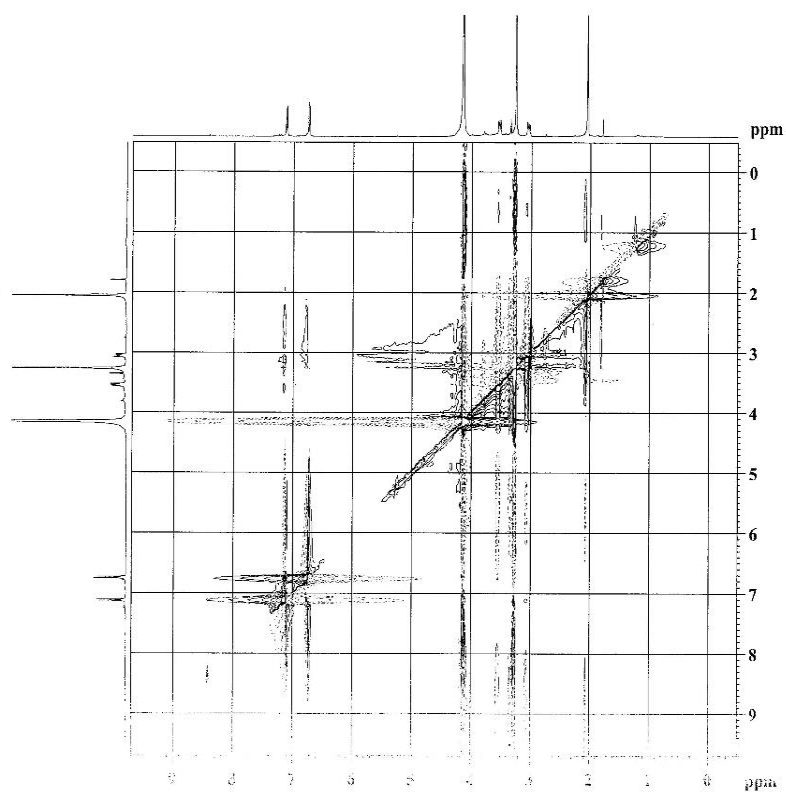
Figure B3 HSQC NMR spectrum (400 MHz, in acetone- d_6) of compound **7**Figure B4 HMBC NMR spectrum (400 MHz, in acetone- d_6) of compound **7**

Figure B5 ^1H - ^1H COSY NMR spectrum (400 MHz, in acetone- d_6) of compound 7

MSP.MeOH.7.6 t5.6 (C8)
Acetone
5.4 mg
19/6/60
NOESY

Figure B6 NOESY NMR spectrum (400 MHz, in acetone- d_6) of compound 7

MSP.MeOH.7.6 t5.6 (C8)
Acetone
5.4 mg
19/6/60

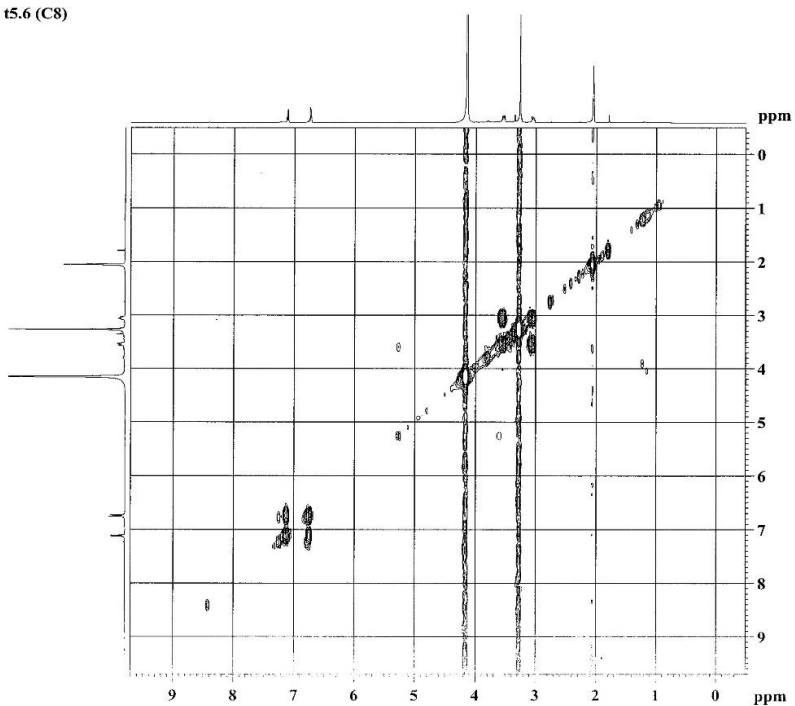
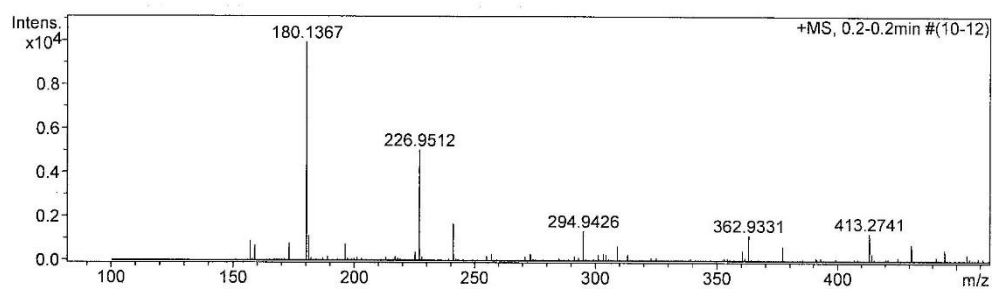


Figure B7 MS spectrum of compound 7



#	m/z	I	Res.
1	157.0831	884	7832
2	158.9631	650	8089
3	172.9783	759	8541
4	180.1367	9926	8555

Figure B8 UV spectrum of compound 7

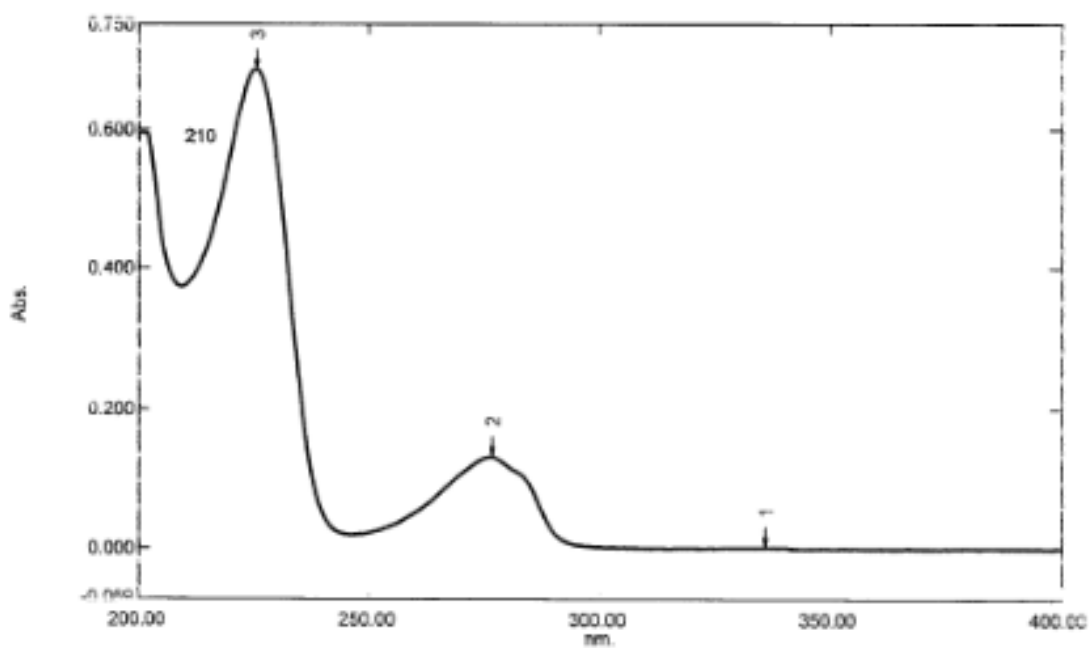


Figure B9 IR spectrum of compound 7

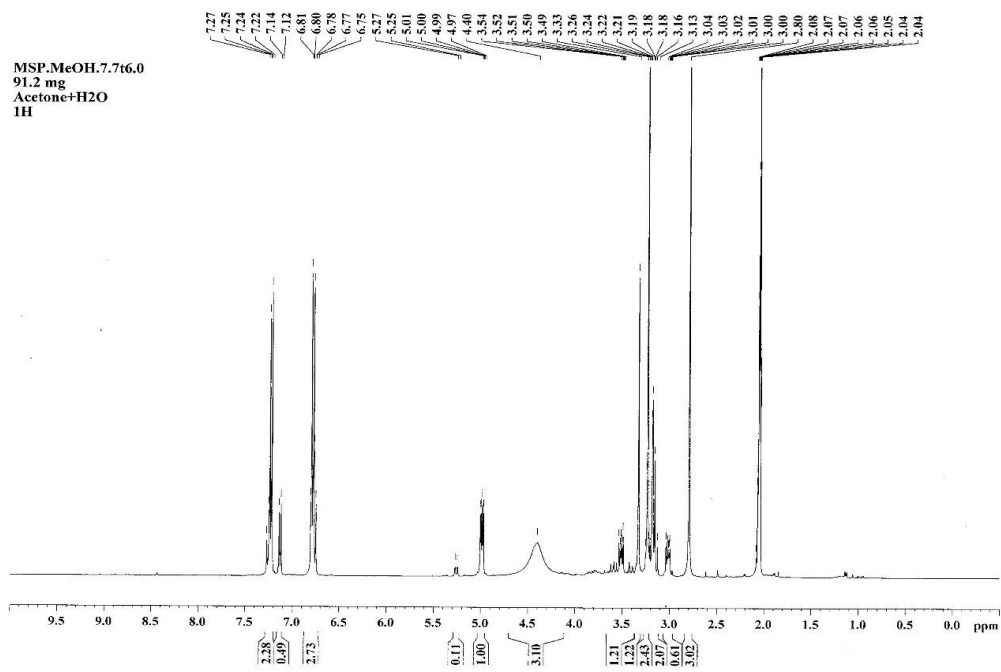
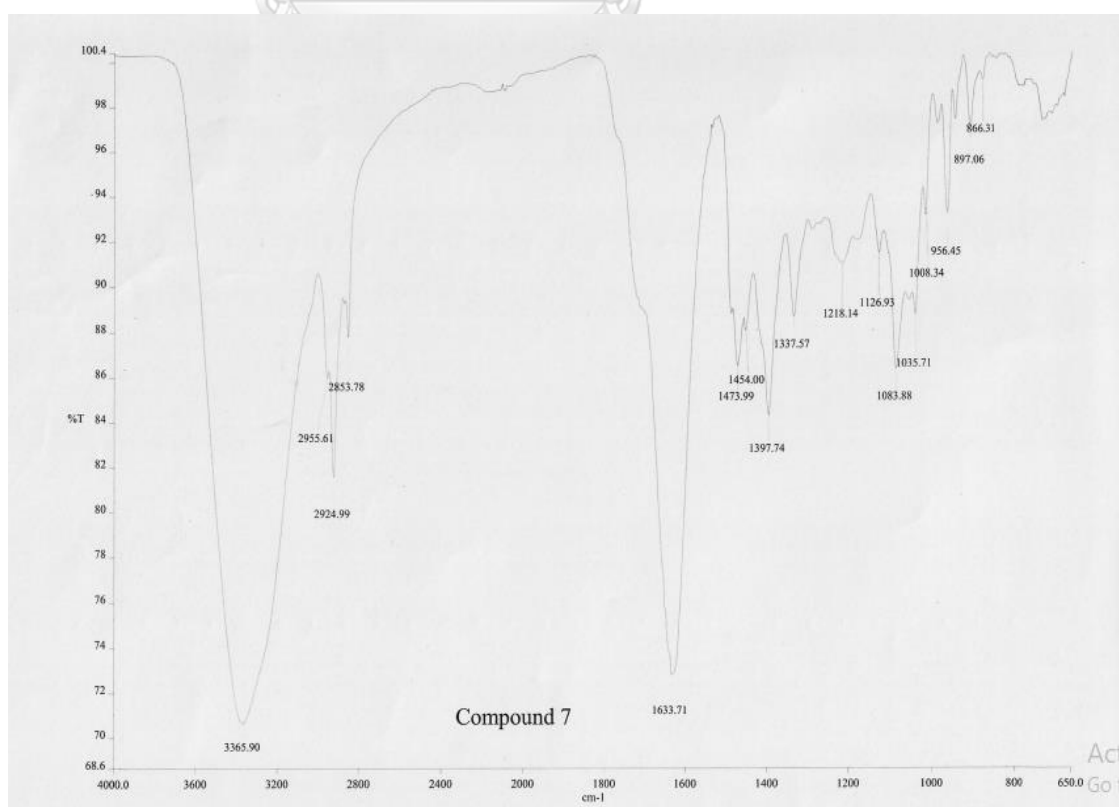
Figure B10 ^1H NMR spectrum (400 MHz, in acetone- d_6) of compound 8

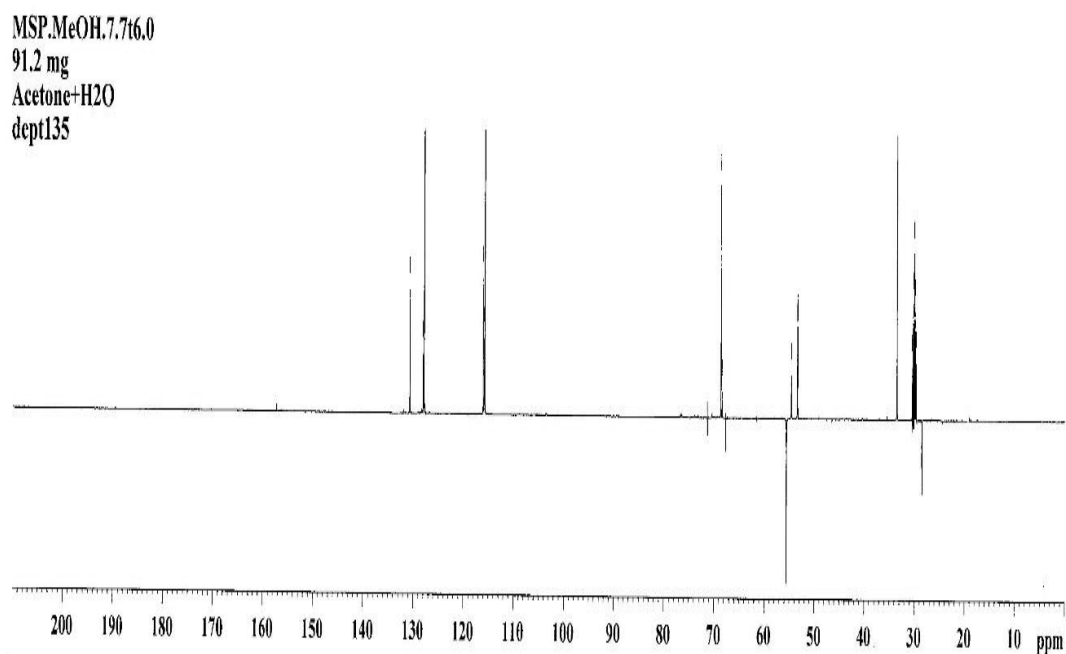
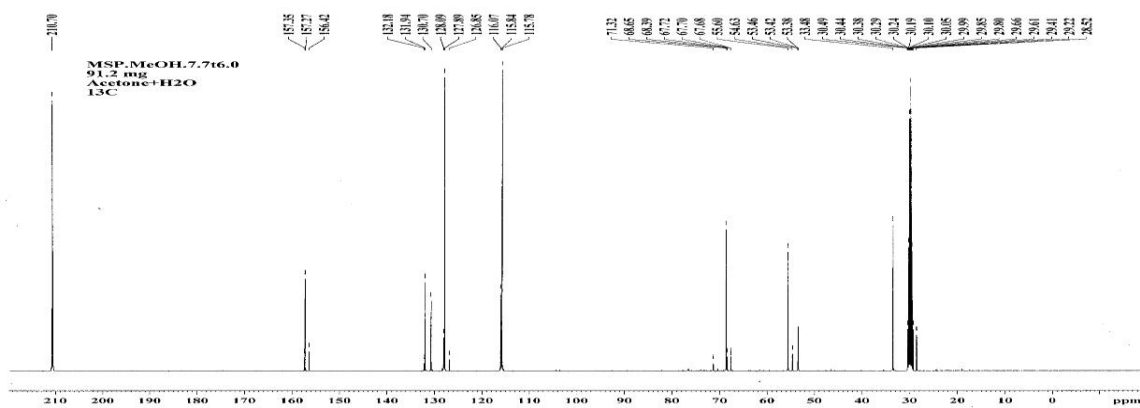
Figure B11 ^{13}C NMR spectrum (400 MHz, in acetone- d_6) of compound **8**Figure B12 DEPT 135 NMR spectrum (400 MHz, in acetone- d_6) of compound **8**

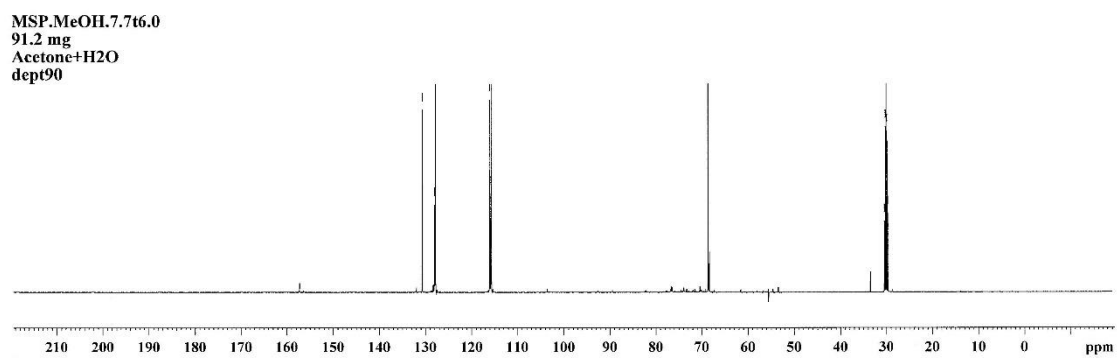
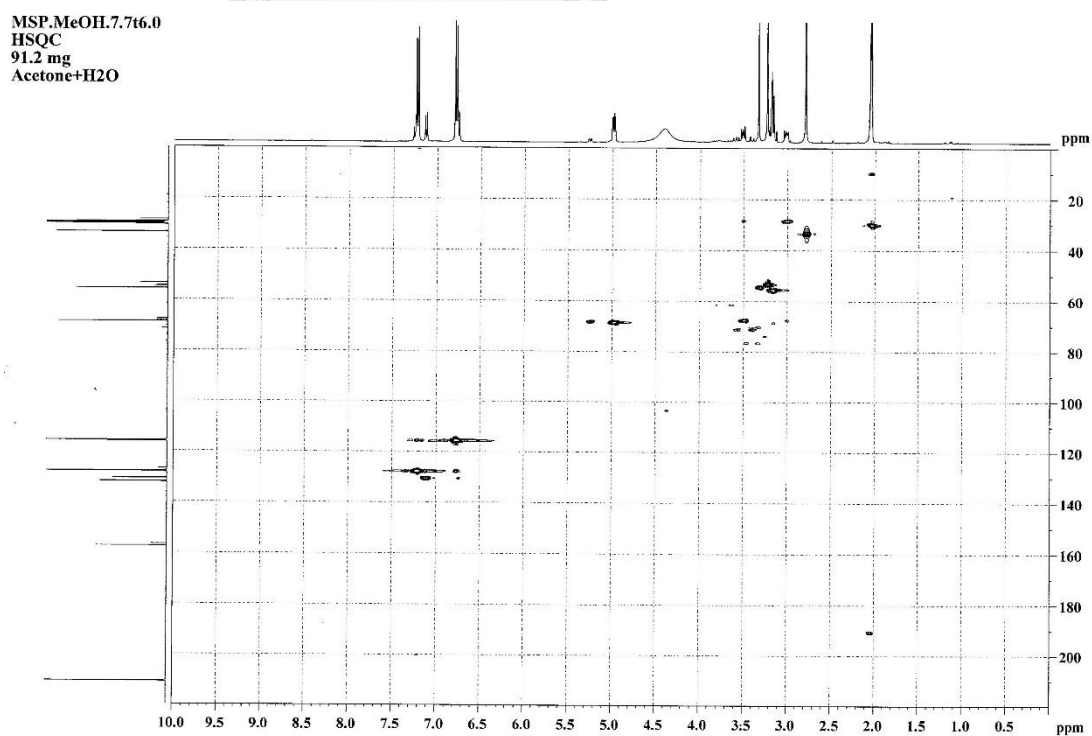
Figure B13 DEPT 90 NMR spectrum (400 MHz, in acetone- d_6) of compound **8**Figure B14 HSQC NMR spectrum (400 MHz, in acetone- d_6) of compound **8**

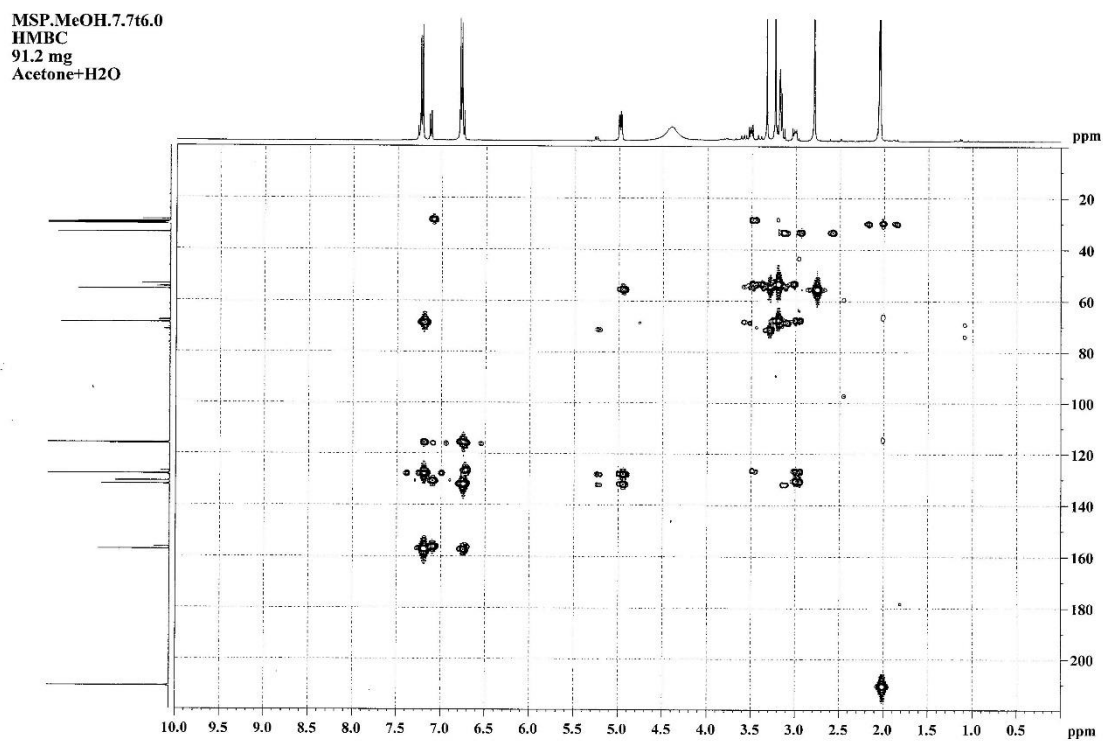
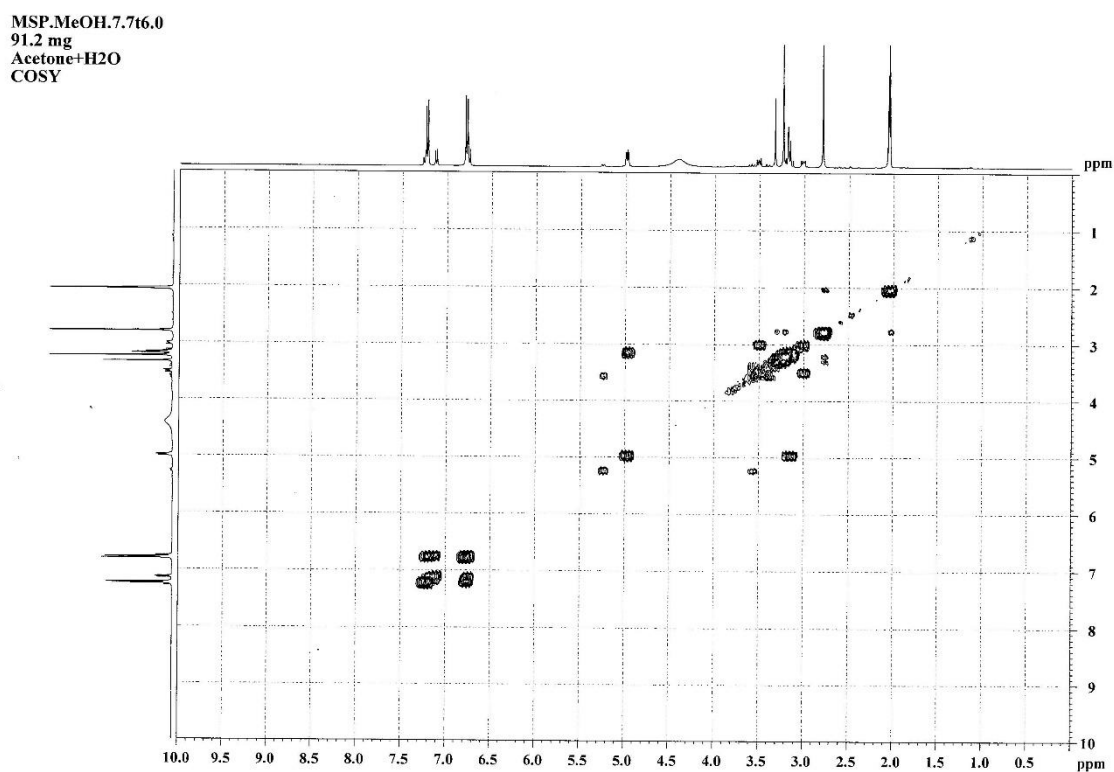
Figure B15 HMBC NMR spectrum (400 MHz, in acetone- d_6) of compound **8**Figure B16 ^1H - ^1H COSY NMR spectrum (400 MHz, in acetone- d_6) of compound **8**

Figure B19 UV spectrum of compound 8

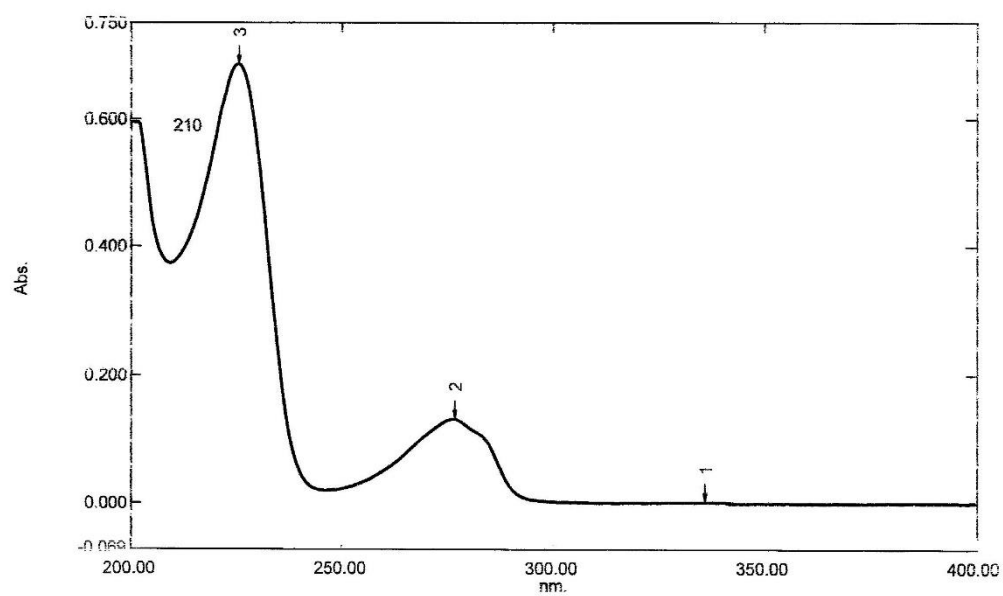
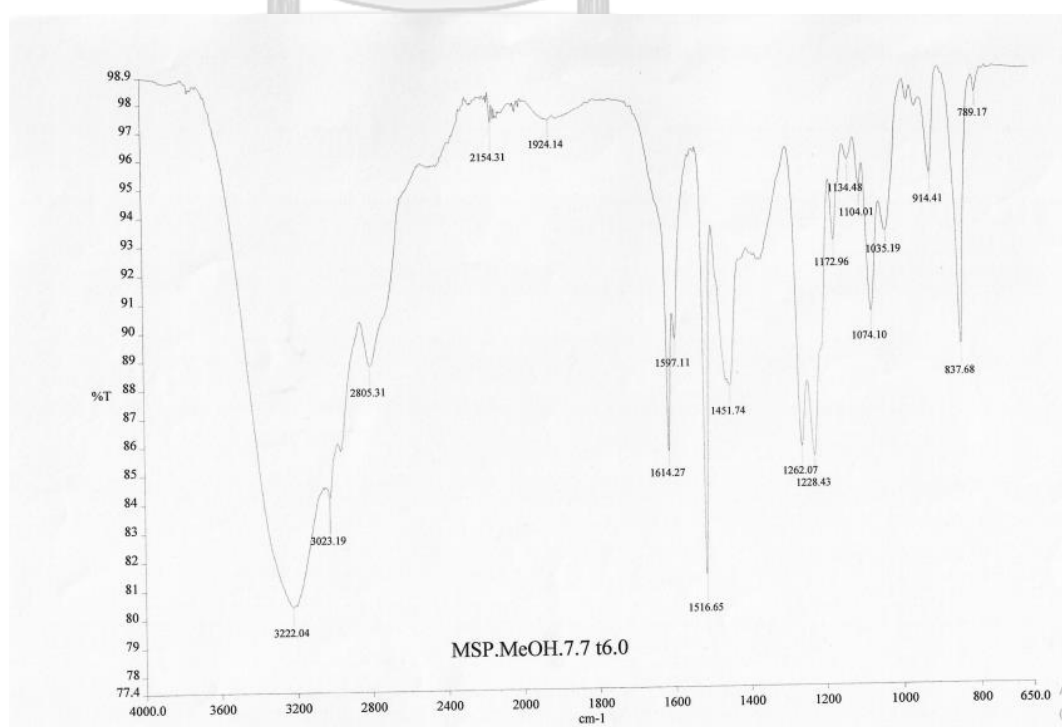
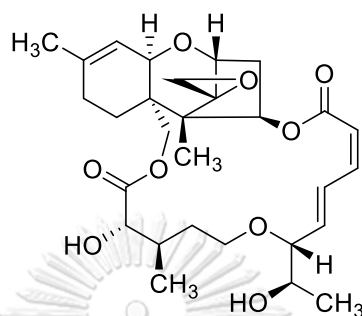


Figure B20 IR spectrum of compound 8



Part C: Bioactive compounds from termite-associated fungus ISFB10

Physicochemical properties of compounds isolated from termite-associated fungus ISFB10

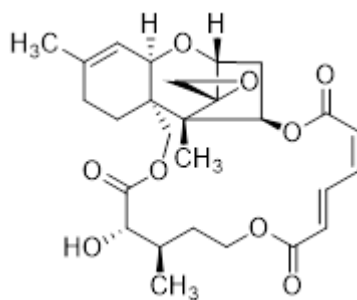


Compound **9** was obtained as yellow solid (150 mg)

ESI-TOF MS: calcd. for C₂₉H₄₀O₉Na, m/z 555.2570 (M+Na)⁺, found 555.2562.

UV (MeOH) λ_{\max} (log ϵ): 262 (3.83) nm.

IR (UATR) ν_{\max} : 3437, 2963, 2925, 2855, 1732, 1712, 1638, 1598, 1417, 1223, 1171, 1122, 1082, 1036, 1009, 967, 814, 733 cm⁻¹.



Compound **10** was obtained as yellow solid (30 mg)

ESI-TOF MS: calcd. for C₂₇H₃₄O₉Na, m/z 525.2101 (M+Na)⁺, found 525.2086.

UV (MeOH) λ_{\max} (log ϵ): 259 (4.17) nm.

IR (UATR) ν_{\max} : 3482, 2967, 1712, 1634, 1435, 1411, 1383, 1267, 1208, 1186, 1125, 1082, 1029, 996, 879, 820, 734, 701 cm⁻¹.

Figure C1 ¹H NMR spectrum (400 MHz, in acetone-*d*₆) of compound **9**

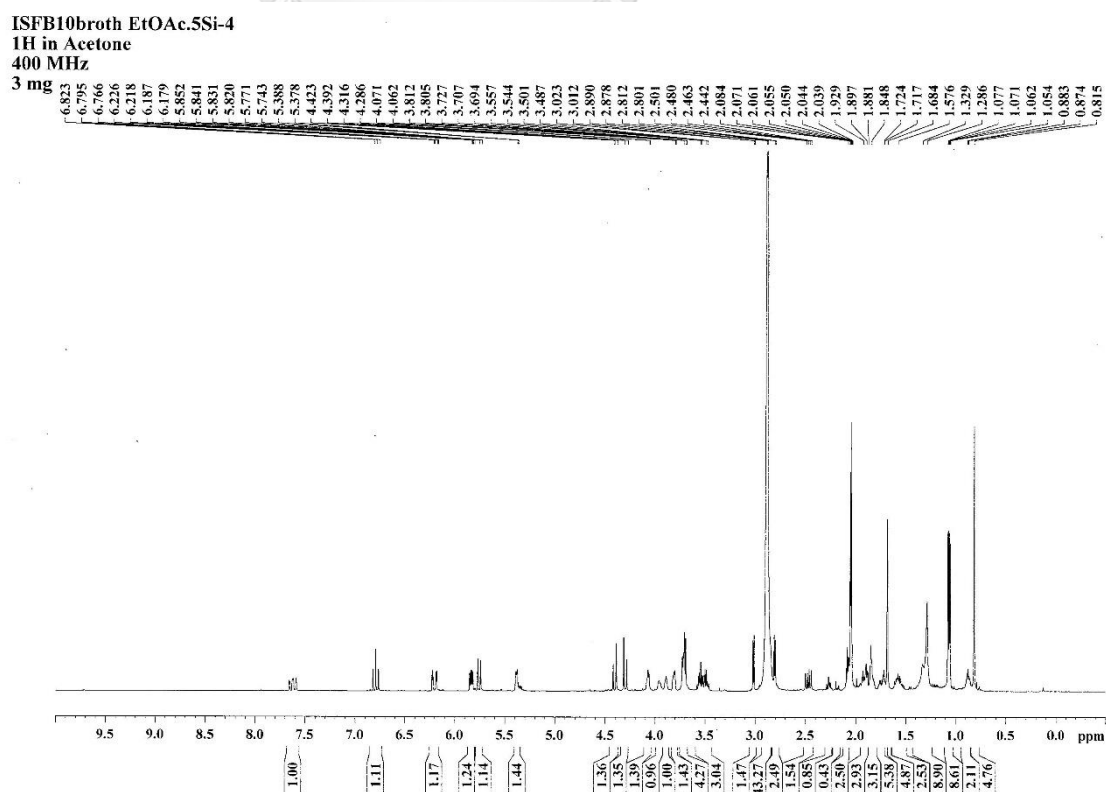


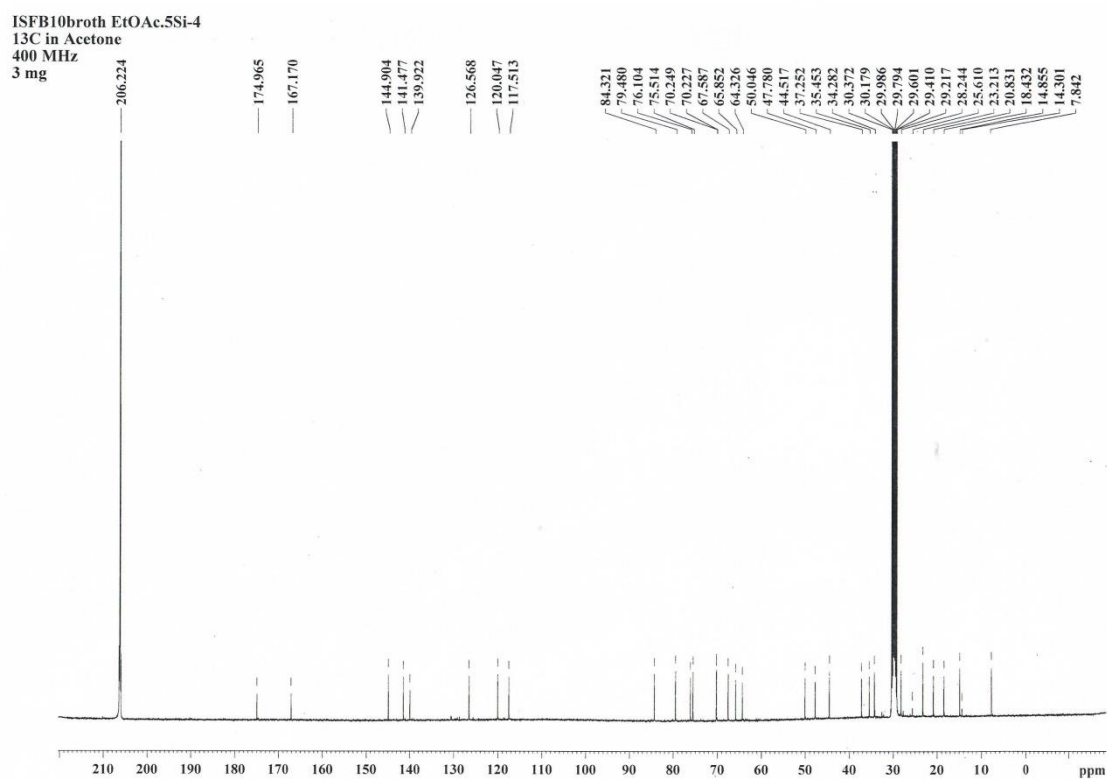
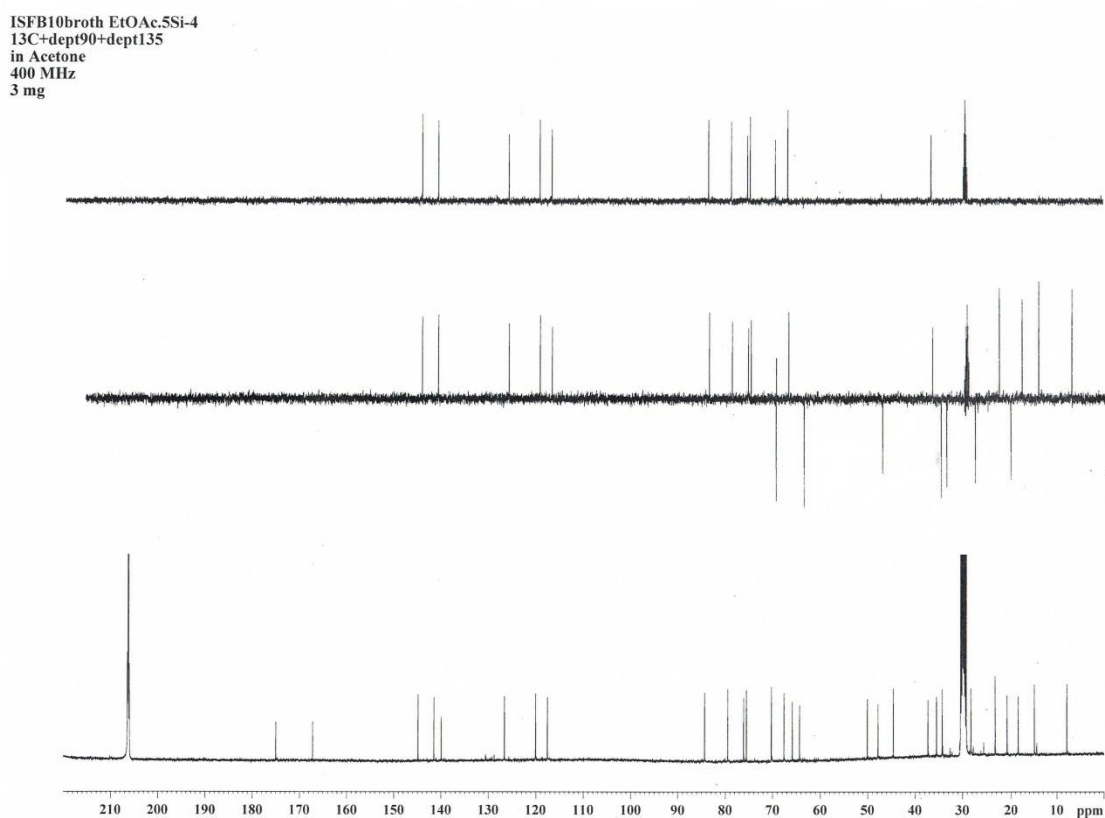
Figure C2 ^{13}C NMR spectrum (400 MHz, in acetone- d_6) of compound **9**Figure C3 DEPT 135 (middle) and DEPT 90 (top) NMR spectrum (400 MHz, in acetone- d_6) of compound **9**

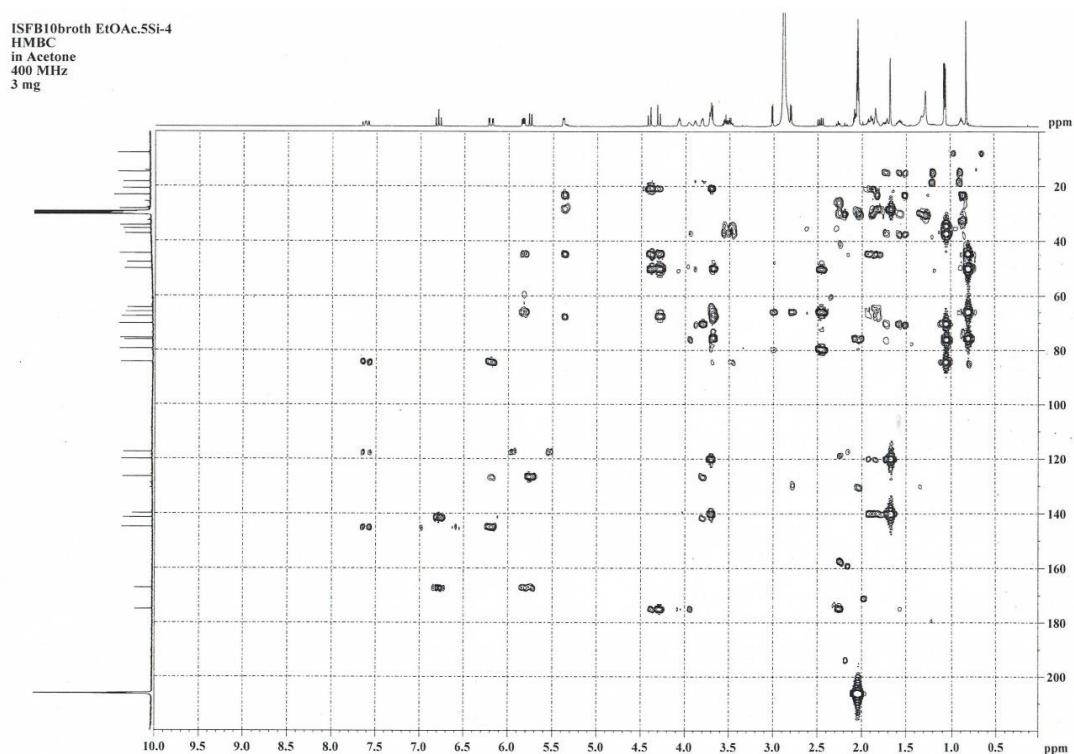
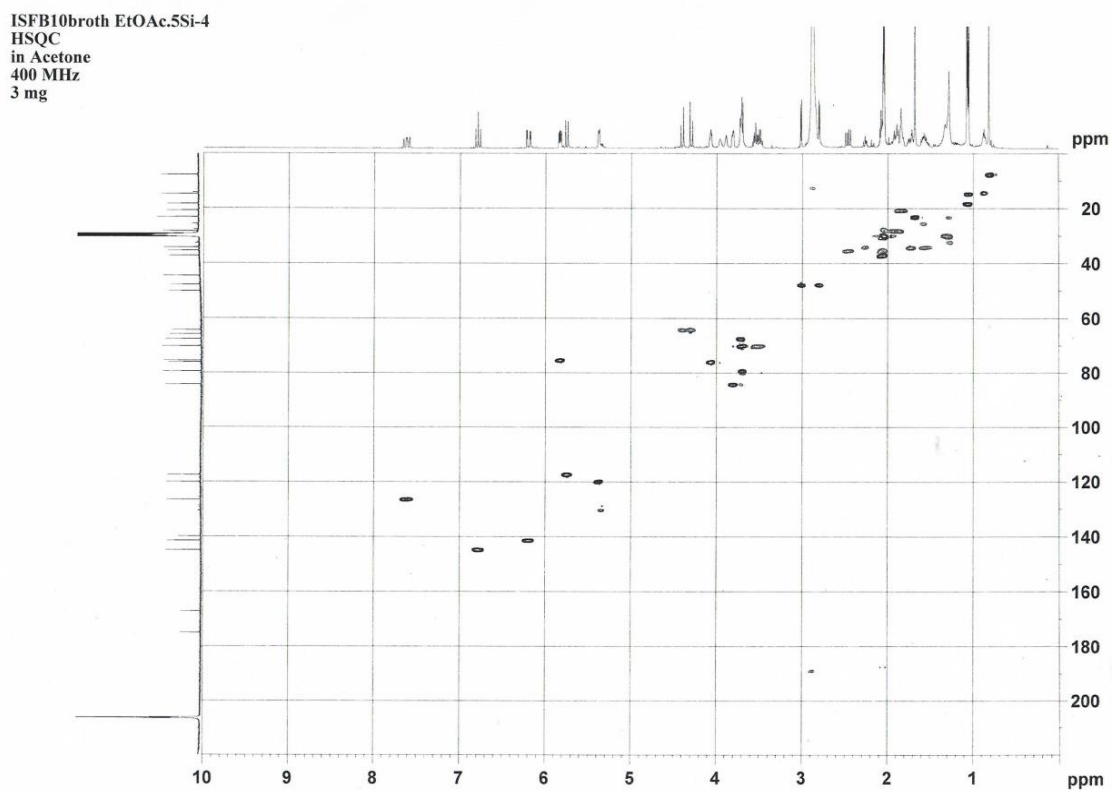
Figure C4 HSQC NMR spectrum (400 MHz, in acetone- d_6) of compound **9**Figure C5 HMBC NMR spectrum (400 MHz, in acetone- d_6) of compound **9**

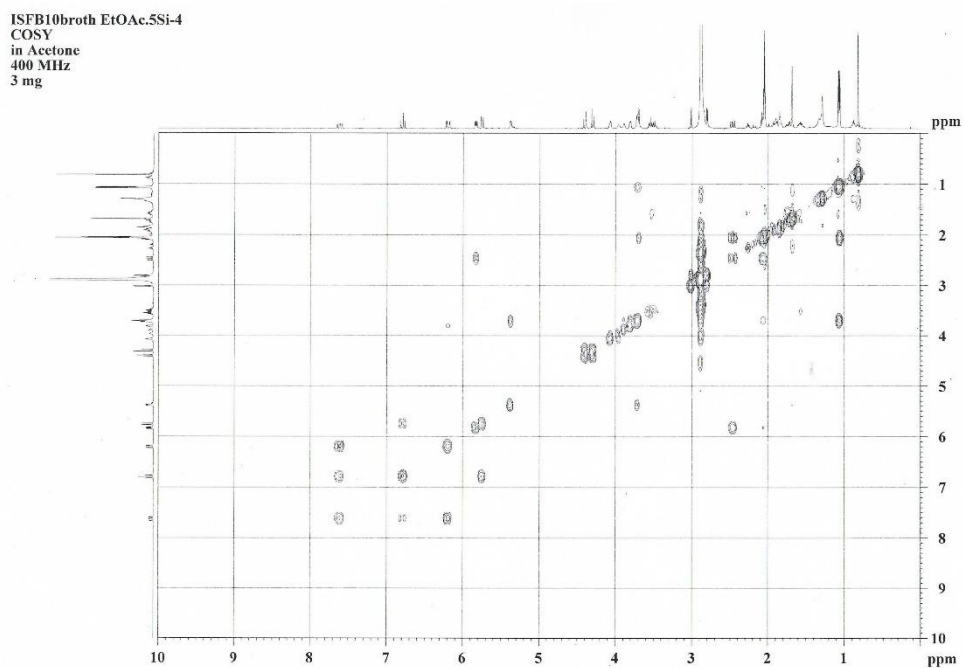
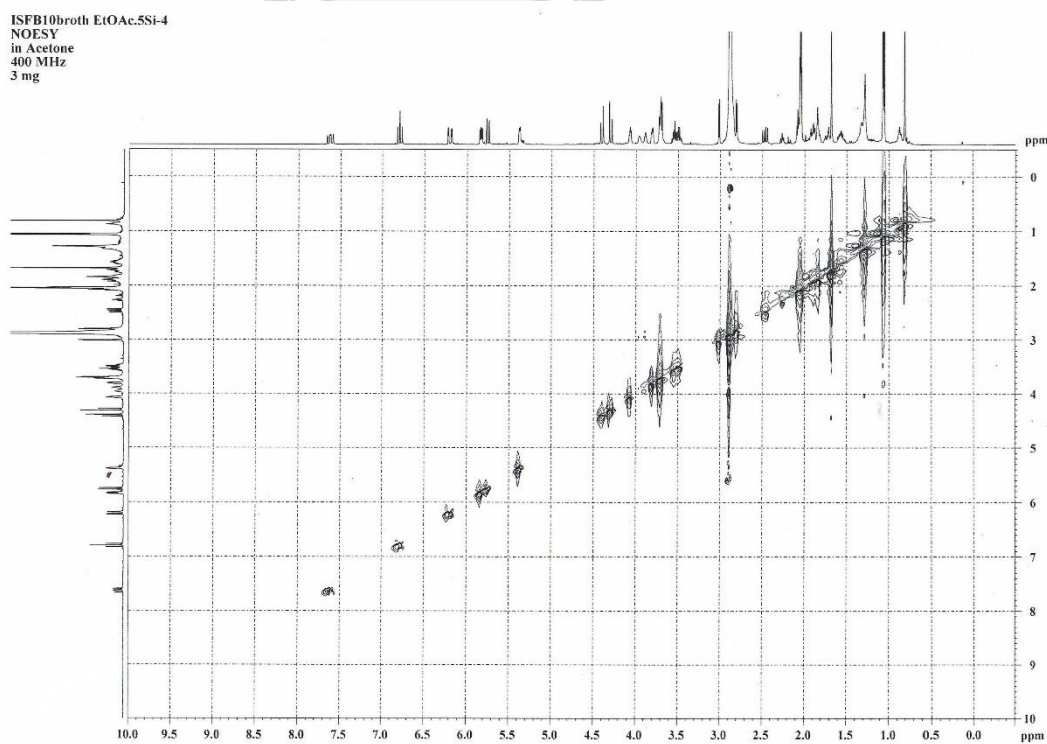
Figure C6 ^1H - ^1H COSY NMR spectrum (400 MHz, in acetone- d_6) of compound **9**Figure C7 NOESY NMR spectrum (400 MHz, in acetone- d_6) of compound **9**

Figure C8 MS spectrum of compound 9

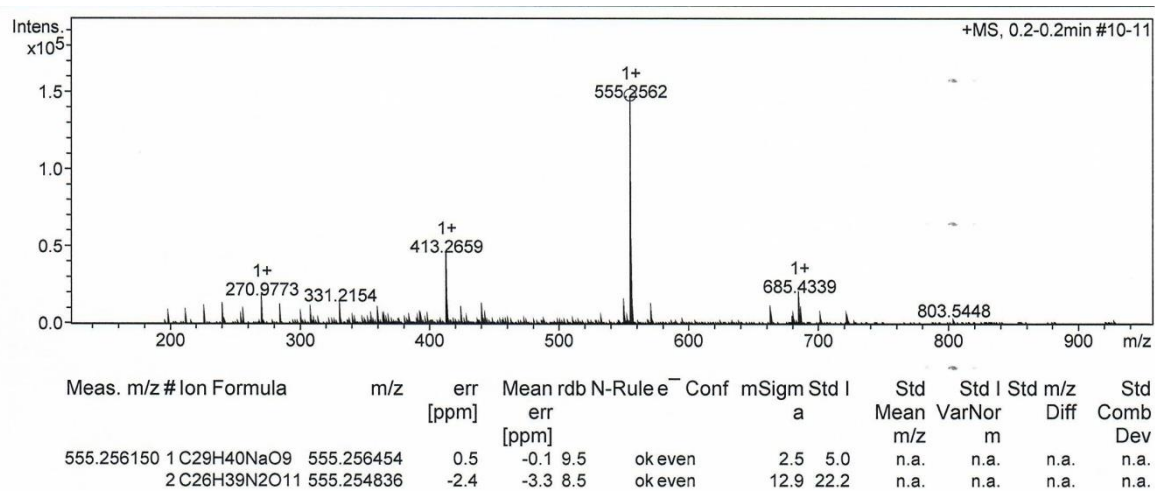


Figure C9 UV spectrum of compound 9

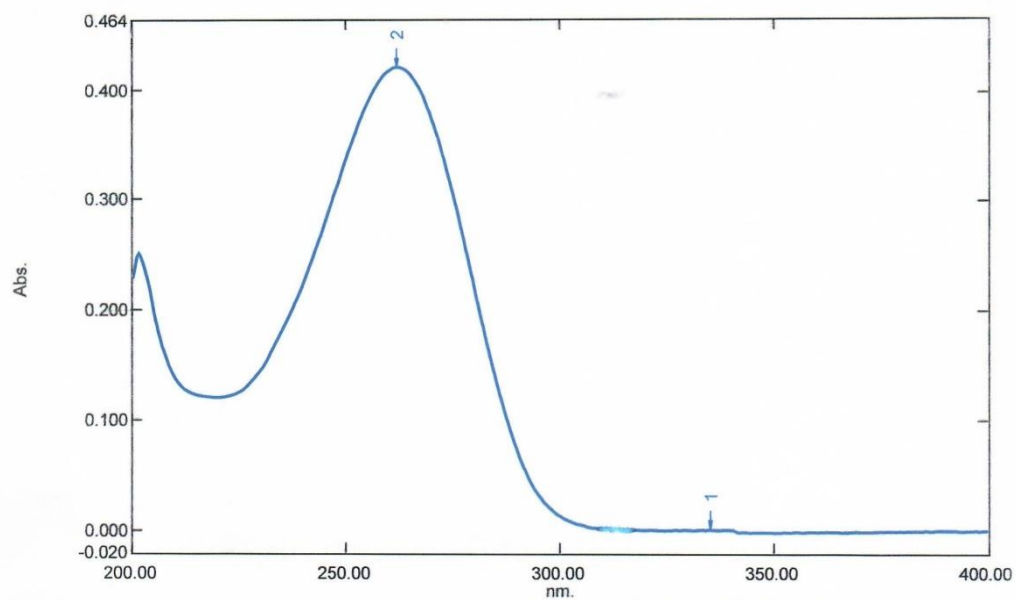


Figure C10 IR spectrum of compound 9

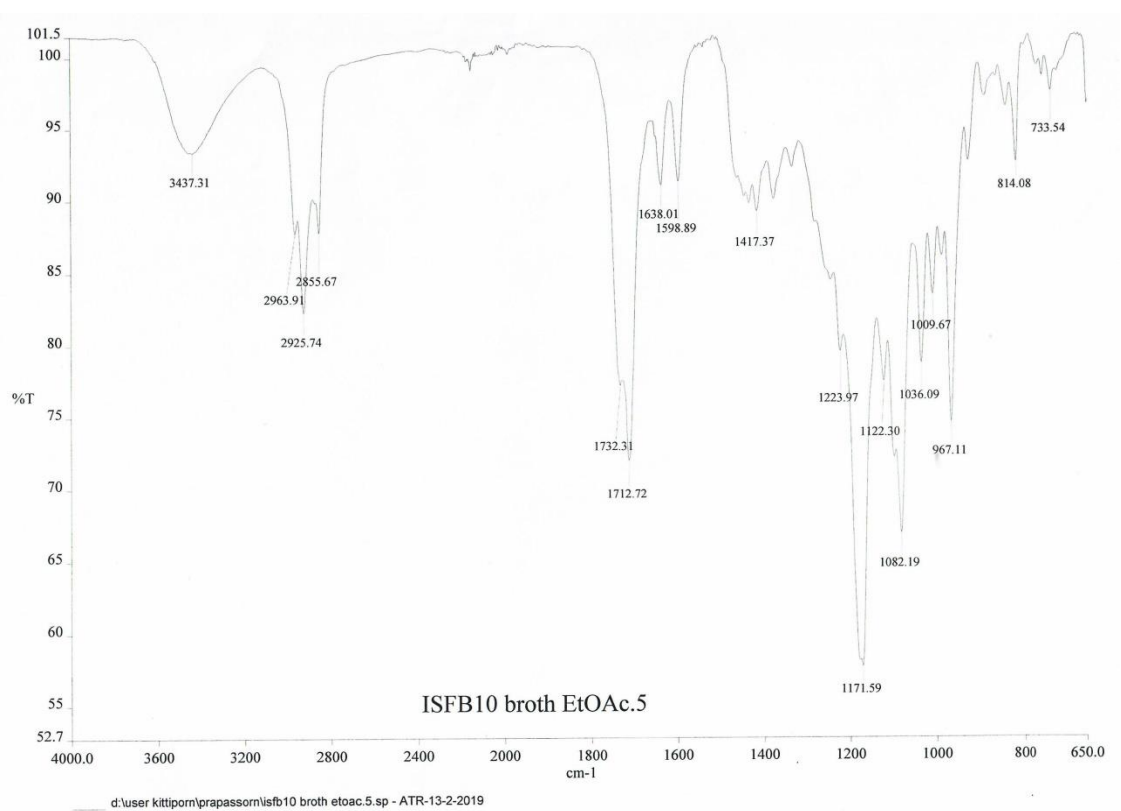
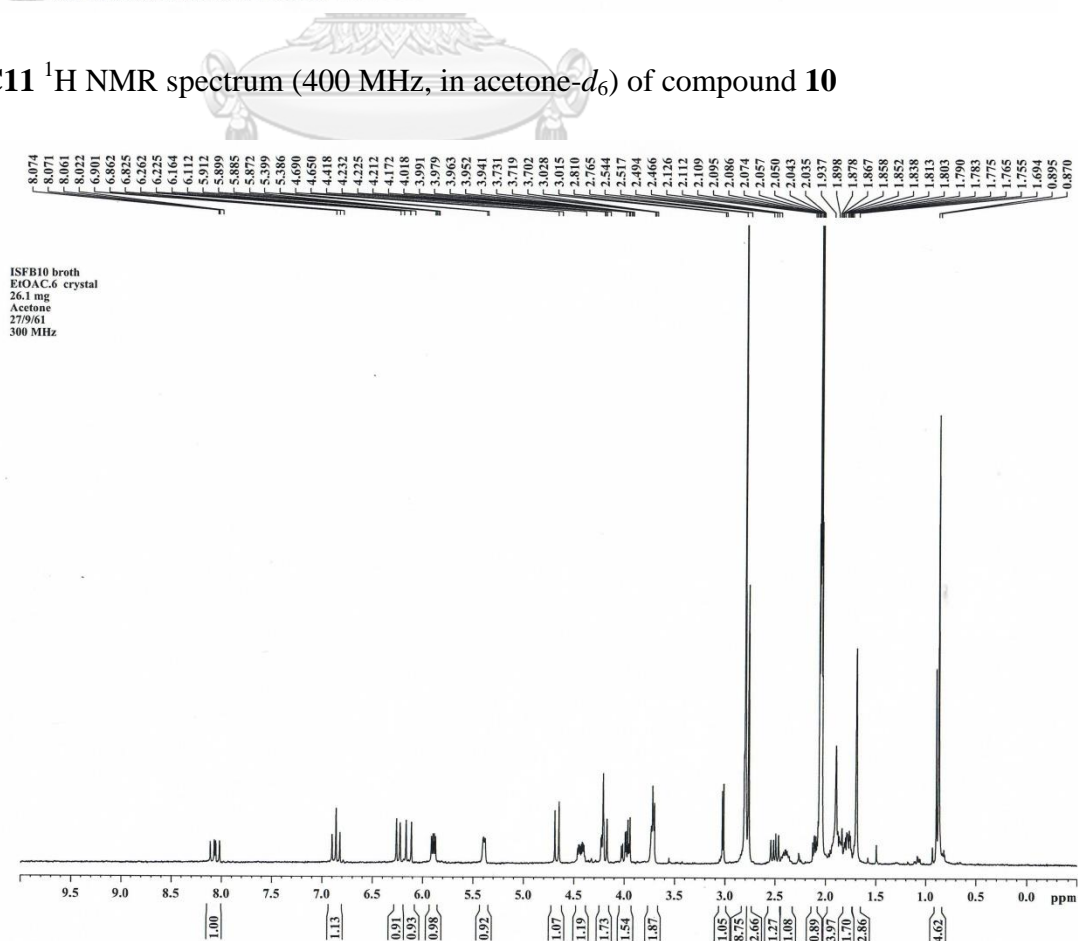
Figure C11 ¹H NMR spectrum (400 MHz, in acetone-*d*₆) of compound 10

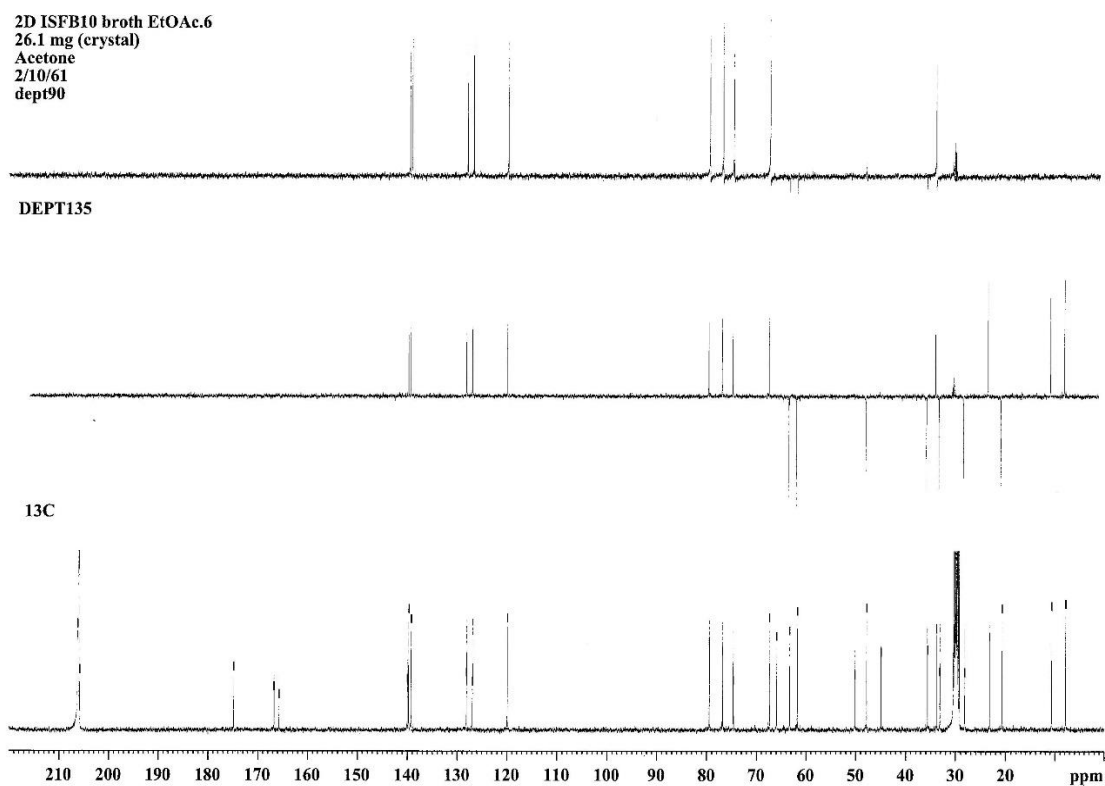
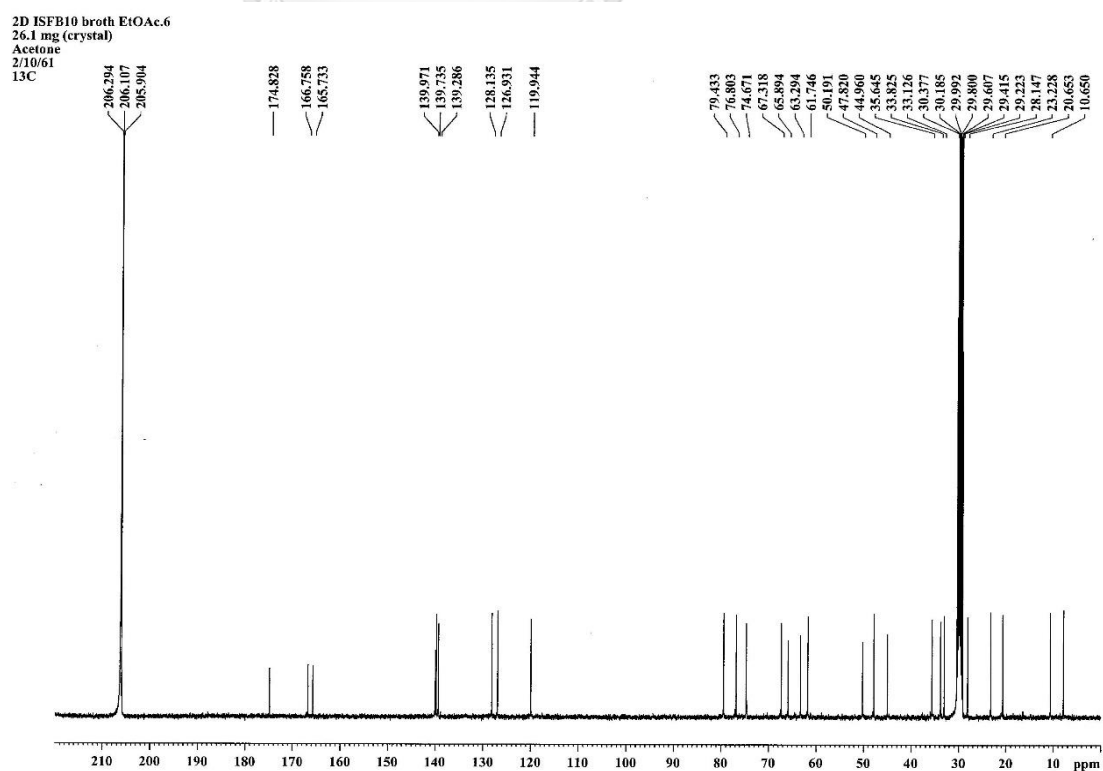
Figure C12 ^{13}C NMR spectrum (400 MHz, in acetone- d_6) of compound **10**Figure C13 DEPT 135 (middle) and DEPT 90 (top) NMR spectrum (400 MHz, in acetone- d_6) of compound **10**

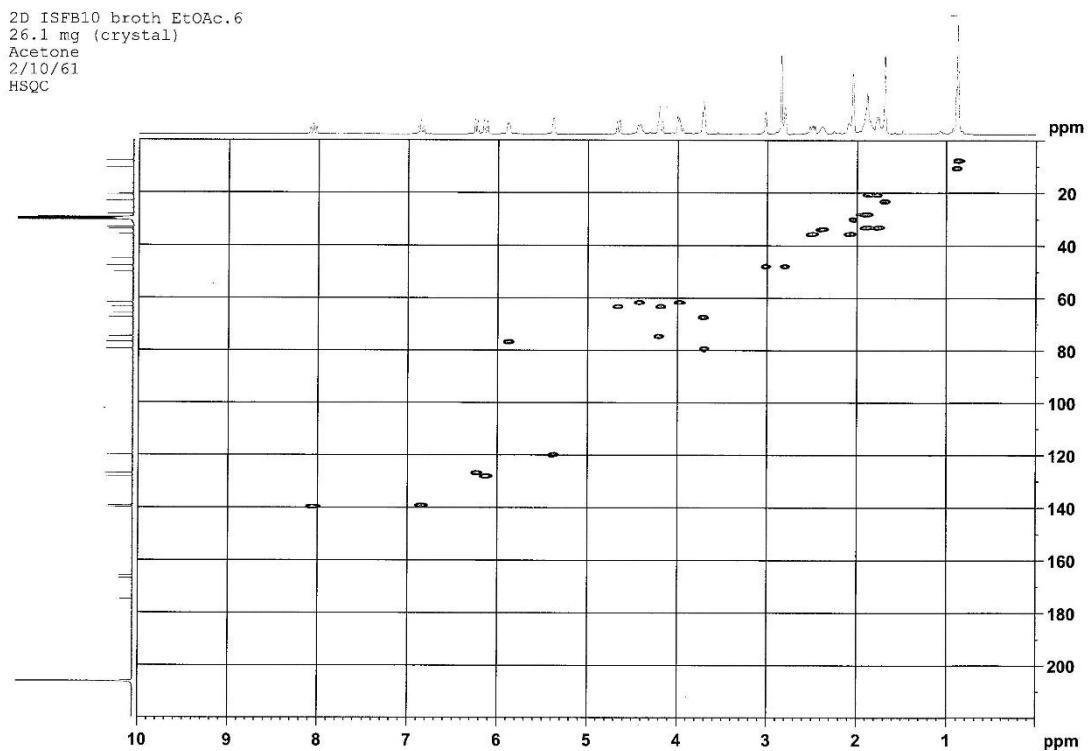
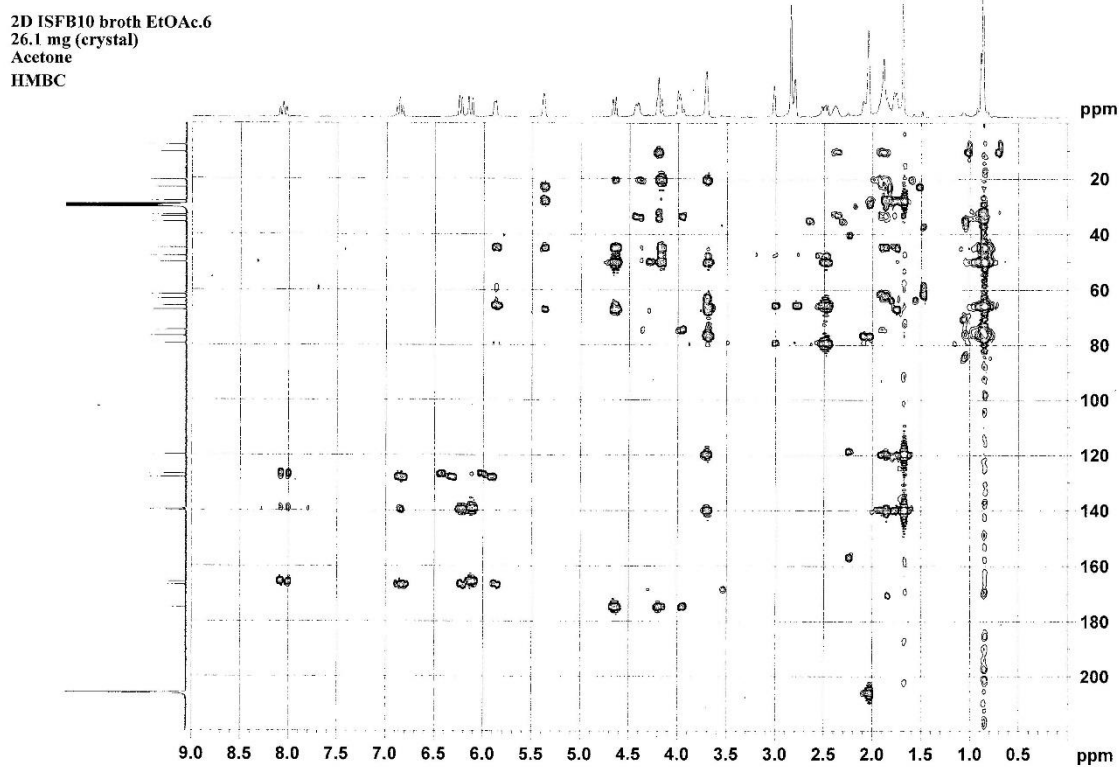
Figure C14 HSQC NMR spectrum (400 MHz, in acetone- d_6) of compound **10**Figure C15 HMBC NMR spectrum (400 MHz, in acetone- d_6) of compound **10**

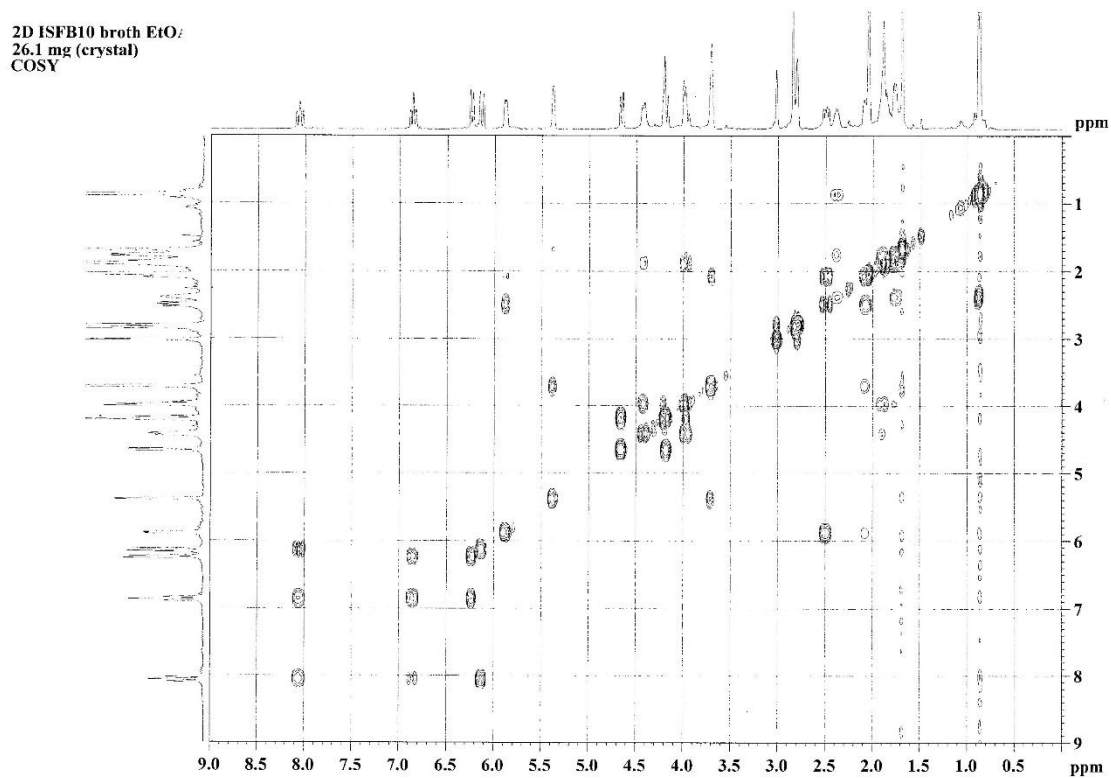
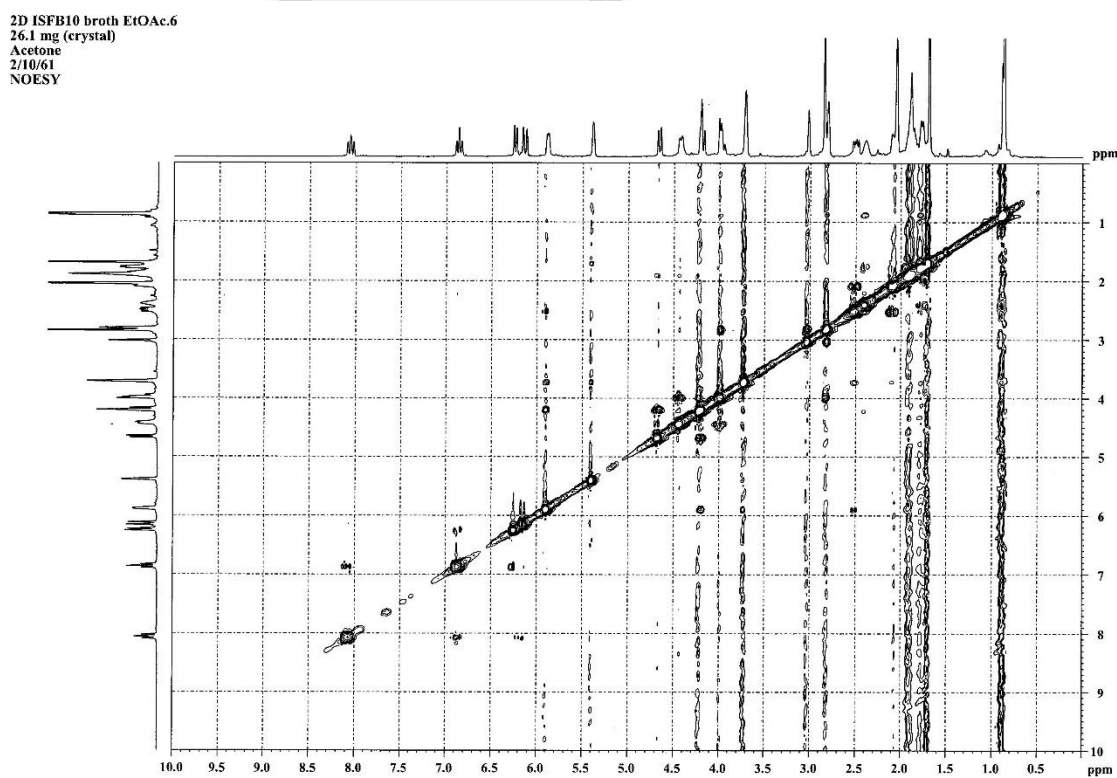
Figure C16 ^1H - ^1H COSY NMR spectrum (400 MHz, in acetone- d_6) of compound **10**Figure C17 NOESY NMR spectrum (400 MHz, in acetone- d_6) of compound **10**

Figure C18 MS spectrum of compound 10

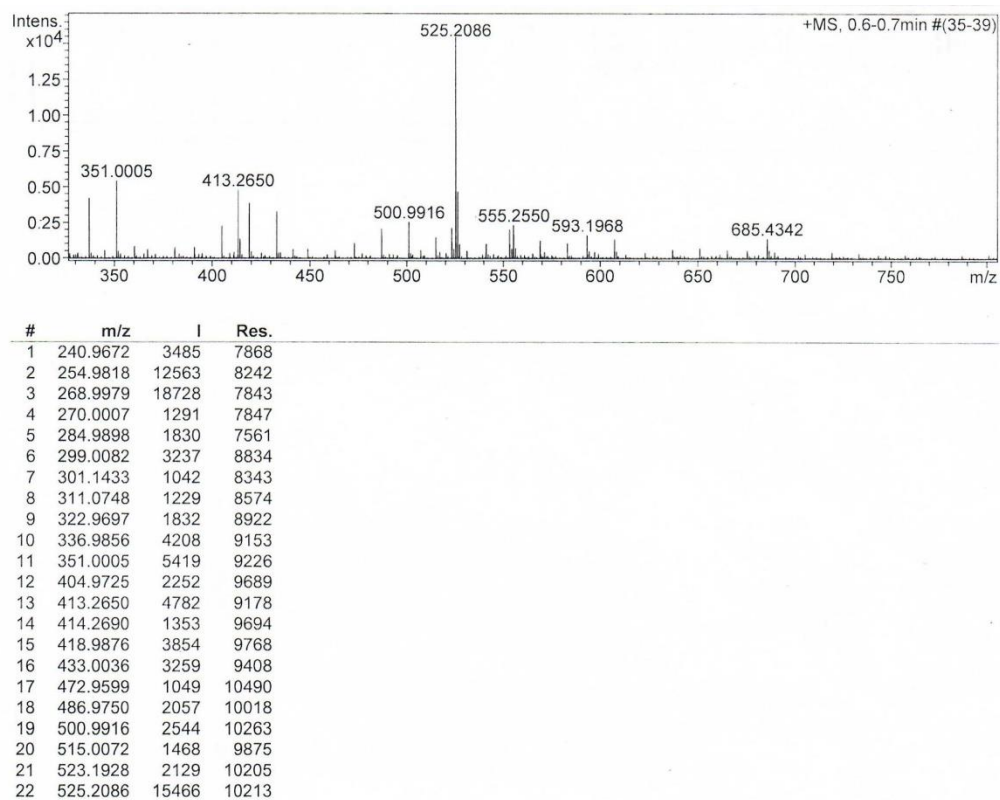


Figure C19 UV spectrum of compound 10

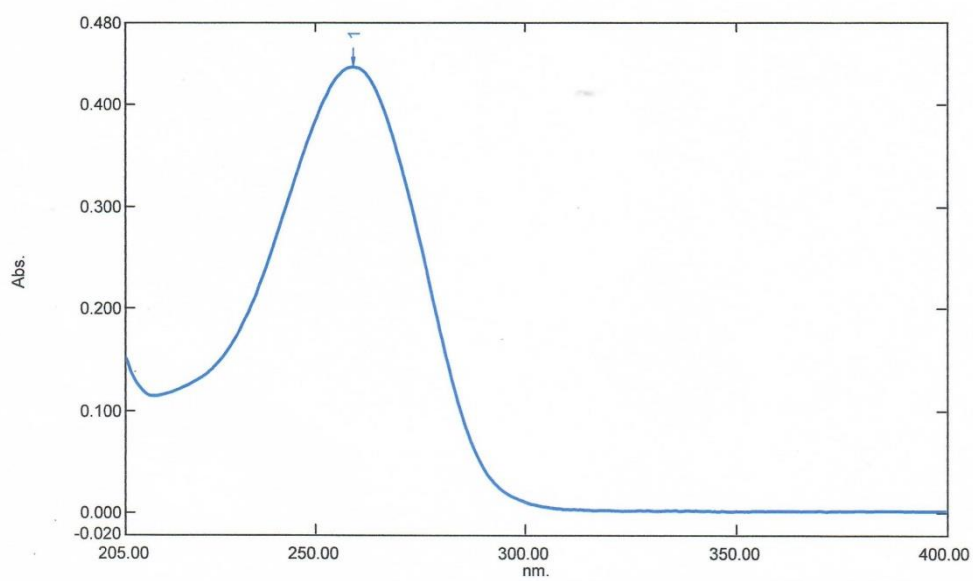
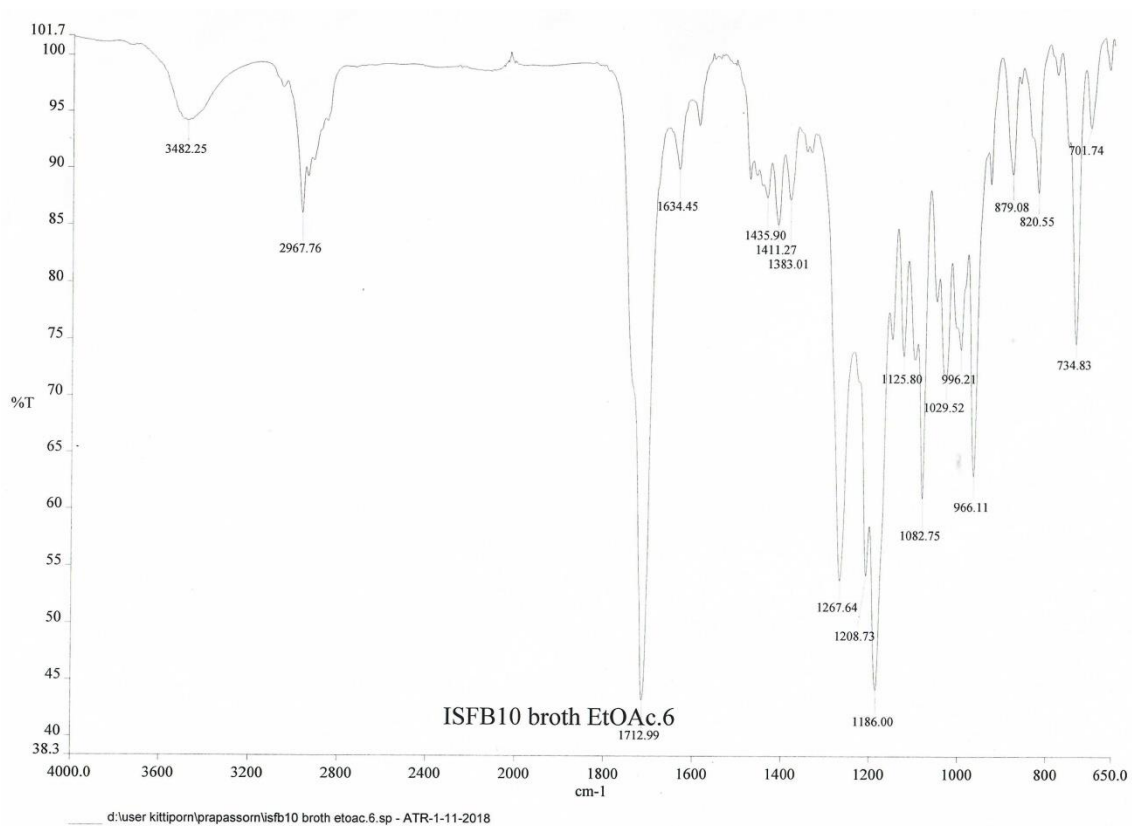


Figure C20 IR spectrum of compound 10





จุฬาลงกรณ์มหาวิทยาลัย
CHULALONGKORN UNIVERSITY

VITA

NAME Prapassorn Poolchanuan

DATE OF BIRTH 2 March 1993

PLACE OF BIRTH Chainat

INSTITUTIONS ATTENDED School of cosmetic science, Mae Fah Luang University.
Faculty of Science, Chulalongkorn University.

HOME ADDRESS 157/1 M.5 Thachanuan Manorum Chainat 17110

PUBLICATION Poolchanuan, P.; Unagul, P.; Thongnest, S.; Wiyakrutta, S.; Ngamrojanavanich, N.; Mahidol, C.; Ruchirawat, S.; Kittakoop, P., An anticonvulsive drug, valproic acid (valproate), has effects on the biosynthesis of fatty acids and polyketides in microorganisms. *Sci. Rep.* 2020, 10, 9300.

AWARD RECEIVED 2015- 2020 The 100th Anniversary Chulalongkorn University for Doctoral Scholarship.
2019 Certificate of training and testing biosafety guidelines for modern biotechnology, CU, Thailand.
2013 Certificate of Scientific Training and Testing, program on Good Lab Practice, Scientific and Technological Instrument Center, MFU, Thailand.
2012-2013 Certificate of outstanding academic performance award, MFU, Thailand.
2011-2012 Certificate of outstanding academic performance award, MFU, Thailand.